DESY 96-015

Physics with ARGUS

The ARGUS Collaboration

H. Albrecht, A. A. Andam, U. Binder, P. Böckmann, G. Drews, H. Ehrlichmann, R. Gläser, T. Hamacher, G. Harder, H. Hasemann, R. P. Hofmann, H. Kapitza, T. Kirchhoff, A. Krüger, I. Lembke-Koppitz, A. Nau, A. W. Nilsson, A. Nippe, S. Nowak[1], A. Philipp, M. Reidenbach, M. Schäfer, H. Schröder, H. D. Schulz, F. Sefkow, F. Selonke, U. Volland, M. Walter[1], R. Wurth, A. Yagil
DESY, Hamburg, Germany

R. D. Appuhn, U. Buchner, J. P. Donker, A. Drescher, H. J. Graf, B. Gräwe, C. Hast, G. Herrera, D. Kamp, H. Kolanoski, A. Kosche, A. Lange, A. Lindner, R. Mankel, A. Markees, U. Matthiesen, H. Scheck, M. Schieber, G. Schweda, T. Siegmund, B. Spaan, H. Thurn, D. Töpfer, A. Walther, D. Wegener, S. Westerhoff
Institut für Physik[2], Universität Dortmund, Germany

M. Bittner, P. Eckstein, C. Frankl, J. Graf, R. Holtzhauer, M. Schmidtler, M. Schramm, K. R. Schubert, R. Schwierz, M. Töpfer, R. Waldi
Institut für Kern- und Teilchenphysik[3], Technische Universität Dresden, Germany

M. Paulini, K. Reim, H. Wegener
Physikalisches Institut[4], Universität Erlangen-Nürnberg, Germany

O. Behnke, R. Eckmann, M. Hapke, H. Kuipers, O. Mai, R. Mundt, T. Oest, R. Reiner, A. Rohde, W. Schmidt-Parzefall, P. Weyers
II. Institut für Experimentalphysik, Universität Hamburg, Germany

U. Becker, C. Ehmann, K. Fritz, W. Funk, F. Heintz, R. Heller, T. Klinger, R. Salomon, B. Schwingenheuer, J. Stiewe, P. Utzat, S. Werner
Institut für Hochenergiephysik[5], Universität Heidelberg, Germany

S. Ball, K. Ehret, J. C. Gabriel, C. Geyer, W. Hofmann, A. Hölscher, B. Holzer, A. Hüpper, S. Khan, K. T. Knöpfle, M. Seeger, M. Spahn, J. Spengler
Max-Planck-Institut für Kernphysik, Heidelberg, Germany

D. I. Britton[6], N. N. Brown[6], C. E. K. Charlesworth[7], K. W. Edwards[8], R. Fernholz[6], W. Frisken[9], C. Fukunaga[9], D. J. Gilkinson[7], D. M. Gingrich[7], M. Goddard[9], E. R. F. Hyatt[6], P. C. H. Kim[7], P. Krieger[7], R. Kutschke[7], D. B. MacFarlane[6], J. A. McKenna[7], K. W. McLean[6], R. S. Orr[7], P. Padley[7], J. A. Parsons[7], P. M. Patel[6], J. D. Prentice[7], P. R. B. Saull[6], S. C. Seidel[7], H. C. J. Seywerd[7], B. J. Stacey[7], J. D. Swain[7], G. Tsipolitis[6], K. Tzamariudaki[6], R. G. Van de Water[7], T.-S. Yoon[7] J. C. Yun[8]

---

[1] DESY, IfH Zeuthen

[2] Supported by the German Bundesministerium für Forschung und Technologie, under contract number 054DO51P.

[3] Supported by the German Bundesministerium für Forschung und Technologie, under contract number 056DD11P.

[4] Supported by the German Bundesministerium für Forschung und Technologie, under contract number 054ER12P.

[5] Supported by the German Bundesministerium für Forschung und Technologie, under contract number 055HD21P.

[6] McGill University, Montreal, Quebec, Canada.

[7] University of Toronto, Toronto, Ontario, Canada.

[8] Carleton University, Ottawa, Ontario, Canada

[9] York University, Downsview, Ontario, Canada

Institute of Particle Physics[10], *Canada*

R. Ammar, D. Coppage, R. Davis, S. Kanekal, N. Kwak
University of Kansas[11], *Lawrence, KS, USA*

C. Ratz, D. Reßing, T. Ruf, S. Schael, M. Schneider, K. Strahl, J. Tamminga, S. Weseler
Institut für Experimentelle Kernphysik[12], *Universität Karlsruhe, Germany*

B. Boštjančič, G. Kernel, P. Križan, E. Križnič, M. Pleško, T. Podobnik, T. Živko
Institut J. Stefan and Oddelek za fiziko[13], *Univerza v Ljubljani, Ljubljana, Slovenia*

H. I. Cronström, L. Jönsson, Y. Oku
Institute of Physics[14], *University of Lund, Sweden*

A. Arefiev, A. Babaev, V. Balagura, S. Barsuk, I. Belyaev, V. Blinov[15], S. Chechelnitsky, R. Chistov, M. Danilov, A. Droutskoy, V. Eiges, B. Fominykh, E. Gershtein, Yu. Gershtein, A. Golutvin, I. Gorelov, O. Igonkina, I. Korolko, G. Kostina, D. Litvintsev, V. Lubimov, V. Matveev, P. Murat, V. Nagovitsin, P. Pakhlov, F. Ratnikov, N. Root[15], A. Rostovtsev, V. Ryltsov, A. Semenov, S. Semenov, Yu. Semenov, V. Shevchenko †, V. Shibaev, A. Snizhko, V. Soloshenko, V. Sopov, V. Tchistilin, I. Tichomirov, A. Undrus[15], Yu. Zaitsev, V. Zhilich[15]
Institute of Theoretical and Experimental Physics[16], *Moscow, Russia*

R. Childers, C. W. Darden, H. Gennow
University of South Carolina[17], *Columbia, S.C., USA*

[10] Supported by the Natural Sciences and Engineering Research Council, Canada.
[11] Supported by the U.S. National Science Foundation.
[12] Supported by the German Bundesministerium für Forschung und Technologie, under contract number 055KA11P.
[13] Supported by the Ministry of Science and Technology of the Republic of Slovenia and the Internationales Büro KfA, Jülich.
[14] Supported by the Swedish Research Council.
[15] On leave of absence from the Institute of Nuclear Physics, Novosibirsk, Russia
[16] Partly Supported by the International Science Foundation with grants MSB000 and MSB300.
[17] Supported by the U.S. Department of Energy, under contract DE-AS09-80ER10690.

Contents

1 Introduction **1**

2 B Physics **6**

2.1 Introduction 6
2.2 Exclusive Hadronic Decays 9
2.2.1 Reconstruction of exclusive B Decays into Mesons with Charm 11
2.2.2 Search for Exclusive Hadronic $b \to u$ Decays 19
2.2.3 Search for Rare "Penguin" B Decays 20
2.2.4 Summary of exclusive B reconstruction 21
2.3 Inclusive Hadronic Decays 22
2.3.1 Inclusive D^0, D^+ and D^{*+} Production 22
2.3.2 Inclusive D_s^+ Production 22
2.3.3 Inclusive Charmonium Production 24
2.3.4 Inclusive Baryon Production 24
2.3.5 Inclusive Kaon Production 25
2.4 Inclusive Semileptonic B decays 26
2.5 Semileptonic $b \to u$ decays and Determination of $|V_{ub}|$ 29
2.6 Exclusive Semileptonic B decays and the Measurement of $|V_{cb}|$ 32
2.6.1 The decay $\overline{B}^0 \to D^{*+}\ell^-\overline{\nu}$ 32
2.6.2 The decay $B^- \to D^{*0}\ell^-\overline{\nu}$ 36
2.6.3 The decays $\overline{B^0} \to D^+\ell^-\overline{\nu}$ and $B^- \to D^0\ell^-\overline{\nu}$ 38
2.6.4 Observation of D^{**} mesons in semileptonic B decays 39
2.6.5 Search for exclusive semileptonic $b \to u$ decays 40
2.7 Summary of semileptonic B decays 41
2.8 $B^0\overline{B}^0$Mixing and the Measurement of $|V_{td}|$ 41
2.9 Conclusions 46

3 Charm Physics **47**

3.1 Introduction 47
3.2 Spectroscopy of Charmed Hadrons 48
3.2.1 Ground State Charmed Mesons 48
3.2.2 Excited Charmed Mesons 51
3.2.3 Charmed Baryon Ground States 57
3.2.4 First Observation of an Excited Charmed Baryon State 59
3.3 Weak Decays of Charmed Hadrons 62
3.3.1 The measurement of the lifetimes of charmed mesons 62
3.3.2 Observation of the Decay $D^0 \to \phi\overline{K}^0$ 63
3.3.3 Evidence for W Exchange Contribution to Charmed Baryon Decays 65
3.3.4 Evidence for Parity Violation in the Decay $\Lambda_c^+ \to \Lambda\pi^+$ 67
3.3.5 Semileptonic decays of charmed mesons 68
3.3.6 Observation of Semileptonic Charmed Baryon Decays 70

3.3.7 Measurement of Branching Ratios for Hadronic D Decays . . . 72
3.4 Summary of Charm Physics with ARGUS . . . 77

4 τ Physics **78**
4.1 Introduction . . . 78
4.2 Decay Branching Ratios of the τ Lepton . . . 80
4.2.1 The Charged Current in τ Decays . . . 80
4.2.2 Leptonic Decays . . . 80
4.2.3 Hadronic Decays . . . 81
4.2.4 Non-Standard Decays . . . 83
4.3 Properties of Hadronic τ Decays . . . 85
4.3.1 Vector currents . . . 85
4.3.2 Axial-vector currents . . . 90
4.3.3 Tau Decays Involving Kaons . . . 93
4.4 Test of Lepton Universality . . . 94
4.4.1 The Leptonic Decay Width . . . 94
4.4.2 The τ Lifetime . . . 94
4.4.3 The Masses of the τ Lepton and its Neutrino . . . 95
4.4.4 Status of Lepton Universality in τ Decays . . . 97
4.5 Tests of the Lorentz Structure of Tau Decays . . . 98
4.5.1 Probing the Electro-Weak Coupling by the Hadronic Final State . . . 98
4.5.2 Leptonic Decays and the Michel Parameters . . . 103
4.5.3 Combing the Results on Michel Parameters and the ν_τ Helicity . . . 107
4.6 Summary of the ARGUS Tau Results . . . 107

5 Bottomonium Spectroscopy **109**
5.1 Upsilon Mass Measurement . . . 110
5.2 Determination of Γ_{ee} and $\Gamma_{\rm tot}$ . . . 111
5.2.1 Radiative Corrections . . . 112
5.2.2 Determination of the Resonance Parameters . . . 112
5.2.3 Lepton Pair Production . . . 114
5.2.4 The Width of the $\Upsilon(4S)$ . . . 115
5.2.5 Electromagnetic Transitions . . . 115
5.3 Hadronic Transitions from $\Upsilon(2S)$ to $\Upsilon(1S)$ . . . 117
5.3.1 $\Upsilon(2S) \to \Upsilon(1S)\,\eta$ . . . 119
5.3.2 Summary . . . 119

6 Two–Photon Physics **120**
6.1 Introduction . . . 120
6.2 Data Analysis Methods . . . 121
6.2.1 Partial Wave Analysis . . . 122
6.2.2 Treatment of the Final States . . . 122
6.2.3 Systematic Errors . . . 123
6.3 Two–Photon Production of a Pair of Vector Mesons . . . 123
6.3.1 $\gamma\gamma \to \rho\rho$ . . . 124
6.3.2 $\gamma\gamma \to \rho^0\omega$ . . . 124
6.3.3 $\gamma\gamma \to \rho^0\phi$ . . . 126
6.3.4 $\gamma\gamma \to \omega\omega$ . . . 126
6.3.5 $\gamma\gamma \to \omega\phi$ . . . 126
6.3.6 $\gamma\gamma \to K^*\bar{K}^*$ . . . 126

6.3.7 Summary and Discussion of Vector Meson Pair Production . . . 127
6.4 Resonance Production . . . 127
6.4.1 $\gamma\gamma \to K^+K^-$ . . . 128
6.4.2 $\gamma\gamma \to \pi^+\pi^-\pi^0$ . . . 128
6.4.3 $\gamma\gamma \to \eta'(958) \to \pi^+\pi^-\gamma$ . . . 129
6.4.4 $\gamma\gamma \to \eta_c$ . . . 131
6.4.5 Summary and discussion of resonance production . . . 131

7 Fragmentation **133**
7.1 Introduction . . . 133
7.2 General Features of the Hadronic Final States . . . 134
7.2.1 Jet-Structure . . . 134
7.2.2 Measurements of α_s . . . 135
7.3 Fragmentation into Mesons and Baryons with Light Valence Quarks . . . 137
7.3.1 Production of Stable Mesons . . . 138
7.3.2 Production of Unstable Mesons . . . 138
7.3.3 Baryon Production . . . 143
7.3.4 Color Coherence Effects . . . 151
7.4 Charmed Quark Fragmentation . . . 154
7.4.1 Charmed Meson Production . . . 154
7.4.2 Charmed Baryon Production . . . 158
7.4.3 Charm Production in Gluon Jets . . . 159
7.5 Summary . . . 160

8 Summary **162**

9 Acknowledgement **163**

10 ARGUS Publications **164**
10.1 B Physics . . . 164
10.2 Charm Physics . . . 166
10.3 τ Physics . . . 168
10.4 Υ Spectroscopy . . . 169
10.5 Two Photon Physics . . . 169
10.6 Fragmentation . . . 170
10.7 Searches . . . 171
10.8 Detector Instrumentation . . . 171

References **173**

Abstract

The impact of the ARGUS experiment to elementary particle physics is reviewed. More than 10 years of data taking has allowed ARGUS to contribute significantly to our understanding of beauty and charmed hadrons, τ leptons, Υ mesons, $\gamma\gamma$ interactions and fragmentation processes. In particular the ARGUS measurements of CKM matrix elements opened up a new window on the Standard Model.

Chapter 1

Introduction

The ARGUS detector at the e^+e^- storage ring DORIS II at DESY has taken data for more than one decade from 1982 to 1992. The experiment has been remarkably prolific and has contributed to our knowledge with many important discoveries, among which the first observation of $B^0\overline{B}^0$ mixing is the most significant [1]. So far, more than 150 papers have been published by the ARGUS collaboration. About half of all papers report on new observations while the other half deal with improvements of previous measurements or searches for new effects. The number of ARGUS PhD thesis amounts to more than 70 and nearly 100 diploma or master thesis have been submitted. In this report we summarize the input of ARGUS to the various fields of elementary particle physics.

The planning of the project goes back to the year 1977, when the c quark and the heavy lepton τ were well established and the b quark has just been discovered through the observation of the Υ mesons [2]. In October 1978 a proposal was submitted by 30 physicists from Germany, Sweden, USSR and USA to DESY to build "ARGUS - A New Detector for DORIS" [3]. In order to study the properties of hadrons containg a b quark, the double ring DORIS was first transformed into a single ring machine and then, in 1982, essentially rebuilt using the existing components. This new machine DORIS II reached a luminosity 20 times higher than before, delivering a maximum luminosity of 1.8 pb^{-1} per day [4], and was thus very competitive with the other existing e^+e^- storage rings. The excellent performance of DORIS II was a necessary condition for the success of the ARGUS experiment.

The ARGUS detector was designed as a universal 4π magnetic spectrometer to cover a wide research program. It detected and identified hadrons, leptons and photons with good momentum resolution and particle discrimination. Its design was based on the experience with previous e^+e^- detectors with the aim to reach better performance. The size of the detector was dictated by the structure of the beam focussing elements of DORIS II. The vertically focussing mini-β quadrupole of the storage ring was integrated into the detector. The huge horizontally focussing quadrupole had to stay outside and thus determined the longitudinal extension of the detector. The lateral dimensions of the detector were fixed by the design goal to reach a uniform detector performance over a more than 95% of the solid angle. This hermiticity of the detector was of great importance for many analyses and enabled ARGUS to detect neutrinos by missing energy and missing momentum measurements.

The ARGUS detector (Figure 1.1) and its performance has been described in detail elsewhere [5]. The detection of charged tracks was performed by two drift chambers. The inner one, the vertex drift chamber (5), worked with a pressurized gas and achieved a resolution of better than 25 μ m for the track coordinates and 40 μ m for the impact parameter. In 1991 a silicon counter system was introduced to the detector which improved the impact parameter resolution by more than a factor of 2. The main tracking device was a cylindrical drift chamber (4) which combined efficient pattern recognition, good spatial resolution and good particle identification by the measurement of

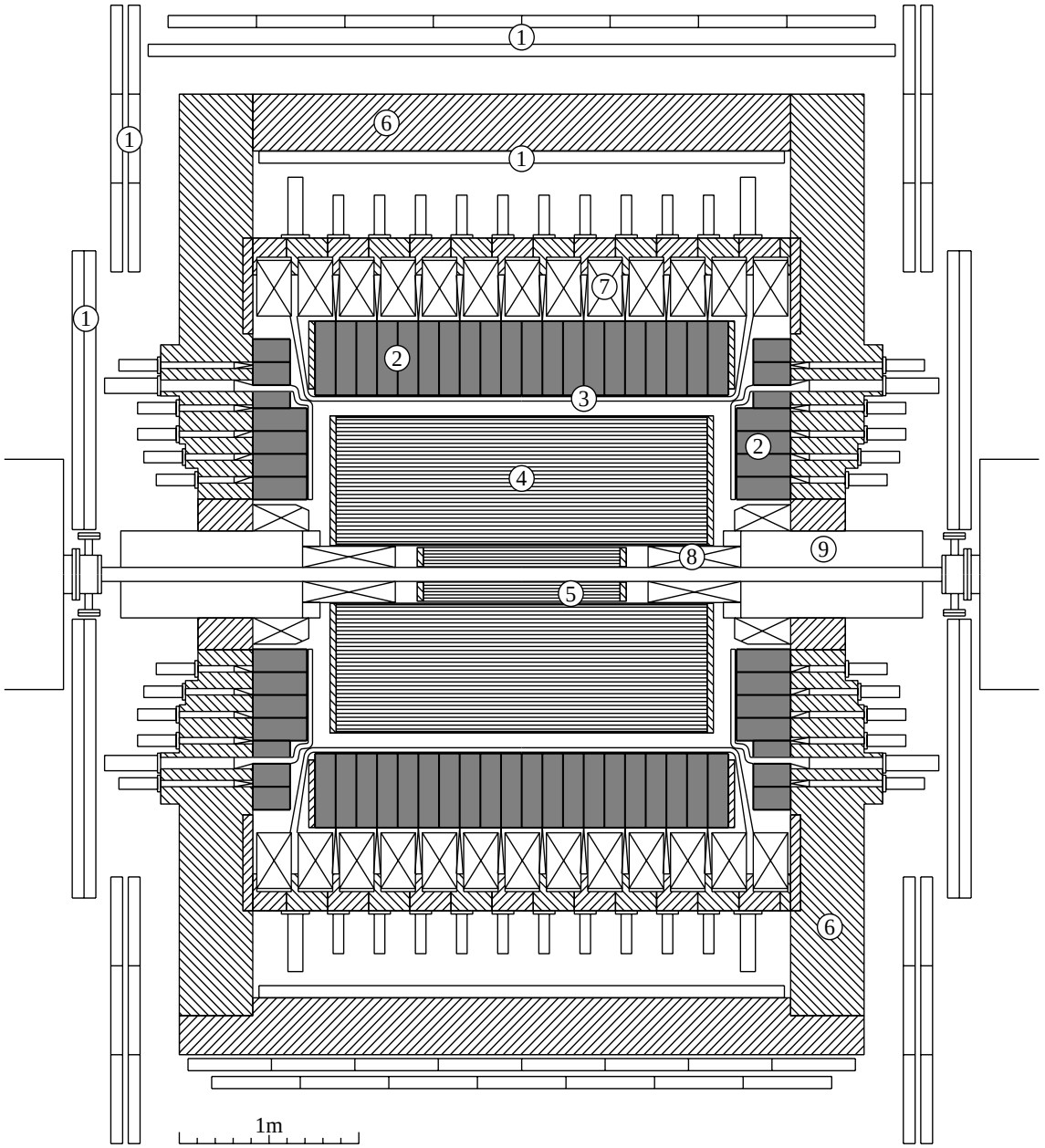

Figure 1.1: *The ARGUS Detector [3].*

1 Muon chambers
2 Shower counters
3 Time of flight counters
4 Driftchamber
5 Vertex chamber
6 Iron yoke
7 Solenoid coils
8 Compensation coils
9 Mini β quadrupole

the specific ionisation loss of charged particles. The outstanding feature of this chamber was the fact that none of the requirements for the optimizing one of these measurements led to compromizes reducing the quality of the other measurements. The drift chamber had 5940 drift cells with more than 30,000 wires in total in one gas volume. The chamber operated stably during the whole data taking period and no wires were even broken.

The particle identification was improved by the time-of-flight system (3) which surrounded the main drift chamber. The time-of-flight measurement allowed for charged particle separation of a quality similar to that obtained from the measurement of the specific ionisation loss. Both measurements were combined and led to a remarkably reliable and stable particle type assignment.

The magnetic field of the detector was chosen to be 0.8 Tesla which still could be achieved by a normal conducting copper coil (7). This choice was the result of an optimization between the demands of a high magnetic field for high momentum resolution and the one for a low magnetic field to avoid losses of low momentum particles spiraling into the beam tube.

For the detection of electrons as well as photons, a novel structure of an electromagnetic calorimeter (2) was invented. In earlier designs the calorimeter was placed behind the solenoid coils which caused a strong degradation of energy resolution and acceptance. In the ARGUS detector the calorimeter consisted of a lead-scintillator sandwich type with wavelength shifter readout. The wavelength shifter passed the solenoid through slits inbetween the individual coils. The light detection took place in the region free of field outside the solenoid where phototubes can operate. Thus the full intrinsic energy resolution of the calorimeter was maintained.

Finally, the detector is surrounded by a muon identification system (1). It consisted of proportional tube chambers behind the shower counters (2) and behind the iron yoke (7). These two components served as muon filters, and signals in the proportional tubes allowed a safe identification of muons.

For more than a decade of operation this detector worked very reliably with only little beam time loss due to detector malfunctions. An efficient monitoring of the detector and a safe data acquisition chain also caused only little deadtime.

An important feature of the ARGUS experiment was the sophisticated software. It not only allowed an efficient reconstruction of the events but also a very powerful analysis package was provided to dig out the physics of interest. This was possible by a newly developed analysis language "KAL" which made it possible to concentrate on the understanding of the physical processes. This piece of software complemented the excellent hardware of the ARGUS detector.

In the years 1980 to 1982 the detector was set up by a small collaboration of about 50 people from the following institutes:
DESY, Hamburg
University of Dortmund
University of Heidelberg
Institute of Particle Phyisics, Canada
University of Kansas
University of Lund
Institute of Theoretical and Experimental Physics, Moscow
University of South Carolina.

The collaboration grew during data taking to a group of 80-90 physicists and more institutions were involved:
Technical University Dresden
University of Erlangen-Nürnberg
University of Hamburg
Max-Planck-Institute of Heidelberg
University of Karlsruhe
University of Ljubljana.

The physics at an e^+e^- collider at center-of-mass energies around 10 GeV is potentially very rich.

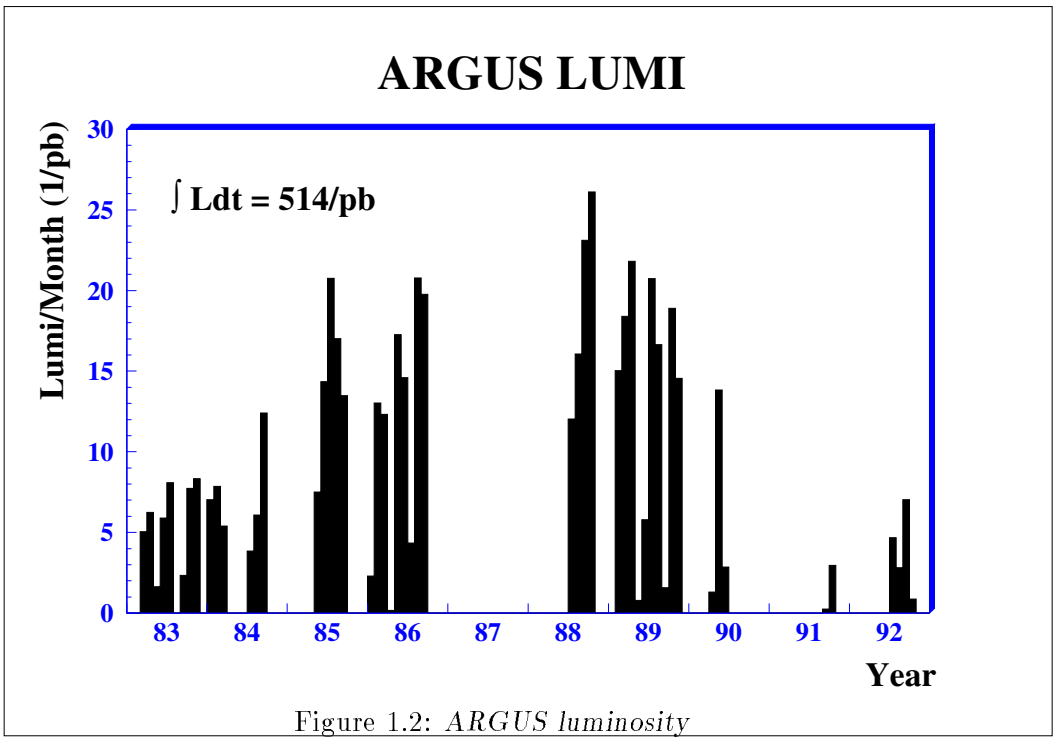

Figure 1.2: *ARGUS luminosity*

Table 1.1: *ARGUS data*

Event types	Number of events
Multihadrons/ Multileptons	3 250 000
$e^+e^- \rightarrow c\overline{c}$	600 000
$e^+e^- \rightarrow \tau^+\tau^-$	500 000
$e^+e^- \rightarrow \Upsilon(4S) \rightarrow B\overline{B}$	210 000
$e^+e^- \rightarrow \Upsilon(1S) \rightarrow hadrons$	400 000
$e^+e^- \rightarrow \Upsilon(2S) \rightarrow hadrons$	130 000

In particular, ARGUS was able to contribute substantially to the study of heavy flavours. A total integrated luminosity $\int Ldt = 514pb^{-1}$ was collected by ARGUS and more than 300 million triggers were accepted. The luminosity per month taken by ARGUS is shown in Figure 1.2 as a function of the running time. Large data samples (Table 1.1) were available for analysis of charmed and beauty hadrons, τ leptons, Υ mesons, $\gamma\gamma$ interactions and continuum processes.

The aim of this paper is to demonstrate the impact of the ARGUS experiment to different fields of elementary particle physics. Chapter 2 deals with the study of B mesons and contains the most important ARGUS results, the first observation of $B^0\overline{B}^0$mixing [1] in 1987, the first reconstruction of exclusive hadronic [6] and semileptonic [7] B decays in 1986 and 1987 and the beauty-to-up quark transition in 1990 [8]. These measurements opened up a sector of the CKM matrix which was not accessible before ARGUS. The observation of a large $B^0\overline{B}^0$mixing demonstrated that the mass of the top quark has to be large as was confirmed in 1995 [9]. The large $B^0\overline{B}^0$mixing implied that a measurement of CP violation in the neutral B system is feasible and therefore opened up a new window on the Standard Model. Projects for the measurement on CP violation in the neutral B system are under way [10, 11, 12]. In Chapter 3 the ARGUS results on charmed hadrons are summarized. They comprise the first observation of an excited charmed meson in 1985 [13] as well as the discovery of the first excited charmed baryon in 1993 [14]. The most important contribution to

our knowledge of weak decays of charmed particles was the first observation of the decay $D^0 \to \phi \overline{K}^0$ [1] [15] which is strongly suppressed in a pure spectator model but was measured by ARGUS as large as 1%. This large value still waits for a convincing explanation. The analysis of the large sample of τ leptons described in chapter 4 led to the determination of basic properties of the τ and its neutrino. The mass of the τ and a limit on the mass of the ν_τ have been measured. The space-time structure of τ decays was investigated for the first time in detail and led to the first observation of parity violation in τ decays as well as the determination of four Michel parameters. In chapter 5 the ARGUS results on bottomonium spectroscopy are presented. The study of the fragmentation of quarks and gluons by ARGUS is the content of chapter 6. ARGUS made also substantial contribution to two photon physics by observing most of the vector-vector final states as demonstrated in chapter 7.

Finally, the impact of ARGUS on particle physics is demonstrated by a summary of the ARGUS highlights.

[1] Unless otherwise stated references in this paper to a specific charged state are to be interpreted as implying the charge-conjugate state as well.

Chapter 2

B Physics

2.1 Introduction

The b quark was proposed together with the t quark by Kobayashi and Maskawa in 1973 [16] who introduced a six-quark model with three families, consisting of quark doublets, in order to get a description for the observed CP violation in K meson decays:

$$\begin{array}{l} Q = +\frac{2}{3} \\ Q = -\frac{1}{3} \end{array} \quad \left(\begin{array}{c} u \\ d \end{array} \right) \left(\begin{array}{c} c \\ s \end{array} \right) \left(\begin{array}{c} t \\ b \end{array} \right).$$

The existence of these two heavy quarks was experimentally established at Fermilab, the b quark through the discovery of the Υ bound states in 1977 [2] and the t quark in 1995 [9]. While the t quark decays very fast, the b quark lives sufficiently long to form B hadrons with lighter quarks. Through the decay of these B hadrons the main features of b quark decays have been most extensively investigated at e^+e^- machines. In particular, the results from machines near threshold for open beauty production, CESR at Cornell and DORIS II at DESY, improved our knowledge considerably. The ARGUS results are based on a sample of 209,000$\pm$ 10,000 pairs of B mesons collected at DORIS II.

In the Standard Model of particle physics the weak eigenstates of the quarks are mixtures of the mass eigenstates. The rotation of (d, s, b) mass eigenstates into weak eigenstates (d', s', b') is given by the CKM matrix V_{CKM}:

$$V_{CKM} = \left(\begin{array}{ccc} V_{ud} & V_{us} & V_{ub} \\ V_{cd} & V_{cs} & V_{cb} \\ V_{td} & V_{ts} & V_{tb} \end{array} \right)$$

$$\left(\begin{array}{c} d' \\ s' \\ b' \end{array} \right) = \left(\begin{array}{ccc} V_{ud} & V_{us} & V_{ub} \\ V_{cd} & V_{cs} & V_{cb} \\ V_{td} & V_{ts} & V_{tb} \end{array} \right) \left(\begin{array}{c} d \\ s \\ b \end{array} \right).$$

In the Standard Model the CKM matrix is introduced in the Lagrangian which describes the interaction of the fermions with the Higgs field. This description provides a connection between the pattern of fermion masses and the CKM matrix elements which, however, is not explicitly known. Specific approaches to this connection can be tested and could give insight into the mechanism which attributes mass to the particles.

The CKM matrix elements describe for three quark families the nine $|\Delta Q| = 1$ transitions between the six quarks. The CKM matrix is unitary and, for three quark families, given by three Euler angles θ_{12}, θ_{23} and θ_{13} and one phase δ_{13} which allows for complex matrix elements. In the Standard Model

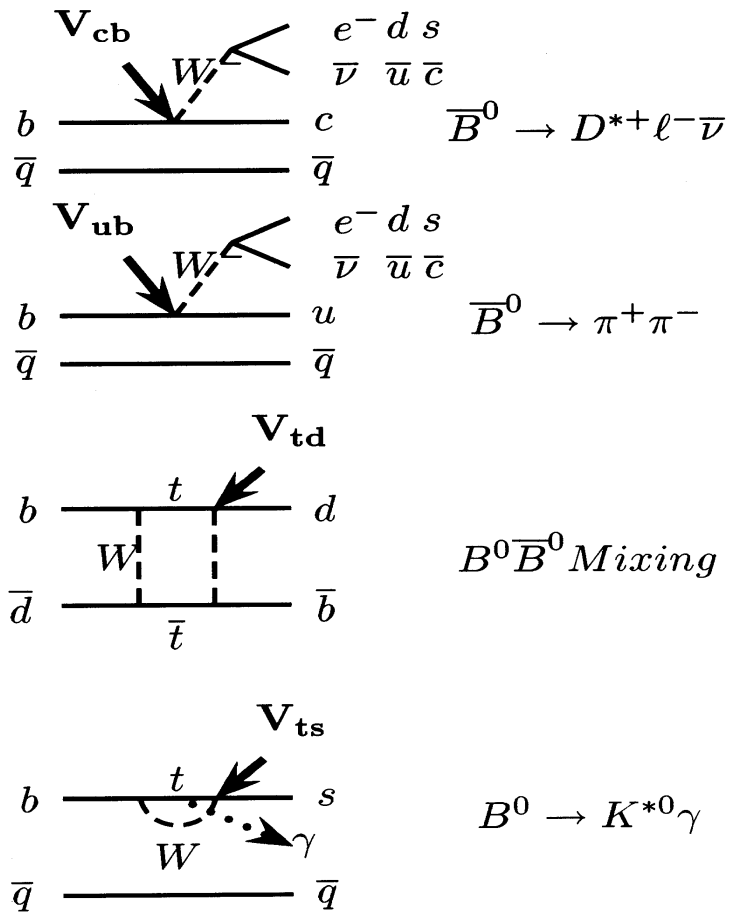

Figure 2.1: *Measurements of CKM matrix elements*

this phase $\delta_{13} \neq (0, \pi)$ is responsible for CP violation. The "standard" parametrization yields [17]:

$$V_{CKM} = \begin{pmatrix} c_{12}c_{13} & s_{12}c_{13} & s_{13}e^{-i\delta_{13}} \\ -s_{12}c_{23} - c_{12}s_{23}s_{13}e^{i\delta_{13}} & c_{12}c_{23} - s_{12}s_{23}s_{13}e^{i\delta_{13}} & s_{23}c_{13} \\ s_{12}s_{23} - c_{12}c_{23}s_{13}e^{i\delta_{13}} & -c_{12}s_{23} - s_{12}c_{23}s_{13}e^{i\delta_{13}} & c_{23}c_{13} \end{pmatrix}.$$

Here $c_{ij} = cos\theta_{ij}$ and $s_{ij} = sin\theta_{ij}$ where i, j are the 'family' labels ($i, j = 1, 2, 3$). These mixing angles and the phase are fundamental parameters of the Standard Model and cannot be predicted within the frame of the Standard Model but have to be determined experimentally through measurements of the CKM matrix elements. The four elements involving the u, d, s and c quarks were already well determined experimentally before b quark studies began. These matrix elements are mainly sensitive to the mixing angle between the first and the second family θ_{12}, the Cabibbo angle. The only way to measure the mixing angles between the second and third family, θ_{23}, and first and third family, θ_{13}, as well as the phase δ_{13} is through B decays. $|V_{cb}|$ and $|V_{ub}|$ are measured through the detection of direct B decays into lighter particles whereas the matrix elements $|V_{td}|$ and $|V_{ts}|$ can be obtained from investigations of B decays involving virtual transitions. Figure 2.1 shows some examples.

The measurement of the CKM matrix elements allows to test the Standard Model and to fix its parameters. The unitarity of the CKM matrix can be tested by determining all matrix elements precisely in independent measurements. The nine matrix elements are deduced from only four real parameters of the the Standard Model leading to a strongly overconstrained measurement. A

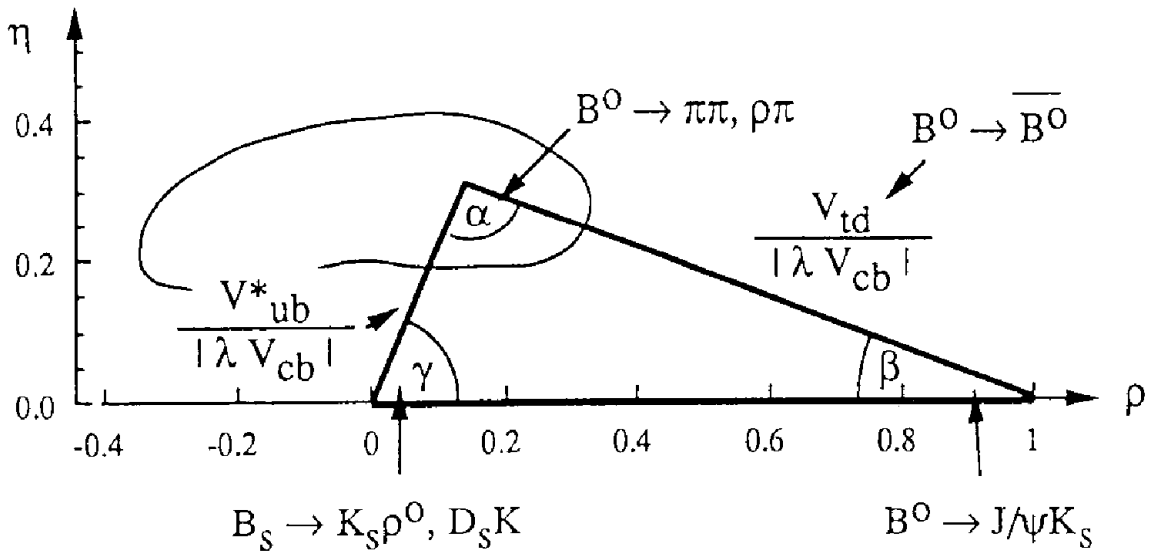

Figure 2.2: *Description of the unitarity triangle (see text).*

breakdown of the unitarity of the CKM matrix is an indication for a fourth quark family or physics beyond the Standard Model.

Probably the most important feature of the CKM matrix is the fact that it provides a description for CP violation through the existence of a non-trivial phase δ_{13}. The unitarity conditions

$$\sum_j V_{ij} V_{kj}^* = \sum_j V_{ji}^* V_{jk} = \delta_{ik}$$

lead to the so-called unitarity triangles in the complex plane of which the most familiar is:

$$c_{13} V_{td} + c_{12} c_{23} c_{13} V_{ub}^* = s_{12} V_{cb}.$$

This relation is visualized in Figure 2.2 using the Wolfenstein parameters $\lambda = sin\theta_{12}, A = sin\theta_{23}/\lambda^2, \rho = (sin\theta_{13} \cdot cos\delta_{13})/(A \cdot \lambda^3)$ and $\eta = (sin\theta_{13} \cdot sin\delta_{13})/(A \cdot \lambda^3)$. The area of this triangle is a measure of the strength of CP violation in B decays. Measurements of the quantities depicted in Figure 2.1 allow the determination of $|V_{cb}|, |V_{ub}|$ and $|V_{td}|$ and thus the lengths of the sides of the triangle. This was the task of ARGUS. A different approach to testing the Standard Model predictions is to determine the angles of the triangle by measuring CP violation in B decays. The possible decays associated with the different angles are depicted in Figure 2.2. The measurement of the angles is the main goal of several experiments presently under construction: the HERA-B experiment at DESY and the B-factories BABAR and BELLE [10, 11, 12].

Another aspect of B physics is that certain processes such as flavour oscillations or radiative B decays, which are induced by loop diagrams involving virtual particles, are sensitive to new physics at much higher energy scales. An example is $B^0\overline{B}^0$mixing which is sensitive to the mass of the top quark. The measurement of the $B^0\overline{B}^0$oscillation frequency allowed an estimate on the mass of the top quark eight years before it was actually discovered.

The study of B hadrons was particularly important for the development of a theory which is able to describe weak decays of heavy quarks in the presence of other strongly bound quarks. The b quark is the heaviest quark bound in a hadron, and its large mass simplifies the theoretical analysis. Early attempts tried to explain decay properties of B mesons using form factor models [18]. In the last few years a better understanding of B decays has been achieved with the development of the

Heavy Quark Effective Theory (HQET) [19] and the Heavy Quark Expansion(HQE)[20]. ARGUS has been particularly influential in the development of the HQET by analysing in detail and for the first time exclusive semileptonic B decays.

The simplest weak Hamiltonian, neglecting QCD effects, for the first diagram in Figure 2.1 for the decay $W^- \to \overline{c}s$ is given by

$$H^0_{eff} = \frac{G_F}{\sqrt{2}} V_{cb} V^*_{cs} (\overline{c}b)_{V-A} (\overline{s}c)_{V-A} \tag{2.1}$$

where G_F is the Fermi constant and

$$(\overline{c}b)_{V-A} (\overline{s}c)_{V-A} \equiv (\overline{c}\gamma_\mu (1-\gamma_5) b)(\overline{s}\gamma_\mu (1-\gamma_5) c) = Q_2 \tag{2.2}$$

is the weak current-current operator denoted as Q_2. The presence of additional quarks and interactions complicates the situation and gives rise to several operators Q_i:

$$H_{eff} = \frac{G_F}{\sqrt{2}} V_{CKM} \sum_i C_i(\mu) Q_i \tag{2.3}$$

where $C_i(\mu)$ are the Wilson coefficients which are calculable, μ represents the ordinary hadronic energy scale ($\mu < 1\ GeV$) and Q_i are the operators generated by QCD and the electroweak interaction.

The treatment of this complicated Hamiltonian became more transparent through the observation that, for very heavy quarks Q, the properties of heavy hadrons are independent its spin and flavour [19]. The statement 'large mass of the heavy quark Q' was turned into a systematic expansion in powers of μ/m_Q. As an example, the width for a decay $B \to f$ is obtained from an expansion in powers of μ/m_b. Since the b quark is heavy the expansion converges quickly. In case of infinite quark masses only the weak part of the decay rate survives together with perturbative QCD corrections since the non-perturbative parts of the decay rate scale with powers $n \geq 2$ in μ/m_b [20]. The improved understanding of systems containing heavy quarks in general, and B mesons in particular, is significant for the extraction of the CKM matrix element from the experimental data.

For the ARGUS experiment, the source for the lightest B mesons and their antiparticles is the $\Upsilon(4S)$ meson which is produced in e^+e^- annihilation

$$e^+e^- \to \Upsilon(4S) \to B^0\overline{B}^0 \text{or } B^+B^- .$$

The peak cross section for the formation of the $\Upsilon(4S)$ at DORIS II is : $\sigma(e^+e^- \to \Upsilon(4S)) = (0.99 \pm 0.05)$ nb (Figure 2.3) [21, 22]. The continuum cross section at $\Upsilon(4S)$ energies amounts to $\sigma(e^+e^- \to q\overline{q}) = (2.5 \pm 0.2)$ nb with $q = u, d, s, c$. For inclusive distributions of B decays measured at the $\Upsilon(4S)$ resonance, the continuum contribution has to be subtracted. This contribution is determined from data taken in the continuum at energies below the $\Upsilon(4S)$ resonance. A total of $\int Ldt = 246$ pb^{-1} was accumulated on the $\Upsilon(4S)$ resonance and $\int Ldt = 112$ pb^{-1} at energies below the $\Upsilon(4S)$ mass in the e^+e^- continuum. Throughout this paper we shall assume that the $\Upsilon(4S)$ meson decays 100% of the time into $B^0\overline{B}^0$or B^+B^- pairs with no additional particles. In fact, no evidence for other decay modes of the $\Upsilon(4S)$ has been observed.

2.2 Exclusive Hadronic Decays

The reconstruction of exclusive B meson decays has provided both a direct proof of their existence and valuable information about their properties. The masses of neutral and charged B's are most accurately determined in exclusive studies. The mass splitting between B^0 and B^+ is interesting for studying quark bindings and is, in particular, an important ingredient for estimating the ratio of branching ratios

$$\frac{\Upsilon(4S) \to B^+B^-}{\Upsilon(4S) \to B^0\overline{B}^0}$$

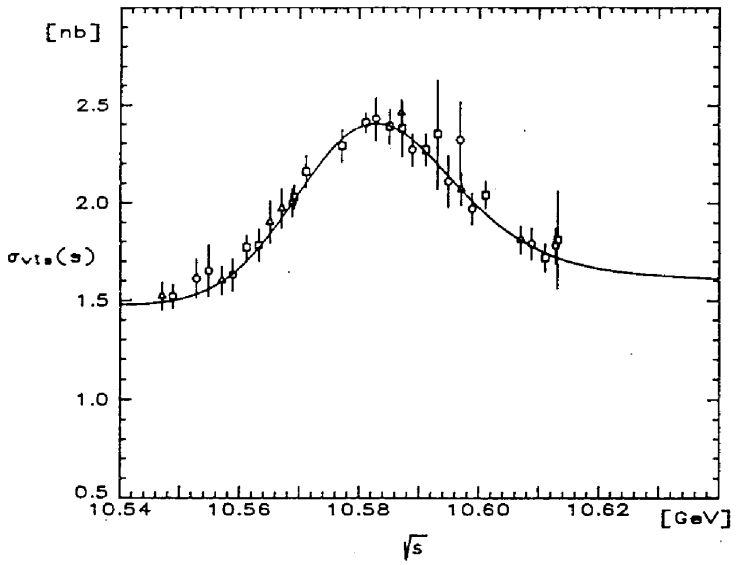

Figure 2.3: $\Upsilon(4S)$ *resonance cross section [21, 22]*

which is, in turn, the basis for determining absolute branching ratios of B mesons produced at the $\Upsilon(4S)$. The spin of the B mesons can be determined from the characteristic distribution in the production angle in e^+e^- annihilations at the $\Upsilon(4S)$ resonance.

Measurements of exclusive B meson decay rates test theoretical models of weak decays of heavy quarks. Due to the large mass of the b quark, the influence of the strong interaction can be calculated more reliably than for the decays of lighter mesons. A sample of tagged B mesons with known charge and b-flavour allows one to study the decay of the other b quark in the event with reduced systematic uncertainties. Exclusive reconstruction of B mesons without charmed particles in the final state yields a measurement for the strength of $|V_{ub}|$. Decays of $\Upsilon(4S)$ mesons constitute an ideal testing ground for studying the properties of B^+ and B^0 mesons since other b hadrons (B_s, beauty baryons, *etc.*) cannot be produced due to their high masses.

In exclusive analyses of B mesons produced in $\Upsilon(4S)$ decays, one can exploit the fact that the two B's are the only decay particles. Thus, all final state particles can be, at least in principle, attributed to one of the two B mesons. Due to the two-particle kinematics, the energy of the B's is given by the beam energy, E_{beam}, which is known *a priori* with high precision. This precision depends on the energy resolution of e^+e^- storage rings and on the width of the $\Upsilon(4S)$ resonance. In the case of the DORIS storage ring, this corresponds to an energy resolution of 4 MeV, about one order of magnitude better than the resolution of the energy derived from the measured momenta of the reconstructed final state particles. The masses m_B of the B mesons are determined from an energy constrained fit using this information

$$m_B^2 = E_{beam}^2 - |\sum_i \vec{p_i}|^2$$

where $\vec{p_i}$ are the momenta of the particles used in the reconstruction.

The mass of the $\Upsilon(4S)$ turns out to be only slightly larger than two times the mass of B^+ and B^0 mesons. Thus, the momenta of the B mesons in $\Upsilon(4S)$ decays are small, about 330 MeV/c with some uncertainty due to the energy resolution of 4 MeV mentioned above. This small momentum is of enormous advantage for the study of exclusive semileptonic decays where it can often be neglected,

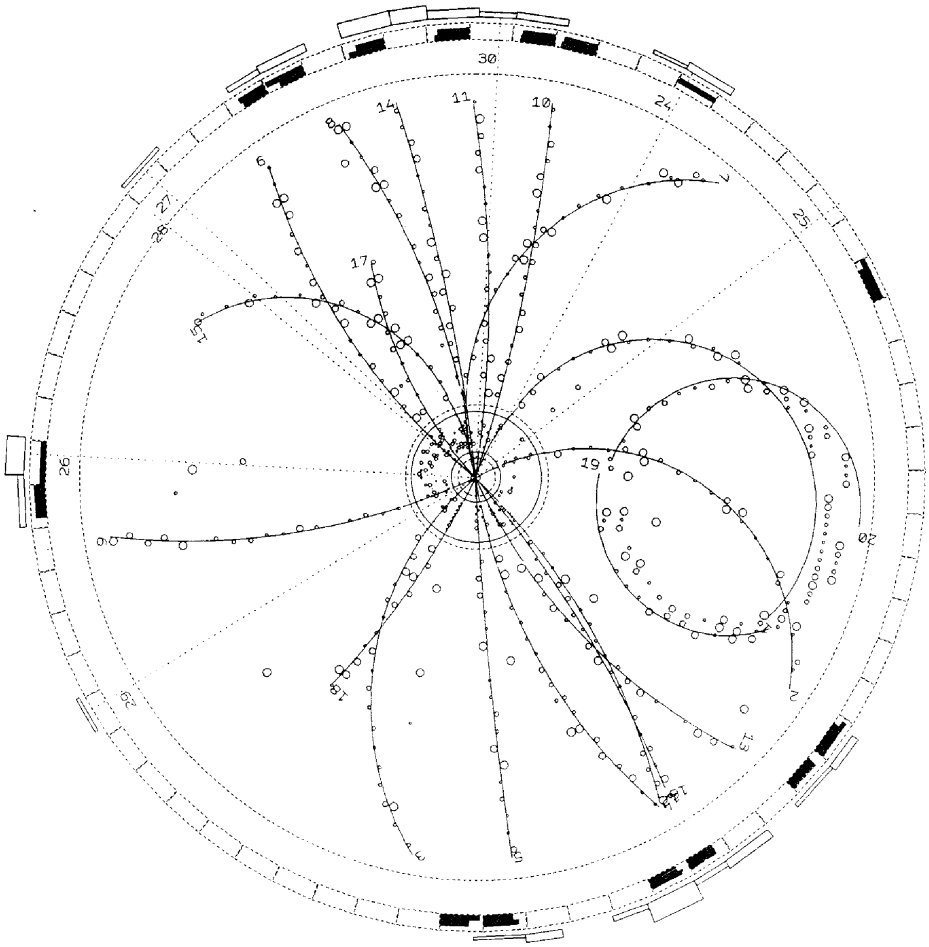

Figure 2.4: *View of a fully reconstructed* $\Upsilon(4S) \rightarrow B^- B^+$ *decay along the beam axis (see text)*

thus allowing for a "pseudo"-exclusive reconstruction in spite of the unobserved neutrino in the final state.

The small value of the B momentum in $\Upsilon(4S)$ decays implies that the B mesons have only a small velocity of $\beta\gamma \approx 0.06$. This leads to the consequence that the decay particles of both B mesons are completely mixed up in space; they don't show the back-to-back behavior observed in LEP data. The topology of $\Upsilon(4S)$ decays may be visualized by one fully reconstructed event $\Upsilon(4S) \rightarrow B^- B^+$ with $B^- \rightarrow D^{*+}\pi^-\pi^-$, $D^{*+} \rightarrow D^0\pi^+$, $D^0 \rightarrow K^-\pi^+\pi^+\pi^-$ given by the charged tracks 5,6,8,11,12,14 and 15 and $B^+ \rightarrow \overline{D}^0 5\pi^+ 5\pi^- 3\pi^0$, $\overline{D}^0 \rightarrow K^+\pi^-\pi^0$ (Figure 2.4).

Problems due to combinatorial background for exclusive reconstruction of hadronic B decays are large; this limits the maximum decay multiplicity which can be exclusively reconstructed. However, the fact that $\Upsilon(4S)$ decays have a spherical event topology can be exploited for suppressing background from non-resonant continuum events with a more jet-like event shape.

2.2.1 Reconstruction of exclusive B Decays into Mesons with Charm

Since b quarks decay mainly into c quarks (section 2.3.1), B mesons predominatly decay into final states containing charmed mesons. Since the B decay multiplicity is high (section 2.3) only a few decay chains can be used to efficiently suppress the combinatorial background in the absence of precise vertex detectors. A severe limitation in the reconstruction of B mesons is given by the existence of π^0 mesons in the final state which suffer from large combinatorial backgrounds; therefore the ARGUS B reconstruction allowed for at most two π^0 candidates in the decay chain.

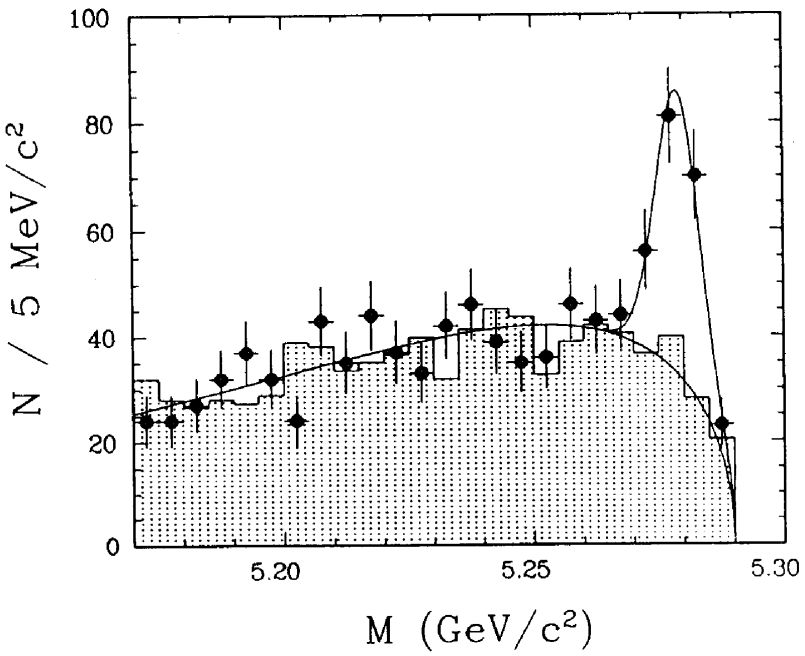

Figure 2.5: *Mass distributions for B candidates in the decay channels $D^{*+}n\pi(n \leq 3)$ [25]. The hatched area shows the same spectrum for wrong-charge combinations.*

The decay channels providing the cleanest reconstruction of B mesons are those with a J/ψ in the final state. Historically, however, the first successful attempts to reconstruct B mesons were based on the channels $B \to Dn\pi$ and $B \to D^*n\pi$ for which the largest branching fractions were expected. Moreover, decays containing a $D^{*\pm}$ provide a relatively clean signature: the channel $D^{*+} \to D\pi^+$ has a favourable signal-to-background ratio due to the small Q-value of this decay (see chapter 3.2).

A first claim of the reconstruction of B mesons was made in 1983 by the CLEO collaboration [23] which observed an enhancement of 18 events at masses close to the beam energy. This enhancement was attributed to exclusive B decays. The mass determined agreed within 2σ with the present value [17]. However, the size of the reported enhancement was far too large to result from exclusive reconstruction of B mesons and is in strong disagreement with present knowledge of B-, D^*-, and D branching fractions.

The first successful reconstruction of B mesons was reported by ARGUS in 1986 [6]. Five decay channels of charged and neutral B mesons decaying into a D^{*+} meson and up to three pions were observed. Statistical and systematical uncertainties on branching fractions were still very large but within these errors the reported values agree with our present knowledge [17] and have been confirmed by CLEO [24]. A later ARGUS publication [25] based on higher statistics contains more decay channels, including those with a J/ψ in the final state. The mass distributions of reconstructed B candidates are shown in Figure 2.5 and 2.6 for all decay channels containing a D^* and for clean decay channels, respectively. The fitted mass values, obtained by fixing the mass of the $\Upsilon(4S)$ to 10580 MeV/c^2, are given in Table 2.1. Within less than 1 MeV the masses of the charged and neutral B mesons agree. This, and the fact that no evidence for other decay modes has been seen, justifies the assumption that the $\Upsilon(4S)$ meson decays with equal probability into the B^+B^- and $B^0\overline{B}^0$final states. This fraction is used for the determination of branching ratios of the charged and neutral B mesons.

The spin J_B of the B mesons can be inferred from the distribution of the production angle θ, defined as the angle of the B with respect to the beam axis. Since the $\Upsilon(4S)$ with $J^P = 1^-$ is formed transversely polarized in e^+e^- annihilation, one expects a $\sin^2\theta$ distribution for $J_B = 0$ mesons. The distribution in $|\cos\theta|$ for B meson candidates, first observed by ARGUS, is in agreement with a $J_B = 0$ assignment (Figure 2.7; [25]).

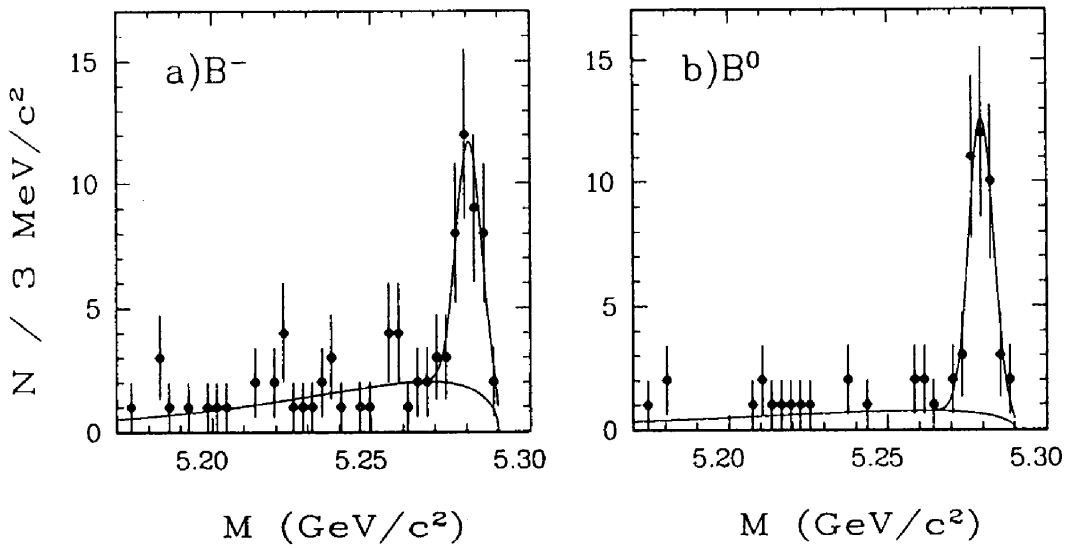

Figure 2.6: *Mass distributions for B candidates in clean two-body channels [25]:* **(a)** B^- *candidates from the channels* $B^- \to D^0\pi^-$, $D^{*0}\pi^-$, $D_J^{(*)0}\pi^-$, $J/\psi(K^-, K^{*-})$, *and* $\psi' K^-$; **(b)** $\overline{B}^0$ *candidates from the channels* $D^+\pi^-$, $D^{*+}\pi^-$, *and* $J/\psi(K_s^0, K^{*0})$

Table 2.1: *Masses of B mesons (MeV)*

	ARGUS [25]	CLEO 1.5 [26]	CLEO II [27]
$M(B^+)$	$5280.5 \pm 1.0 \pm 2.0$	$5278.3 \pm 0.4 \pm 2.0$	$5278.8 \pm 0.54 \pm 2.0$
$M(B^0)$	$5279.6 \pm 1.0 \pm 2.0$	$5278.0 \pm 0.4 \pm 2.0$	$5279.2 \pm 0.54 \pm 2.0$
ΔM	$-0.9 \pm 1.2 \pm 0.5$	$-0.4 \pm 0.6 \pm 0.5$	$0.41 \pm 0.25 \pm 0.19$

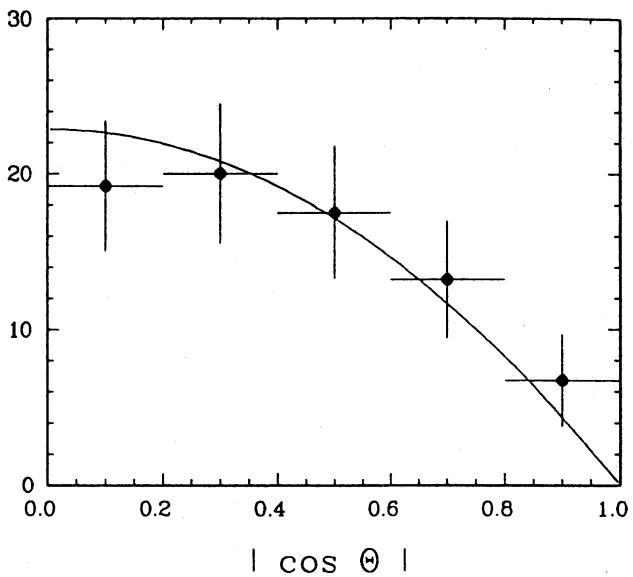

Figure 2.7: $|\cos\theta|$ *distribution for B mesons [25]. The curve is a fit using a* $\sin^2\theta$ *distribution.*

Table 2.2: *Branching ratios for decays* $B \to D^{(*)} n \cdot \pi$ *(%)*

Decay Mode	ARGUS [25]	CLEO 1.5 [26]	CLEO II [27]
$B^- \to D^0\pi^-$	$0.21 \pm 0.09 \pm 0.06$	$0.48 \pm 0.08 \pm 0.05$	$0.55 \pm 0.04 \pm 0.05 \pm 0.02$
$B^- \to D^0\rho^-$	$1.3 \pm 0.4 \pm 0.4$		$1.35 \pm 0.12 \pm 0.04$
$B^- \to D^{*0}\pi^-$	$0.38 \pm 0.14 \pm 0.12$	$0.94 \pm 0.23 \pm 0.19$	$0.52 \pm 0.07 \pm 0.06 \pm 0.04$
$B^- \to D^{*0}\rho^-$	$1.0 \pm 0.5 \pm 0.4$		$1.68 \pm 0.21 \pm 0.25 \pm 0.12$
$B^- \to D^{*+}\pi^-\pi^-$	$0.21 \pm 0.13 \pm 0.06$		$0.19 \pm 0.07 \pm 0.03 \pm 0.01$
$\overline{B}^0 \to D^+\pi^-$	$0.49 \pm 0.11 \pm 0.11$	$0.24 \pm 0.06 \pm 0.04$	$0.29 \pm 0.04 \pm 0.03 \pm 0.05$
$\overline{B}^0 \to D^+\rho^-$	$0.9 \pm 0.5 \pm 0.3$		$0.81 \pm 0.11 \pm 0.12 \pm 0.13$
$\overline{B}^0 \to D^{*+}\pi^-$	$0.23 \pm 0.08 \pm 0.04$	$0.47 \pm 0.12 \pm 0.06$	$0.26 \pm 0.03 \pm 0.04 \pm 0.01$
$\overline{B}^0 \to D^{*+}\rho^-$	$0.6 \pm 0.3 \pm 0.3$	$2.2 \pm 0.9 \pm 1.3$	$0.74 \pm 0.10 \pm 0.14 \pm 0.03$
$\overline{B}^0 \to D^+\pi^-\pi^-\pi^+$	$1.0 \pm 0.3 \pm 0.4$	$1.37 \pm 0.24 \pm 0.27$	$0.63 \pm 0.10 \pm 0.03 \pm 0.11 \pm 0.02$

Table 2.3: *Branching ratios for decays* $B \to J/\psi/\chi_c K^*$ *(%)*

Decay Mode	ARGUS [25]	CLEO 1.5 [26]	CLEO II [27]
$B^- \to J/\psi K^-$	$0.08 \pm 0.03 \pm 0.01$	$0.10 \pm 0.02 \pm 0.02$	$0.110 \pm 0.015 \pm 0.009$
$B^- \to J/\psi K^{*-}$	$0.18 \pm 0.12 \pm 0.03$	$0.15 \pm 0.11 \pm 0.04$	$0.178 \pm 0.051 \pm 0.023$
$B^- \to \chi_{c1} K^-$	$0.19 \pm 0.13 \pm 0.06$		$0.097 \pm 0.040 \pm 0.009$
$\overline{B}^0 \to J/\psi \overline{K}^0$	$0.09 \pm 0.07 \pm 0.02$	$0.07 \pm 0.04 \pm 0.02$	$0.075 \pm 0.024 \pm 0.008$
$\overline{B}^0 \to J/\psi \overline{K}^{*0}$	$0.13 \pm 0.06 \pm 0.02$	$0.13 \pm 0.06 \pm 0.03$	$0.169 \pm 0.031 \pm 0.018$

A comparison of branching ratios measured by CLEO and ARGUS is given in Tables 2.2 and 2.3. The ARGUS results indicate that for two-body decays where the four-momentum squared of the off-shell W^- is small, *i.e.* corresponds to the mass of a π or ρ, the rate of D and D^* production is very similar. This is in marked contrast to inclusive D and D^* productions where approximately 75 % of the inclusive D-mesons originate from D^* decays (section 2.3). The other vector-to-pseudoscalar ratios

$$\mathrm{BR}(B \to D\rho)/\mathrm{BR}(B \to D\pi) = 3.2 \pm 1.2,$$

$$\mathrm{BR}(B \to D^*\rho)/\mathrm{BR}(B \to D^*\pi) = 2.5 \pm 1.2,$$

show that there is a significant enhancement of ρ over π production. These results are compatible with the Heavy Quark Effective Theory (HQET) which predicts, in the heavy quark limit, due to the spin symmetry [29]:

$$\mathrm{BR}(B \to D\pi^-(\rho^-))/\mathrm{BR}(B \to D^*\pi^-(\rho^-)) = 1.0$$

and

$$\mathrm{BR}(B \to D^*\rho^-)/\mathrm{BR}(B \to D^*\pi^-) = 2.8$$

Exclusive B decays can be used to study various topics. The two-body are decays allow one to test theoretical models of weak decays. The exclusive B meson decays into final states containing D_s mesons are of particular interest since the weak decay constant of the D_s, f_{D_s}, can be derived. The B decays involving J/ψ, $\psi\prime$, and χ_c mesons in the final state are of importance for future measurements of CP violation.

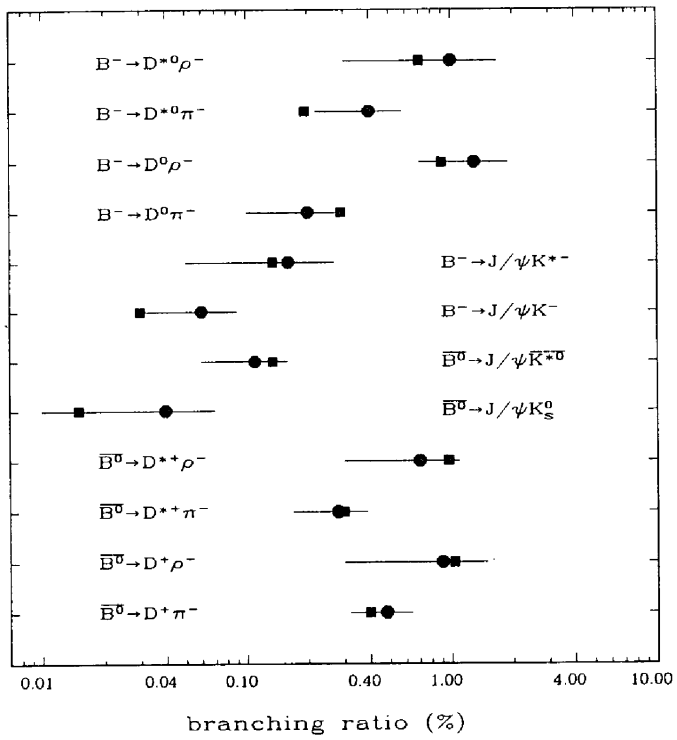

Figure 2.8: *Comparison between the experimentally measured branching ratios (points with combined statistical and systematic errors; [25]) and the prediction of Bauer, Stech, and Wirbel [18] with* $a_1 = 1.03$ *and* $a_2 = -0.20$ *(squares)*

One model supplying predictions for a list of some exclusive two-body B meson decays is that due to Bauer, Stech, and Wirbel [18]. Decays are grouped into three classes described by parameters a_1, a_2, or a combination of both. The parameter a_1 is associated with the external spectator diagram (Figure 2.1, top), and a_2 represents with internal spectator diagram where the c quark forms a hadron with the $\overline{u}$ quark from the W^- decay. This results from first order QCD corrections to the weak hamiltonian (Equation 2.1). The effect of a first order QCD correction can be shown by a Fierz transformation to be equivalent to renormalizing the strength of the existing weak operator and adding a term which appears as a neutral current:

$$H_{eff}^{QCD} = \frac{G_F}{\sqrt{2}} V_{cb} V_{ud}^* \left[c_1 (\overline{c}b)(\overline{d}u) + c_2 (\overline{c}u)(\overline{d}b) \right] . \tag{2.4}$$

The scale-dependent coefficients depend on the b mass scale and are predicted to $c_1 \approx 1.1$ and $c_2 \approx -0.24$. The phenomenological approach [18] assumes that factorization and subsequent replacement of quark currents by hadron currents can be used:

$$H_{eff}^{had} = \frac{G_F}{\sqrt{2}} V_{cb} V_{ud}^* \left[a_1 (\overline{c}b)_H (\overline{d}u)_H + a_2 (\overline{c}u)_H (\overline{d}b)_H \right] . \tag{2.5}$$

Fitting the parameters a_1 and a_2 to the measured branching ratios, one obtains two possible solutions given in Table 2.4. A comparison between data and the first solution is shown in Figure 2.8.

The weak decay constant of the D_s, f_{D_s}, can be derived from $B \to D_s^{(*)-} D^{(*)0,+}$ assuming that factorization holds in these decays. In this case the decay rate is proportional to $f_{D_s}^2$. By comparing the measured branching ratios to the above mentioned theoretical models f_{D_s} can be deduced. The decay constant is a measure of the probability that both constituent quarks of the meson annihilate

Table 2.4: *Parameters a_1 and a_2 of the model of Bauer, Stech, and Wirbel*

a_1	a_2	χ^2/DoF	prob
1.03 ± 0.09	-0.20 ± 0.03	6.5/10	77 %
0.87 ± 0.08	0.19 ± 0.03	9.2/10	51 %

Table 2.5: *Branching ratios for decays $B \to D_s^{(*)} D^{(*)}$ (%)*

Decay Mode	ARGUS [30]	CLEO 1.5 [26]	CLEO II [28]
$B^- \to \overline{D}^0 D_s^-$	$1.8 \pm 0.9 \pm 0.4$	$1.8 \pm 0.8 \pm 0.8$	$1.18 \pm 0.21 \pm 0.24 \pm 0.22$
$B^- \to \overline{D}^0 D_s^{*-}$	$1.2 \pm 0.9 \pm 0.2$		$0.84 \pm 0.26 \pm 0.16 \pm 0.20$
$B^- \to \overline{D}^{*0} D_s^-$	$0.8 \pm 0.5 \pm 0.2$		$1.35 \pm 0.41 \pm 0.33 \pm 0.32$
$B^- \to \overline{D}^{*0} D_s^{*-}$	$1.8 \pm 1.0 \pm 0.3$		$3.00 \pm 0.85 \pm 0.62 \pm 0.72$
$\overline{B}^0 \to D^+ D_s^-$	$1.1 \pm 0.9 \pm 0.4$	$0.7 \pm 0.4 \pm 0.4$	$0.87 \pm 0.24 \pm 0.20 \pm 0.21$
$\overline{B}^0 \to D^+ D_s^{*-}$	$1.8 \pm 1.1 \pm 0.6$		$1.01 \pm 0.35 \pm 0.22 \pm 0.24$
$\overline{B}^0 \to D^{*+} D_s^-$	$0.8 \pm 0.5 \pm 0.2$	$1.4 \pm 0.8 \pm 0.3$	$0.90 \pm 0.22 \pm 0.16 \pm 0.22$
$\overline{B}^0 \to D^{*+} D_s^{*-}$	$1.5 \pm 0.8 \pm 0.3$		$1.96 \pm 0.48 \pm 0.35 \pm 0.47$

to form a virtual W-boson. Knowledge of the decay constant is essential for the extraction of fundamental CKM parameters from the measurement of weak decays, including $B - \overline{B}$ mixing.

Exclusive B meson decays into D_s have been reconstructed in eight decay channels $B^{-,0} \to D_s^{(*)-} D^{(*)0,+}$ where $D^{(*)}$ stands for D or D^* [30]. A large number of decay channels (*e.g.* 8 for the D_s, 4 for the D^0, and 3 for the D^+) have been taken into account in order to compensate for the small indiviual branching ratios. The mass distribution of the B meson candidates is shown in Figure 2.9; the branching rates are given in Table 2.5 where the branching ratio $\mathrm{BR}(D_s \to \phi\pi)$ is assumed to be 3.5 %. A comparison of the measured branching ratios with theoretical predictions is best performed on the basis of ratios of branching ratios (Figure 2.10) where many assumptions for branching ratios of charmed mesons, life times, *etc.* cancel. The predictions of the BSW model [18] and of the Heavy Quark Effective Theory (Mannel-Roberts-Ryzak [33]) fit best to the data.

In order to derive the weak decay constant f_{D_s} from the measured branching ratios, theoretical models have to be used. With the Bauer-Stech-Wirbel model, one obtains a value

$$f_{D_s} = (280 \pm 46)\mathrm{MeV} \cdot (2.7\%)/\mathrm{BR}(D_s^+ \to \phi\pi))^{1/2}.$$

A measurement of the polarization in the $B \to J/\psi K^*$ decay channel is of special interest for CP violation studies [34]. The J/ψ mesons can be in a helicity $\lambda = 0$ (longitudinally polarized) or $\lambda = \pm 1$ (transversely polarized) state. The longitudinally polarized helicity state of the decay $B^0 \to J/\psi K^{0*}$ followed by $K^{0*} \to K_s^0 \pi^0$ is a pure CP eigenstate. If this state is dominant, this decay can be used as an important complement to the "gold plated" decay $B^0 \to J/\psi K_s^0$ the most promosing channel for CP violation measurements.

The expected angular distribution for pure helicity states are:

$$d\Gamma_L/d(\cos\theta_{J/\psi}) = \frac{3}{4} sin^2\theta_{J/\psi}$$

$$d\Gamma_T/d(\cos\theta_{J/\psi}) = \frac{3}{8}(1 + cos^2\theta_{J/\psi})$$

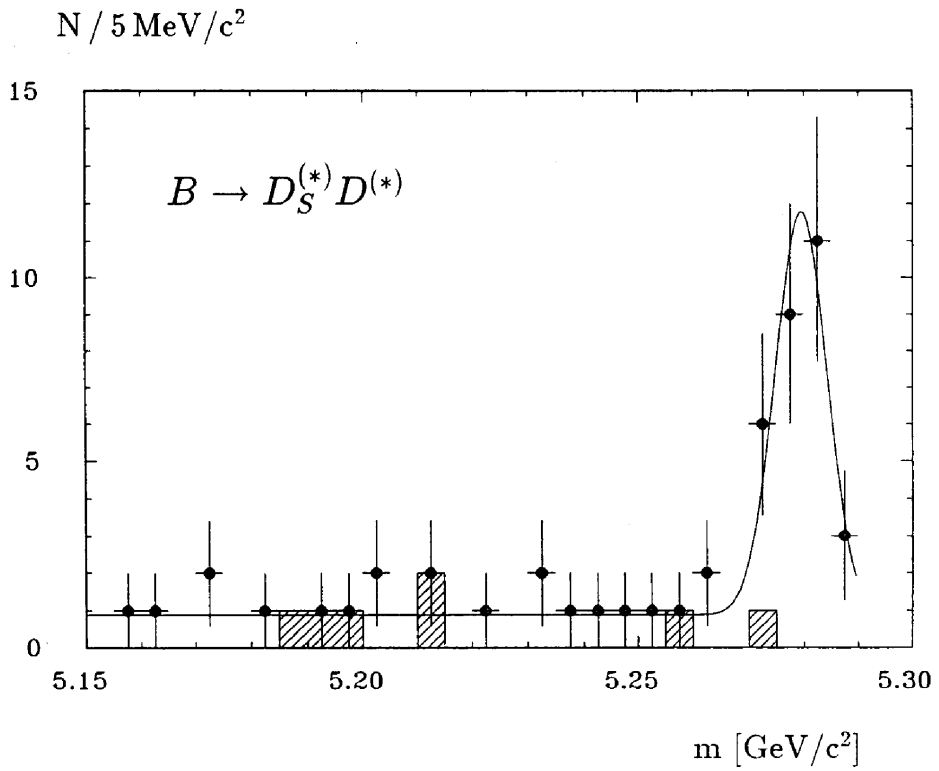

Figure 2.9: *Invariant mass distribution for all eight decay modes* $B \to D_s^{(*)} D^{(*)}$ *(points with error bars; [30]). The solid line is the result of a fit using a Gaussian for the signal plus a constant to parametrize the background. The corresponding distribution for the continuum contribution is shown as a hatched histogram.*

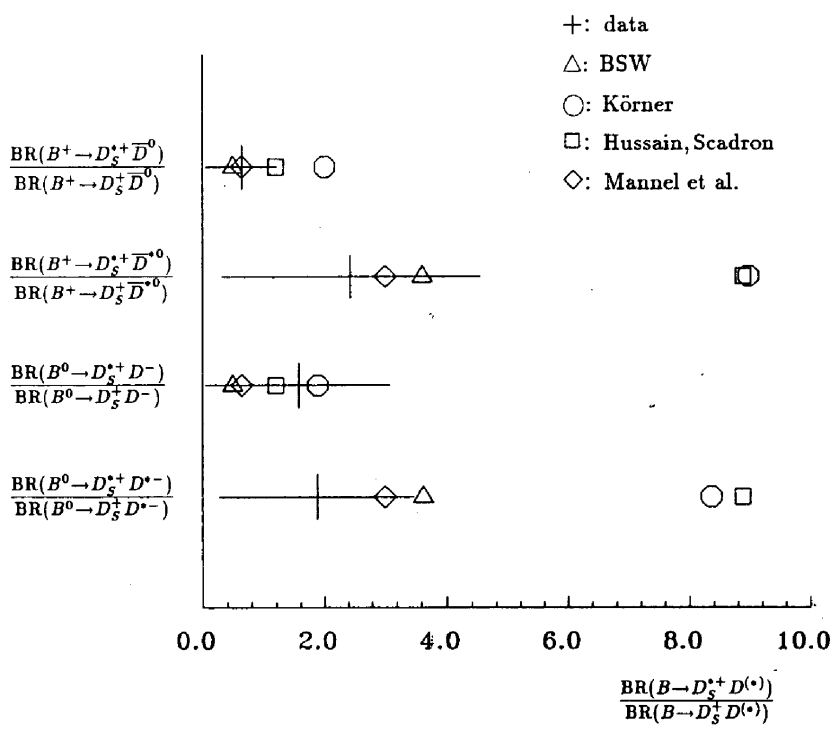

Figure 2.10: *Comparison of the ratio of branching ratios* $BR(B^+ \to D_s^{*+}\overline{D}^0)/BR(B^+ \to D_s^+\overline{D}^0)$, $BR(B^+ \to D_s^{*+}\overline{D}^{*0})/BR(B^+ \to D_s^+\overline{D}^{*0})$, $BR(B^0 \to D_s^{*+}D^-)/BR(B^+ \to D_s^+D^-)$, *and* $BR(B^0 \to D_s^{*+}D^{*-})/BR(B^+ \to D_s^+D^{*-})$ *[30] with theoretical predictions of Bauer-Stech-Wirbel [18] (triangles), Körner [31] (circles), Hussain-Scadron [32] (squares), and Mannel-Roberts-Ryzak [33] (diamonds)*

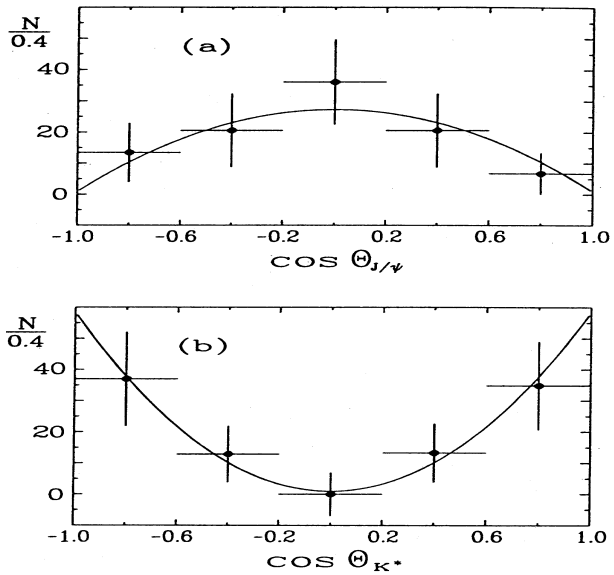

Figure 2.11: *Angular distributions for the decay $B \to J/\psi K^*$ [35]. The solid lines show the fit results to the (a) $\cos\theta_{J/\psi}$ and (b) $\cos\theta_{K^*}$ angular distributions*

$$d\Gamma_L/d(\cos\theta_{K^*}) = \frac{3}{2} cos^2\theta_{K^*}$$

$$d\Gamma_T/d(\cos\theta_{K^*}) = \frac{3}{4} sin^2\theta_{K^*}$$

where $\theta_{J/\psi}$ is the angle between the J/ψ direction in the rest frame of the B meson and the direction of the positive lepton from $J/\psi \to \ell^+\ell^-$ in the J/ψ rest frame. θ_{K^*} is the corresponding angle for the $K^* \to K\pi$ system. The acceptance corrected and normalized angular distributions for the decay $B \to J/\psi K^*$ are shown in Figure 2.11 [35]. Both angular distributions are well described by longitudinally polarized J/ψ and K^* mesons only. A simultanous fit of both distributions is consistent with a vanishing rate Γ_T for transverse polarization:

$$\frac{\Gamma_T}{\Gamma} = 0.03 \pm 0.16 \pm 0.15$$

Therefore, the decay $B^0 \to J/\psi K^{0*}$ can be effectively used in future measurements of CP violation.

Another B decay into charmonium states is also useful for CP violation studies. In 1992 ARGUS observed an unexpectedly large rate for the decay $B \to \chi_{c1} K^-$ [36]: $\mathrm{BR}(B \to \chi_{c1} K^-) = 0.0019 \pm 0.0013 \pm 0.0006$. This was confirmed by CLEO [27]: $\mathrm{BR}(B \to \chi_{c1} K^-) = 0.0097 \pm 0.0040 \pm 0.0009$. The decay $B \to \chi_{c1} \overline{K}^0$ is expected to have an equally large rate and hence can also be used for CP violation studies.

2.2.2 Search for Exclusive Hadronic $b \to u$ Decays

A search for exclusive B decays into hadronic final states containing no charm has resulted in upper limits for many decay channels. The branching ratios for these decays is expected to be much smaller than the ones for $b \to c$ transitions (Tables 2.2, 2.3 and 2.5). However, the reconstruction efficiency for $b \to u$ is much higher, since the reconstruction of intermediate states is more favorable. While the reconstruction efficiency for the decay $B^0 \to \pi^+\pi^-$ is about 40%, the one for the corresponding $b \to c$ decay $B^0 \to D^+\pi^-$ is about 20 times less.

Table 2.6: *Limits on charmless B decays from ARGUS [37]*

Decay mode	BR (90% C.L.)
$B^+ \to \pi^+\pi^0$	$< 2.5 \cdot 10^{-4}$
$B^0 \to \pi^+\pi^-$	$< 1.3 \cdot 10^{-4}$
$B^+ \to \pi^+\pi^+\pi^-$	$< 4.5 \cdot 10^{-4}$
$B^+ \to \rho^0\pi^+$	$< 1.5 \cdot 10^{-4}$
$B^0 \to \pi^+\pi^-\pi^0$	$< 7.2 \cdot 10^{-4}$
$B^0 \to \rho^0\pi^0$	$< 4.0 \cdot 10^{-4}$
$B^0 \to \rho^+\pi^-$	$< 5.2 \cdot 10^{-4}$
$B^+ \to \rho^+\pi^0$	$< 5.5 \cdot 10^{-4}$
$B^+ \to \pi^+\pi^0\pi^0$	$< 8.9 \cdot 10^{-4}$

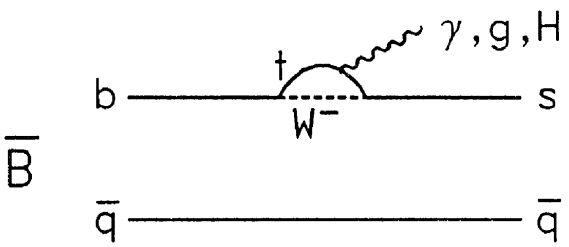

Figure 2.12: *Penguin diagrams for B decays*

In the search for $b \to u$ transitions ARGUS tried to reconstruct B mesons in the channels $B \to n\pi(n \leq 7)$ with up to two π^0's in the final states. No signal was found. Some of the corresponding upper limits are shown in Table 2.6 [37].

A search for rare B decays into D_s^+ mesons like $B^0 \to D_s^+\pi^-$ has also resulted in upper limits which lie in the region of 10^{-3} [38]. In principle, the observed upper limits can be converted into measurements of upper limits for the CKM-matrix element $|V_{ub}|$. However, the limits are less sensitive than the ones derived from the end-point of the lepton spectrum in B decays (Section 2.4). For example, the obtained upper limit for the branching ratio $BR(B^0 \to \pi^+\pi^-) < 1.3 \cdot 10^{-4}$ corresponds to an upper limit of $|V_{ub}/V_{cb}| < 0.22$ [18]. For $b \to u$ transitions involving D_s^+ mesons the predictied branching ratios are of the order of 10^{-4}.

2.2.3 Search for Rare "Penguin" B Decays

Penguin decays of B mesons are of great interest since they provide insight into higher order weak and electromagnetic interactions and are particularly useful for the determination of the CKM matrix element $|V_{ts}|$ (see Figure 2.12). Inclusive contributions from penguin-diagrams can be calculated in the framework of the standard model using perturbative QCD analysis. Measurements of penguin decays allow therefore tests of the Standard Model.

Penguin decays can be studied much better with B than with K mesons since the B mesons are more that ten times heavier than K mesons, and special B decays, such as the decay $B \to \phi K^0$ or $B \to K^*\gamma$ can only occur via penguin diagrams. Since the exchanged quarks can couple to gluons and photons or other neutral bosons, there exist different types of penguin diagrams which can be studied experimentally. Moreover, the contribution from the heaviest quark dominates the loop amplitude and therefore a measurement of these loop-induced processes is sensitive to the existence of a fourth

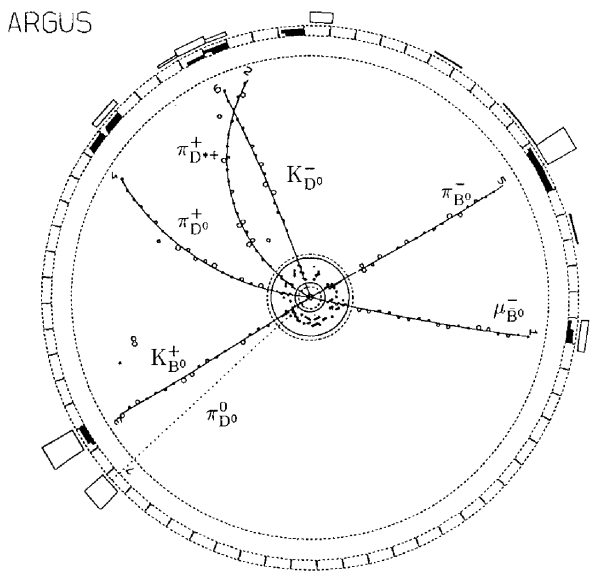

Figure 2.13: *Completely reconstructed event with a $B^0 \to K^+\pi^-$ candidate [42]*

quark family. In the standard model with three families the transition amplitudes depend on the mass of the t quark and the coupling of the t quark to the s quark, $|V_{ts}|$. The inclusive branching ratio for the $b \to s\gamma$ transition has been measured by CLEO [39]

$$\mathrm{BR}(b \to s\gamma) = (2.32 \pm 0.67) \cdot 10^{-4}$$

close to theoretical predictions [40]. The inclusive rate for the transitions $b \to s$ *gluon* (Figure 2.12) is predicted to be [41]:

$$BR(b \to s\ gluon) \approx 1 - 2\%,$$

where s *gluon* stands for all types of penguin transitions: $sg, sq\overline{q}, sgg, ...$

The ARGUS search for hadronic penguin decays $B \to K n\pi^{\pm}$ with $n \leq 7$ has resulted in two completely reconstructed $\Upsilon(4S) \to B\overline{B}$ events with two B decays which are interpreted as $b \to s$ *gluon* decays (Figure 2.13) [42]. If these two decays are attributed to $b \to s$ *gluon* decays the resulting inclusive branching ratio would be $\approx 2\%$ as expected.

ARGUS has also searched for other exclusive penguin decays through the reconstruction of B mesons in the decays $B \to 'K'\pi^+, 'K'\rho^0, 'K'\phi$ and $K^*\gamma$. $'K'$ represents K^0_s, K^+, K^{*0}, and K^{*+} for which the theoretical estimates depend strongly on the poorly known hadronization process. No significant signals have been observed for exclusive hadronic decays of such penguin-type by ARGUS [44]. The obtained upper limits like $\mathrm{BR}(B^0 \to K^-\pi^+) < 2.7 \cdot 10^{-4}$ or $\mathrm{BR}(B^0 \to K^{*0}\gamma) < 2.9 \cdot 10^{-4}$ are much smaller than the branching ratios obtained for decays allowed by spectator diagrams with $b \to c$ transitions (see Table 2.2), indicating that penguin-type diagrams contribute only little to the total decay rate of B mesons.

2.2.4 Summary of exclusive B reconstruction

In summary, only about one quarter of the hadronic decay channels of B mesons has been reconstructed exclusively, comprising those channels with a relatively small multiplicity in the final state. On the other hand, these small multiplicities, and in particular two-body final states, have allowed for detailed comparisons of measured data with theoretical predictions.

2.3 Inclusive Hadronic Decays

An alternative approach to the understanding of B meson decays is to study the hadronic decay products inclusively. Inclusive decays contain global information on B meson decay properties which have to be reproduced by any model describing these decays. They are particularly useful as a testing ground for Monte-Carlo event generators which are indispensible tools in planning experiments at future B factories, fixed-target experiments, and hadron colliders.

The average multiplicity of charged particles in $\Upsilon(4S)$ events is $10.81 \pm 0.05 \pm 0.23$ [43]. The momentum spectra for charged pions, kaons, and protons can be found in [45]. Multiplicities of ω, ρ^0, K^{*0}, K^{*+}, and ϕ mesons are described in ref. [46].

2.3.1 Inclusive D^0, D^+ and D^{*+} Production

The dominance of $b \to c$ transition implies that D and D^* mesons are abundantly produced in B decays. At the $\Upsilon(4S)$ resonance the measured branching ratios for $B \to DX$ refer to a 1:1 mixture of B^0 and B^- mesons. ARGUS measures for the inclusive production of the pseudoscalar D mesons: $\mathrm{BR}(B \to D^0 X) = (58.4 \pm 3.8)\%$ and $\mathrm{BR}(B \to D^+ X) = (24.8 \pm 2.6)\%$. The difference between these two branching ratios is due to the D^* production in B decays which result in more than five times more D^0 than D^+ originating from D^{*+} and D^{*0} decays, assuming equal production rates for the latter.

The momentum spectrum of D and D^* mesons are shown in Figure 2.14. The spectra are soft and do not show a strong contribution from two-body B decays. This agrees nicely with the fact that the exclusive hadronic decay channels reconstructed so far, consisting mainly of two-body decays, cover only a small fraction of all hadronic decay channels.

Remarkably small is the inclusive production of D^* mesons in B decays of $\mathrm{BR}(B \to D^{*+} X) = (23.0 \pm 2.0)\%$. Assuming equal rates for D^{*+} and D^{*0} production in B decays one obtains for the inclusive production of D^0 and D^+ mesons in B decays *not* originating from D^* decays (D^0_{dir} and D^+_{dir} : $(\mathrm{BR}(B \to D^0_{dir} X) + (\mathrm{BR}(B \to D^+_{dir} X) = (37.2 \pm 5.4)\%$ or

$$\frac{2 \cdot \mathrm{BR}(B \to D^{*+} X)}{\mathrm{BR}(B \to D^0_{dir} X) + (\mathrm{BR}(B \to D^+_{dir} X)} = 1.24 \pm 0.20.$$

This ratio is in contrast to the prediction from factorization models [48] which predict

$$\left(\frac{2 \cdot \mathrm{BR}(B \to D^{*+} X)}{\mathrm{BR}(B \to D^0_{dir} X) + (\mathrm{BR}(B \to D^+_{dir} X)} \right)_{WW} = 2.6.$$

We conclude that D mesons, not originating from D^* mesons, are more abundant in B decays than expected from factorization models. The inclusive properties of B decays are not described by the factorization model [48].

2.3.2 Inclusive D_s^+ Production

In contrast to the momentum spectrum of D^0 or D^+ mesons the one for D_s mesons (Figure 2.15) shows a clear component from two-body decays. Indeed, the sum of all investigated exclusive decay modes yields a two-body branching ratio of $(5.6 \pm 1.7)\%$ for $B^- \to D_s^{(*)-} D^{(*)0}$ and $(5.2 \pm 1.7)\%$ for $B^0 \to D_s^{(*)-} D^{(*)-}$. Comparing these numbers with the inclusive rate $B \to D_s$ anything $= (7.9 \pm 1.4)\%$, there is evidence that a large fraction of the D_s production occurs via two-body decays [30].

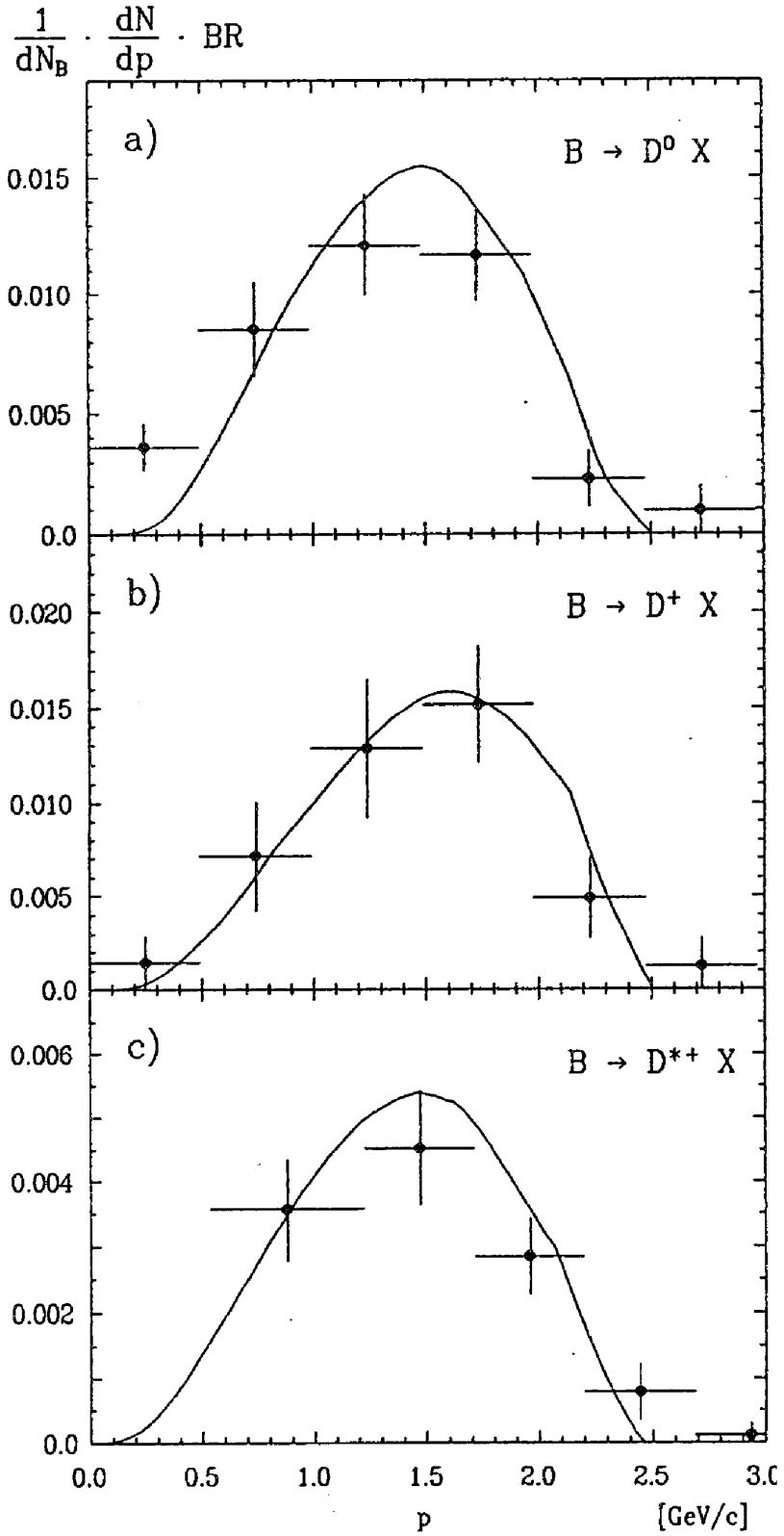

Figure 2.14: *Momentum spectra for (a) D^0, (b) D^+, and (c) D^{*+} mesons from inclusive B decays in the $\Upsilon(4S)$ rest frame [47]. The curves are the results of a calculation of Wirbel and Wu [48], normalized to the data.*

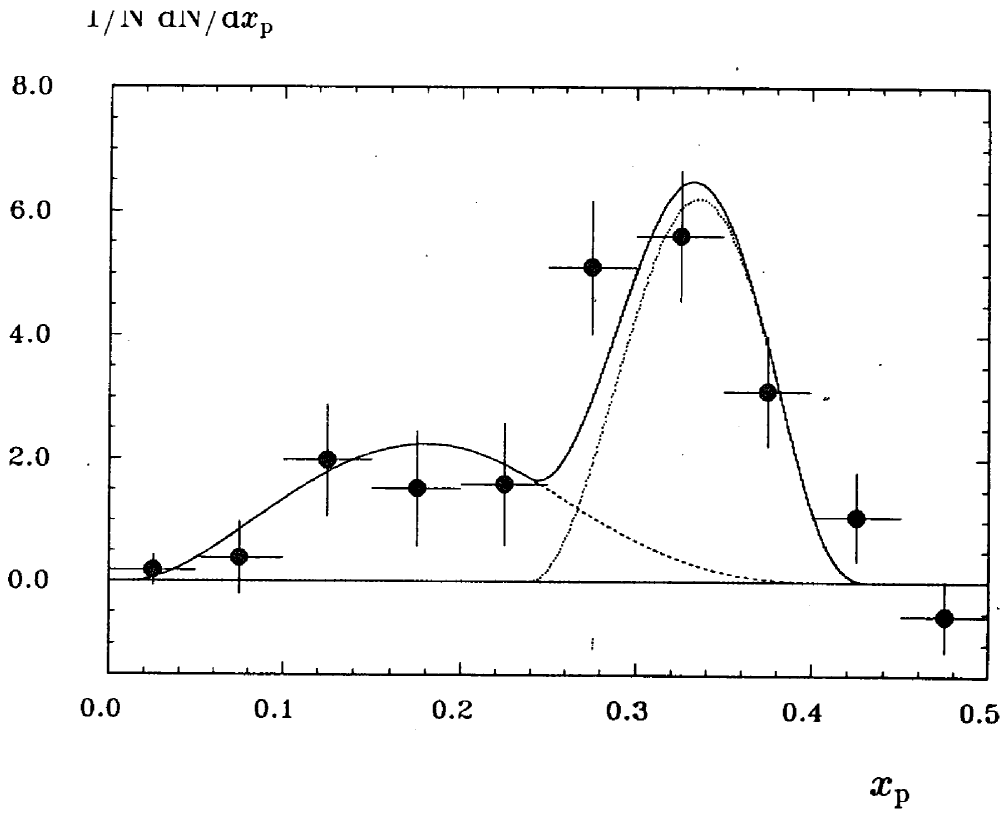

Figure 2.15: *Momentum spectrum of D_s mesons from B decays [30]. The curves are the result of a fit of expected spectra for two-body decays $B \to D_s^{(*)} D^{(*)}$ and three-body decays $B \to D_s^{(*)} D^{(*)} \pi/\rho/\omega$*

2.3.3 Inclusive Charmonium Production

Decays of B mesons into J/ψ mesons are expected to proceed mainly through the so-called "internal spectator" diagram where a c quark from a W boson decay and a $\overline{c}$ quark from $b \to c$ transitions form the J/ψ. This process is called colour-suppressed because colour matching between c and $\overline{c}$ is required. How this matching is accomplished by hard and soft gluon exchange is a question which has attracted considerable theoretical attention.

ARGUS and CLEO simultanously reported in 1985 the first observation of J/ψ mesons in B decays [49, 50]. The ARGUS measurement has been updated and yielded the inclusive branching ratios [51]

$$\mathrm{BR}(B \to J/\psi X) = (1.07 \pm 0.16 \pm 0.22)\%;$$

$$\mathrm{BR}(B \to \psi\prime X) = (0.46 \pm 0.17 \pm 0.11)\%.$$

First evidence for χ_c production in B meson decays was obtained by ARGUS in 1992 [36] yielding

$$\mathrm{BR}(B \to \chi_c X) = (1.05 \pm 0.35 \pm 0.25)\%.$$

This result has been confirmed by CLEO [52]: $\mathrm{BR}(B \to \chi_c X) = (0.40 \pm 0.06 \pm 0.04)\%$.

The results for the charmonium production confirm the important role of colour suppression in these decays.

2.3.4 Inclusive Baryon Production

B mesons provide a unique laboratory in which to study baryon pair production in weak decays of mesons. The $b \to$baryon X decays could proceed through two different mechanisms: (a) through an external W process and (b) through an internal W process. In case (a) the quarks from the W decay

do not participate in the production of the baryon pairs. The baryon-antibaryon is formed from two quark pairs popped up between the c quark and the spectator quark (Figure 2.1). The presence of such a process would imply that semileptonic B decays with a baryon in the final state compared to all baryonic B decays are as abundant as semileptonic B decays with a charmed meson in the final state compared to all mesonic B decays, namely of the order of 10%. In process (b) the quark from the W decay is bound to the c quark and only one quark pair is popped between the c and the spectator quark. This process is not expected to be colour suppressed to the same extent as B decays into charmonium. Process (b) would not allow for semileptonic $b\rightarrow$baryon ℓ^- X decays.

In both mechanisms charmed baryons are produced. The production of Λ_c baryons in B decays was first measured by ARGUS [53] by observing a $\Lambda_c^+ \rightarrow pK^-\pi^+$ signal in $\Upsilon(4S)$ decays. The product branching ratio was determined to be

$$\mathrm{BR}(B \rightarrow \Lambda_c X) \cdot \mathrm{BR}(\Lambda_c \rightarrow pK^+\pi^-) = (0.28 \pm 0.05)\%.$$

Protons and Λ's as well as undetected neutrons are expected to arise either from Λ_c decays which are produced via $b \rightarrow c$ transitions, or from the fragmentation of the spectator quark. The investigation of proton, Λ, and Λ_c multiplicities might give some insight into the production mechanism and allows, in addition, for a determination of Λ_c branching ratios.

ARGUS has determined the inclusive baryonic branching ratio by investigating p and Λ multiplicities [53, 54]:

$$\mathrm{BR}(B \rightarrow pX) = (8.2 \pm 0.5 \pm 1.3)\%.$$
$$\mathrm{BR}(B \rightarrow \Lambda X) = (4.2 \pm 0.5 \pm 0.6)\%.$$

where the protons can also originate from Λ decays.

A simultaneous analysis of p and Λ yields, $p\overline{p}$ and Λp correlations, and various lepton-baryon and lepton-baryon-antibaryon correlations [55] was performed to obtain the inclusive $b\rightarrow$baryonX which is independent of any assumption on the neutron yield in B decays. The result of this analysis is

$$\mathrm{BR}(B \rightarrow \mathrm{baryons}X) = (6.8 \pm 0.5 \pm 0.3)\%.$$

Assuming that the decays $B \rightarrow \Xi_c X$ and $B \rightarrow \Omega_c X$ are small, the decay of a B meson into a charmed baryon proceeds via a Λ_c, *i.e.* $\mathrm{BR}(B \rightarrow \mathrm{baryons}) = \mathrm{BR}(B \rightarrow \Lambda_c X)$. This allows the determination of the branching ratio

$$\mathrm{BR}(\Lambda_c \rightarrow pK^+\pi^-) = (4.0 \pm 0.3 \pm 0.8)\%.$$

A further study of $\overline{p}\ell^+$ [22] events allowed to obtain a limit (90% C.L.) on semileptonic B decays into baryons:

$$\mathrm{BR}(B \rightarrow \overline{p}\ell^+ X) < 0.16\%.$$

This result implies that the external W process contributes only little to baryonic B decays.

2.3.5 Inclusive Kaon Production

The most frequent production mechanism of kaons in B decays is via the decay chain $b \rightarrow \overline{c} \rightarrow s$, and consequently there is a correlation between the flavour of the B meson (containing b or $\overline{b}$) and the kaon produced in this way. Additional kaons are produced through $s\overline{s}$ quark pairs from the vacuum or through the decay of virtual W bosons $W^+ \rightarrow c\overline{s}$.

Measurements of kaon production in B meson decays can thus serve as a test of our understanding of the different mechanisms in these decays, and probe the ability of the spectator model to explain data. Charged kaons are expected to provide a means of tagging the flavour of B mesons in future experiments, particularly in experiments planned to measure CP violation. The quality of the tagging depends both on the tagging efficiency and the number of incorrectly tagged B mesons.

Table 2.7: *Mean kaon multiplicities in B meson decays. Mixing of B^0 mesons is taken into account*

Decay	ARGUS [56]	CLEO[57]
$B^+/B^0 \to K^+X$	$0.620 \pm 0.013 \pm 0.038$	$0.66 \pm 0.05 \pm 0.07$
$B^+/B^0 \to K^-X$	$0.165 \pm 0.011 \pm 0.036$	$0.19 \pm 0.05 \pm 0.02$
$B^+/B^0 \to K^0_s X$	$0.321 \pm 0.005 \pm 0.021$	$0.315 \pm 0.03 \pm 0.03$

ARGUS has measured the multiplicities of K^+ and K^- mesons, separated for B hadrons containing either a b or a $\overline{b}$ quark, by using fast leptons as a flavour tag [56]. The results, including K^0 multiplicities, are given in Table 2.7 and compared with results of the CLEO collaboration [57]. All numbers are consistent with a large majority of the B mesons decaying according to the spectator model through the quark transition $b \to \overline{c} \to s$. Using charged kaons as a means of tagging the flavour of B mesons is possible but one has to take into account that approximately one out of five kaons tags the B flavour incorrectly.

2.4 Inclusive Semileptonic B decays

Inclusive semileptonic B decays (see Figure 2.1) are of particular interest since these β-decay like processes can be used for a determination of the CKM matrix elements $|V_{cb}|$ and $|V_{ub}|$ and for tagging the flavour of the b quark. The total semileptonic decay rate is given by:

$$\Gamma_{sl} = \gamma_c \, |V_{cb}|^2 + \gamma_u \, |V_{ub}|^2 \, . \tag{2.6}$$

where the factors γ_c and γ_u in front of $|V_{cb}|^2$ and $|V_{ub}|^2$ are given by phase space and QCD correction factors. They depend on the b and c as well as on u quark masses. For γ_c the predictions were $\gamma_c = (40 \pm 8)\text{ps}^{-1}$[58] and $\gamma_c = (42 \pm 8)\text{ps}^{-1}$ [59]. Recently large progress has been achieved in the framework of the Heavy Quark Expansion with $\gamma_c = (41 \pm 3)\text{ps}^{-1}$ [60]. For $b \to u\ell\nu$ decays one expects that γ_u is about a factor of 2 larger than γ_c due to the larger phase space which is available [61].

The ARGUS detector provides excellent $e^\pm$ and $\mu^\pm$ identification by coherently using the whole detector information. Electrons can be identified down to momenta of $p_e = 0.4$ GeV/c with small fake rates. Figure 2.16 shows the electron spectrum measured by ARGUS at the $\Upsilon(4S)$ resonance [22]. The low-momentum range of the spectrum consists mainly of "cascade" leptons from the decay $b \to c \to eX$ and is not shown in this figure. At momenta below 2.3 GeV/c^2 the spectrum is dominated by contributions from B decays; above p = 2.3 GeV/c^2 the contributions of leptons from the e^+e^- continuum predominate. After subtraction of this continuum contribution the measured electron spectrum from direct $\Upsilon(4S)$ decays (Figure 2.17) is well described by assuming only primary leptons from $b \to c\ell\nu$ transitions (solid curve) and cascade decays $b \to cX, c \to s\ell\nu$ (dashed curve).

A distinction between $b \to u$ and $b \to c$ transitions can be made by exploiting the fact that, in the $\Upsilon(4S)$ rest system which is approximately also the B rest system, the leptons accompanying $b \to u$ transitions can have larger momenta (up to 2.7 GeV/c) than the corresponding leptons from $b \to c$ transitions where the kinematic limit is at 2.3 GeV/c. The absence of a significant signal beyond the latter limit indicates that contributions from $b \to u$ transitions are small. This point will be discussed in detail in the next section. Since the $\Upsilon(4S)$ mesons decay with equal probability into $B^0\overline{B}^0$and B^+B^- pairs an average semileptonic branching ratio $B \to \ell X$ where B stands for an equal mixture of B^0 and B^+ mesons is obtained from the integration of the lepton spectrum. Due to the large contribution from cascade decays at low lepton momenta an extrapolation to $p_\ell = 0$ GeV/c has to be performed with the aid of specific models. This procedure introduces systematic errors on

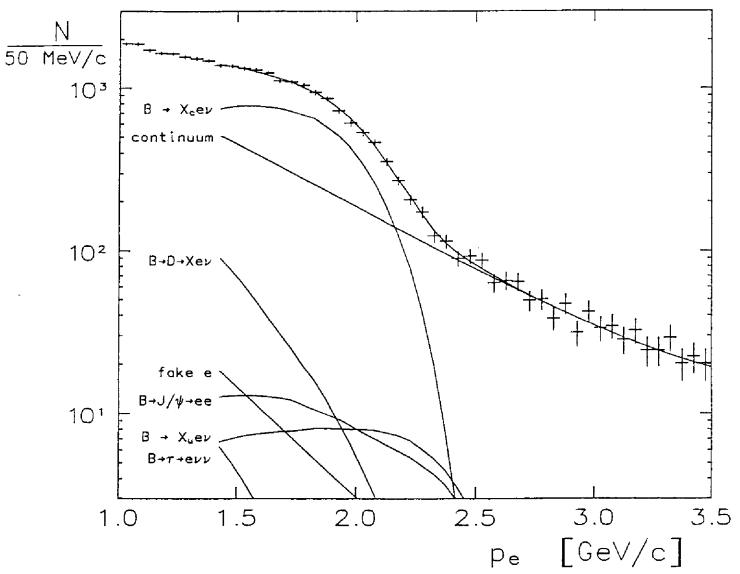

Figure 2.16: *Lepton spectra on the* $\Upsilon(4S)$ *[22]*

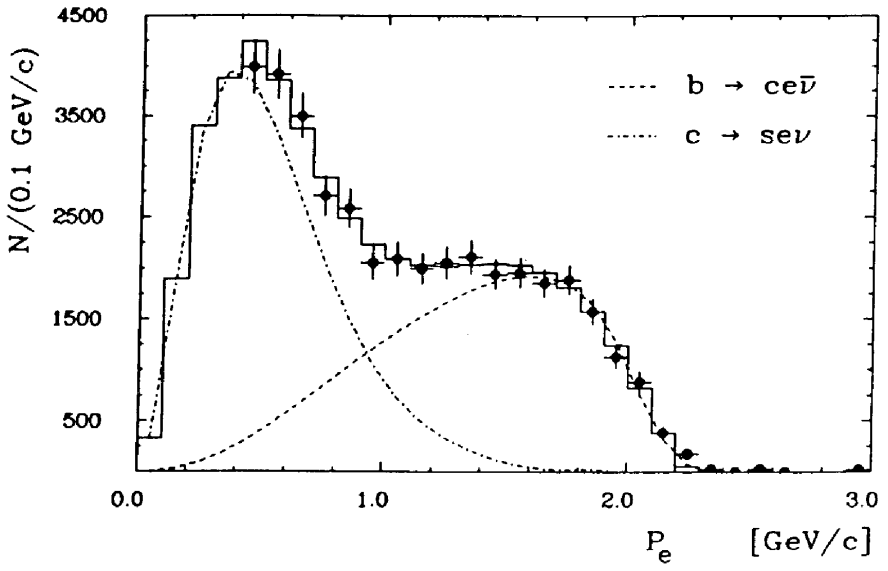

Figure 2.17: *Lepton spectra from* $\Upsilon(4S)$ *decays; continuum subtracted [64]*

Table 2.8: *Semileptonic branching ratios of B mesons [22]*

Model	Branching Ratio [%]	$\|V_{cb}\|$
ACM [58]	$10.2 \pm 0.5 \pm 0.2$	0.039 ± 0.004
GISW [59]	9.8 ± 0.5	0.038 ± 0.005

the branching ratio since different models lead to different results. The branching ratios given in Table 2.8 are obtained from extrapolations with a quark decay model [58] and with a form factor model [59].

The observed semileptonic branching ratio is unexpectedly small. This result was first presented by ARGUS and CLEO in 1988 [62] and confirmed by recent measurements at LEP [39]. Spectator models predict branching ratios in excess of 12% [63]. At present, there remains no convincing explanation for this discrepancy between theory and experiment.

Also shown in Table 2.8 are the values for the CKM matrix element $|V_{cb}|$ which are determined from the semileptonic decay rates of B mesons, Γ_{sl}, given by eq. 2.6. Γ_{sl} is experimentally determined from the measured semileptonic branching ratio BR_{sl} by

$$\Gamma_{sl} = \frac{BR_{sl}}{\tau_b} \tag{2.7}$$

where τ_b is the average lifetime of B^0 and B^+ mesons. Using $\tau_b = (1.63 \pm 0.07)$ ps [39] and assuming negligible contributions from $b \to u$ transitions, ARGUS obtains $|V_{cb}| \approx 0.039$ (Table 2.8).

The model dependence of the integration of the whole lepton spectrum can be reduced considerably if the spectrum of the primary leptons is measured down to low lepton momenta. This is possible if the background from cascade leptons can be suppressed. For this purpose, ARGUS has developed a technique which uses the fact that B mesons from $\Upsilon(4S)$ decays can be efficiently tagged by fast leptons where the contributions from cascade leptons are small (Figure 2.17). Using electrons and muons in the momentum range between 1.4 and 2.3 GeV/c as tags for the second B, the primary leptons from the first B are identified from the charges of the two leptons which have to be of opposite sign. Like sign lepton pairs, on the other hand, tag mainly the cascade background in $e^+e^- \to \Upsilon(4S) \to B\overline{B}$ events. Corrections to this approach arise from $B\overline{B}$ oscillations and events where both leptons originate from the same B meson. Additional backgrounds arise from faked leptons, photon conversions and $B \to J/\psi X, J/\psi \to \ell^+\ell^-$. Most of the backgrounds can be determined from the data itself, and only very little Monte Carlo simulation is necessary. With all backgrounds subtracted one obtains the electron spectrum for primary $B \to e\nu X$ decays shown in Figure 2.18 [64].

Integration of the obtained electron spectrum in Figure 2.18 leads to

$$\mathrm{BR}(B \to e\nu X, p_e > 0.6\mathrm{GeV}/c) = (9.1 \pm 0.5 \pm 0.4)\%.$$

This result is independent of any B meson decay model. It is consistent with the model dependent results described earlier. Therefore it strongly indicates that the discrepancy between experiment and theory is not due to a model dependent treatment of the data. Extrapolation to $p_e = 0$ requires a model, but the momentum region below 0.6 GeV/c contains only $(5.7 \pm 1.0)\%$ of all electrons. The final result of

$$\mathrm{BR}(B \to e\nu X) = (9.6 \pm 0.5 \pm 0.4)\%$$

is therefore essentially model independent and in good agreement with the first measurement as well as with a more recent CLEO measurement using the method developed by ARGUS [65]. The

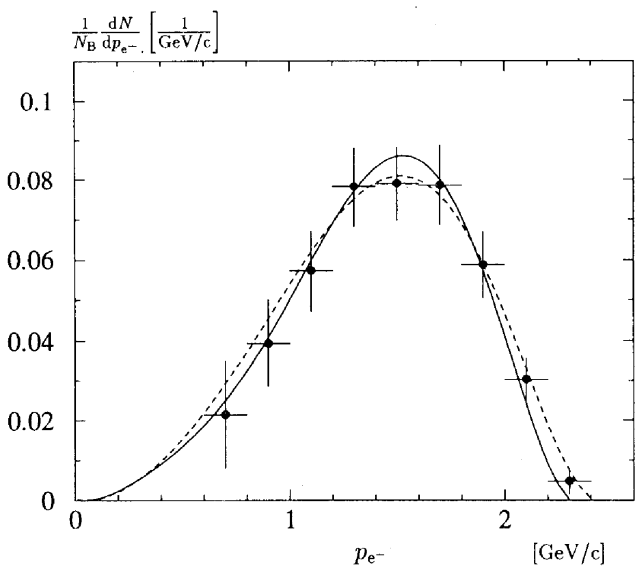

Figure 2.18: *Electron spectrum of $B \rightarrow e\nu X$ decays [64] The solid line is the fit with the ACM model [58] to the data, the dashed line that of the GISW model [59]*

ACM [58] and GISW models [59] both describe the shape of the spectrum well and give branching ratios in agreement with the above value. Using the best predicted value for γ_c (Equation 2.6) of $\gamma_c = (41 \pm 3)\text{ps}^{-1}$ [60] ARGUS obtains from the model independent measurement:

$$|V_{cb}| = 0.0379 \pm 0.0012 \pm 0.0014$$

where the first error is due to the measurement and the second one due to the uncertainty in the theoretical prediction. Adding both errors yields a precision in $|V_{cb}|$ of better than 5%.

2.5 Semileptonic $b \rightarrow u$ decays and Determination of $|V_{ub}|$

Due to their apparent smallness in semileptonic B decays, the most sensitive place to look for $b \rightarrow u$ transitions is the endpoint region of the lepton spectrum where $b \rightarrow c$ transitions do not contribute. The kinematic limit for contributions from $b \rightarrow c\ell\nu$ decays to the lepton spectrum obtained in direct $\Upsilon(4S)$ decays is $p_l \approx 2.3$ GeV/c (Figure 2.17) whereas the limit for $b \rightarrow u\ell\nu$ is $p_l \approx 2.6$ GeV/c. In 1989 ARGUS presented the first statistically significant evidence for $b \rightarrow u$ transitions from the observation of $\Upsilon(4S)$ decays having leptons in the momentum range from $p_l \approx 2.3$ GeV/c to $p_l \approx 2.6$ GeV/c which proved the existence of charmless B decays [8]. The same effect with smaller significance was simultanously observed by CLEO [66].

The lepton spectrum in this region, measured on the $\Upsilon(4S)$ resonance, is dominated by contributions from the continuum below the $\Upsilon(4S)$ resonance (see Figure 2.16). The strategy for observing $b \rightarrow u$ transitions in the lepton spectrum consequently consists of suppressing the continuum contributions in this region with respect to the direct $\Upsilon(4S)$ contribution by exploiting the differences in event topologies that were discussed earlier. Moreover there is a neutrino in semileptonic B decays whereas many of the continuum leptons are misidentified hadrons which are not accompanied by neutrinos. These facts result in a large missing momentum p_{miss} for events with semileptonic B decays and a small p_{miss} for most of the continuum events. Due to the hermiticity of the ARGUS detector one is able to measure p_{miss} with sufficient accuracy to efficiently suppress purely hadronic decays at the $\Upsilon(4S)$.

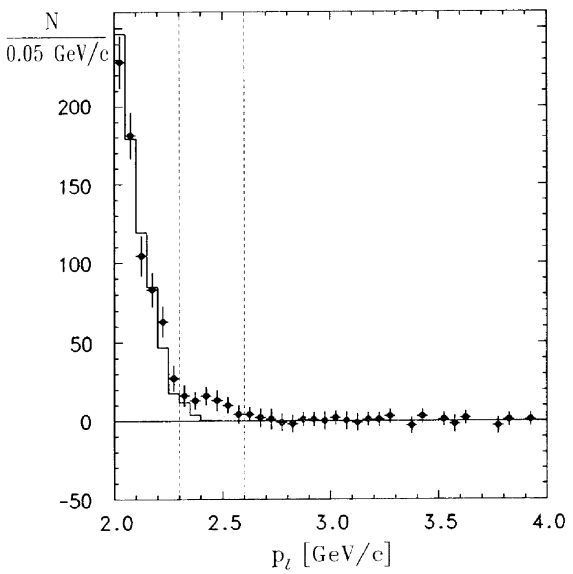

Figure 2.19: *Combined lepton momentum spectrum for direct* $\Upsilon(4S)$ *decays [8]. The histogram is the* $b \to c$ *contribution normalized in the region* $2.0 - 2.3\,GeV/c$.

The ARGUS analysis [8, 67] suppresses the continuum contributions to a 1% level while retaining an efficiency for $B\overline{B}$ decays as high as about 50%. This is achieved either by requiring a single fast lepton, and applying additional restrictions on the event topology and missing momentum, or demanding two leptons.

The lepton spectrum for events which satisfy these selection criteria is shown in Figure 2.19 for direct $\Upsilon(4S)$ decays. The breakdown of the yields for the single and dilepton samples is given in Table 2.9. In the signal region between 2.3 and 2.6 GeV/c 81 leptons are observed in the $\Upsilon(4S)$ data while only 3 are found in the continuum sample. A conservative estimate for the continuum contribution in the signal region was obtained by using the average background level observed in the continuum data over the whole momentum interval 2.0 to 2.9 GeV/c, corresponding to 8.0 events in the signal region. This number has to be scaled by a factor 2.9 to account for different luminosities and center-of-mass energies. The total estimated background, broken down in detail in Table 2.9, is 40.0 ± 5.3 lepton candidates. In total, after subtraction of this background a signal of 41.0 ± 10.4 events remain from charmless semileptonic B decays.

An update of this analysis using more data was performed in 1991 [67] and resulted in a signal from charmless semileptonic B decays of 77.1 ± 13.4 events. In order to show that this excess of high momentum leptons ($2.3 < p_{\ell^-} < 2.6$ GeV/c) does indeed originate from $b \to u\ell^-\overline{\nu}$ transitions, a systematic attempt to completely reconstruct these events has been performed. The reconstruction efficiency using many B decay channels involving D mesons [1] is about 1.6 %. Therefore one expects approximately one completely reconstructable event in the ARGUS single lepton sample.

As a result of a search for a hadronic B tag in the data, indeed one fully reconstructed event was found. The event is shown in Figure 2.20 and consists of a $\Upsilon(4S)$ decay into a pair of $\overline{B}^0$mesons, indicating that one B^0 meson has oscillated into a $\overline{B}^0$. Thus, the event simultaneously demonstrates the existence of $b \to u$ transitions and $B^0\overline{B}^0$mixing [1]. The hadronic $\overline{B}^0$tag was reconstructed in the mode $\overline{B}^0 \to D^{*+}\rho^-$. The second $\overline{B}^0$meson was seen in the channel $\overline{B}^0 \to \pi^+\mu^-\overline{\nu}$, representing the first direct observation of a $b \to u$ transition.

[1] Here D meson should be interpreted as D^0, D^+, D^{*0}, D^{*+}. The final state of the B decay was required to contain no more than 8 charged particles and 6 photons.

Table 2.9: *Observed single-lepton and dilepton events in the momentum interval* $2.3 < p_\ell < 2.6$ *GeV/c and estimated backgrounds (ARGUS [8])*

	Single Leptons		Dileptons	
	e	μ	e	μ
$\Upsilon(4S)$	31	29	11	11
Backgrounds:				
Continuum (scaled)	6.8	14.5	1.0	1.0
$b \to c$	4.0	4.4	1.1	1.2
J/ψ	0.6	0.4	0.2	0.1
Fakes	0.9	1.7	0.7	1.4
Total background	12.4 ± 32.8	21.0 ± 4.0	3.0 ± 1.0	3.7 ± 1.1
Signal	18.7 ± 6.2	8.0 ± 6.7	8.0 ± 3.5	6.3 ± 3.4
Combined signal	41.0 ± 10.4			

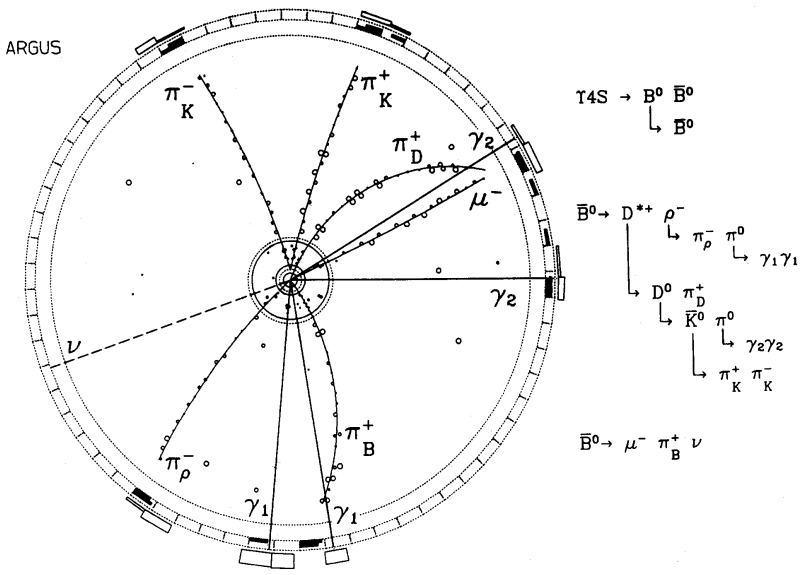

Figure 2.20: *Completely reconstructed event containing the decay* $\Upsilon(4S) \to B^0\overline{B}^0$, $B^0 \to \overline{B}^0$ *where one* $\overline{B}^0$ *decays into* $\pi^+\mu^-\overline{\nu}$ *and the other into* $D^{*+}\rho^-$ *[67]*

Having explicitly shown that $b \to u\ell^-\nu$ transitions are responsible for the excess of leptons with momenta above the kinematical limit for $b \to c\ell^-\nu$ transitions, the strength of the $b \to u$ coupling can be obtained from the inclusive spectra. The shape of the spectrum in Figure 2.19 in this region is compatible with the predictions for semileptonic $b \to u\ell^-\overline{\nu}$ decays [58, 59, 68, 69]. However, using only this very restricted portion of the full momentum spectrum, it is not possible to discriminate between the available models which have to be used to extrapolate the spectrum down to $p_\ell = 0$. Since the predicted spectra vary considerably according to the chosen model the extracted ratios $|V_{ub}/V_{cb}|$ also have different values. Using the ACM model [58] one obtains $|V_{ub}/V_{cb}| \approx 0.10 \pm 0.01$. Similar results are found by using the WBS [68] and KS models [69] while the GISW prediction [59] yields a larger value. Taking into account the model dependence of the result, a value of $|V_{ub}/V_{cb}| = 0.08 \pm 0.03$ is accepted today which demonstrates that $b \to u$ transitions contribute only with a small percentage to the total B decay rate.

2.6 Exclusive Semileptonic B decays and the Measurement of $|V_{cb}|$

2.6.1 The decay $\overline{B}^0 \to D^{*+}\ell^-\overline{\nu}$

The study of exclusive semileptonic decays of B mesons was pioneered by ARGUS in 1987 with the introduction of the recoil mass technique first developed for the decay $\overline{B}^0 \to D^{*+}\ell^-\overline{\nu}$ [7]. Since then, many important applications of the ARGUS method have been made which has allowed for a systematic study of exclusive semileptonic B decays. The decay $\overline{B}^0 \to D^{*+}\ell^-\overline{\nu}$ is of particular importance as a means for determining the CKM matrix element $|V_{cb}|$, for testing the Lorentz structure of the weak hadronic current, and for selecting models which consistently describe the dynamics of exclusive semileptonic B decays. Even the first studies of this decay by ARGUS [7] showed that specific models [70, 71] could be ruled out. Better theoretical understanding of exclusive semileptonic B decays have been obtained in the last few years, both in the context of Heavy Quark Effective Theory (HQET) [19, 72] and by using QCD sum rules [73]. Within the HQET approach it has been shown [74] that the decay $\overline{B}^0 \to D^{*+}\ell^-\overline{\nu}$ is not affected by $O(1/m_Q)$ corrections at the point of zero recoil, *i.e.* at the maximum momentum transfer $q^2 = q^2_{max}$ which allows in principle a model independent determination of $|V_{cb}|$ from the study of the q^2 spectrum.

The decay $\overline{B}^0 \to D^{*+}\ell^-\overline{\nu}$ can be reconstructed despite the neutrino in the final state which escapes detection. The square of the mass of the neutrino, M^2_ν is given by

$$M^2_\nu = (E_B - E_{D^{*+}} - E_{\ell^-})^2 - (\vec{p}_{B^0} - (\vec{p}_{D^{*+}} + \vec{p}_{\ell^-}))^2 . \quad (2.8)$$

At the $\Upsilon(4S)$ resonance the energy of the B^0 meson is given by the beam energy: $E_B = E_{beam}$. The energies E and momenta $\vec{p}$ of the D^{*+} meson and the lepton ℓ^- are measured. The only unknown quantity is the direction of the B^0 meson whose momentum, however, is as small as 330 MeV/c. Neglecting this B^0 momentum, a signal for the reaction $\overline{B}^0 \to D^{*+}\ell^-\overline{\nu}$ is obtained from the distribution of the recoil-mass squared:

$$M^2_{rec} = (E_{beam} - E_{D^{*+}} - E_{\ell^-})^2 - (\vec{p}_{D^{*+}} + \vec{p}_{\ell^-})^2 . \quad (2.9)$$

The M^2_{rec} distribution for the decay $\overline{B}^0 \to D^{*+}\ell^-\overline{\nu}$ peaks at $M^2_{rec} = 0$ since the $\overline{B}^0$ momentum is small, and therefore M^2_{rec} is approximately the square of the neutrino rest mass. The contribution from higher excited D resonances which decay into $D^{*+}\pi^-$ is shifted to positive M^2_{rec} values due to the non-vanishing $(\overline{\nu}\pi)$ invariant mass. Figure 2.21 shows the measured M^2_{rec} distributions for the two decay chains $D^{*+} \to D^0\pi^+$, followed by $D^0 \to K^-\pi^+$ and $D^0 \to K^-\pi^+\pi^+\pi^-$, respectively [75]. A prominent signal at $M^2_{rec} = 0$ is observed, as expected for the decay $\overline{B}^0 \to D^{*+}\ell^-\overline{\nu}$. The small number of events at $M^2_{rec} < -2\mathrm{GeV}^2/c^4$ indicates that there are only minor background sources

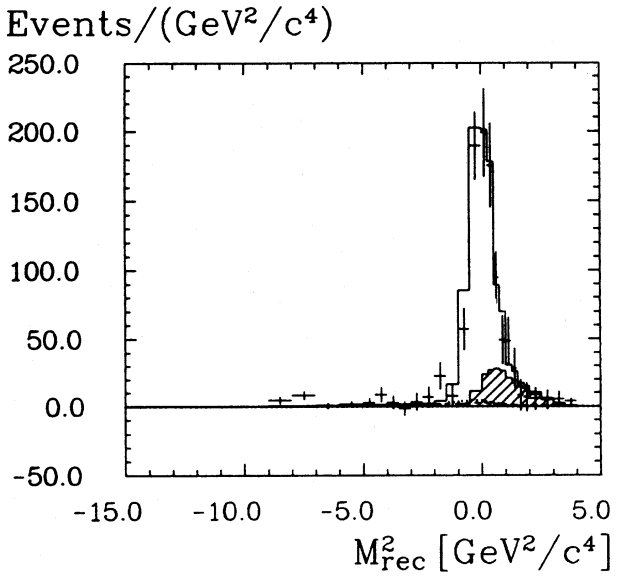

Figure 2.21: *Measured M^2_{rec} distributions (points with error bars) for the two D^0 decay channels [75] The blank and shaded areas correspond to the rates for the signal process and the feeddown process, respectively. The continuum process is shown as a dashed line*

from uncorrelated $D^{*+}\ell^-$ combinations and the continuum. For positive M^2_{rec} values one observes a shoulder which is attributed to the process $\overline{B} \to D^{**}\ell^-\overline{\nu}$. From a fit to the M^2_{rec} distribution one obtains $235\pm24 \pm 11$ events for the decay $\overline{B}^0 \to D^{*+}\ell^-\overline{\nu}$ and $63 \pm 15 \pm 6$ events from the decay $\overline{B} \to D^{**}\ell^-\overline{\nu}$ where D^{**} refers to the higher excited D states or $D^{*+}n\pi$ phase space. The decay $\overline{B} \to D^{**}\ell^-\overline{\nu}$ will be discussed in section 2.7. The rate for the continuum process $e^+e^- \to q\overline{q} \to D^{*+}\ell^-X$ has been determined from measurements at energies below the $\Upsilon(4S)$ mass.

Assuming lepton universality, the fitted number of $(D^{*+}\ell^-)$ events for the process $\overline{B}^0 \to D^{*+}\ell^-\overline{\nu}$ lead to a branching ratio of [75]:

$$\mathrm{BR}(\overline{B}^0 \to D^{*+}\ell^-\overline{\nu}) = (4.8 \pm 0.5 \pm 0.5)\%$$

using the relevant charm branching ratios [17] $\mathrm{BR}(D^{*+} \to D^0\pi^-) = 68.1\%$, $\mathrm{BR}(D^0 \to K^-\pi^+) = 4.01\%$, and $\mathrm{BR}(D^0 \to K^-\pi^+\pi^+\pi^-) = 8.1\%$. This measurement is in agreement with the original ARGUS result [7].

The Lorentz structure of the decay $\overline{B}^0 \to D^{*+}\ell^-\overline{\nu}$ has been studied by measuring the D^{*+} polarization, given by the parameter α_{pol}, and the forward-backward asymmetry A_{FB} defined by

$$\alpha_{pol} = 2 \cdot \frac{\Gamma^L}{\Gamma^T} - 1$$

and

$$A_{FB} = \frac{3}{4} \cdot \frac{\Gamma^- - \Gamma^+}{\Gamma}$$

The total width Γ is given by $\Gamma = \Gamma^L + \Gamma^T$, where Γ^L and Γ^T are the longitudinal and transverse decay rates with $\Gamma^T = \Gamma^- + \Gamma^+$ for the negative and positive helicities.

The ARGUS measurement of α_{pol} shows that the longitudinal D^{*+} polarization equals about the transverse and that the $b \to c$ transitions are left-chiral as seen from the non-zero forward-backward asymmetry A_{FB} which reflects parity violation in the $b \to c$ decay [75]. The values for A_{FB} and α_{pol}

Table 2.10: A_{FB} and α_{pol} in the decay $\overline{B}\to D^*\ell^-\overline{\nu}$ [75]

	A_{FB}	α_{pol}
ARGUS	$0.20 \pm 0.08 \pm 0.06$	$1.1 \pm 0.4 \pm 0.2$
HQET [76]	0.22	1.37

are in agreement with the predictions from the HQET and QCD sum rule models [19, 69, 73, 74, 76] (Table 2.10).

One obtains a model-independent determination of $|V_{cb}|$ from a fit to the squared momentum transfer, q^2, spectrum in the decay $\overline{B}^0 \to D^{*+}\ell^-\overline{\nu}$ or, equivalently, to the y spectrum with

$$y = \frac{m_B^2 + m_{D^*}^2 - q^2}{2 m_B m_{D^*}}$$

where m_B and m_{D^*} are the masses of the B^0 and D^{*+} mesons, respectively. In the framework of HQET, the decay rate is given, apart from kinematical quantities and CKM matrix element $|V_{cb}|$, by one universal form factor, the Isgur-Wise function $\xi(y)$ with the normalization $\xi(1) = 1$. The existence of finite quark masses implies corrections of order $1/m_Q^2$. It has been shown [74, 76] that, specifically for the decay $B \to D^*\ell\nu$, these corrections are small at the point of zero recoil, $y = 1$.

The differential width for this decay is given by :

$$\begin{aligned} \frac{1}{\tau_{\overline{B}^0}} \cdot \frac{d\mathrm{BR}(\overline{B}^0 \to D^{*+}\ell^-\overline{\nu})}{dy} &= \frac{G_F^2}{48\pi^3} m_{D^*}^3 (m_B - m_{D^*})^2 \cdot \eta_A \cdot |V_{cb}|^2 \xi^2(y) \sqrt{y^2-1} \\ &\times \left[4y(y+1) \frac{1 - 2y m_r + m_r^2}{(1-m_r)^2} + (y+1)^2 \right], \end{aligned} \tag{2.10}$$

with $m_r = m_{D^*}/m_B$ and $\eta_A = 0.91 - 0.94$ [60, 77]. The measured $|V_{cb}| \cdot \xi(y)$ distribution is shown in Figure (2.22) [75]. The values of $|V_{cb}|$ are determined by the intersection of the fitted function $\xi(y)$ with the ordinate since $\xi(1) = 1$.

From the value of $|V_{cb}| \cdot \xi(y)$ at $y = 1$ ARGUS obtains

$$|V_{cb}| = 0.040 \pm 0.004 \pm 0.003$$

for $\tau_{B^0} = (1.63 \pm 0.07) ps$ [39], $\eta_A = 0.94$ and an Isgur-Wise function of the form $\xi(y) = 1 - \rho^2(y-1)$ with the charge radius $\rho = 1.08 \pm 0.11 \pm 0.03$. The agreement with the value of $|V_{cb}|$ from the inclusive semileptonic decay rate is excellent.

The reconstruction of B^0 mesons in the channel $B^0 \to D^{*-}\ell^+\nu$ also works well when the D^0 from the decay $D^{*-} \to \overline{D}^0\pi^-$ remains undetected [78]. The energy release in this decay is only about 6 MeV , so the direction of the pion is close to that of the D^* meson and their momentum are strongly correlated. The momenta of the D^{*-} meson can be approximated by the pion momenta by $p_{D^*} = \alpha p_\pi + \beta$ with empirical parameters $\alpha = 8.23$ and $\beta = 0.41$ GeV/c [78]. This method has the advantage of yielding higher statistics than the previous one.

Figure 2.23 shows the M_{rec}^2 spectra for right-sign ($\ell^+\pi^-$) and wrong-sign ($\ell^+\pi^+$) combinations. The prominent peak at $M_{rec}^2 \sim 0$ is attributed to $B \to D^*$ (π) ℓ ν decays. No signal can be seen in the wrong-sign spectrum. The contributions from continuum events and faked leptons have been subtracted.

The shapes of the spectra for right- and wrong-sign $\ell\pi$ combinations are well reproduced by a Monte Carlo simulation of $\Upsilon(4S) \to B\overline{B}$ events. Moreover, the shape of the background for the right-sign combinations is the same as that for the wrong-sign, with a well reproduced relative

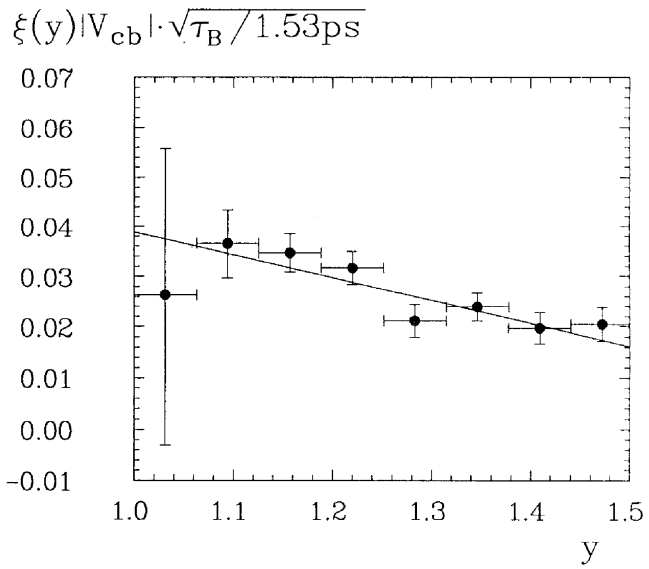

Figure 2.22: *Measured distribution* $\Delta BR(\overline{B}^0 \to D^{*+}\ell^-\overline{\nu})/\Delta y$ *transformed to correspond to* $|V_{cb}|\cdot\xi(y)$ *[75]. The dotted line corresponds to* $\xi(y) = 1 - \rho^2(y-1)$ *for the Isgur-Wise Function where* ρ *is the charge radius*

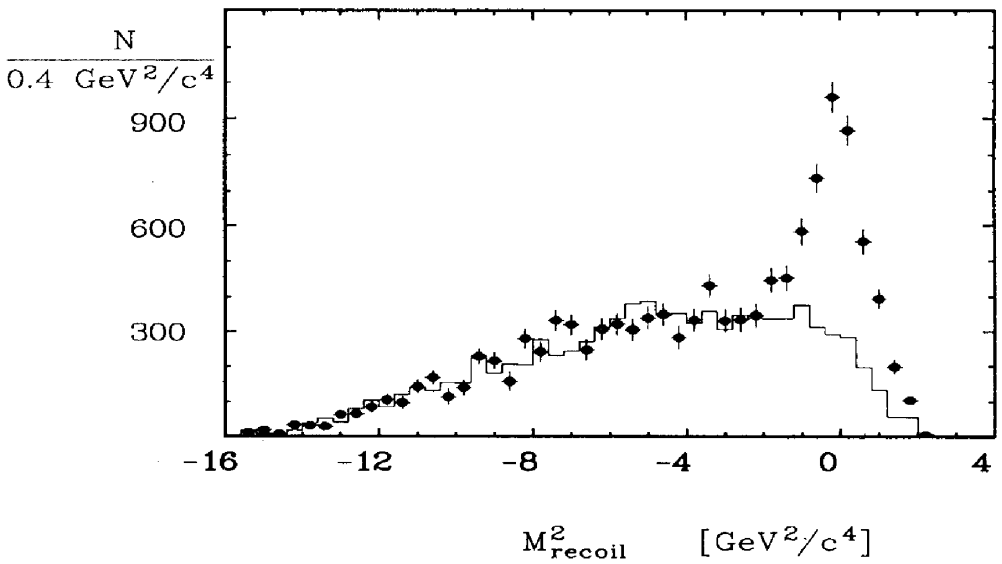

Figure 2.23: *Continuum and fake lepton subtracted* M^2_{rec} *spectrum for* $l^+\pi^-$ *(points with errors) and* $l^+\pi^+$ *(histogram) combinations [78]*

normalization. This means that the pion is generally soft enough so as not to have a strong correlation with the lepton and that this correlation is charge independent. The influence of the correlations on the wrong-sign distribution was estimated by taking particles from different events, *i.e.* replacing all correlated pairs by uncorrelated ones. No significant difference was seen in the M^2_{rec} spectra for mixed and real events.

Subtracting the background using the wrong-sign M^2_{rec} spectrum ARGUS obtained the distribution shown in Figure (2.24). The resulting spectrum was fitted by using contributions from both the D^{*+} and D^{**} channels. The expected shapes of these contributions for the M^2_{rec} distribution were derived from a Monte Carlo simulation based on the GISW model. Possible backgrounds from $B \to \tau X, \tau \to \ell Y$ and $B \to D_s x, D_s \to \ell Y$ were estimated using a Monte Carlo simulation and found to be negligible. From the fit we find

$$N_{D^*} = 2693 \pm 183 \pm 105$$

and

$$N_{D^{**}} = 423 \pm 138 \pm 35.$$

The acceptance was obtained from a Monte Carlo simulation using the GISW model [59]. The overall efficiency was determined to be 0.201 ± 0.015. With $\mathrm{BR}(D^{*+} \to D^0\pi^+) = (68.1 \pm 1.0 \pm 1.3)\%$ [17] ARGUS obtains

$$\mathrm{BR}(\overline{B}^0 \to D^{*+}\ell^-\overline{\nu}) = (4.5 \pm 0.3 \pm 0.4)\%$$

The systematic error reflects uncertainties in the fit procedure, the acceptance determination, the number of B^0 mesons, and the D^{*+} branching ratio.

Averaging both measurements on the branching ratio for the decay $\overline{B}^0 \to D^{*+}\ell^-\overline{\nu}$, ARGUS obtains finally

$$\mathrm{BR}(\overline{B}^0 \to D^{*+}\ell^-\overline{\nu}) = (4.6 \pm 0.5)\%.$$

From this branching ratio a value of $|V_{cb}|$ can also be deduced [59, 68, 69]:

$$|V_{cb}| = 0.034 \pm 0.002 \pm 0.005.$$

2.6.2 The decay $B^- \to D^{*0}\ell^-\overline{\nu}$

ARGUS was also the first experiment to measure the decay $B^- \to D^{*0}\ell^-\overline{\nu}$ [79]. Again, the unobserved neutrino is inferred from the recoil mass squared, M^2_{rec}. D^{*0} mesons are reconstructed in the decay chain $D^{*0} \to D^0\gamma$ followed by the decay of the D^0 meson into the $K^-\pi^+, K^-\pi^+\pi^-\pi^+$ or $K^0_s\pi^+\pi^-$ final states. The main difficulty in the D^{*0} reconstruction arises from the large combinatorial background created by the many soft photons from π^0 decays. In order to reduce this background no more than 5 photons were allowed per event and photons from π^0 decays were efficiently removed by eliminating those photon pairs whose invariant mass lay within $\pm 50 MeV/c^2$ of the nominal π^0 mass. The invariant $D^0\gamma$ mass is shown in Figure 2.25 for cuts in the recoil mass squared $|M^2_{rec}| < 1 GeV^2/c^4$ and after subtraction of the background under the D^0 signal and the contribution from faked leptons. The background to the decay $B^- \to D^{*0}\ell^-\overline{\nu}$ arises mainly from other semileptonic B decays into D^0 and ℓ^- where the D^0 does not come from a D^{*0}. This background has been modelled according to the GISW model. The solid curve in Figure 2.25 shows the result of the fit which finds 244 ± 46 events for the D^{*0} signal.

Part of the D^{*0} signal results from continuum events, $B^0\overline{B}^0$mixing, $\overline{D}^{*0}$ misinterpreted as D^{*0}, or D^{*0} plus cascade leptons. Subtracting this background leaves 224 ± 47 events for the decay $B^- \to D^{*0}\ell^-\overline{\nu}$ which translates into a branching ratio

$$\mathrm{BR}(B^- \to D^{*0}\ell^-\overline{\nu}) = (5.4 \pm 1.3 \pm 1.2)\%$$

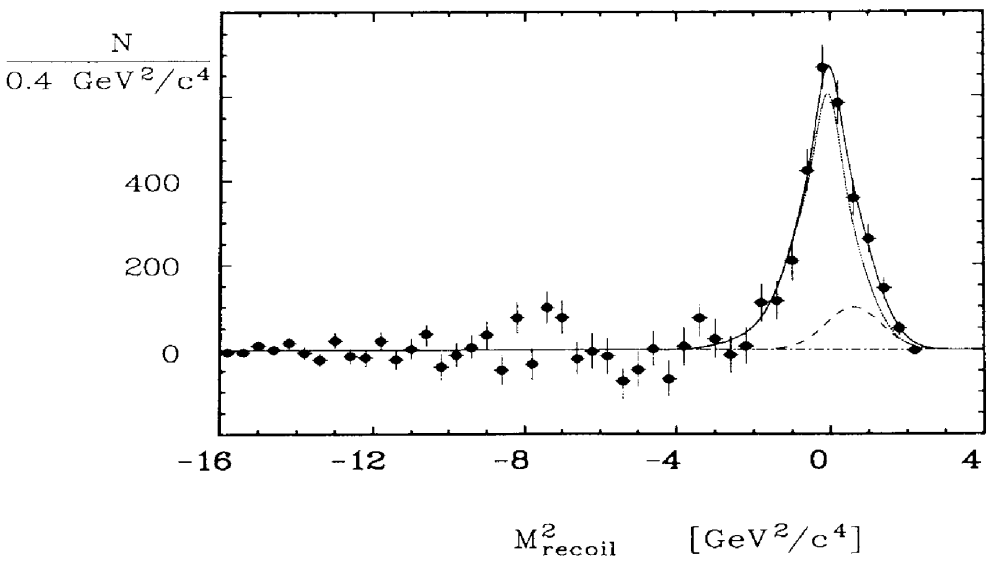

Figure 2.24: *Background subtracted M^2_{rec} spectrum for right-sign ($\ell^+\pi^-$) combinations [78]. The curves show the result of the fit described in the text*

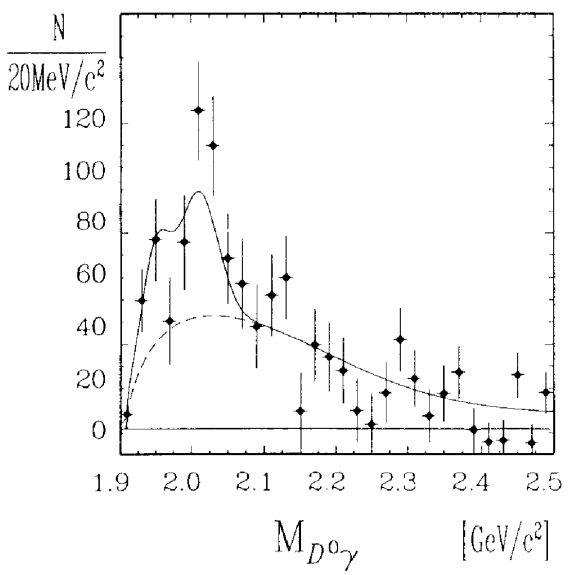

Figure 2.25: *$D^0\gamma$ invariant mass distribution for $|M^2_{rec}| < 1$ GeV$^2/c^4$ after subtraction of the background under the D^0 signal and of the contribution from faked leptons [79]. The solid line represents the fit result for the D^{*0} signal, the calculated background is shown as the dashed line*

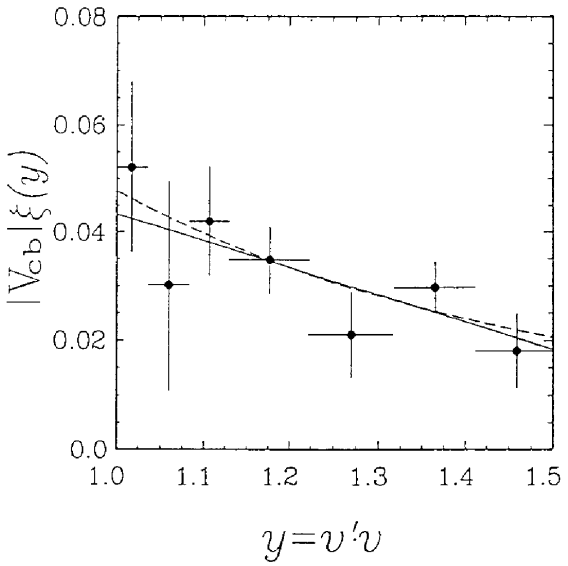

Figure 2.26: $|V_{cb}| \cdot \xi(y)$ *distribution for* $\tau_{B^0} = 1.27$ ps *[79]. The solid line shows the fit result for a linear parametrization of the Isgur-Wise Function. The dotted line shows the fit result with a single pole parametrization*

with D^0 branching ratios from [17]. This branching ratio is consistent with the one from the corresponding B^0 decay (previous section).

This measurement also allows for a determination of $|V_{cb}|$ from the y distribution of this decay shown in Figure 2.26. With a linear parametrization of the Isgur-Wise function the y distribution for the decay $B^- \to D^{*0}\ell^-\overline{\nu}$ results, at $y = 1$, in a value of $|V_{cb}| = 0.034 \pm 0.006$ using $\tau_{B^0} = 1.63$ ps [39].

2.6.3 The decays $\overline{B^0} \to D^+\ell^-\overline{\nu}$ and $B^- \to D^0\ell^-\overline{\nu}$

Extending the recoil mass technique, ARGUS was also able to investigate the exclusive semileptonic decays $\overline{B^0} \to D^+\ell^-\overline{\nu}$ and $B^- \to D^0\ell^-\overline{\nu}$ [80] [81]. These decay rates are of particular interest since they depend, in the form factor approach, only on one form factor which can be calculated rather reliably. Therefore these measurements are also very useful for a determination of $|V_{cb}|$.

The M^2_{rec} spectrum for the decay $\overline{B^0} \to D^+\ell^-\overline{\nu}$ is shown in Figure 2.27 after subtraction of backgrounds coming from the continuum under the $\Upsilon(4S)$ resonance, uncorrelated D^+ and ℓ^+ from different B decays, fake leptons and cascade decays. Taking into account also the feeddown from the cascade decay $B^0 \to D^{*-}\ell^+\nu$, $D^-(\pi^0,\gamma)\ell^+\nu$ which is analogous to the well understood decay mode $B^0 \to D^{*-}\ell^+\nu, D^0\pi^-\ \ell^+\nu$ ARGUS obtains :

$$\mathrm{BR}(B^0 \to D^+\ell^-\overline{\nu}) = (1.6 \pm 0.5 \pm 0.5)\%$$

A combined fit to $D^0\ell^-$, $D^+\ell^-$ and $D^{*+}\ell^-$ missing energy spectra [81] yields also a branching ratio for the decay $B^- \to D^0\ell^-\overline{\nu}$:

$$\mathrm{BR}(B^- \to D^0\ell^-\overline{\nu}) = (1.7 \pm 0.6 \pm 0.4)\%$$

which is consistent with the corresponding neutral B meson branching ratio.

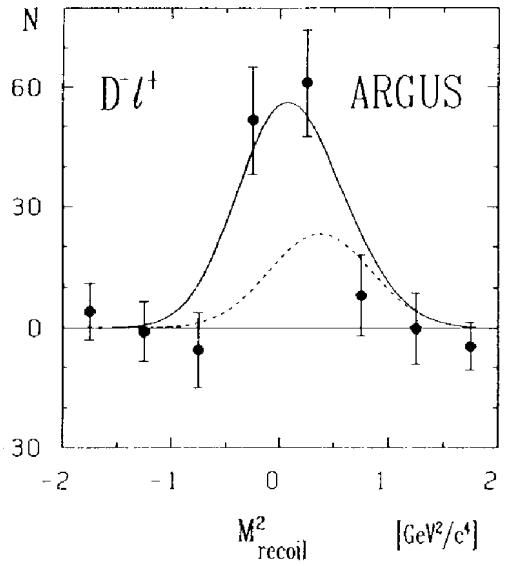

Figure 2.27: *M^2_{rec} distribution for the $D^-\ell^+$ system [80]. The dashed curve shows the contribution from the cascade decay $B^0 \to D^{*-}\ell^+\nu, D^-(\pi^0,\gamma)\ell^+\nu$*

Table 2.11: *Summary on exclusive semileptonic B decays*

Decay	*Branching ratio [%]*	$\|V_{cb}\|$
$\overline{B}^0 \to D^{*+}\ell^-\overline{\nu}$	4.6 ± 0.5	0.040 ± 0.005
$\overline{B}^0 \to D^{+}\ell^-\overline{\nu}$	1.6 ± 0.7	0.035 ± 0.008
$B^- \to D^{*0}\ell^-\overline{\nu}$	5.4 ± 1.8	0.039 ± 0.006
$B^- \to D^{0}\ell^-\overline{\nu}$	1.7 ± 0.7	0.036 ± 0.008
$\overline{B}^0 \to D^{**+}\ell^-\overline{\nu}$	2.4 ± 0.7	

These results correspond to a decay rate

$$\Gamma(B \to D\ell^-\overline{\nu}) = (0.010 \pm 0.04)\text{ps}^{-1}$$

using $\tau_B = 1.63$ ps [39]. A comparison with a theoretical prediction [69] :

$$\Gamma_{th}(B \to D\ell^-\overline{\nu}) = 8.3 \cdot |V_{cb}|^2\text{ps}^{-1}$$

leads to

$$|V_{cb}| = 0.035 \pm 0.007$$

in good agreement with the other determinations of $|V_{cb}|$.

2.6.4 Observation of D^{**} mesons in semileptonic B decays

The ARGUS results on exclusive semileptonic $b \to c$ decays are summarized in Table 2.11. One observes that the results are very consistent. However, it is also obvious that the sum of the measured exclusive semileptonic branching ratios into D or D^* mesons does not saturate the inclusive rate. The average branching ratio for exclusive semileptonic B^0 and B^+ decays into exclusive final states with D or D^* mesons is only $(6.7 \pm 1.1)\%$ compared to the measured inclusive rate of $(9.6 \pm 0.6)\%$ from the model independent approach (see section 2.4). Additional exclusive semileptonic B decays with higher excited D mesons must exist.

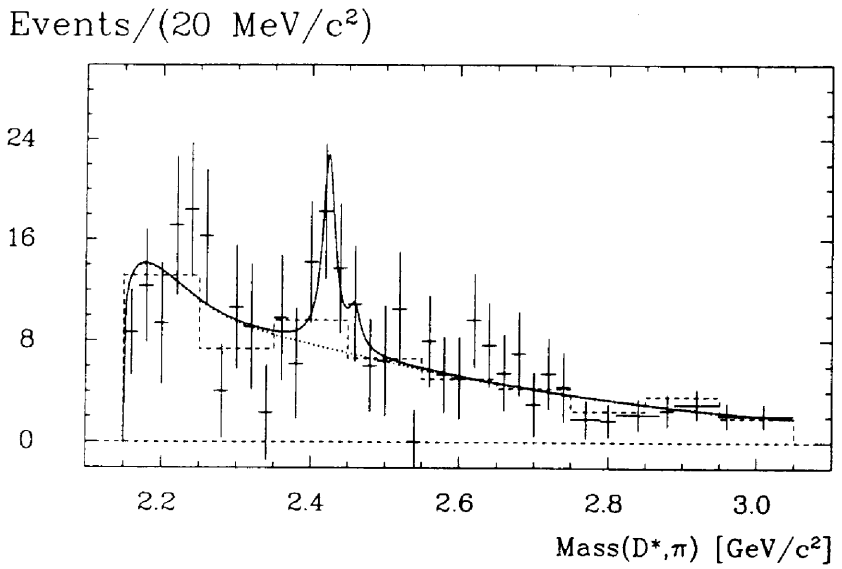

Figure 2.28: *Invariant $(D^{*+}\pi^-)$ mass (points with error bars) obtained for $M^2_{rec} > 0$ [75]. The dotted curve describes the background obtained from the $(D^{*+}\pi^-)$ mass distribution for $M^2_{rec} < 0$*

These decays $\overline{B}^0 \to D^{**+}\ell^-\overline{\nu}$ have been observed for the first time by ARGUS as a by-product of the investigation of the decay $\overline{B}^0 \to D^{*+}\ell^-\overline{\nu}$ as mentioned earlier. In Figure 2.21 contributions from higher excited D mesons appear mainly at positive values of M^2_{rec} with $63 \pm 15 \pm 6$ candidates. Figure 2.28 shows the measured invariant $D^{*+}\pi^-$ mass for these events. An enhancement of 30 ± 10 candidates at the known masses of the P-wave D states (see section 3.2) is observed which are attributed to the decay $\overline{B}^0 \to D^{**+}\ell^-\overline{\nu}$. From the observed shoulder in the M^2_{rec} distribution we expect 35 ± 9 D^{**} candidates. An estimate of the branching ratio for this process has been made by using model predictions for the relative production rate of the higher excited D states in semileptonic B decays [59]. ARGUS obtains:

$$\mathrm{BR}(\overline{B}^0 \to D^{**+}\ell^-\overline{\nu}) = (2.4 \pm 0.5 \pm 0.5)\%$$

This result implies that, within still rather large errors, the inclusive semileptonic branching ratio is saturated by the exclusive semileptonic B decays to D, D^* and D^{**} and that there is only little room left for semileptonic non $b \to c$ decays. The existence of D^{**} mesons in semileptonic B decays has been confirmed by recent LEP results [83].

2.6.5 Search for exclusive semileptonic $b \to u$ decays

Searches for exclusive semileptonic $b \to u$ decays have resulted in the detection of one event with a $\overline{B}^0 \to \pi^+\ell^-\overline{\nu}$ decay (Figure 2.20). However, no branching ratio could be given for this decay. Only upper limits for exclusive semileptonic $b \to u$ decays like $\overline{B}^0 \to \pi^+\ell^-\overline{\nu}$ or $B^- \to \rho^0\ell^-\overline{\nu}$ could be determined. None of these results is in conflict with the observed inclusive semileptonic $b \to u$ rate [84].

2.7 Summary of semileptonic B decays

The ARGUS results on inclusive and exclusive semileptonic B decays give a consistent picture. The measured model independent branching ratio

$$\mathrm{BR}(B \to e\nu X) = (9.6 \pm 0.6)\%$$

is smaller than theoretically expected. It is saturated by the exclusive semileptonic B decays into final states with D, D^* and D^{**} mesons. All determinations of $|V_{cb}|$ are consistent which each other. The most precise value is obtained from the model independent inclusive decay rate together with the Heavy Quark Expansion [60]:

$$|V_{cb}| = 0.0379 \pm 0.0018.$$

The value of $|V_{ub}|$ is about an order of magnitude smaller.

The semileptonic B decays can also be used to determine the lifetime assuming equal semileptonic rates for charged and neutral B mesons:

$$\frac{\tau_{B^+}}{\tau_{B^0}} = \frac{BR(B^+ \to \ell X)}{BR(B^+ \to \ell X)}$$

and approximating [85]

$$\frac{BR(B^+ \to \ell X)}{BR(B^0 \to \ell X)} = \frac{BR(B^+ \to D^{*0}, D^0 \ell^- \nu)}{BR(B^0 \to D^{*+}, D^+ \ell^- X)}$$

The resulting value of $\frac{\tau_{B^+}}{\tau_{B^0}} = 1.14 \pm 0.36 \pm 0.25$ is in good agreement with the now directly measured value $\frac{\tau_{B^+}}{\tau_{B^0}} = 0.98 \pm 0.09$ [17].

2.8 $B^0\overline{B}^0$Mixing and the Measurement of $|V_{td}|$

The most important ARGUS result was the discovery of $B^0\overline{B}^0$mixing in 1987 [1]. $B^0\overline{B}^0$mixing occurs in the Standard Model through second order weak interactions as described by the "box-diagrams" (Figure 2.29) where contributions from the t quark dominate. Since in 1987 the mass of the top quark was believed to be about 40 GeV/c^2 [86], only a small and undetectable effect for $B^0\overline{B}^0$ mixing was expected. The ARGUS observation has far reaching consequences which will be discussed at the end of this section.

$B^0\overline{B}^0$mixing leads to a mass difference ΔM between the CP-eigenstates. ΔM is obtained from the evaluation of the "box"-diagrams and is given by [87, 88]:

$$x = \frac{\Delta M}{\Gamma} = \frac{G_F^2}{6\pi^2} B_B f_B^2 M_B \tau_b \left|V_{tb}^* V_{td}\right|^2 m_t^2 F(\frac{m_t^2}{M_W^2}) \eta_{QCD}. \tag{2.11}$$

with $\Gamma = 1/\tau_{B^0}$.

In this expression, reasonably well known quantities are G_F, the mass of the B^0mesons, the B^0lifetime, the QCD correction η_{QCD}, and the functional dependence $F(\frac{m_t^2}{m_W^2})$. There are estimates from lattice QCD for the decay constant f_B and the bag factor B_B. The mass of the top quark m_t is obtained from the CDF and D0 measurements [9] and the correction factor η_{QCD} has been calculated to be about $\eta_{QCD} = 0.55$ [89]. Thus, x can be used as a measure of the CKM matrix element $|V_{td}|$.

At the $\Upsilon(4S)$ the determination of the CKM matrix element $|V_{td}|$ can be made by measuring the mixing parameter r which is defined as the ratio of the probability that an initially produced B^0 meson decays as a $\overline{B}^0$to the probability that an initially produced B^0 meson decays as a B^0:

$$r = \frac{Prob(B^0 \to \overline{B}^0)}{Prob(B^0 \to B^0)} = \frac{x^2}{2 + x^2}.$$

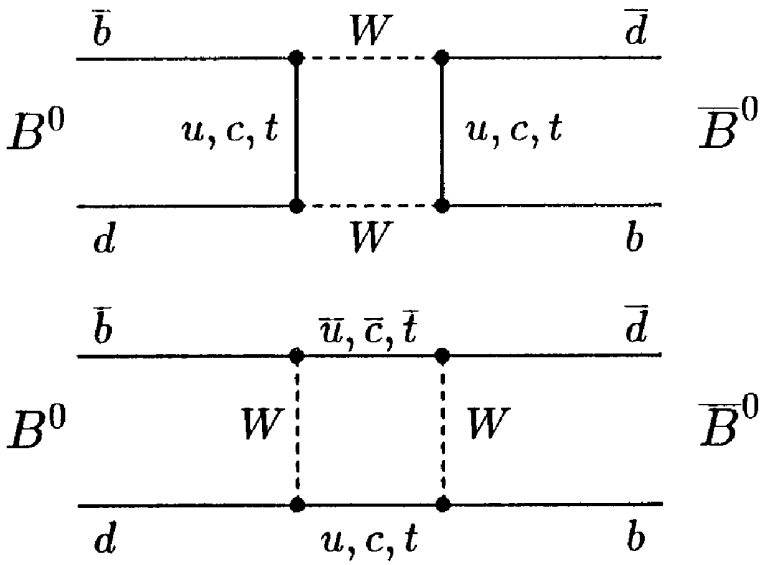

Figure 2.29: *Box diagrams for $B^0\overline{B}^0$transitions*

At the $\Upsilon(4S)$ resonance, $B^0\overline{B}^0$mixing manifests itself in the production of B^0B^0 or $\overline{B}^0$Baz mesons in the final state. The straightforward strategy for the observation of $B^0\overline{B}^0$mixing is to completely reconstruct the two neutral B mesons in the $\Upsilon(4S)$ decay. This, however, is not trivial because of the small reconstruction efficiency. Nevertheless, the approach of searching for fully reconstructed $\Upsilon(4S)$ decays into B^0B^0 or $B^0\overline{B}^0$pairs led to the discovery of $B^0\overline{B}^0$mixing. ARGUS succeeded in completely reconstructing a decay $\Upsilon(4S)\rightarrow B^0B^0$ where both B^0 mesons decay as $B^0\rightarrow D^{*-}\ell^+\nu$ with the following decay chains:

$$\begin{array}{llll} B^0\rightarrow & D_1^{*-} & \mu_1^+ & \nu_1 \\ & \hookrightarrow & \overline{D}^0 & \pi_{1s}^- \\ & & \hookrightarrow & K_1^+\pi_1^- \end{array} \quad and \quad \begin{array}{llll} B^0\rightarrow & D_2^{*-} & \mu_2^+ & \nu_2 \\ & \hookrightarrow & D^- & \pi^0 \\ & & \hookrightarrow & K_2^+\pi_2^-\pi_2^- \end{array}$$

In this simple event (Figure 2.30) all particles are well identified and the masses of the intermediate states agree well with the table values. Kinematic considerations show that the event is completely reconstructed. The background for this event was found to be completely negligible.

This one event demonstrates that the phenomenon of $B^0\overline{B}^0$mixing does exist. However, a determination of the $B^0\overline{B}^0$mixing parameter r needs other analysis methods which provide much better statistics but also give flavor identification of both B mesons at the time of their decay. This can be done by the reconstruction of one B meson and tagging the flavor of the other B by the charge of the lepton emitted in its semileptonic decay. The $B^0\overline{B}^0$oscillation strength r is then given by

$$r = \frac{N(\overline{B}^0\ell^-) + N(B^0\ell^+)}{N(\overline{B}^0\ell^+) + N(B^0\ell^-)}. \tag{2.12}$$

With the partial reconstruction of $\overline{B}^0$mesons in the decay $\overline{B}^0 \rightarrow D^{*+}\ell^-\overline{\nu}$ as described in the previous section the results shown in Table 2.12 are obtained. After background subtraction ARGUS obtains from the measured signals: $r = 0.231 \pm 0.118 \pm 0.034$ [90].

The statistical uncertainty can be considerably reduced by reconstructing B^0 mesons in the channel $B^0\rightarrow D^{*-}\ell^+\nu$ where, besides the undetectable neutrino, the $\overline{D}^0$ from the decay $D^{*-}\rightarrow\overline{D}^0\pi^+$ remains also undetected (see section 2.6.1). Figure 2.31 shows the M_{rec}^2 spectra for events which contain,

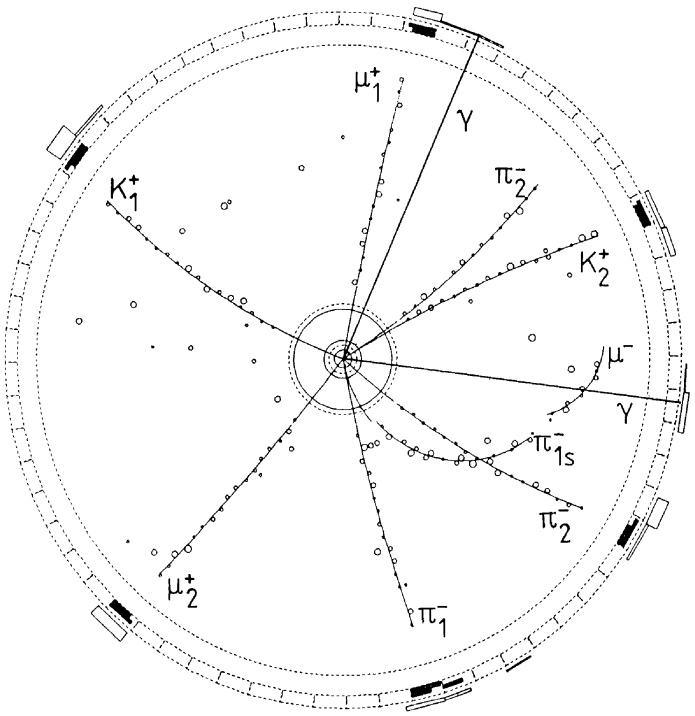

Figure 2.30: *Completely reconstructed event consisting of the decay* $\Upsilon(4S) \to B^0 B^0$ *(see text; [1])*

Table 2.12: *Observed* $\overline{B}^0 \ell^{\pm}$ *rates [90]*

	$\overline{B}^0 \ell^-$	$\overline{B}^0 \ell^+$
$\Upsilon(4S)$	10	33
Background D^{*+} combinatorics + D^{**} contributions	1.9 ± 0.9	3.3 ± 1.3
Cascade decays	0.76 ± 0.3	0.15 ± 0.04
Fakes	0.6 ± 0.15	0.5 ± 0.15
Signal	$6.7 \pm 3.2 \pm 1.0$	$29.1 \pm 5.7 \pm 1.3$

Table 2.13: *Dilepton rates from ARGUS [90]*

	Like-sign	Unlike-sign
	Dileptons	
$\Upsilon(4S)_{dir}$	96.4	551.5
Fakes	16.1	32.6
Secondaries	32.2	13.9
Signal	$48.1 \pm 11.4 \pm 8.3$	$505.1 \pm 25.4 \pm 9.9$

besides the $\ell^+\pi^-$ combination from which M^2_{rec} is calculated, also a high momentum lepton. If this tagging lepton has negative charge, the event is considered to be a mixed candidate.

The term $N(\overline{B}^0\ell^-) + N(B^0\ell^+)$ which enters equation 2.12 is given by the content in the peak at $M^2_{rec} = 0$ in Figure 2.31a and $N(\overline{B}^0\ell^+) + N(B^0\ell^-)$ by the corresponding one in Figure 2.31b. The analysis of the spectra in Figure 2.31 leads to

$$N(\overline{B}^0\ell^+) + N(B^0\ell^-) = 26.5 \pm 8.0$$

and

$$N(\overline{B}^0\ell^-) + N(B^0\ell^+) = 129.8 \pm 14.0$$

events. After correcting for the exclusion of leptons from J/ψ decays, one obtains a mixing parameter of [90]

$$r = 0.194 \pm 0.062 \pm 0.054.$$

in agreement with the value of the first measurement.

The second method of measuring $B^0\overline{B}^0$oscillation parameter r is based on tagging both B^0 mesons with fast leptons. The like-sign lepton pairs again provide candidates for mixed events. In calculating r one has to account for the decay $\Upsilon(4S) \to B^+B^-$ which produces only primary $\ell^+\ell^-$ pairs, by a factor:

$$\lambda = \frac{f^+}{f^0}(\frac{\tau_{B^+}}{\tau_{B^0}})^2$$

which enters the formula for r:

$$r = \frac{N_{\ell^\pm\ell^\pm}(1+\lambda)}{N_{\ell^+\ell^-} - N_{\ell^\pm\ell^\pm}\cdot\lambda}.$$

f^+ is the branching ratio for the $\Upsilon(4S)$ decay into B^+B^- f^0 the corresponding one for the decay into $B^0\overline{B}^0$. The determination of the fraction $\frac{f^+}{f^0}$ is based on the small mass difference between charged and neutral B mesons [25] and results in $\frac{f^+}{f^0} = 1.0 \pm 0.05$. Using $\frac{\tau_{B^+}}{\tau_{B^0}} = 0.98 \pm 0.09$ (section 2.7) λ is found to be 0.96 ± 0.19.

From the combined electron and muon dilepton rates shown in Table 2.13 the mixing parameter is determined to be

$$r = 0.205 \pm 0.054 \pm 0.069$$

where the first error is statistical and the second systematic. The uncertainty on the correction factor λ is included in the systematic error.

This measurement is in agreement with the original measurement [1] and with the one from the first method. The dilepton measurement should, however, *not* be combined with the result of the B^0 reconstruction using the partial D^{*-} reconstruction since the results are strongly correlated. Combining the dilepton results with the first measurements and taking into account 3 mixed and 13 unmixed events which are present in both data samples, the ARGUS number on the mixing rate is

$$r = (20.6 \pm 7.0)\%.$$

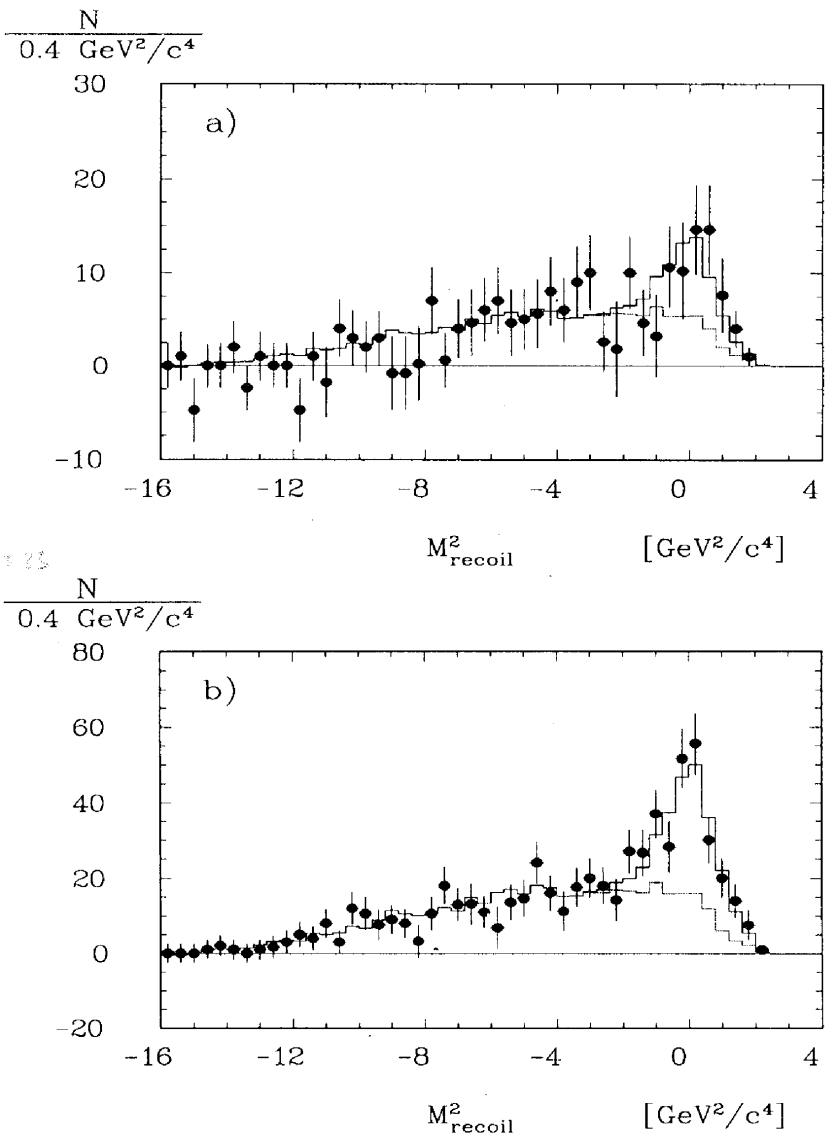

Figure 2.31: M^2_{rec} *spectra [90] for* $l^+\pi^-$ *(points with errors) for events with an additional lepton with momentum* $1.4 < p_l < 2.5$ *: background (dotted histogram) and the result of the fit (full histogram) a) for like-sign leptons; b) for unlike-sign leptons*

For the mixing parameter x the ARGUS result implies:

$$x = 0.72 \pm 0.15.$$

Using formula 2.11 the CKM matrix element $|V_{td}|$ can be determined. Since the value $\eta_{QCD} = 0.55$ is calculated in the $\overline{MS}$ scheme [89], consistency requires that the mass of the top quark be rescaled from its pole mass of $m_t = (174 \pm 15)$ GeV/c^2 [9]to the value $\overline{m_t}$ in the $\overline{MS}$ scheme, which is typically 9 MeV smaller. Using $B_B f_B^2 = (1.0 \pm 0.2)(180 \pm 50)^2 \mathrm{MeV}^2$ [91] ARGUS finds for $|V_{td}|$:

$$|V_{td}| = (0.98 \pm 0.10 \pm 0.11 \pm 0.27 \pm 0.10 \pm 0.036) \cdot 10^{-2}$$

where the errors come from the errors on x_d, m_t, f_B, B_B and τ_b. The largest error comes from the uncertainty in f_B. Combining all errors the ARGUS result is

$$|V_{td}| = (0.0098 \pm 0.0033).$$

The ARGUS observation of $B^0\overline{B}^0$mixing was confirmed in 1989 by CLEO [92]. Later, in 1993, the LEP experiments were able to determine the oscillation frequency ΔM_d from the time evolution of $B^0\overline{B}^0$mixing. It is amazing to see how well all results on $B^0\overline{B}^0$mixing coincide with the original ARGUS measurement.

2.9 Conclusions

ARGUS has made significant contributions to our knowledge of B physics. The experiment has shown in a convincing manner that B physics is of great interest and provides a key for a better understanding of the Standard Model. ARGUS paved the way for the determination of the fundamental CKM matrix elements $|V_{cb}|, |V_{ub}|$, and in particular $|V_{td}|$ by measuring inclusive and exclusive semileptonic B decays as well as $B^0\overline{B}^0$mixing. ARGUS performed the first successful reconstruction of exclusive B decays in several hadronic channels. The many results on exclusive and inclusive B decays were confronted with various models in order to improve theoretical concepts. The results also serve as input for future measurements of the top quark and searches for new particles like the Higgs.

The first observation of $B^0\overline{B}^0$mixing represents the most important of the many discoveries made by ARGUS which had far reaching consequences for new experiments and machines [10, 11, 12]. This discovery opened up prospects for understanding the origin of CP violation by studying this phenomenon in B decays: the unexpectedly large $B^0\overline{B}^0$mixing potentially implies large CP violation in the neutral B system as well since any asymmetry between decay rates for B^0 and $\overline{B}^0$is proportional to the mixing parameter x.

The best candidate for the study of CP violation is to search for an asymmetry A in the decays $B^0, \overline{B}^0 \to J/\psi K_s^0$ for which a prediction exists which is free of any uncertainty:

$$A = \frac{\Gamma(B^0 \to J/\psi K_s^0) - \Gamma(\overline{B}^0 \to J/\psi K_s^0)}{\Gamma(B^0 \to J/\psi K_s^0) + \Gamma(\overline{B}^0 \to J/\psi K_s^0)}$$

$$= \frac{x}{1 + x^2} \sin 2\beta$$

where x is the $B^0\overline{B}^0$mixing parameter and β is an angle in the unitarity triangle (Figure 2.2). Large, expensive and challenging projects are under way to perform this measurement in the near future [10, 11, 12]. First results are expected by 1998 [10].

B physics has acquired a large importance over the last 10 years, in particular through the ARGUS experiment. For the new hadron machines at CERN and FNAL the physics of B hadrons represents an essential scientific goal.

Chapter 3

Charm Physics

3.1 Introduction

The existence of the charm quark was first postulated by Glashow, Iliopoulos, and Maiani [93] in 1970 in order to explain the absence of flavour changing neutral currents. This fourth quark remained hypothetical until the 1974 discovery of the J/ψ meson by groups working at SLAC[94] and Brookhaven[95]. The J/ψ is a $c\bar{c}$ bound-state decaying to non-charmed final states and is said therefore to carry hidden charm. The first particles with open charm (D^0 and D^+ mesons) were discovered at SLAC in 1976[96].

Since that time, the study of the production, spectroscopy and decays of charmed mesons and later charmed baryons has been an extremely fruitful area of elementary particle physics. ARGUS made many significant contributions to this field with the first observations of new charmed hadrons, detailed studies of leptonic and non-leptonic weak decays and measurements of charmed particle lifetimes. The available sample of charmed hadrons collected with the ARGUS detector corresponds to about 600 thousand D^0 mesons, 300 thousand D^+ mesons and about 250 thousand ground-state charmed baryons: Λ_c, Ξ_c, Σ_c and Ω_c which are produced in continuum e^+e^- collisions at center of mass energies around 10 GeV. These numbers result from the measured production cross-sections[47][97]

$$\begin{aligned} \sigma(e^+e^- \to D^0X) &= (1.18 \pm 0.15 \pm 0.08)\text{nb} \\ \sigma(e^+e^- \to D^+X) &= (0.65 \pm 0.09 \pm 0.09)\text{nb} \\ \sigma(e^+e^- \to \Lambda_c^+X) &= (0.30 \pm 0.08)\text{nb} \end{aligned}$$

The Λ_c production rate is estimated to account for roughly 60% of the charmed baryon production. Charmed hadrons are also copiously produced in the decays of the 400 thousand B mesons collected by ARGUS in running on the $\Upsilon(4S)$ peak.

From the earliest stages of its design, one of the primary fields of study at ARGUS was expected to be the investigation of charmed mesons produced in the fragmentation of the leading charm quarks produced in the process $e^+e^- \to c\bar{c} \to$ hadrons. The distinct feature of this method of charm quark production is the hard fragmentation function. This is visible in Figure 3.1 which shows the scaled momentum (x_p) distribution for D^{*+} mesons produced in continuum e^+e^- collisions where $x_p = p/P_{max}$, $P_{max} = (E_{beam}^2 - M^2)^{1/2}$[98]. Since the product of B meson decays are kinematically restricted to have $x_p \leq 0.5$, and because combinatorial background peaks at low values of x_p, in most analyses a clear signal for charmed hadrons can be obtained using a cut of $x_p \geq 0.5$. Alternatively, cuts in the scaled energy of $x_E \geq 0.5$ are applied, where x_E is analogously defined by $x_E = E/E_{beam}$. The study of fragmentation of charmed quarks is discussed further in chapter 7.

In this chapter the ARGUS results on the spectroscopy of charmed hadrons and the study of the weak decays of charmed particles are presented. Many of these results represented first observations

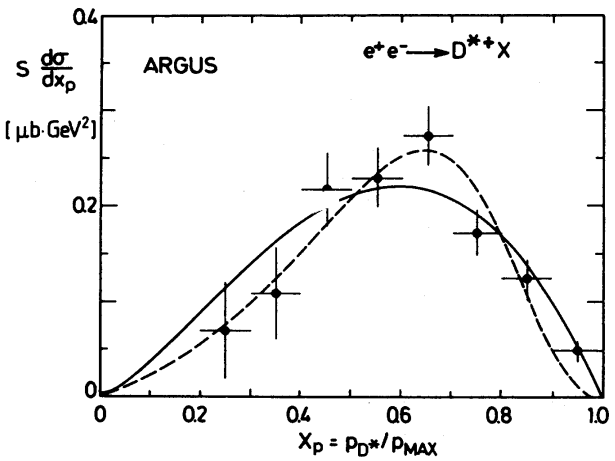

Figure 3.1: *$d\sigma/dx_p$ for the D^{*+} mesons produced in charm fragmentation [98]. The dotted and solid curves result from fits to theoretical models [99] [100].*

such as the discovery of P-wave charmed mesons, of the first excited baryons, or of particular weak decays of which the most important is the detection of the decay $D^0 \to \phi \bar{K}^0$, which was a big surprise. Other results improved on existing knowledge by providing more precise measurements.

3.2 Spectroscopy of Charmed Hadrons

3.2.1 Ground State Charmed Mesons

We use the term ground state here to include both the $^1S_1$ and $^3S_1$ $c\bar{q}$ states where $\bar{q}$ represents a light anti-quark $(\bar{u}, \bar{d}, \bar{s})$. The kinematic properties of the decay $D^{*+} \to D^0\pi^+$, which has a Q value of only 5.8 MeV, result in extremely good resolution for the mass difference $M(D^{*+}) - M(D^0)$. At ARGUS, D^{*+} mesons were first reconstructed[98] in the decay channels

$$\begin{aligned} D^{*+} \quad &\to \quad D^0\pi^+ \\ &\qquad \hookrightarrow K^-\pi^+, K^-\pi^+\pi^+\pi^- \end{aligned}$$

The resulting mass difference plots are shown in Figure 3.2. Clear peaks are seen in both channels. Overlaid on each plot is the result of a fit with a Gaussian to describe the signal and a polynomial to describe the background. The fitted mass difference averaged for two distributions was $\Delta M = (145.46 \pm 0.07 \pm 0.03)$ MeV/c^2. This value compared well with the then current world average of $\Delta M = (145.41 \pm 0.24)$ MeV/c^2[101] but had significantly improved errors. This result, obtained with only 40 pb^{-1} of early data at ARGUS, without a vertex chamber, is comparable to the 1994 world average of $\Delta M = (145.42 \pm 0.04)$ MeV/c^2 [17]. This is an indication of the capabilities of the ARGUS detector.

The vector mesons D^{*+} and D^{*0} may decay either via the strong interaction to $D\pi$ final states or electromagnetically to $D\gamma$. The rate for the electromagnetic decay is proportional to the magnetic moment of the constituent quarks [102], which allows an important test of Standard Model predictions for the heavy c-quark. The previous world average [103] of BR$(D^{*+} \to D^+\gamma) = (\ 18 \pm 4\ )\%$, could be explained only by invoking non-standard models, e.g. assuming a large anomalous magnetic moment for the charm quark [104]. A recent measurements from CLEO [105], confirmed by ARGUS[106], permits a solution of this discrepancy within the framework of the Standard Model. The ARGUS analysis yielded BR$(\ D^{*+} \to D^+\gamma) < 5.2\%$ (90% CL), which was much lower than the

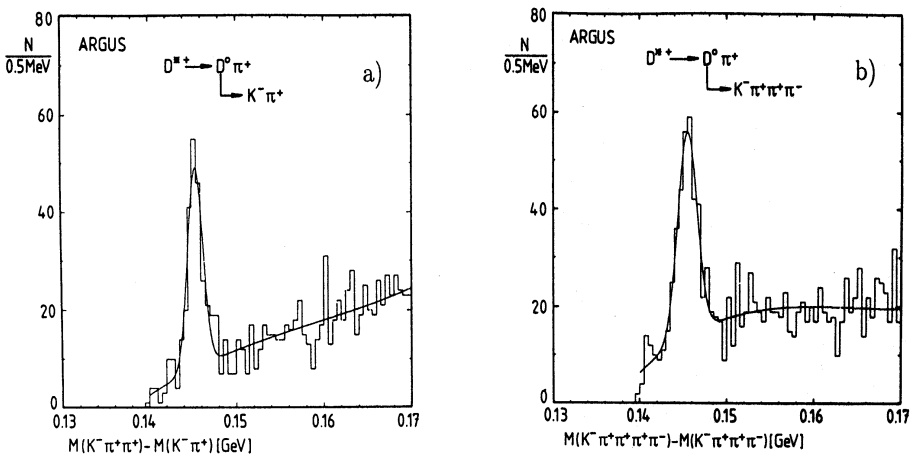

Figure 3.2: *Mass difference plots from D^{*+} analysis for $K^-\pi^+$ and $K^-\pi^+\pi^+\pi^-$ D^0 final states. Combinations in (c) are required to have $x_E > 0.6$ [98].*

earlier PDG value[103] and in good agreement with both the CLEO result and with Standard Model predictions. ARGUS has also measured the branching ratios BR($D^{*0}\to D^0\gamma$) = $(40.4 \pm 3.5 \pm 2.8)\%$ and BR($D^{*0}\to D^0\pi^0$) = $(59.6 \pm 3.5 \pm 2.8)\%$ Both are in good agreement with the current world averages [17].

Exploiting the excellent momentum resolution obtainable for converted photons, ARGUS used D^{*0} signals for a determination of the $D^{*0} - D^0$ mass difference. This result of $\Delta M = (142.2 \pm 0.3 \pm 0.2)$MeV/c^2 is in a good agreement with a precise measurement from the CLEO collaboration of $(142.12 \pm 0.05 \pm 0.05)$MeV/c^2 [107].

ARGUS contributions to the properties of the ground state charmed-strange mesons were also significant. The observation of the $D_s^+(1970)$ by the CLEO collaboration[108] was confirmed by both the TASSO[109] and ARGUS[110] collaborations. All these groups based their results on analysis of the decay channel

$$\begin{array}{rcl} D_s^+ & \to & \phi\pi^+ \\ & & \hookrightarrow K^-K^+ \end{array}$$

although ARGUS also included the channel $D_s^+ \to \phi\pi^+\pi^-\pi^+$. The ARGUS $\phi\pi^+$ and $\phi\pi^+\pi^-\pi^+$ invariant mass distributions from this analysis are shown in Figure 3.3. The masses obtained from the two channels were consistent and yielded a weighted average of $M_{D_s} = (1973.6 \pm 2.6 \pm 3.0)$ MeV/c^2. This compared well with the CLEO and TASSO results, $(1970 \pm 5 \pm 5)$ and $(1975 \pm 9 \pm 10)$ MeV/c^2 respectively, but had significantly smaller errors.

For the $c\bar{s}$ system, the quark model also predicts a spin-parity 1^- state analogous to the D^* state of the $c\bar{q}$ system. However, unlike the D^* meson, the D_s^* cannot decay strongly to the pseudoscalar state and a pion as this is forbidden by isospin invariance. This leaves the radiative decay as the dominant mode. Searching in the $D_s^+\gamma$ decay mode with the D_s^+ reconstructed in the $\phi\pi^+$ final state, ARGUS provided the first experimental evidence for this state[111]. In order to determine the mass of the D_s^{*+} the number of D_s^+ events was fitted in bins of the $\phi\pi^+\gamma$ invariant mass. The mass value obtained from the fit was then corrected for the fact that, due to limited photon energy resolution, the photon energy cut suppresses the lower tail of the D_s^{*+} peak, effectively shifting the peak upwards in mass. This procedure yielded a final D_s^{*+} mass of $(2109 \pm 9 \pm 7)$ MeV/c^2.

Using a much larger data sample, this measurement was improved by ARGUS in 1988[112]. The fitted D_s^+ mass was $(1969 \pm 1.4 \pm 1.4)$ MeV/c^2. D_s^{*+} candidates were searched for by combining $\phi\pi^+$

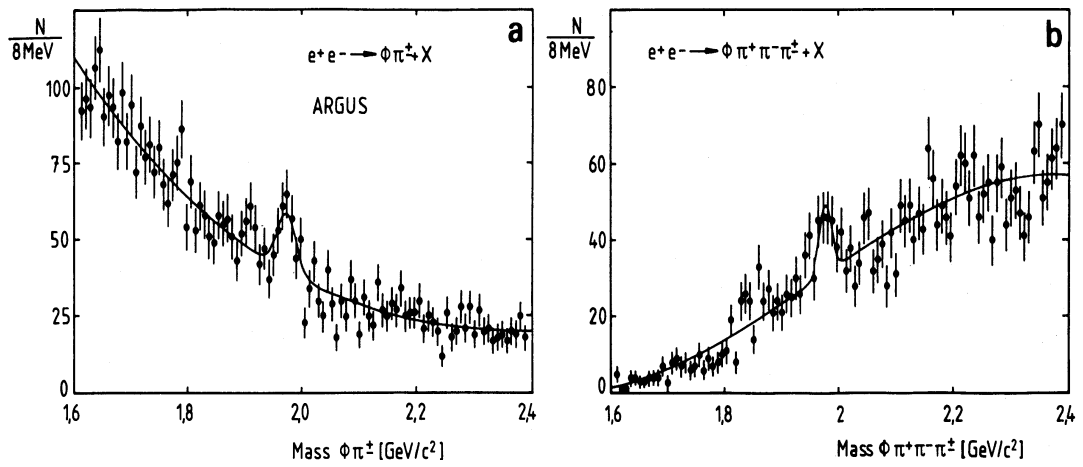

Figure 3.3: *$\phi\pi^+$ and $\phi\pi^+\pi^-\pi^+$ invariant mass distributions from D_s^+ analysis [110].*

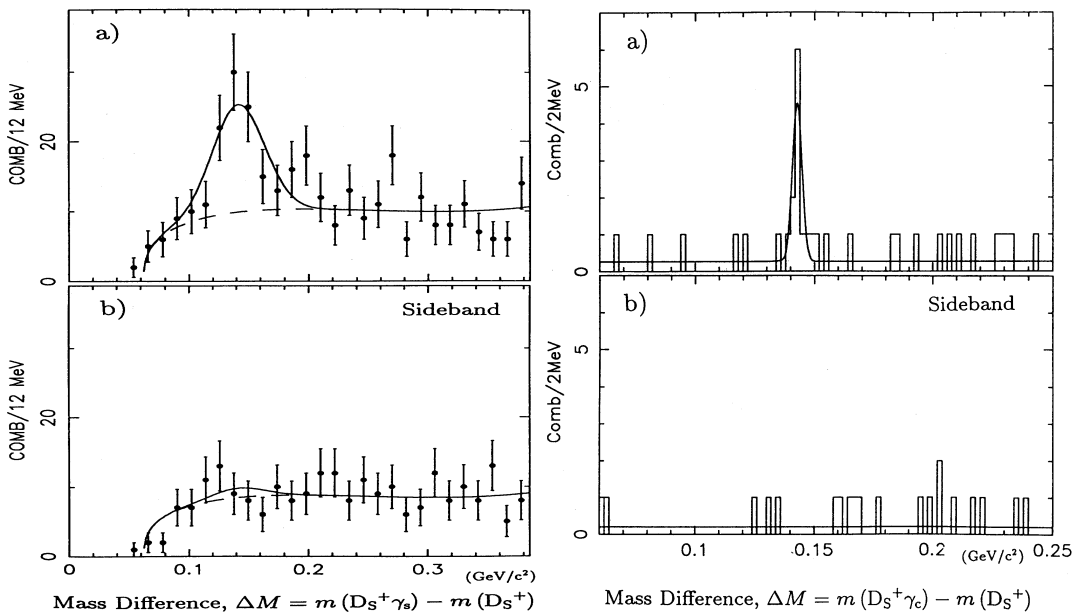

Figure 3.4: *Plots from analysis of $D_s^{+*} - D_s^+$ mass difference from the updated ARGUS analysis of 1988 [112]. the left and right plots respectively, show the $D_s^+\gamma$ invariant mass distributions obtained using shower photons (γ_s) and converted photons (γ_c). In each case both signal and sideband distributions are provided ((a) and (b)).*

candidates with photons in the appropriate kinematical region. Using the photons (γ_s) reconstructed from neutral energy deposits in the ARGUS electromagnetic calorimeter yielded the mass difference distribution shown in Figure 3.4(a). A clear peak is seen near threshold. The fitted mass difference, corrected for the photon energy cut as previously described, was

$$\Delta\mathrm{M} = M(D_s^+\gamma_s) - M(D_s^+) = (138.6 \pm 4.8 \pm 4.0)\ \mathrm{MeV/c^2}$$

The precision of the mass determination is greatly improved by performing a similar analysis using the converted photons (γ_c). This improvement in energy resolution is illustrated by the difference in

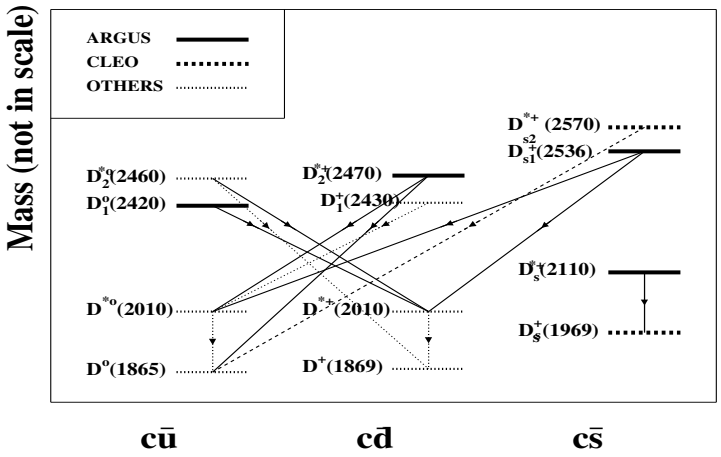

Figure 3.5: *Observed charmed mesons (schematic)*

the detector resolutions for π^0 reconstruction in the $\gamma_s\gamma_s$ and $\gamma_c\gamma_c$ final states which are (23.4 ± 0.4) and (5.2 ± 0.4) MeV/c^2 respectively. The resulting mass difference spectrum is shown in Figure 3.4(b) for the signal and sideband regions. Fitting with a Gaussian, allowing for a radiative tail, and assuming the background to be flat yielded

$$\Delta\mathrm{M} = M(D_s^+\gamma_c) - M(D_s^+) = (142.9 \pm 0.8)\ \mathrm{MeV/c^2}.$$

The two independent measurements of the mass difference yield a combined result of

$$\Delta\mathrm{M} = M(D_s^+\gamma) - M(D_s^+) = (142.5 \pm 0.8 \pm 1.5)\mathrm{MeV/c^2}$$

3.2.2 Excited Charmed Mesons

The 1985 discovery, by the ARGUS collaboration, of the first L=1 excited charmed meson[13] initiated a flurry of experimental activity and calls for the re-examination of early theoretical expectations for the properties of these states. This re-examination suggested analysis techniques useful in the study of these sates[113]. One feature of the mass predictions for the L=1 charmed mesons that complicates their description is that, in a heavy-light quark system, there is no quantum number which prevents the two $J^P = 1^+$ states from mixing. However, simple non-relativistic models show that in the limit as the charm quark mass is taken to infinity, this mixing produces a narrow 1^+ state degenerate with the 2^+ state, and a wide one degenerate with the 0^+ state.

Figure 3.5 illustrates the present experimental knowledge about charmed mesons. All 6 of the relatively narrow resonances expected have been observed by both ARGUS and CLEO as well as by a variety of other experiments.

The full decay sequences used for the ARGUS reconstruction of the first observed P-wave excited charmed meson [13] were

$$\begin{aligned} D_J^{(*)0} \;\rightarrow\; & D^*(2010)^+\pi^- \\ & \hookrightarrow D^0\pi^+ \\ & \quad\hookrightarrow K^-\pi^+ \end{aligned}$$

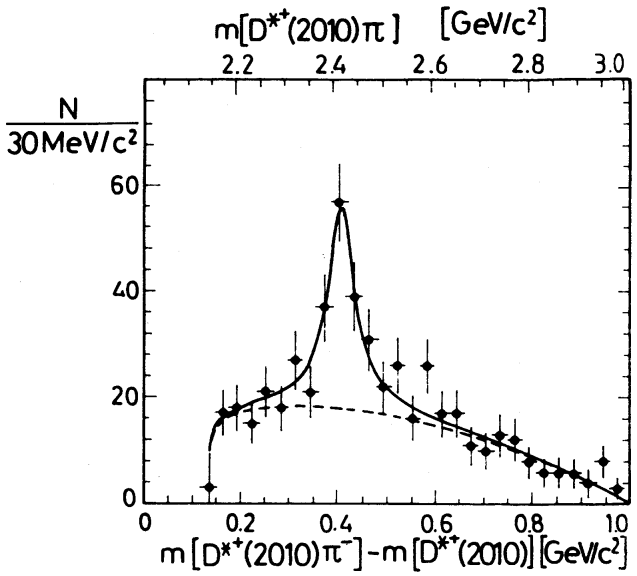

Figure 3.6: $D^{*+}\pi^-$ *invariant mass distributions for all final states [13].*

$$\hookrightarrow K^-\pi^+\pi^+\pi^-$$
$$\hookrightarrow K^-\pi^+(\pi^0)$$

In plotting the $D^{*+}\pi^-$ invariant mass distribution the mass-difference technique was used in order to obviate the need for π^0 reconstruction in the $K^-\pi^+\pi^0$ final state. The decay $D^0 \to K^-\pi^+\pi^0$ produces a satellite peak in the $K^-\pi^+$ invariant mass distribution which can be utilized without π^0 reconstruction if the mass-difference technique is used; this results in only a slightly degraded mass resolution. The resulting mass-difference spectra are shown combined in Figure 3.6. The distribution shows a significant enhancement just above $\Delta M = 400$ MeV/c^2. Overlaid on the distribution is the the result of a fit with polynomial background functions and non-relativistic Breit-Wigner distributions convoluted with Gaussian resolution functions to describe the signal. The fitted mass-difference and width were (410 ± 6) MeV/c^2 and (70 ± 21) MeV/c^2 respectively.

This resonance was interpreted as one of the lowest lying orbitally excited charmed mesons. Spin-parity conservation rules out the $J^P = 0^+$ assignment so the observed state was assumed to be either the 2^+ state, one of the 1^+ states, or a composite of some combination of these states. The ARGUS observation of the $D^{*0}(2420)$[1] in its decay to $D^{*+}\pi^-$ was confirmed by the E691 collaboration at Fermilab which simultaneously published evidence for the charged isospin partner of this state and the observation of an excited charmed meson decaying to $D^+\pi^-$[114]. The mass and width of this state, $(2459\pm3\pm2)$ MeV/c^2 and $(20\pm10\pm5)$ MeV/c^2 respectively, made it likely that it was the 2^+ resonance since that is expected to be the highest mass state and since the 0^+, which decays as an S-wave, is expected to be considerably broader. The existence of this state was confirmed by the ARGUS collaboration[115]. Examining the decay sequence

$$D_J^{(*)0} \to D^+\pi^-$$
$$\hookrightarrow K^-\pi^+\pi^+$$

ARGUS obtained the $D^+\pi^-$ mass-difference distribution shown in Figure 3.7(a). A clear peak is

[1] The symbol $D^{*0}(2420)$ is intended to refer to the composite $D^{*+}\pi^-$ resonance. Following the conventions of the Particle Data Group, the symbols $D_J^{(*)0}$ refer to specific J^P states.

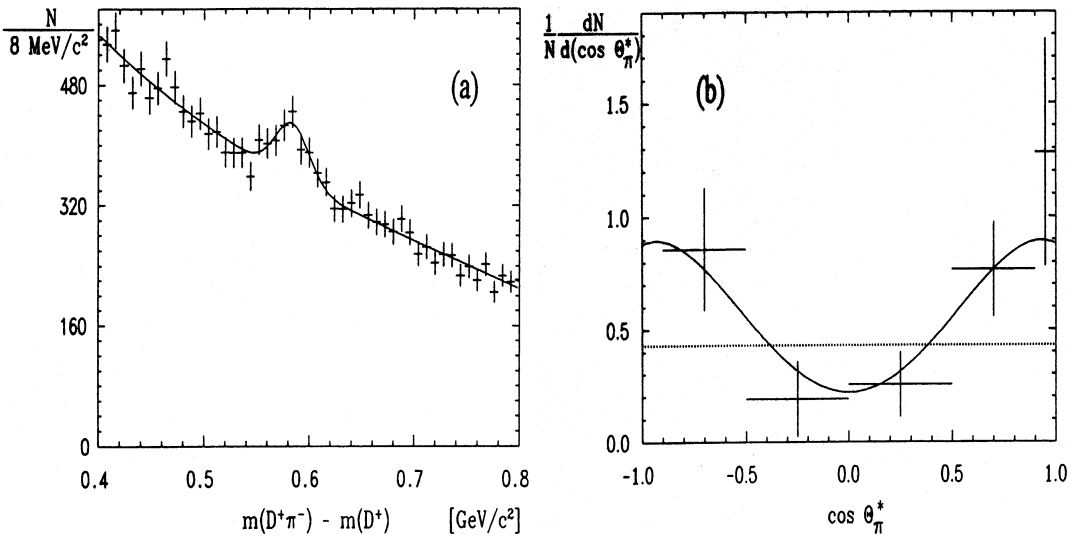

Figure 3.7: *Plots from analysis of the $D^+\pi^-$ final state. (a) shows the invariant mass distribution obtained using selection criteria described in the text. (b) shows the $\cos\theta_\pi$ angular distribution for signal (data points) and background (histogram). In both plots the overlaid lines are the results of the fits described in the text [115].*

observable at a mass difference around 585 MeV/c^2. The fitted mass-difference and width were $(585.4 \pm 2.7 \pm 5)$ MeV/c^2 and (15^{+13+5}_{-10-10}) MeV/c^2 respectively. The corresponding mass was $(2455 \pm 3 \pm 5)$ MeV/c^2 in agreement with the E691 result.

As a check on the spin-parity assignment, which earlier was based on expectations for the mass and widths of the 0^+ and 2^+ states, ARGUS examined the $\cos\theta_\pi$ angular distribution, where θ_π is defined as the angle between the pion flight direction and $D\pi$ boost direction, as measured in the $D\pi$ rest frame. For the 0^+ state decaying to $D^+\pi^-$ this distribution should be flat, while for a 2^+ decay the distribution can be non-isotropic if the states are produced with non-zero alignment. The acceptance corrected angular distribution is shown in Figure 3.7(b) and shows a marked deviation from isotropy. This is in contrast to the background distribution, overlaid as a histogram, which, as expected, peaks towards $\cos\theta_\pi = -1$. Parametrizing the distribution in terms of amplitudes to the different helicity states and fitting the resulting function to the measured distribution yielded a population of the ± 2 helicity states consistent with zero. Setting these identically to 0 and assuming equal population of the helicity ± 1 states yielded approximately equal populations for the helicity -1 ,0, and $+1$ states with a χ^2 of 1.4 for three degrees of freedom. The result of this fit is overlaid as a dashed line. Also shown as a dotted line is the result of a fit to an isotropic distribution which produces a much poorer χ^2/dof (11.4/4). Along with the arguments based on the high mass and narrow width of the observed state, this angular analysis provided compelling evidence for the 2^+ spin-parity assignment.

The discovery of a state decaying to $D^+\pi^-$ at a mass close to that observed for the enhancement in the $D^{*+}\pi^-$ invariant mass spectrum led quite naturally to the hypothesis that the state originally identified as the $D^{*0}(2420)$ was a composite comprised primarily of contributions from the $D_2^{*0}(2459)$ and the narrow 1^+ state. ARGUS led the way in establishing this fact using an analysis based on decay angular distributions. The three L=1 charmed mesons decaying to $D^{*+}\pi^-$ are expected to do so with very different distributions in the angle α, defined as the angle between the momentum vectors of the pions from the $D_J^{(*)0}$ and D^{*+} decays in the D^{*+} rest frame. The expected distribution for a 2^+ decay is of the form $\sin^2\alpha$. For a 1^+ state the situation is more complicated since there

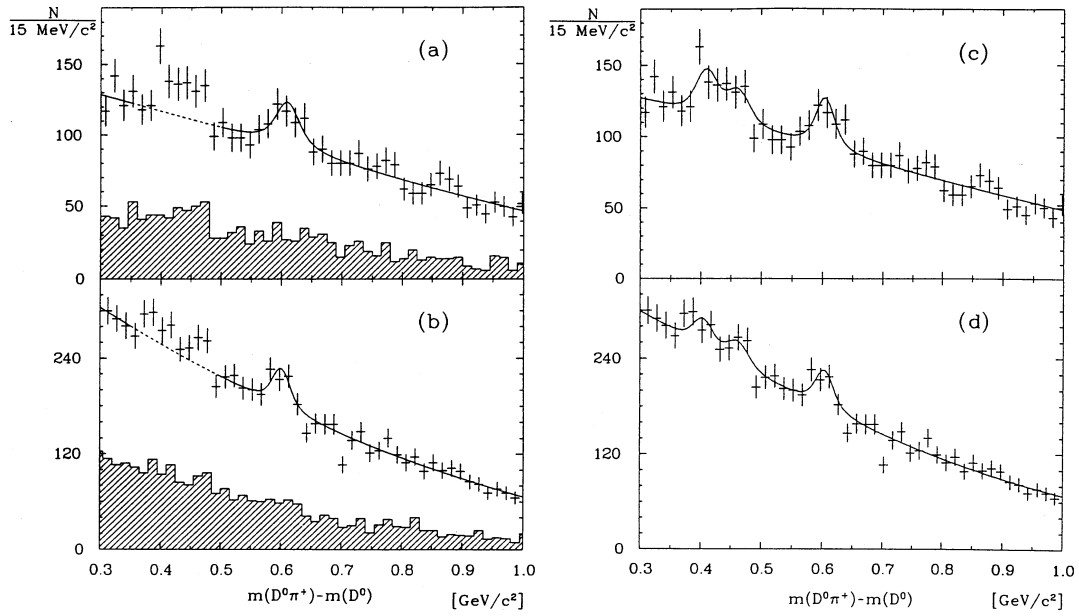

Figure 3.8: *Mass difference plots from analysis of $D^0\pi^+$ final states for each of the two D^0 final states. (a) and (b) were fitted using a polynomial background function and a single Breit-Wigner to describe signal contributions. Signal contributions in (c) and (d) were fitted with three Breit-Wigners in order to account for the feeddown contributions described in the text [117].*

are two allowed partial waves in the decay $D_1^0 \to D^*\pi$: an S-wave decay which should produce an isotropic distribution and a D-wave decay producing a distribution of the form $1 + 3\cos^2\alpha$. The ARGUS analysis of these angular decay distributions showed [116] that the $D^{*0}(2420)$ is consistent with being the a mixture of the narrow 1^+ and 2^+ states.

ARGUS was also the first collaboration to present evidence for the charged isospin partners of both the $D_2^{*0}(2459)$[117], and the $D_1^0(2414)$[118] although evidence for the charged isospin partner of the composite resonance had been published by E691[114]. The charged 2^+ state can be directly reconstructed in the decay sequence

$$\begin{aligned} D_2^{(*)+} \quad &\to \quad D^0\pi^+ \\ &\qquad \hookrightarrow K^-\pi^+ \\ &\qquad \hookrightarrow K^-\pi^+\pi^+\pi^- \end{aligned}$$

The mass difference spectra $\mathrm{M(D^0\pi^+) - M(D^0)}$ are shown in Figure 3.8 for both D^0 final states (data points). Overlaid as shaded histograms in a) and b) are the corresponding distributions for $D^0\pi^+$ combinations satisfying $|\cos\theta_\pi| < 0.4$. The motivation for this is the knowledge, obtained in the $D_2^{*0}(2459)$ analysis, of the $\cos\theta_\pi$ angular distribution which indicates that little signal contribution is expected in this kinematic region. Overlaid also are the results of fits using a polynomial background function and a Breit-Wigner convoluted with a Gaussian to describe the signal. The background region between $\Delta\mathrm{M} = 0.35 - 0.45$ is affected by feeddown from other decay sequences and was excluded from this fit. Better determination of the signal parameters is obtained if one first requires $|\cos\theta_\pi| > 0.4$. The final experimentally determined mass and width for the observed state were $2469 \pm 4 \pm 6$ and $27 \pm 12 \pm 10$ MeV/c^2, respectively. The widths of the two isospin partners are consistent with each other and the isospin mass-splitting for the 2^+ state is thus $M(D_2^{*+}) - M(D_2^{*0}) = (14 \pm 5 \pm 8)$ MeV/c^2.

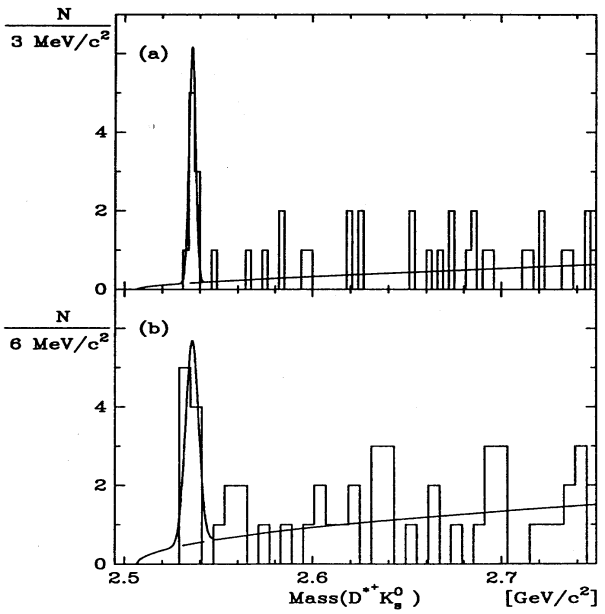

Figure 3.9: *Plots from the $D^{*+}K_s^0$ analysis using the (a) $K^-\pi^+$,$K^-\pi^+\pi^+\pi^-$ (b) $K^-\pi^+\pi^0$ for the D^0 reconstruction [119].*

The ARGUS evidence for the charged 1^+ state (D_1^+) is less direct but still convincing[118]. The $D^{*0}\pi^+$ final state was used to search for the D_1^+. The low Q-value for the decay $D^{*0} \to D^0\pi^0, D^0\gamma$ means that the slow neutral cannot be reconstructed. However, due to the low Q-value for the D^{*0} decay, the kinematics of the decay sequence are not greatly affected by the loss of the neutral. The effect of the missing neutral is to produce a mass shift and a slightly degraded resolution. Evidence for the D_1^+ state is apparent in the mass difference plots $M(D^0\pi^+) - M(D^0)$ obtained in the search for the $D_2^{*+}(2469)$ shown in Figure 3.8. The structure at mass-differences below 500 MeV/c^2 can be attributed to feeddown from the decays $D_J^{(*)+} \to D^{*0}\pi^+$ where the neutral from the D^{*0} decay is unobserved. Figures 3.8(c) and (d) show the same mass distributions as Figures 3.8(a) and (b). Overlaid, however, are the results of fits to the distributions using a polynomial function to parametrize the background and three Breit-Wigners convoluted with Gaussian resolution functions to describe the contributions to the spectrum from

- Direct $D_2^{*+}(2469) \to D^0\pi^+$ decays.
- Feeddown from $D_2^{*+}(2469) \to D^{*0}\pi^+$ decays.
- Feeddown from $D_1^+ \to D^{*0}\pi^+$ decays.

The detector resolutions for the feeddown contributions were obtained from Monte Carlo studies, as was the expected mass of the $D_2^{*+}(2469)$ feeddown peak. Fixing these quantities to their expected values and fitting yielded a mean mass-difference for the 1^+ contribution of $\Delta M = 407.7 \pm 7.0$ MeV/c^2 which corresponds to a D_1^+ mass of $(2415 \pm 7 \pm 5)$ MeV/c^2. The mean fitted width was 20.4 ± 9 MeV/c^2. This is consistent with the measured width for the $D_1^0(2414)$. The isospin mass-splitting for the observed 1^+ state is $M(D_1^+) - M(D_1^0) = (1 \pm 7 \pm 7)$ MeV/c^2.

ARGUS also made the first observation of orbitally excited charmed-strange mesons with the discovery of the D_{s1}^+ in 1989[119]. With reconstruction in the channels

$$D_{sJ}^{(*)+} \quad \to \quad D^*(2010)^+ K_s^0$$

$$
\begin{array}{l}
\hookrightarrow D^0\pi^+ \\
\quad \hookrightarrow K^-\pi^+ \\
\quad \hookrightarrow K^-\pi^+\pi^+\pi^- \\
\quad \hookrightarrow K^-\pi^+\pi^0
\end{array}
$$

ARGUS observed a narrow state just above threshold at a mass of 2536 MeV/c^2 in invariant mass spectra obtained in the $K\pi$ and $K\pi\pi\pi$ final states (which have the same resolution) and in the $K\pi\pi^0$ final state which has a somewhat poorer resolution due to the π^0 reconstruction. These mass spectra are shown in Figure 3.9. The signal parameters were extracted by fitting the two spectra simultaneously, keeping the central value of the Gaussian describing the signals equal, and allowing all other fit parameters to vary. The 18 events observed represented an excess of more than 5σ over the expected number of background events. In order to obtain an upper limit on the $\Gamma_{D_{s1}^+}$, the signal shape was parametrized as a Breit-Wigner convoluted with a Gaussian resolution function. This fit yielded an upper limit on the natural width of $\Gamma_{D_{s1}^+} < 4.9$ MeV/c^2 at the 90% confidence level.

A similar search performed in the decay channel $D^+K_s^0$ yielded no signal and an upper limit of

$$\frac{\mathrm{BR}(D_{sJ}^+(2536) \to D^+\ K^0)}{\mathrm{BR}(D_{sJ}^+(2536) \to D^{*+}K^0)} < 0.43\ @\ 90\%\ \mathrm{C.L.}$$

The absence of a signal in the $D^+K_s^0$ final state is most easily understood if the observed state is one of the 1^+ states which is forbidden to decay to DK.

Further compelling evidence for the existence of this state was later provided by the ARGUS reconstruction[120] of the decay sequence

$$
\begin{array}{rcl}
D_{s1}^+(2536) & \to & D^{*0}K^+ \\
 & & \quad \hookrightarrow D^0(\pi^0,\gamma) \\
 & & \quad\quad \hookrightarrow K^-\pi^+ \\
 & & \quad\quad \hookrightarrow K_s^0\pi^+\pi^- \\
 & & \quad\quad \hookrightarrow K_s^0K^+K^-
\end{array}
$$

which produced the invariant mass spectra shown in Figure 3.10. The $D^0\pi^0$ and $D^0\gamma$ final states have different resolutions and are shown separately. These distributions were fitted with a polynomial background function and the sum of two Gaussians, one of which parametrizes cross-talk between the two channels and feeddown from the $D^0\pi^0$ channel arising when one or both photons from the pion are unobserved. For the $D^0\pi^0$ channels the ratio of the amplitudes for the two Gaussians was fixed to the value determined in Monte Carlo studies. Variation of the ratio resulted in small differences in the fitted number of events which were included in the systematic error. These fits yielded 15.8 ± 4.0 and 12.2 ± 5.6 events at masses of (2535.4 ± 0.6) and (2534.8 ± 0.8) MeV/c^2 respectively, in good agreement with the mass obtained in the $D^{*+}K_S^0$ channel. An upper limit on the signal width was also obtained in this channel, yielding $\Gamma_{D_{s1}^+} < 3.9$ MeV/c^2 at the 90% confidence level.

As a final confirmation of these results, the D^0K^+ invariant mass spectrum was examined[120]. The $D_{s1}^+(2536)$ can produce an enhancement in this spectrum at a mass of $\mathrm{M}(D_{s1}^+) - \mathrm{M}(D^{*0}) + \mathrm{M}(D^0)$ if the π^0 or γ is unobserved. After application of somewhat more stringent selection criteria, due to higher background than in the analysis of $D^{*0}K^+$ combinations, the invariant mass distribution shown in Figure 3.10(c) was obtained. The shaded histogram represents the invariant mass distribution of wrong-sign D^0K^- combinations obtained using only the $D^0 \to K^-\pi^+$ channel in order to distinguish D^0 from $\bar{D}^0$. These spectra were fitted with polynomial background functions and two Gaussians with widths fixed to the values expected for the $D^0\gamma$ and $D^0\pi^0$ channels and the

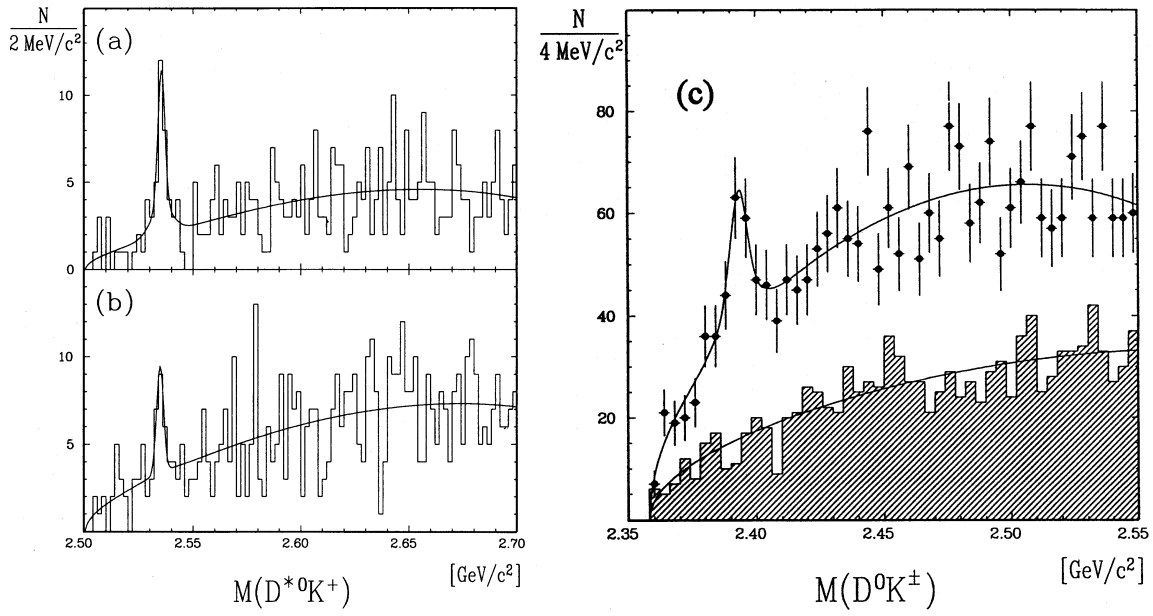

Figure 3.10: *Plots from analysis of $D^{*0}K^+$ final state. (a) and (b) are from the full reconstruction of using the $D^0\pi^0$ and $D^0\gamma$ D^{*0} final states respectively. (c) is from the partial reconstruction where the neutral from the D^{*0} decay is unobserved [120].*

same central values. The fit to the right-sign distribution yielded $71 \pm 17 \pm 10$ events at a mass of (2393.2 ± 1.2) MeV/c^2. This number of events was consistent with the 103 ± 23 events expected based on the results of the $D^{*0}K^-$ analysis and the mass was in good agreement with the expected value of 2393.1 MeV/c^2, obtained from Monte Carlo simulation in which the mass of the $D_{s1}^+(2536)$ was fixed to 2535.2 MeV/c^2.

Recently, CLEO observed the last predicted narrow P-wave charmed-strange meson $D_{s2}^+(2573)$ decaying into D^0K^+ [121]. The values of its mass and natural width were found to be $(2573.2^{+1.7}_{-1.6} \pm 0.8 \pm 0.5)$ and $(16^{+5}_{-4} \pm 3)$ MeV/c^2 respectively. ARGUS has confirmed the observation of this resonant state [122]. Figure 3.11 shows the D^0K^+ invariant mass distribution. There is a peak at the expected 2^+ mass as well as a narrow structure near threshold which is a reflection from the partially reconstructed decay chain $D_{s1}^+(2536) \to D^{*0}K^+$, $D^{*0} \to D^0\pi^0(\gamma)$, with π^0 or γ missing. Contributions of reflections from $D_1(2420)$ and $D_2(2460)$ decays are shown in the figure. The measured values of M = $(2574.5 \pm 3.3 \pm 1.6)$ MeV/c^2 and $\Gamma = (10.4 \pm 8.3 \pm 3.0)$ MeV/c^2 are consistent with the values obtained by CLEO [121].

In summary, the signal properties for all the states discussed in this section are comparable to 1994 world averages, with the exception of the $D_1^0(2414)$ mass which is somewhat lower than the world average, and the $D_1^+(2415)$ mass for which there is no PDG value. No significant deviations from the results presented here have arisen in subsequently performed ARGUS analyses. Experimental results are in good qualitative agreement with model predictions (Table 3.2.2).

3.2.3 Charmed Baryon Ground States

ARGUS has also produced significant contributions to the current knowledge of charmed baryon spectroscopy. Λ_c^+ and Σ_c's are rather well established charmed baryon states, observed in several e^+e^- and fixed target experiments [131]. The Λ_c^+ baryon was already quite well established when ARGUS started to take data. However, only a few Σ_c candidates had been reproted by that time.

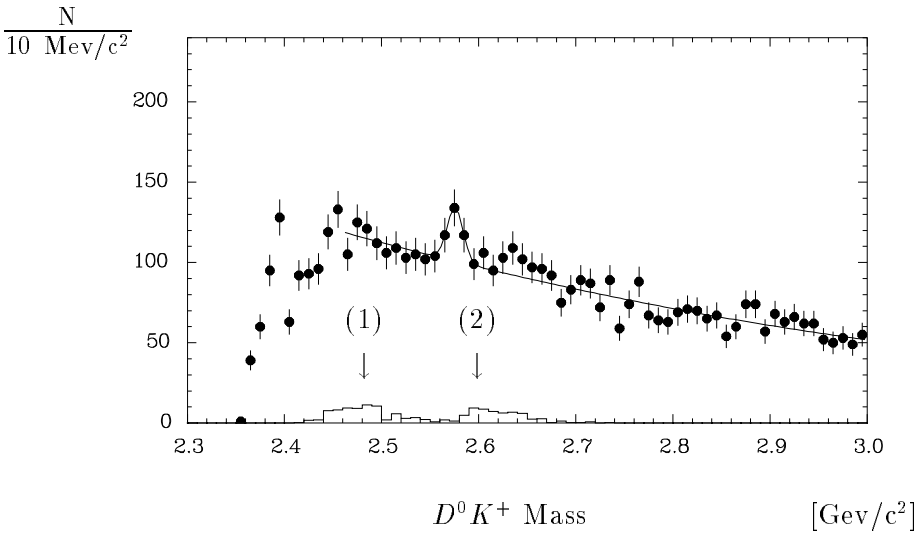

Figure 3.11: *Invariant mass spectrum for all accepted D^0K^+ combinations. The histogram represents the total contribution of feed-down structures described in the text. The arrows (1) and (2) point to the region populated by the reflections from decays $D_1^+(2420) \to D^{*0}\pi^+$ and $D_2^{*+}(2460) \to D^{*0}\pi^+$, and the feed-down from the decay $D_2^{*+}(2460) \to D^0\pi^+$ respectively [122].*

Table 3.1: *Experimental (ARGUS) measurements and theoretical predictions for masses of P-wave charmed excited mesons.*

State	ARGUS	HQET [123]	Quark-Gluon String Model [124]	Potential model, Zeng *et al.* [125]
$D_1^0(2420)$	$2414 \pm 2 \pm 5$		2420 ± 20	2410
$D_1^+(2420)$	$2415 \pm 7 \pm 5$			
$D_2^{*0}(2460)$	$2455 \pm 3 \pm 5$		2430 ± 30	2460
$D_2^{*+}(2460)$	$2469 \pm 4 \pm 6$			
$D_{s1}^+(2536)$	$2535.2 \pm 0.5 \pm 1.5$ ($\to D^{*+}K_S^0$)	2526	2530 ± 40	2520
	$2535.9 \pm 0.6 \pm 2.0$ ($\to D^{*0}K^+$)			
$D_{s2}^{*+}(2573)$	$2574.5 \pm 3.3 \pm 1.6$	2561	2550 ± 30	2580

At ARGUS the Λ_c^+ was reconstructed in a variety of decay channels (Table 3.2.3), the most useful being the $pK^-\pi^+$ final state. Λ_c^+ signals were used to reconstruct ${\Sigma_c}^{++}$ and ${\Sigma_c}^0$ states in the decays ${\Sigma_c}^{++} \to \Lambda_c^+\pi^+$ and $\Sigma_c^0 \to \Lambda_c^+\pi^-$. Signals for both of these states are shown in Figure 3.12 [129]. The mass difference of $M_{\Sigma_c^{++}} - M_{\Sigma_c^0} = (1.2 \pm 0.7 \pm 0.3)$ MeV/c^2, consistent with more recent data, was first reported by ARGUS.

Ξ_c baryons were reconstructed in final states containing a Ξ. Signals for the charged and neutral states, reconstructed in the $\Xi\pi^+$ and $\Xi\pi^+\pi^-$ final states respectively, are shown in Figure 3.13 [128]. In addition to confirmation of previously observed channels, ARGUS produced the first evidence for the decay $\Xi_c^0 \to \Xi\pi^+\pi^+\pi^-$.

The situation with the heaviest ground state baryon, the Ω_c^0, was quite controversial for some time. In 1985, searching in the $\Xi^- K^-\pi^+\pi^+$ final state, the WA-62 Collaboration observed a cluster of three events at a mass around 2740 GeV/c^2 which was attributed to Ω_c^0 decays [132]. ARGUS has searched for the Ω_c^0 in the same final state, as well as in the $\Omega^-\pi^-\pi^+\pi^+$ system[130],[133]. Signals were observed in both channels leading to a weighted mass average of $(2716 \pm 5 \pm 4)$MeV/c^2. The invariant mass distribution for the $\Xi^- K^-\pi^+\pi^+$ final state is shown in Figure 3.14. The E687 Collaboration has observed a signal of 11.7 ± 3.8 events in the $\Omega^-\pi^+$ invariant mass spectrum at a mass of $(2705.9 \pm 3.3 \pm 2.0)$ MeV/c^2 [134]. More recently E687 has shown significant evidence (42.5 ± 8.8 events) for the presence of the Ω_c^0 in the $\Sigma^+ K^- K^-\pi^+$ final state[135]. A confirmation of the Ω_c^0 from the CLEO Collaboration is still missing.

The results of the ARGUS measurements of charmed baryon ground states are summarized in Table 3.2.3. The table exhibits, for each particle investigated, the measured mass, the production cross-section times branching ratio ($\sigma \cdot$Br) into the decay channel observed, and the ϵ value from a fit of the Peterson fragmentation function to the observed momentum spectrum. Production cross-sections and "absolute" branching fractions are given where known, i.e. in the case of the Λ_c^+. If more than one decay channel has been observed, the mass value quoted is the weighted average of the results obtained in the listed final states. For comparison, the 1994 world average masses are provided in the final column[17].

Table 3.2: *Summary of ARGUS ground state baryons measurements.*

	Decay mode	Mass [MeV/c^2]	$\sigma\cdot$BR [pb]	ϵ	PDG94 [MeV/c^2]
Λ_c	$\Lambda_c \to pK^-\pi^+$	$2283.1 \pm 1.7 \pm 2.0$	$12.0 \pm 1.9 \pm 1.2$	0.24 ± 0.04	2284.9 ± 0.6
	$\Lambda_c \to \Lambda\pi^+\pi^+\pi^-$		$8.3 \pm 1.3 \pm 1.7$		
	$\Lambda_c \to \Lambda\pi^+$		$2.2 \pm 0.3 \pm 0.4$		
	$\Lambda_c \to \overline{K^0}p$		$6.6 \pm 1.0 \pm 1.3$		
	$\Lambda_c \to \Sigma^0\pi^+$		$1.8 \pm 0.5 \pm 0.3$		
Σ_c^{++}	$\Sigma_c^{++} \to \Lambda_c^+\pi^+$	$2451.3 \pm 0.5 \pm 2.5$		0.29 ± 0.06	2453.1 ± 0.6
Σ_c^0	$\Sigma_c^0 \to \Lambda_c^+\pi^-$	$2450.1 \pm 0.5 \pm 2.5$		0.29 ± 0.06	2452.4 ± 0.7
Ξ_c^0	$\Xi_c^0 \to \Xi^-\pi^+$	$2472.1 \pm 2.7 \pm 1.6$	$0.77 \pm 0.24 \pm 0.16$	0.24 ± 0.08	2470.4 ± 2.0
	$\Xi_c^0 \to \Xi^-\pi^+\pi^+\pi^-$		$2.55 \pm 0.64 \pm 0.39$		
Ξ_c^+	$\Xi_c^+ \to \Xi^-\pi^+\pi^+$	$2465.1 \pm 3.6 \pm 1.9$	$1.50 \pm 0.39 \pm 0.23$	0.29 ± 0.04	2465.4 ± 1.6
Ω_c	$\Omega_c \to \Xi^- K^-\pi^+\pi^+$	$2716 \pm 4 \pm 2$	$1.5 \pm 0.6 \pm 0.6$		2710 ± 5
	$\Omega_c \to \Omega^-\pi^+\pi^+\pi^-$				

3.2.4 First Observation of an Excited Charmed Baryon State

The spectrum of charmed baryons contains not only the $J^P = 1/2^+, 3/2^+$ ground states, but also excited states. A number of models have been developed to provide explicit predictions for the masses of excited charmed baryons [136].

A search for an excited Λ_c state, which we will call Λ_c^*, can be performed in the channel $\Lambda_c^+\pi^+\pi^-$. A Λ_c^*, having (I = 0), should decay preferentially into a Λ_c^+ and two pions, or into a Σ_c and one pion. The decay into $\Lambda_c^+\pi$ is clearly forbidden.

ARGUS searched for a signal in $\Lambda_c^+\pi^+\pi^-$ combinations [14], using Λ_c^+ candidates reconstructed in the $pK^-\pi^+$, pK_s^0, $\Lambda\pi^+$, and $\Lambda\pi^+\pi^+\pi^-$ final states. The resulting mass distribution is displayed in

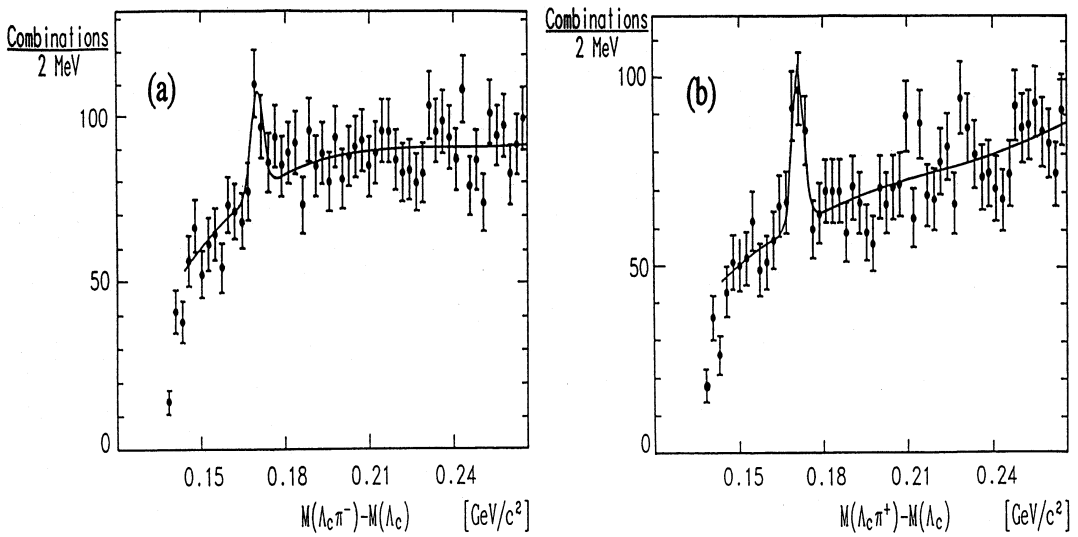

Figure 3.12: *ARGUS signals for the* Σ_c^0 *and* Σ_c^{++} *states. Mass difference spectra for (a)* $\Lambda_c^+\pi^-$ *and (b)* $\Lambda_c^+\pi^+$ *combinations, using* $\Lambda_c{}^+$ *candidates from the decay modes* $pK^+\pi^-$, $\Lambda\pi^+\pi^-\pi^+$, *and* $\overline{K^0}p$. *The overlaid lines are from fits using a Gaussian and a polynomial background [129].*

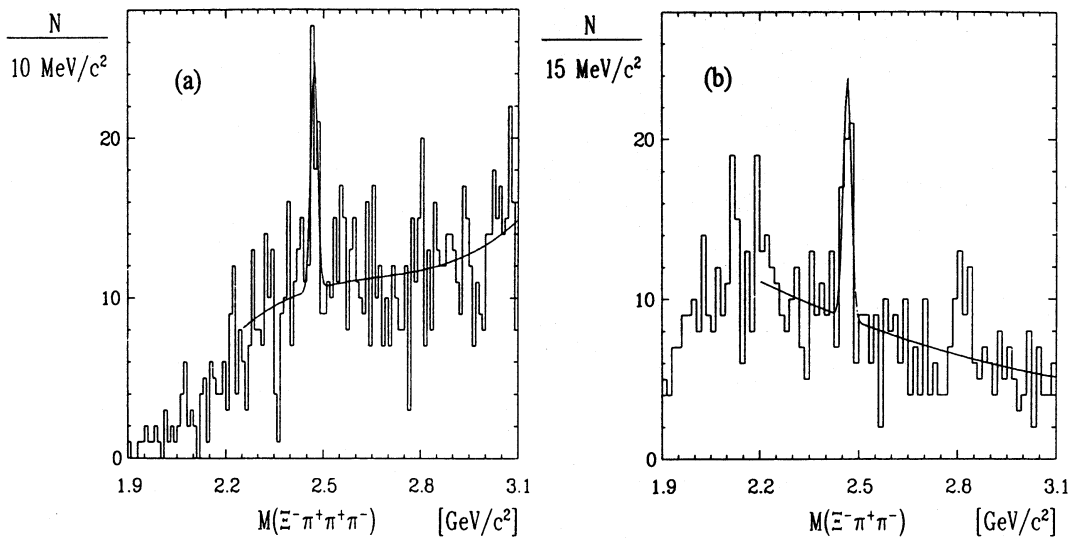

Figure 3.13: *ARGUS signals for the a)* $\Xi_c{}^0$ *and b)* $\Xi_c{}^+$ *states reconstructed in the* $\Xi\pi^+\pi^+\pi^-$ *and* $\Xi\pi^+\pi^+$ *final states respectively. Overlaid are fit results using a Gaussian for the* Ξ_c *signal and a polynomial to describe the background [128].*

Figure 3.15. It exhibits a clear peak at a mass of about 2625MeV/c^2. A fit using a Gaussian for the signal and a second order polynomial to model the background yielded 42.4 ± 8.8 events at a mass of $(2626.6 \pm 0.5 \pm 1.5)$ MeV/c^2. This result represented the first observation of an excited charmed baryon

In order to obtain an upper limit on the natural width Γ of the Λ_c^{*+}, the signal shape was parametrized using a non-relativistic Breit-Wigner convoluted with a Gaussian resolution function. This fit yielded a upper limit of $\Gamma < 3.2$ MeV/c^2 at the 90% confidence level.

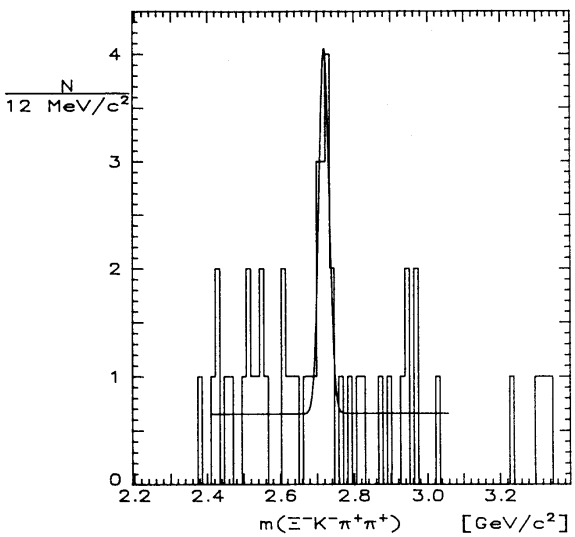

Figure 3.14: *ARGUS signal for Ω_c in the $\Xi^- K^- \pi^+ \pi^+$ final state [130].*

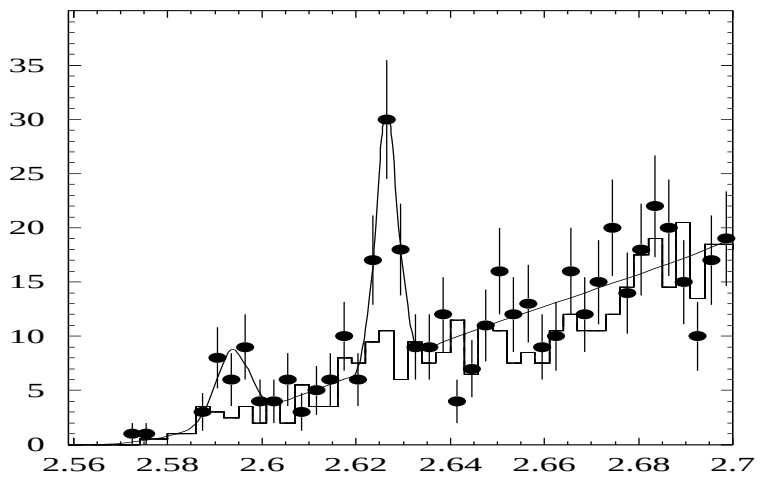

Figure 3.15: *Invariant mass distribution for all accepted $\Lambda\pi^+\pi^-$ combinations. The solid histogram results from using the Λ_c^+ sidebands. Overlaid is the result of the fit described in the text [14].*

The efficiency corrected x_p distribution (Figure 3.16) is hard as expected and is well described by a Peterson [99] fragmentation function with $\epsilon = 0.044 \pm 0.018$. When one compares the corresponding values for Λ_c^+ and Σ_c production, namely $\epsilon_{\Lambda_c^+} = 0.24 \pm 0.04$ [127], and $\epsilon_{\Sigma_c} = 0.29 \pm 0.06$ [129], one finds them to be significantly larger, corresponding to a softer fragmentation spectrum. This might be an indication that a large fraction of Λ_c^+ and Σ_c baryons are produced in the decays of higher excited states. The measured product of cross section and branching ratio was

$$\sigma \cdot \mathrm{BR}(\Lambda_c^{*+} \to \Lambda_c^+ \pi^+ \pi^-) = (11.5 \pm 2.5 \pm 3.0)\mathrm{pb},$$

where the ARGUS result $BR(\Lambda_c \to pK^-\pi^+) = (4.0 \pm 0.3 \pm 0.8)\%$[55] has been used.

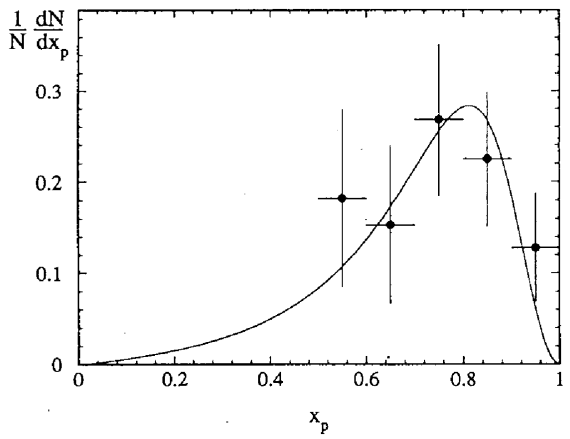

Figure 3.16: *The x_p spectrum of the Λ_c^{*+}. The solid curve is the result of the fit with the Peterson fragmentation function [14].*

The $\Lambda_c^+\pi^+\pi^-$ final state can be generated through the decay of either a Λ_c^* or Σ_c^*. In the present case there are no direct means of determining the identity of the parent particle. However, for charmed baryons just above threshold the phase space for the $\Lambda_c^+\pi$ decay is much larger than that for the $\Lambda_c^+\pi^+\pi^-$. The Σ_c^* would therefore decay mainly to $\Lambda_c^+\pi$, while this decay mode is forbidden for the Λ_c^* due to isospin conservation. No signal was observed in the $\Lambda_c^+\pi^0$ channel. Furthermore, model calculations predict substantially higher masses for excited Σ_c states, while predictions for P-wave Λ_c^* states lie close to the mass of the observed state. This object, the first observed excited charmed baryon, can therefore be identified as an excited Λ_c state.

This mass value has been confirmed by the CLEO Collaboration [121] which also identified a second peak, closer to threshold, at a mass of about 2590 MeV/c^2. ARGUS also observes a small (18.0 ± 7.1 events) enhancement at this mass. In the fit to the distribution in Figure 3.15 a second Gaussian was added to account for this signal.

3.3 Weak Decays of Charmed Hadrons

3.3.1 The measurement of the lifetimes of charmed mesons

In the spectator model of heavy flavour decays light quarks play a minor role and it was expected that the lifetimes of all charmed hadrons were approximately equal [140]. However, even the first measurements of the lifetimes of charmed particles indicated that this was not the case [137]. Several mechanisms were proposed to account for the observed difference [138], but agreement with experiment was still unsatisfactory. Accurate measurements performed by ARGUS[139] provided a check of previous results and constrained models which attempted to explain the large observed lifetime differences.

ARGUS reported measurements of the D^0, D^+ and D_s^+ lifetimes. For these analyses, D mesons were reconstructed in the following decay channels :

$D^{*+} \to D^0\pi^+$, $D^0 \to K^-\pi^+$ and $D^0 \to K^-\pi^+\pi^+\pi^-$;

$D^+ \to K^-\pi^+\pi^+$;

$D_s{}^+ \to \phi\pi^+$, $D_s{}^+ \to \phi K^+K^-$.

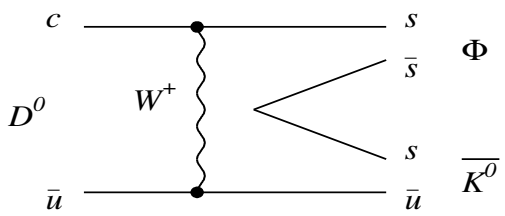

Figure 3.17: *W-exchange diagram for the decay* $D^0 \rightarrow \phi\overline{K}^0$

The lifetimes of D^0 , D^+ and ${D_s}^+$ mesons were determined to be

$\tau_{D^0} = (4.8 \pm 0.4 \pm 0.3) \cdot 10^{-13}$ s,

$\tau_{D^+} = (10.5 \pm 0.8 \pm 0.7) \cdot 10^{-13}$ s,

$\tau_{{D_s}^+} = (5.6^{+1.3}_{-1.2} \pm 0.8) \cdot 10^{-13}$ s.

The ratio of charged to neutral D lifetimes, was found to be $\tau_{D^+}/\tau_{D^0} = 2.2 \pm 0.3 \pm 0.2$. The ${D_s}^+$ and D^0 measurements yield the ratio $\tau_{{D_s}^+}/\tau_{D^0} = 1.2 \pm 0.3 \pm 0.2$. These results were among the most precise charmed meson lifetime measurements available at that time. They continue to agree well with world averages [17]. The difference in D meson lifetimes can be qualitatively understood with the aid of a simple picture of quark diagrams and factorization, based on two principles: two-body spectator decay domination, and destructive interference of two spectator diagrams in the case of D^+ decays. Evidence for non-spectator contributions to the weak decays of these states, as well as in the decays of charmed baryons, is discussed in the next section.

3.3.2 Observation of the Decay $D^0 \rightarrow \phi\overline{K}^0$

According to simple quark models [140], the decays of heavy mesons should be dominated by the spectator mechanism with contributions from quark annihilation being extremely small due to helicity and colour suppression. Other models predict that this suppression can be reduced or eliminated by non-perturbative aspects of QCD. A crucial test of these ideas would be the observation of the decay $D^0 \rightarrow \overline{K}^0\phi$ which should occur predominantly through the W-exchange diagram shown in Figure 3.17. W-exchange enhanced models predict that the branching ratio for this decay could be as large as $\simeq 1.0\%$ [141]. The spectator mechanism can contribute to this decay only through an OZI forbidden process, for which the calculated branching ratio is less than 10^{-5} [141].

ARGUS reported the first observation of the decay $D^0 \rightarrow \overline{K}^0\phi$ in 1985 [15]. This study was later repeated with a larger data sample [142].

Figure 3.18 shows the $K^0_s K^+ K^-$ invariant mass distribution. There is a clean D^0 signal of 205 ± 38 events at a mass of (1864.3 ± 1.5)MeV/c^2. The two-body contributions to the three-body decay $D^0 \rightarrow \overline{K}^0 K^+ K^-$ can be determined by examining the K^+K^- subsystem. Requiring $|M(K^0_s K^+ K^-) - M(D^0)| < 16.2$ MeV/c^2 yielded the K^+K^- invariant mass spectrum shown in Figure 3.19.

Clearly visible is a prominent ϕ signal with the expected mass and shape. The part of the K^+K^- mass spectrum which is not correlated with the $D^0 \rightarrow \overline{K}^0\phi$ decay is determined from the sidebands above and below the D^0 (hatched histogram). The distribution for the helicity angle Θ, defined as the angle between the K^+ and the K^0_s in the rest frame of the ϕ, exhibits the expected $cos^2\Theta$ behaviour, allowing for only small K^+K^- S-wave contribution below the ϕ.

The ratio $\mathrm{Br}(D^0 \rightarrow \overline{K}^0\phi)/\mathrm{Br}(D^0 \rightarrow K^0_s\pi^+\pi^-)$ was found to be 0.155 ± 0.033 resulting in a value of

$$\mathrm{Br}(D^0 \rightarrow \overline{K}^0\phi) = (0.82 \pm 0.17 \pm 0.08)\%,$$

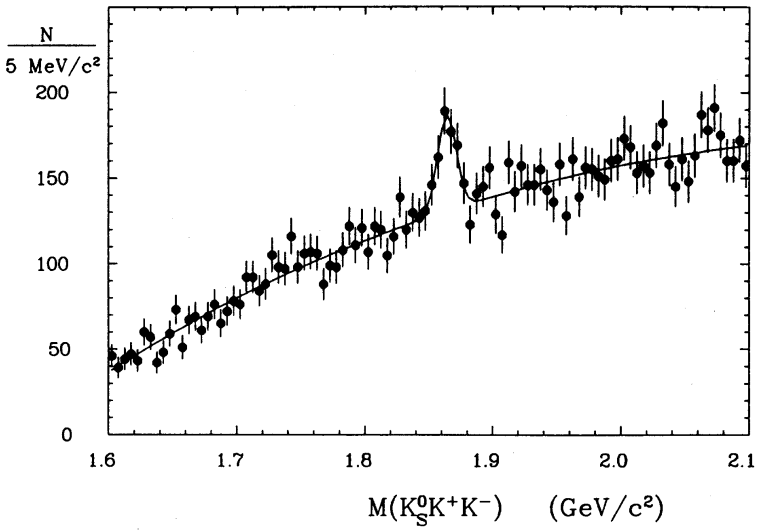

Figure 3.18: $K^0_s K^+ K^-$ *invariant mass distribution [142].*

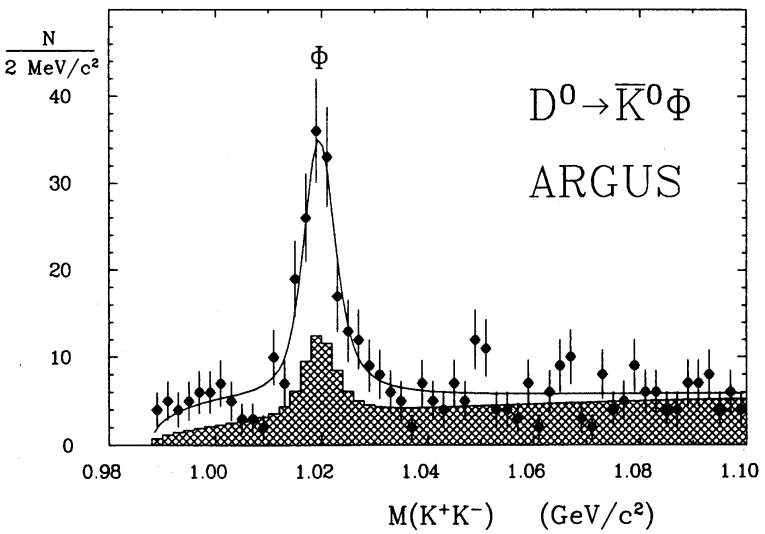

Figure 3.19: $K^+ K^-$ *invariant mass distribution from* $K^0_s K^+ K^-$ *combinations in the* D^0 *mass region [142].*

using the updated value of $\mathrm{Br}(D^0 \to \overline{K}^0 \pi^+ \pi^-) = 5.3 \pm 0.6\%$ from [17]. For the remaining fraction of the $D^0 \to \overline{K}^0 K^+ K^-$ decay, $Br(D^0 \to \overline{K^0}(K^+ K^-)_{non-\phi}) = (0.46 \pm 0.11 \pm 0.04)\%$ was obtained.

This surprising result stimulated a number of publications on models which attempted to describe the observed $D^0 \to \overline{K}^0 \phi$ branching ratio [143, 144, 145, 146]. One possible explanation was that flavour annihilation does indeed make a strong contribution to D meson decays. However, there is also a qualitative argument[147] that final state interactions may strongly enhance or simulate annihilation processes if nearby resonances contribute. The D meson mass lies in a resonance region, where rescattering effects of the outgoing mesons are very important.

ARGUS also presented a first measurement of the branching ratio of $D_s{}^+ \to \overline{K}^{*0} K^+$ decay [150],

which can occur either through the annihilation diagram or through a colour suppressed spectator diagram. 87 ± 20 events were observed in the decay $D_s{}^+ \to \overline{K}{}^{*0} K^+$ yielding

$$\frac{Br(D_s{}^+ \to \overline{K}{}^{*0} K^+)}{Br(D_s{}^+ \to \phi\pi^+)} = 1.44 \pm 0.37.$$

Thus the $\overline{K}{}^{*0} K^+$ decay mode of the $D_s{}^+$ meson, which proceeds only through annihilation and colour-suppressed spectator diagrams, occurs at a rate comparable with that for the colour-favoured spectator decay $D_s{}^+ \to \phi\pi^+$.

The ARGUS investigations, along with the results of other experiments, showed that the simple spectator model [140] was inadequate for the interpretation of nonleptonic D meson decays and promoted therefore the development of other theoretical approaches [144, 145, 146, 148]. ARGUS results showed that the contributions of annihilation diagrams are not small, although the large $\mathrm{Br}(D^0 \to \overline{K}{}^0 \phi)$ can be partially due to the final state interactions. Moreover, it should be noted that these two mechanisms are not mutually exclusive but represent dual pictures of the same phenomenon [138].

3.3.3 Evidence for W Exchange Contribution to Charmed Baryon Decays

Although non-spectator effects are important in charmed meson decays and have provided us with a deeper understanding of hadronic decay mechanisms, it is actually charmed baryons which provide the best opportunity to study the W-exchange mechanism. This advantage arises since the helicity-suppression of these contributions in mesonic decays is not present[131] [151].

ARGUS has searched for the following charmed baryon decays[153]:

$$\begin{aligned} \Lambda_c^+ &\to \Xi^- K^+ \pi^+ \\ \Lambda_c^+ &\to \Xi^{*0} K^+ \end{aligned}$$

In the absence of final state interactions, the only way in which the last decay can occur is via W-exchange. Observation of these decays therefore provides strong evidence for W-exchange in charmed baryon decays. Observation of the channel $\Lambda_c^+ \to \Xi^- K^+ \pi^+$ and its subchannel $\Lambda_c^+ \to \Xi^{*0} K^+$ was first reported by the CLEO collaboration [152].

In the Λ_c^+ analysis, the $\Xi^- K^+ \pi^+$ final state was reconstructed, and the extent to which the two body channel contributed to the total $\Xi^- K^+ \pi^+$ signal was determined. The $\Xi^- K^+ \pi^+$ mass spectrum (Figure 3.20(a)) displays a clear peak at the Λ_c^+ mass. The signal contains (33.6 ± 6.7) events at a mass of (2284.8 ± 1.8) MeV/c^2 in excellent agreement with the nominal value [17]. In Figure 3.20(b) the wrong sign mass spectrum ($\Xi^- K^+ \pi^-$ combinations) is plotted. This distribution shows no enhancement at the position of the Λ_c^+ mass.

The $\Xi^- K^+ \pi^+$ distribution obtained by requiring the $\Xi^- \pi^+$ invariant mass to be within ± 12 MeV/c^2 of the nominal Ξ^{*0} mass is shown in Figure 3.21. A total of (13.1 ± 3.9) events were observed in the signal. The $\Xi^- K^+ \pi^+$ distribution from 60 MeV/c^2 sidebands above and below the accepted Ξ^{*0} region was also obtained. When fitted, this distribution yielded (8.4 ± 3.4) events in the accepted Λ_c^+ mass region. Since the sideband region taken was five times wider than that of the signal region, the latter number was scaled down by a factor of five to (1.7 ± 0.8) events. Subtracting the two numbers yielded (11.4 ± 3.9) events which can be attributed to the decay $\Lambda_c^+ \to \Xi^{*0} K^+$.

The final results for the products of production cross-section and branching ratio are

$$\sigma(\Lambda_c^+) \cdot (\Lambda_c^+ \to \Xi^- K^+ \pi^+) = (1.7 \pm 0.3 \pm 0.2)\mathrm{pb} \ ,$$

$$\sigma(\Lambda_c^+) \cdot (\Lambda_c^+ \to \Xi^{*0} K^+) = (0.6 \pm 0.2 \pm 0.1)\mathrm{pb} \ ,$$

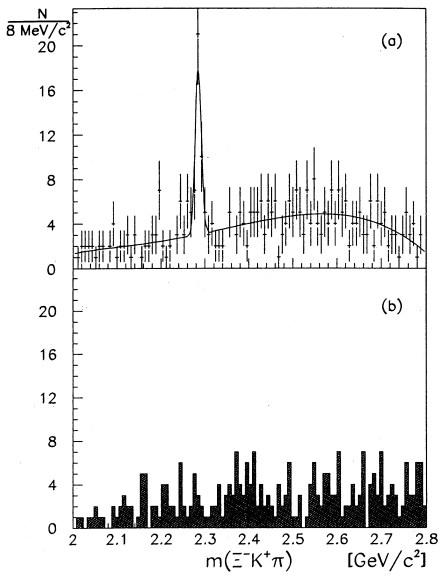

Figure 3.20: *(a) The invariant mass of all accepted $\Xi^- K^+ \pi^+$ combinations. (b) The wrong sign distribution [153].*

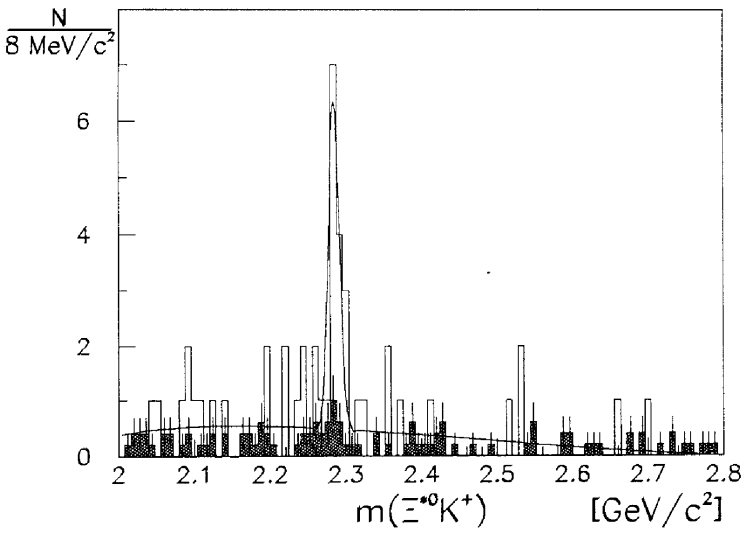

Figure 3.21: *The $\Xi^- K^+ \pi^+$ invariant mass spectrum after a cut around the Ξ^{*0} signal (unshaded histogram). Shaded: The scaled mass spectrum obtained from the Ξ^{*0} sidebands; it displays no enhancement in the Λ_c^+ signal region [153].*

implying that $(35 \pm 17)\%$ of the decay $\Lambda_c^+ \to \Xi^- K^+ \pi^+$ proceeds via a two body intermediate state. Using the ARGUS result [97]

$$\sigma \cdot \mathrm{BR}(\Lambda_c^+ \to p K^- \pi^+) = (12.0 \pm 1.1 \pm 1.3)\mathrm{pb}$$

yields the two ratios

$$\mathrm{BR}(\Lambda_c^+ \to \Xi^- K^+ \pi^+)/\mathrm{BR}(\Lambda_c^+ \to p K^- \pi^+) = 0.14 \pm 0.03 \pm 0.02,$$

$$\mathrm{BR}(\Lambda_c^+ \to \Xi^{*0} K^+)/\mathrm{BR}(\Lambda_c^+ \to pK^-\pi^+) = 0.05 \pm 0.02 \pm 0.01.$$

Among the decays discussed above, the only theoretical information available concerns the decay $\Lambda_c^+ \to \Xi^{*0} K^+$ for which the branching ratio has been calculated to be 0.5% [154]. Using the PDG value for the $\Lambda_c^+ \to pK^-\pi^+$ branching ratio and the ARGUS value for $\sigma \cdot \mathrm{BR}(\Lambda_c^+ \to pK^-\pi^+)$, the ARGUS measurement for the the $\Lambda_c^+ \to \Xi^{*0} K^+$ branching ratio is (0.2 ± 0.1) %.

3.3.4 Evidence for Parity Violation in the Decay $\Lambda_c^+ \to \Lambda\pi^+$

With the exception of the Σ_c's and the Ξ_c', ground state charmed baryons decay through the weak interaction. These decays are expected to exhibit maximum parity violation due to their V-A nature.

A system suitable for investigation of this phenomenon is the two-body decay $\Lambda_c \to \Lambda\pi^+$ which is exactly analogous to the hyperon decay $\Xi^- \to \Lambda\pi^-$. The latter process is theoretically well understood and provides a formalism which can directly be applied to the decay investigated here [155]. In both of these decays, the Λ is produced with a polarization given by

$$\mathbf{P}_\Lambda = \frac{(\alpha_B + \hat{\Lambda} \cdot \mathbf{P}_B)\hat{\Lambda} - \beta_B(\hat{\Lambda} \times \mathbf{P}_B) - \gamma_B \hat{\Lambda} \times (\hat{\Lambda} \times \mathbf{P_B})}{(1 + \alpha_B \hat{\Lambda} \cdot \mathbf{P}_B)}$$

due to the interference between the S and P wave final states. Here, $\mathbf{P}_B$ is the parent baryon polarization, α_B, β_B and γ_B are the parent baryon asymmetry parameters, and $\hat{\Lambda}$ is a unit vector along the Λ flight direction in its production frame [156]. Averaging over parent baryon polarization, one obtains

$$\mathbf{P}_\Lambda = \alpha_B \hat{\Lambda}.$$

Hence, when the parent is unpolarized or when its polarization is not observed, the Λ is produced with helicity equal to α_B. The angular distribution of the proton from the decay of the Λ is therefore

$$W(\theta) \propto 1 + \alpha_\Lambda \alpha_B cos\theta, \tag{3.1}$$

where α_Λ is the Λ decay asymmetry parameter and θ is the angle between the Λ polarization and the proton flight direction. α_B is therefore determined by measuring the angular distribution of protons from the Λ decay since the Λ decay parameters are well known [17].

In order to determine the Λ_c^+ asymmetry parameter α, the $\Lambda\pi^+$ spectrum was fitted in bins of cosθ, then normalized by the total number of events. The resulting distribution is shown in Figure 3.22. The full circles with error bars represent the distribution of the signal in bins of cosθ on which the result of a straight line fit is superimposed. If parity were conserved, a flat distribution in cosθ would be expected (dotted line). On the other hand, parity violation leads to a distribution of the form given by Equation 3.1, with the slope equal to the product $\alpha_{\Lambda_c}\alpha_\Lambda$. Using a value for α_Λ of 0.642 $\pm$ 0.013 [17], we find α_{Λ_c} to be -0.96 $\pm$ 0.42.

The angular distribution of the background, obtained by summing the number of Λ_c sidebands events in the region of cosθ (open circles with error bars in Figure 3.22). is uniform, in contrast to the Λ_c^+ behaviour.

This result for α_{Λ_c} agrees well in magnitude with the prediction of Pakvasa *et al.* [158] and is in excellent agreement with the predictions of Bjorken [159] and Mannel *et al.* [160] which suggest that α_{Λ_c} be around -1. CLEO [161] has also measured α_{Λ_c} and finds a value of $-1.0 \pm^{0.4}_{0.0}$. A negative sign for α_{Λ_c} indicates that Λ's produced in Λ_c^+ decay have a negative helicity. In the so-called $\alpha\beta\gamma$ formalism, α is defined as $\frac{2ReS^*P}{|S|^2+|P|^2}$, where S and P are the S and P-wave amplitudes respectively [162]. Therefore, a magnitude of 1 for α could indicate that the S and P-wave amplitudes are equal implying that parity is maximally violated in this decay.

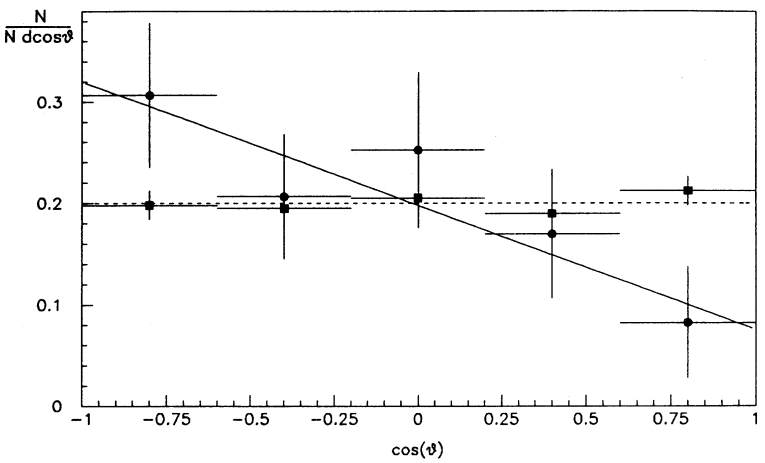

Figure 3.22: *Number of events as a function of cosθ for signal (circles) and background (squares). The shape of the signal distribution is well parametrized by the fit described in the text [157].*

3.3.5 Semileptonic decays of charmed mesons

The degree of attention paid to the measurement of exclusive semileptonic decays is attributable to their simple theoretical interpretation. Only spectator diagrams can contribute to these processes, so there is no uncertainty due to annihilation or exchange-diagram contributions. Existing quark models predict the same branching ratio for semileptonic charm decays to pseudoscalar mesons, $D \to Ke\nu$, and vector mesons, $D \to K^*e\nu$, and suggest that these two modes saturate the semileptonic width [68, 69, 59]. The E691 and CLEO collaborations[163, 164] confirmed the predicted $D \to Ke\nu$ decay width, but obtained only about half the width predicted for the $D \to K^*e\nu$ channel. At about the same time, the MARK III group reported a measurement of the $D^0 \to K^{*-}e^+\nu$ branching ratio in agreement with theory, although within large experimental errors [165].

For the analogous process ${D_s}^+ \to \phi e^+\nu$, one expected similar values for the partial width and polarization, based on SU(3) symmetry in the framework of the spectator model. ARGUS presented the measurement of the first semileptonic ${D_s}^+$ decay and measurements of the $D^0 \to K^{*-}e^+\nu$ and $D^+ \to K^{*0}e^+\nu$ branching ratios [166, 167]. For this purpose, K^*e^+ (or ϕe^+) correlations were studied. Wrong-charge (K^*e^-) combinations cannot be attributed to charm decays and were used for estimating the reliability of the background determination.

In the $K\pi$ invariant mass distributions for the $D^+ \to K^{*0}e^+\nu$ and $D^0 \to K^{*-}e^+\nu$ decay channels respectively (Figures 3.23 and 3.24) K^* peaks are visible. The analysis of these spectra yields, after background subtraction, the following branching ratios:

$$\mathrm{Br}(D^+ \to K^{*0}e^+\nu) = (4.2 \pm 0.6 \pm 1.0)\%,$$

$$\mathrm{Br}(D^0 \to K^{*-}e^+\nu) = (1.8 \pm 0.3 \pm 0.5)\%.$$

These branching ratios agree well with the results of other experiments [163, 164]. Using the PDG values for $\mathrm{Br}(D^+ \to K^0e^+\nu) = (6.6 \pm 0.9)\%$ and $\mathrm{Br}(D^0 \to K^-e^+\nu) = (3.80 \pm 0.22)\%$ [17] yields the ratios of branching ratios:

$$\mathrm{Br}(D^+ \to K^{*0}e^+\nu)/\mathrm{Br}(D^+ \to K^0e^+\nu) = (0.64 \pm 0.21),$$

$$\mathrm{Br}(D^0 \to K^{*-}e^+\nu)/\mathrm{Br}(D^0 \to K^-e^+\nu) = (0.47 \pm 0.16).$$

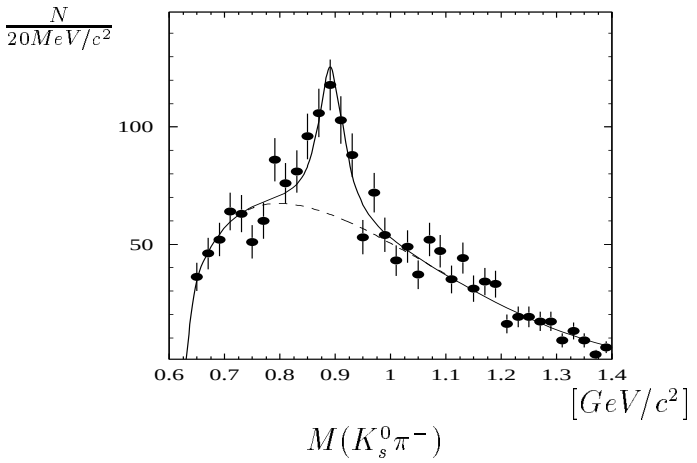

Figure 3.23: *The $K_s^0\pi^-$ invariant mass distribution for events containing a positron candidate [167]*

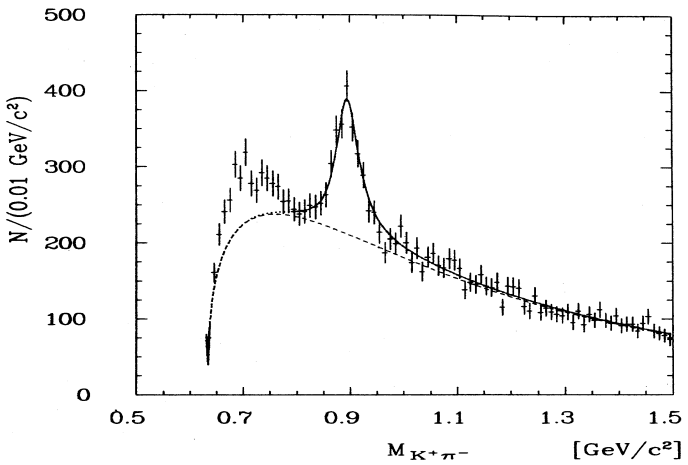

Figure 3.24: *The $K^+\pi^-$ invariant mass distribution for events containing a positron candidate [166]*

Averaging these results, yields a ratio of branching ratios of 0.55 ± 0.13 , which is lower than the early predictions of quark models [68, 69, 59]. However, recent calculations based on sum rules [168] and lattice calculations [169] have reproduced this result.

ARGUS has also measured the absolute branching fraction of inclusive semileptonic D^0 decays [170] using a technique described in detail in section 3.3.7. ARGUS obtains $Br(D^0 \rightarrow e^+\nu_e X) = (6.9 \pm 0.3 \pm 0.5)\,\%$, $Br(D^0 \rightarrow \mu^+\nu_\mu X) = (6.0 \pm 0.7 \pm 1.2)\,\%$. Both results are smaller than the corresponding PDG values which have however large errors [17]. Comparing our results on inclusive and exclusive semileptonic D^0 decays we observe that our sum of the exclusive semileptonic rates coincides within the errors with our measured rate for the inclusive semileptonic rate, leaving only little room for other exclusive semileptonic D^0 decays.

The analogous technique of $\phi - e^+$ correlations was employed for the study of the decay ${D_s}^+ \rightarrow \phi e^+ \nu$. The K^+K^- decay channel was used to reconstruct ϕ mesons.

Fig. 3.25 shows the K^+K^- invariant mass distribution for events containing an electron candidate. There is a clear peak at a mass of the ϕ meson with 200 ± 21 events.

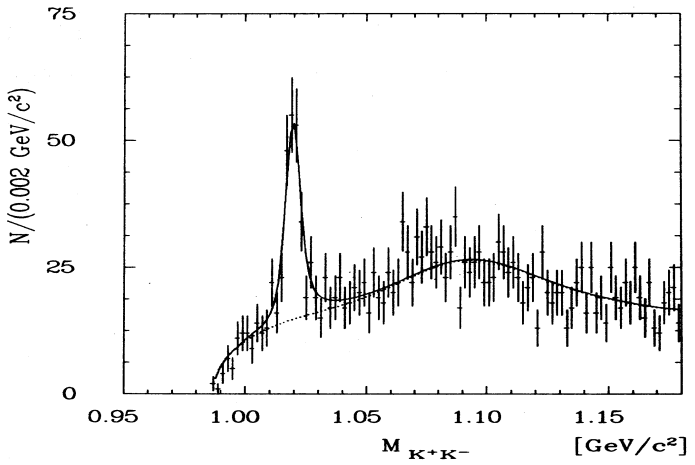

Figure 3.25: K^+K^- *invariant mass distribution for events containing electron candidate [166]*

Analysis of this signal yields, after background subtraction,

$$\frac{Br({D_s}^+ \to \phi e^+ \nu)}{Br({D_s}^+ \to \phi \pi^+)} = 0.57 \pm 0.15 \pm 0.15,$$

which corresponds to Br(${D_s}^+ \to \phi e^+ \nu$) = $2.0 \pm 0.6 \pm 0.6\%$ using Br(${D_s}^+ \to \phi \pi^+$) = $(3.5 \pm 0.4)\%$ [17]. This value agrees well with the results of other experiments [171] and with the ARGUS measurement of Br($D^0 \to K^{*-} e^+ \nu$). This is as expected; since the D^0 and ${D_s}^+$ lifetimes are almost equal, their semilpetonic branching ratios should also be equal.

By measuring the ratio Br(${D_s}^+ \to \phi e^+ \nu$)/Br(${D_s}^+ \to \phi \pi^+$) and combining it with theoretical estimates of $\Gamma({D_s}^+ \to \phi e^+ \nu)/\Gamma(D \to K^* l^+ \nu)$ and measurements of Br($D \to K^* \ell^+ \nu$) and $\tau(D_s^+)$ it is possible to determine the absolute branching fraction for the ${D_s}^+ \to \phi \pi^+$. Using ARGUS measurements for Br(${D_s}^+ \to \phi e^+ \nu$) and Br($D^+ \to K^{*0} e^+ \nu$), yields Br(${D_s}^+ \to \phi \pi^+$) = $(3.3 \pm 1.4)\%$ in a good agreement with the world average[17].

3.3.6 Observation of Semileptonic Charmed Baryon Decays

Theory has also devoted much interest recently to semileptonic decays of charmed baryons. Branching ratios for the decays of the Λ_c^+ and Ξ_c^0 are predicted to be of the order of a few percent[172], depending on the choice of the heavy baryon wave function model and the nature of the q^2-dependence of the hadronic form factors. This section reviews the ARGUS observation of Λ_c^+ and Ξ_c^0 semileptonic decays [173],[174].

Only a few measurements of Λ_c^+ semileptonic decays have been made so far [175, 177], some of them suffering from low statistics, or from only indirect observation of the semileptonic decay channel. The strategy pursued in this analysis is to detect the daughter hyperon Λ in the presence of a lepton with the invariant mass of the combination in the appropriate range, such, that any source for this configuration other than a semileptonic decay can be excluded. This method utilizing particle correlations is similar to the methods applied to semileptonic D meson decays.

The kinematically allowed range for the $\Lambda\ell$ invariant mass is 1.115-2.285 GeV/c^2, where a strong $\Lambda\ell^+$ signal is observed (Figure 3.26). The main three background sources have been taken into account: (1) background due to real Λ's plus a fake lepton and vice versa, (2) background due to random correlations between real Λ's and real leptons, and (3) background from the decay $\Xi_c^0 \to \Xi^- \ell^+ \nu$, the Ξ^- decaying into $\Lambda\pi^-$.

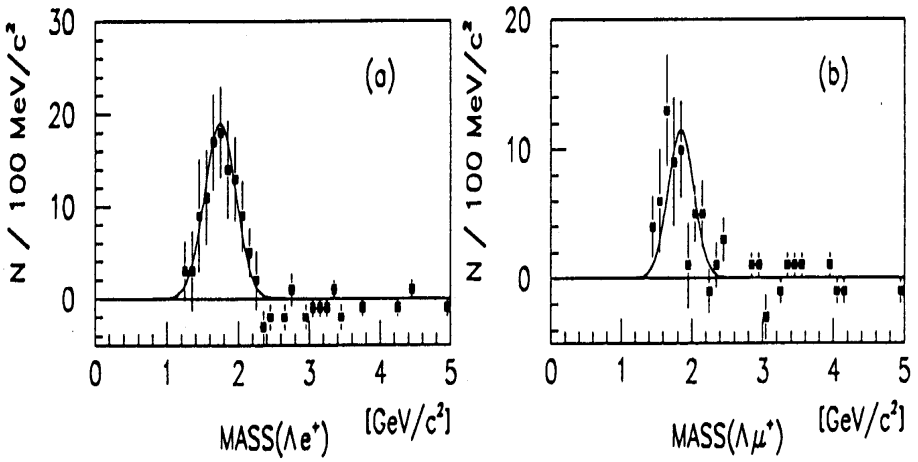

Figure 3.26: *The (a)*Λe^+ *(b)* $\Lambda\mu^+$ *invariant mass distributions for* $x_p > 0.5$*, after wrong-sign subtraction(solid squares). Overlaid are the results of Gaussian fits to the corresponding Monte Carlo distributions. Bins with zero contents are not displayed [173].*

After subtraction of all backgrounds, signals of $73.2 \pm 22.1\Lambda e^+$ and $30.1 \pm 15.5\Lambda\mu^+$ events were observed. The $\Lambda\ell^+$ invariant mass distributions are shown in Figure 3.26. In each case the overlaid line is the result of a Gaussian fit to the corresponding Monte Carlo distribution.

The resulting products of cross section times branching ratio were

$$\sigma(e^+e^- \to \Lambda_c^+ X) \cdot \mathrm{BR}(\Lambda_c^+ \to \Lambda e^+ X) = (4.20 \pm 1.28 \pm 0.71)\mathrm{pb},$$

and

$$\sigma(e^+e^- \to \Lambda_c^+ X) \cdot \mathrm{BR}(\Lambda_c^+ \to \Lambda\mu^+ X) = (3.91 \pm 2.02 \pm 0.90)\mathrm{pb}.$$

.

The absolute semileptonic branching ratios can be obtained by using an estimated production cross section of $\sigma(e^+e^- \to \Lambda_c^+ X) = 0.30 \pm 0.08$ nb yielding

$$\mathrm{BR}(\Lambda_c^+ \to \Lambda e^+ X) = (1.4 \pm 0.4 \pm 0.4)\%,$$
$$\mathrm{BR}(\Lambda_c^+ \to \Lambda\mu^+ X) = (1.3 \pm 0.7 \pm 0.4)\%.$$

An investigation of the decay $\Xi_c^0 \to \Xi^-\ell^+\nu$ was a natural continuation of the study of the decay $\Lambda_c^+ \to \Lambda\ell^+\nu$ The Ξ^- was identified through its decay into $\Lambda\pi^-$, with the Λ reconstructed as in the previous analysis.

The $\Xi^-\ell$ invariant mass distributions, for both right-sign and wrong-sign plus sideband combinations, are shown in Figure 3.27(a), where Ξ^- candidates are all $\Lambda\pi^-$ combinations within 6.6 MeV/c^2 (3σ) of the Ξ^- mass. Contributions from the non-resonant mode $\Xi_c^0 \to \Xi^-\pi^+\ell^+\nu_l$ and from the decay $\Lambda_c \to \Xi^- K^+\ell^+\nu_l$ can be shown to be negligible.

After background subtraction, a signal of 18.1 ± 5.9 events remained. Figure 3.27(b) shows the $\Xi^-\ell^+$ right - sign mass distribution after wrong - sign and sideband background subtraction. For comparison, the figure also shows the Monte Carlo generated $\Xi^-\ell^+$ mass distribution from the decay $\Xi_c^0 \to \Xi^-\ell^+\nu$, normalized to the data [174]. The cross section times branching ratios results are

$$\sigma(e^+e^- \to \Xi_c^0 X) \cdot \mathrm{BR}(\Xi_c^0 \to \Xi^- e^+ X) = (0.71 \pm 0.28 \pm 0.09)\mathrm{pb},$$
$$\sigma(e^+e^- \to \Xi_c^0 X) \cdot \mathrm{BR}(\Xi_c^0 \to \Xi^-\mu^+ X) = (0.83 \pm 0.50 \pm 0.11)\mathrm{pb}.$$

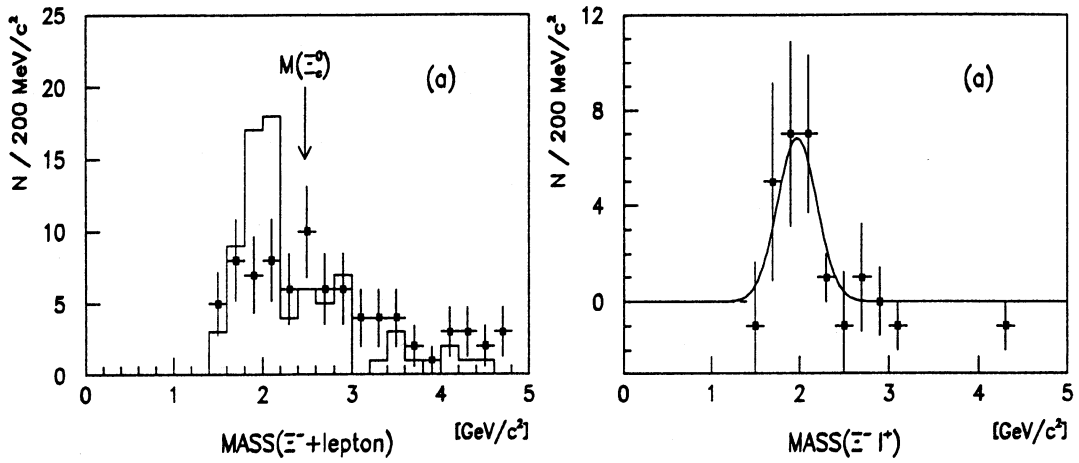

Figure 3.27: *Invariant mass $\Xi^- l^+$ combinations with $x_p > 0.45$ for events with: (a)the right-sign lepton(histogram) and wrong-sign+sideband (solid squares); (b)the right-sign lepton after background subtraction [174].*

Averaging the two values gives

$$\sigma(e^+e^- \to \Xi_c^0 X) \cdot \mathrm{BR}(\Xi_c^0 \to \Xi^- \ell^+ X) = (0.74 \pm 0.24 \pm 0.09)\mathrm{pb}.$$

This result represented the first observation of the decay $\Xi_c^0 \to \Xi^- \ell^+ \nu$. Analyses of the decay $\Lambda_c^+ \to \Lambda \ell^+ \nu$ have also been reported by other experiments. MARK II at SPEAR has measured $\mathrm{BR}(\Lambda_c^+ \to e^+ X) = (4.5 \pm 1.7)\%$ and $\mathrm{BR}(\Lambda_c^+ \to \Lambda e^+ X) = (1.1 \pm 0.8)\%$ [175] while the Fermilab 15 foot bubble chamber neutrino experiment obtains $\mathrm{BR}(\Lambda_c^+ \to \Lambda e^+ X) < 2.2\%$ at the 90 % confidence level [176].

Finally, ARGUS has searched also for evidence of semileptonic Ω_c^0 decays. This analysis searched for correlations between leptons and Ω^- hyperons, in a manner analogous to that described above for Λ_c^+ and Ξ_c semileptonic decays. The analysis is based on Ω_c^0 decays to Ω^- baryons, where the Ω^- is reconstructed in the ΛK^- final state. Λ candidates were reconstructed in the decay channel $\Lambda \to p\pi^-$.

An enhancement of 7.6 ± 3.1 entries was observed at the position of the Ω^- mass in the ΛK^- invariant mass spectrum, in the presence of an additional e^+ [178].

Interpreting these events as the products of semileptonic decays of the charmed and doubly strange baryon Ω_c^0, yields

$$\sigma(e^+e^- \to \Omega_c^0 X_1) \cdot \mathrm{BR}(\Omega_c^0 \to \Omega^- e^+ \nu_e X_2) = (0.52 \pm 0.23 \pm 0.13)\mathrm{pb}.$$

3.3.7 Measurement of Branching Ratios for Hadronic D Decays

Taking into account the importance of precise measurements of normalizing channels and in order to decrease possible sources of systematic errors, ARGUS has measured absolute branching fractions for the $D^0 \to K^-\pi^+$, $D^0 \to K^-\pi^+\pi^+\pi^-$, and $D^0 \to \overline{K}^0\pi^-\pi^+$ decay channels [179] using a method previously employed by the HRS [180] and ALEPH [181] collaborations. In this approach, first the total number of D^0 mesons produced in the decay $D^{*+} \to D^0\pi^+$ is determined using a partial reconstruction technique. Subsequent reconstruction of the exclusive decay chains $D^{*+} \to D^0\pi^+, D^0 \to K^-\pi^+, K^-\pi^+\pi^+\pi^-, K_s^0\pi^+\pi^-$ yields the numbers of D^0 decays of interest, thus allowing a measurement of the absolute branching ratios.

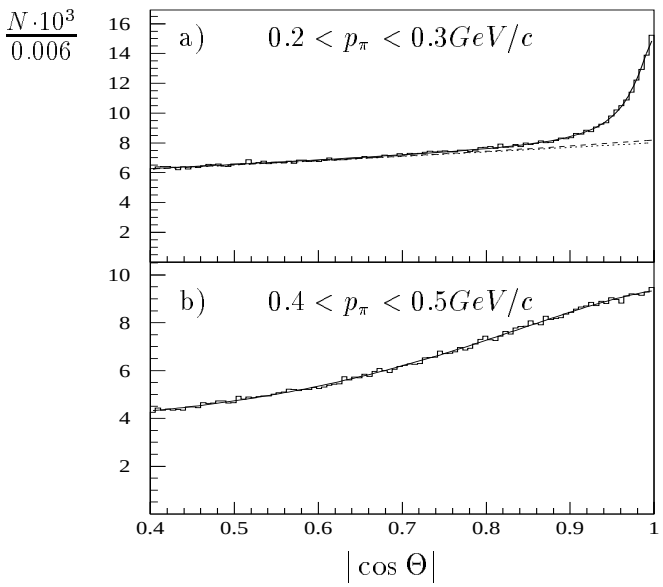

...

Figure 3.28: *Distribution of* cosΘ *for two intervals of pion momenta [179]*

Due to the hard momentum spectrum of D^{*+} mesons produced in charm fragmentation and the small energy release in $D^{*+} \to D^0\pi^+$ decay, one could expect cos Θ close to unity for this decay, where Θ is the angle between the thrust direction and decay pion momentum. The background distribution is expected to have a smooth behaviour near cos Θ = 1.

The cosΘ distribution is shown in Figure 3.28 for two intervals of pion momentum:

a) $0.2 < p_\pi < 0.3$ GeV/c

b) $0.4 < p_\pi < 0.5$ GeV/c

We attribute the sharp structure on the top part of Figure 3.28 to the decay $D^{*+} \to D^0\pi^+$. The smooth distribution on the bottom part of Figure 3.28 was obtained for pion $0.4 < p_\pi < 0.5$ GeV/c which is above the kinematical limit for the slow pion from the D^{*+} decay.

To extract the number of $D^{*+} \to \pi^+ D^0$ decays the cos Θ distribution in Figure 3.28 was fitted with a third order inverse polynomial plus the signal term. A fixed Σ_c contribution (background contribution) was included in the fit. The fit yields $51327 \pm 757 \pm 3080$ D^0s coming from D^{*+}. To determine the shape of the signal the same distribution for completely reconstructed D^{*+} mesons was obtained: $1173 \pm 37 \pm 31$, $1430 \pm 52 \pm 49$ and $284 \pm 22 \pm 17$ D^{*+} mesons in the $K^-\pi^+$,$K^-\pi^+\pi^-\pi^+$, and $K^0_s\pi^+\pi^-$ modes, respectively.

Combining the number of $D^{*+} \to \pi^+ D^0$ with the number of $D^{*+} \to \pi^+ D^0$ for the $D^0 \to K^-\pi^+$, $K^-\pi^+\pi^-\pi^+$, and $K^0_s\pi^+\pi^-$ with the corresponding efficiencies yields

$$\begin{aligned} Br(D^0 \to K^-\pi^+) &= (3.41 \pm 0.12 \pm 0.28)\% \\ Br(D^0 \to K^-\pi^+\pi^-\pi^+) &= (6.80 \pm 0.27 \pm 0.57)\% \\ Br(D^0 \to K^0_s\pi^-\pi^+) &= (5.03 \pm 0.39 \pm 0.49)\%. \end{aligned}$$

The result for the $K^-\pi^+$ channel is consistent with both the PDG value[17] and with the recent CLEO result $(3.91 \pm 0.08 \pm 0.17)\%$ [187].

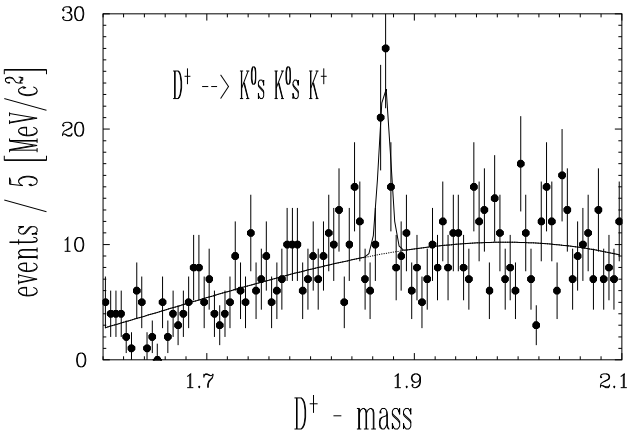

Figure 3.29: $K^0_S K^0_S K^+$ *invariant mass [190] .*

Decay mode	ARGUS	CLEO	BSW model [145]
$D^0 \to \overline{K}^0 \pi^0$	$1.8 \pm 0.2 \pm 0.3$	$2.0 \pm 0.35 \pm 0.4$	2.5
$D^0 \to \overline{K}^0 \eta$	< 2.4	$0.77 \pm 0.08 \pm 0.15$	
$D^0 \to \overline{K}^0 \eta'$	$2.0 \pm 0.7 \pm 0.4$	$1.8 \pm 0.14 \pm 0.37$	1.2
$D^0 \to \overline{K}^0 \pi^- \pi^+ \pi^0$	$9.3 \pm 0.9 \pm 2.0$	$9.5 \pm 1.3 \pm 1.5$	
$D^0 \to \overline{K}^0 \omega$	$1.6 \pm 0.4 \pm 0.4$	$3.0 \pm 0.8 \pm 0.9$	2.7
$D^0 \to \phi K^0_s$	$0.84 \pm 0.21 \pm 0.12$	0.87 ± 0.12	
$D^0 \to \overline{K}^0 K^+ K^-$	$0.46 \pm 0.11 \pm 0.06$		
$D^0 \to \overline{K}^0 \pi^- \pi^+ \pi^- \pi^+$	$0.37 \pm 0.13 \pm 0.08$	0.78 ± 0.16	
$D^0 \to K^0_S K^0_S K^0_S$	$0.18 \pm 0.07 \pm 0.05$	0.085 ± 0.027	
$D^0 \to K^- \pi^+ \pi^- \pi^- \pi^0$	$3.9 \pm 0.4 \pm 1.0$	$4.7 \pm 0.7^{+1.2}_{-1.0}$	
$D^0 \to K^- \pi^+ \omega$	$3.0 \pm 0.4 \pm 0.7$		
$D^0 \to \overline{K}^{*0} \omega$	$1.2 \pm 0.4 \pm 0.3$		
$D^0 \to \overline{K}^{*0} \eta$	< 2.9	$1.8 \pm 0.3 \pm 0.4$	2.5
$D^0 \to \overline{K}^{*-} \pi^-$	5.7 ± 0.7		
$D^0 \to \overline{K}^0 \rho$	1.2 ± 0.2		

Table 3.3: D^0 *decay branching ratios in* % *. Absolute normalization was obtained using PDG [17] branching ratios for* $D^0 \to \overline{K}^0 \pi^+ \pi^-$ *(for channels with* K^0_s *) and* $D^0 \to K^- \pi^+$ *(for all other channels)*

.

Exploiting the excellent resolution for the mass difference between the D^{*+} and the D^0, ARGUS has studied many D^0 decay channels[182, 183, 184]. The measured branching ratios are summarized in Table 3.3. where they are compared with CLEO results [185, 186] and with theoretical predictions [145].

ARGUS has also studied many D^+ and ${D_s}^+$ channels [110, 150, 189, 190]. Figure 3.29 shows the $K^0_s K^0_s K^+$ invariant mass spectrum. A clear peak of 39 ± 9 events is observed at the D^+ mass,

Table 3.4: *Cabibbo-suppressed D Decays*

Decay mode	Ratio of branching ratios	ARGUS	MARK III [194]
$D^0 \to K^- K^+$	$\frac{BR(D^0 \to K^- K^+)}{BR(D^0 \to K^- \pi^+)}$	$0.10 \pm 0.02 \pm 0.01$	$0.122 \pm 0.018 \pm 0.012$
$D^0 \to \pi^- \pi^+$	$\frac{BR(D^0 \to \pi^- \pi^+)}{BR(D^0 \to K^- \pi^+)}$	$0.040 \pm 0.007 \pm 0.006$	$0.033 \pm 0.010 \pm 0.006$
	$\frac{BR(D^0 \to K^- K^+)}{BR(D^0 \to \pi^- \pi^+)}$	2.5 ± 0.7	3.7 ± 1.4
			CLEO [206]
$D^0 \to K^+ \pi^-$	$\frac{BR(D^0 \to K^+ \pi^-)}{BR(D^0 \to K^- \pi^+)}$	< 0.009	$0.0077 \pm 0.0025 \pm 0.0025$

Branching Ratios in %

Decay Mode	ARGUS	CLEO
$D^0 \to K^+ K^- \pi^+ \pi^-$	$0.31 \pm 0.05 \pm 0.04$	0.24 ± 0.08
$D^0 \to K_s^0 K_s^0 \pi^- \pi^+$	$0.17 \pm 0.05 \pm 0.04$	
$D^0 \to \phi \pi^+ \pi^-$	$0.15 \pm 0.04 \pm 0.03$	0.19 ± 0.05
$D^0 \to K^{*0} K^- \pi^+$	$0.32 \pm 0.10 \pm 0.07$	
$D^0 \to \overline{K}^{*0} K^+ \pi^-$	$0.17 \pm 0.10 \pm 0.07$	
$D^+ \to \overline{K}^{*0} K^{*+}$	$2.6 \pm 0.8 \pm 0.7$	

yielding a branching ratio of BR($D^+ \to \overline{K}^0 \overline{K}^0 K^+$) = $(1.1 \pm 0.3 \pm 0.2)\%$. This is the only measured decay mode which involves the popping of an $s\overline{s}$ pair. The ARGUS branching ratio is somewhat smaller than the CLEO result BR($D^+ \to \overline{K}^0 \overline{K}^0 K^+$) = $(2.7 \pm 0.6)\%$ [191].

The study of Cabibbo-suppressed D^0 decays is an important means of probing the interplay between the weak and strong interactions. Only in the last few years have the experiments reached a level of sensitivity which allows the systematic study of the Cabibbo-suppressed channels.

One particularly interesting feature of Cabibbo-suppressed D^0 decays is the ratio of branching ratios for the $D^0 \to K^- K^+$ and $D^0 \to \pi^- \pi^+$ channels. Assuming SU(3) flavour symmetry, one would expect this ratio to be close to unity [192]. However, the MARK II [193] and MARK III [194] collaborations have reported an experimental value of about 3.5 with large errors. There have been theoretical attempts to attribute this discrepancy to final state interactions [195] or even to contributions from penguin diagrams [196].

This ratio of branching ratios was measured by ARGUS with increased accuracy [184] using D^0 mesons reconstructed from the decay $D^{*+} \to D^0 \pi^+$. The study of the Cabibbo-suppressed decays required careful estimation of the backgrounds from the corresponding Cabibbo-allowed decay channel $D^0 \to K^- \pi^+$. After removing these backgrounds we obtained the branching ratios normalized to the Cabibbo-allowed channel $D^0 \to K^- \pi^+$ (Table 3.4). The ratio of branching ratios obtained for the decays $D^0 \to K^- K^+$ and $D^0 \to \pi^- \pi^+$, Br($D^0 \to K^- K^+$)/Br($D^0 \to \pi^- \pi^+$) = 2.5 ± 0.7, is lower than previous results and can be theoretically understood on the basis of SU(3) breaking and final state interactions [195].

Within the framework of ARGUS investigations of Cabibbo-suppressed decays, $D \to KK\pi\pi$ decay channels were also studied in detail[189, 190]. ARGUS reported the first observation of the Cabibbo-suppressed decay $D^+ \to K^- K_s^0 \pi^+ \pi^+$ [189] which was found to proceed predominantly via $\overline{K}^{*0} K^{*+}$. Figure 3.30 shows the mass spectrum of all accepted $\overline{K}^{*0} K^{*+}$ combinations. There is one peak corresponding to the D_s^+ decay into the same final state and a clear peak at the mass of D^+. The resulting branching ratio, BR($D^+ \to \overline{K}^{*0} K^{*+}$) = $(2.6 \pm 0.8 \pm 0.7)\%$ makes this is the

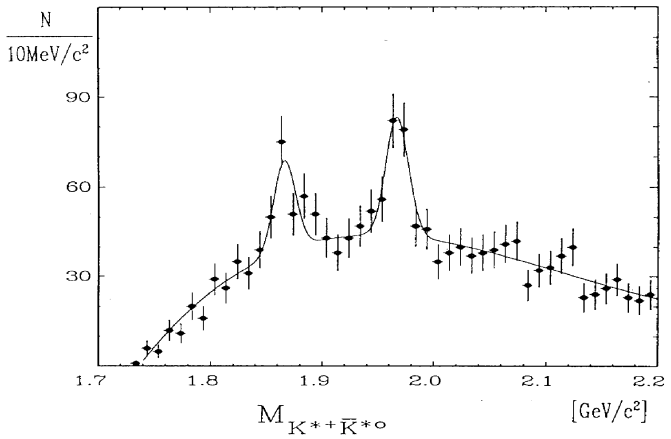

Figure 3.30: *Mass spectrum of accepted* $K^{*+}\overline{K}^{*0}$ *combinations [189] .*

strongest of all known Cabibbo-suppressed D^+ decays. The sum of all known Cabibbo-suppressed D^+ decays[17] together with the decay $D^+ \to \overline{K}^{*0} K^{*+}$ is almost twice as large as the naive spectator model expectation of

$$\sin^2 \Theta_c \cdot \mathrm{BR}(D^+ \to hadrons) \approx 3\%,$$

where Θ_c is the Cabibbo angle. Such an excess could be caused by the suppression of Cabibbo-allowed D^+ decay modes due to interference between the spectator $\overline{d}$-quark and $\overline{d}$ produced in the virtual W^- decay. This interference should reduce the contribution from Cabibbo-allowed decays to the total width of the D^+ meson, resulting in a larger D^+ lifetime (see Section 3.3.1) and higher branching ratios for the Cabibbo-suppressed decays.

ARGUS presented the first measurement of the $D^0 \to K^0_s K^0_s \pi^- \pi^+$ decay and studied the structure in the $K^+K^-\pi^+\pi^-$ final state [190] (Table 3.4). The branching ratios for the $D^0 \to K^-K^+\pi^-\pi^+$ and $D^0 \to \phi\pi^+\pi^-$ channels agree well with the other measurements [191, 197, 198], while for the $D^0 \to K^{*0}K^-\pi^+$ it is the first measurement of the branching ratio.

Exclusive charm decays with $\Delta C = -\Delta S$, such as $D^0 \to K^+\pi^-$ are especially interesting. The transition $D^0 \to K^+\pi^-$ can occur either through $D^0 \to \overline{D^0}$ mixing followed by $\overline{D^0} \to K^+\pi^-$, or through a doubly Cabibbo-suppressed decay (DCSD).

$D^0 \leftrightarrow \overline{D}^0$ transitions are allowed in the Standard Model via "box" diagrams [199], but are strongly suppressed relative to $K^0 \leftrightarrow \overline{K}^0$ and $B^0 \leftrightarrow \overline{B}^0$ transitions [200, 201, 202]. A value for r_D^{mix} of more than 10^{-3} would signify new physics beyond the Standard Model. The value for $r_{DCSD}^{K\pi} = \Gamma(D^0 \to K^+\pi^-)/\Gamma(D^0 \to K^-\pi^+)$ is proportional to $\tan^4 \Theta_c$ in the framework of the Standard Model, with predictions varying from 0.0027 to 0.0054 [202, 203].

The search for $D^0 \to K^+\pi^-$ was made by ARGUS using D^{*+} mesons reconstructed from their daughter particles in the cascade decay $D^{*+} \to D^0\pi^+$, followed by $D^0 \to K^-\pi^+$ [204, 205]. In this case DCSD or $D^0 - \overline{D^0}$ mixing will appear as a signal in the channel $D^{*+} \to \overline{D^0}\pi^+$. The ARGUS result of $r_D^{K\pi} = \dfrac{\Gamma(D^0 \to K^+\pi^-)}{\Gamma(D^0 \to K^-\pi^+)} < 0.9\%$ at 90% C.L. was for some time the best limit on the DCSD of D^0 mesons assuming negligible contribution from $D^0 - \overline{D^0}$ mixing (Table 3.4).

3.4 Summary of Charm Physics with ARGUS

The ARGUS observations of the first excited charmed meson opened up the rich field of charmed meson and baryon spectroscopy. ARGUS made substantial contributions to this field with many discoveries of S-wave and excited P-wave states of charmed hadrons. These results compared favorably with theoretical predictions for the spectra of charmed hadrons.

The weak decays of charmed hadrons were studied intensively with the observation of many new decay channels of charmed mesons and baryons. The relevance of the W-exchange mechanism in the weak decays of charmed hadrons was demonstrated through the observation of the decay $D^0 \to \phi\overline{K}^0$, and also through decays of charmed baryons. Exclusive semileptonic decays of charmed hadrons were investigated in detail.

Absolute branching ratios could be determined for the D^0 meson, by using the $D^{*+} \to D^0\pi^+$ decay for normalization, and for the Λ_c where the B meson decay to charmed baryons served for normalization.

The charm physics results of ARGUS are a valuable input for theory and, in most cases, corroborate existing theoretical predictions. "Charm" has been one of the most fruitful and exciting places in the wide field of physics covered by ARGUS.

Chapter 4

τ Physics

4.1 Introduction

The ARGUS experiment made substantial contributions to the understanding of the leptons of the third fermion generation, the τ-lepton and its neutrino. Compared to our current knowledge [17] relatively little was known about the τ-lepton when the ARGUS experiment started in 1982.

The τ-lepton was discovered at the e^+e^- storage ring SPEAR in 1975 by searching for two leptons of different flavour and unbalanced momentum in the final state [207]:

$$e^+e^- \;\rightarrow\; \tau^+\tau^- \;\rightarrow\; e^+\nu_e\overline{\nu}_\tau\,\mu^-\overline{\nu}_\mu\nu_\tau. \tag{4.1}$$

The observed final state has a very distinguished topology and with good lepton identification it is well separable from other reactions. However, at SPEAR energies, not too far from the τ pair threshold, most of the other decay modes of the τ-lepton are very difficult to extract from the data since the background from hadronic e^+e^- reactions has similar topologies and particle multiplicities.

At higher energies the topologies of τ decays become more distinct from other e^+e^- reactions: the decaying τ's develop narrow jets with low particle multiplicities. However, at the same time the production cross section drops very quickly as the energy rises, proportional to $1/E^2$. It appears that in the ARGUS energy range around $\sqrt{s} = 10$ GeV the experimental conditions for τ physics are quite optimal: The production cross section is still relatively large, the average charged multiplicity of 1.3 in τ events is sufficiently different from 10.8 in $\Upsilon(4S)$ decays and 8.35 in hadronic continuum events [208], and the boost of the τ's ensures a distinct topology of the final state. The topologies are traditionally classified according to the charged particles ('prongs') each τ decays into. The 1-3 topology shown in Figure 4.1 is one of the easiest to recognize as a τ event.

Neglecting radiative corrections the production cross section is given by

$$\sigma(e^+e^- \rightarrow \tau^+\tau^-) \;=\; \frac{4\pi\alpha^2}{3s} \tag{4.2}$$

yielding $868\,pb$ at $\sqrt{s} = 10$ GeV compared to $96\,pb$ at $\sqrt{s} = 30$ GeV, a typical energy of PETRA and PEP. At the Z^0 peak the cross section rises to a similar value as at 10 GeV and therefore the LEP experiments have become quite competitive in the last years. Because of the very small background from hadronic Z^0 decays and two-photon reactions the LEP experiments have advantages, in particular for measurements of topological branching ratios. On the other hand at these higher energies particle identification becomes more difficult and in particular π^0 reconstruction requires higher granularities of the electromagnetic shower detectors. The ARGUS energy range is certainly in this respect advantageous and a unique domain to study exclusive τ decay channels requiring identification of charged and neutral pions and kaons, electrons and muons.

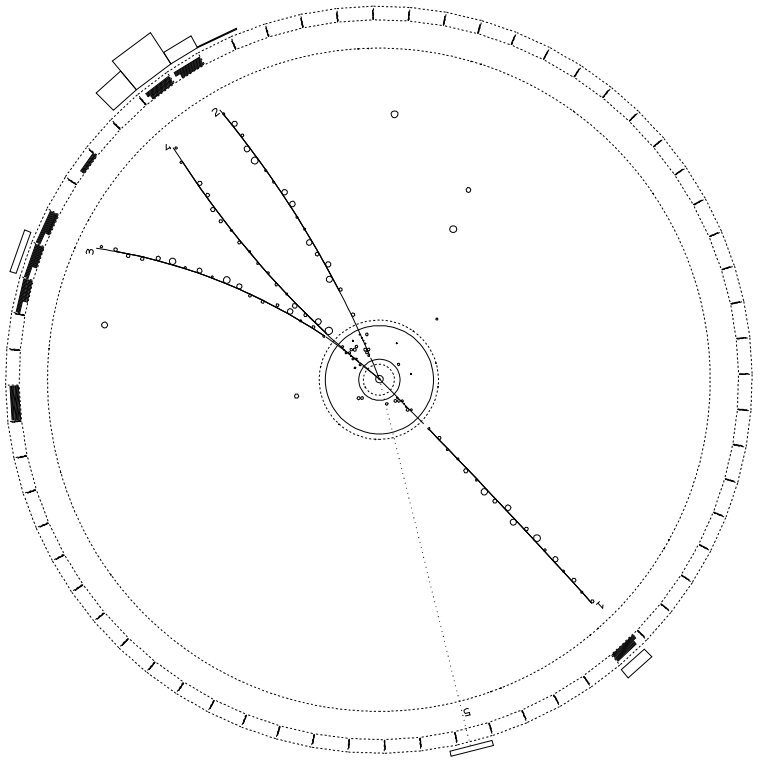

Figure 4.1: *A typical τ event with 1-3 topology produced in e^+e^- annihilation.*

The τ-lepton and its neutrino fit well into the Standard Model scenario as the leptons of the third fermion generation. In the context of this model these leptons are 'sequential' in the sense that they behave like higher mass repetitions of the electron, muon and their neutrinos. In particular, they are spin-$\frac{1}{2}$ fermions with their own absolutely conserved lepton flavour number and massless neutrino and they couple with the standard structure and strength to the electro-weak currents. Since the discovery of the τ-lepton the research goal in τ physics is the testing of these Standard Model properties, always with the hope of finding deviations pointing to new physics. Because of its high mass the τ-lepton may be closer to the scale of 'new physics' and the investigation of τ decay properties may be as sensitive as the muon decay experiments which compensate the mass deficiency through about 10^5 higher statistics.

Amongst all known leptons only the τ-lepton is heavy enough to decay into hadrons. Since the τ mass is below the threshold for open charm the charged current couplings of the τ are constrained to the three lightest quarks. Here a variety of relations for fundamental hadronic currents, such as the hypotheses of conserved vector currents and partially conserved axial vector currents or the selection rules for currents (e.g. second class currents), can be tested. The selection rules of weak currents have also the effect that the hadronic final states exhibit often a clean resonance structure. For example, the best determination of the $a_1(1270)$ resonance parameters comes from τ decay studies.

To date the ARGUS Collaboration has contributed 23 publications [209] - [231] to the understanding of the properties of the τ and its neutrino, with still more papers in preparation. The studies have covered almost all topics of τ physics (except the neutral current couplings) and many of them were pioneering works at the time. Novel methods have, for instance, been developed for the mass measurements of the τ and the ν_τ, the determination of the Michel parameters and the analysis of the Lorentz structure of hadronic τ decays yielding the helicity of the τ neutrino.

4.2 Decay Branching Ratios of the τ Lepton

4.2.1 The Charged Current in τ Decays

According to the Standard Model the τ^- lepton decays by transforming into a ν_τ under the emission of a W^- boson which then couples to a fermion–antifermion pair, either leptons or quarks (Figure 4.2). The τ mass allows for the coupling to the light lepton doublets (e, ν_e), (μ, ν_μ) and to the three lightest quark species, u, d, s. In the Standard Model both W–fermion vertices in the

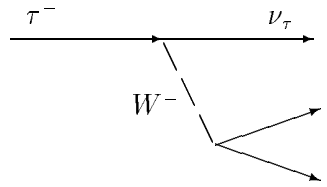

$$\left(\begin{array}{c} f \\ \overline{f} \end{array}\right) = \left(\begin{array}{c} e^- \\ \overline{\nu}_e \end{array}\right), \left(\begin{array}{c} \mu^- \\ \overline{\nu}_\mu \end{array}\right), \left(\begin{array}{c} d\cos\theta_C + s\sin\theta_C \\ \overline{u} \end{array}\right)$$

Figure 4.2: *The decay of a τ lepton via W exchange into a fermion pair.*

diagram have the same universal coupling strength given by the Fermi coupling constant G_F (times the corresponding mixing matrix element for quarks). In the limit where the squared momentum, q^2, of the exchanged W is small compared to m_W^2, which is a very good approximation for τ decays ($q^2 < {m_\tau}^2$), the W propagator becomes constant and the interaction is described by a current-current Lagrangian:

$$\mathcal{L}^{cc} = \frac{G_F}{\sqrt{2}} J^{f\dagger}(x)\, J^{\tau}(x). \tag{4.3}$$

For the lepton vertices the currents are simply calculable from the Dirac spinors with a vector and an axial-vector component.

$$J^l_\mu = \overline{u}_{\nu_l}\gamma_\mu(1-\gamma_5)u_l. \tag{4.4}$$

Also the hadronic currents have a vector and axial-vector component,

$$J^h_\mu = V_\mu + A_\mu, \tag{4.5}$$

which are, however, not easily expressed in terms of free-quark spinors. The strong interaction projects out hadronic final states h with well defined quantum numbers.

4.2.2 Leptonic Decays

The partial width for τ decays into a lepton l and neutrinos ($l = e, \mu$)

$$\tau^- \to l^-\overline{\nu}_l\nu_\tau, \tag{4.6}$$

can be calculated from the interaction of two leptonic currents (4.4) and yields:

$$\Gamma(\tau^- \to l^-\overline{\nu}_l\nu_\tau) = \frac{G_F^2}{192\pi^3}\, m_\tau^5\, f\left(\frac{m_l^2}{m_\tau^2}\right)(1-\delta_{QED})(1+\delta_{EW}) \tag{4.7}$$

The function $f(x)$ is a phase space factor accounting for the mass of the lepton l:

$$f(x) = 1 - 8x + 8x^3 - x^4 - 12x^2\ln x\,, \tag{4.8}$$

yielding $f(x) \approx 1$ for electrons and $f(x) = 0.9726$ for muons. The two additional factors account for radiative corrections and the (very small) effect of the W-propagator. The whole correction amounts to about -0.4% [232]. Differential decay distributions of the leptons will be discussed in Sect. 4.5.2 in connection with the determination of the Michel parameters.

The experimentally measurable quantities are the leptonic branching ratios B_e and B_μ of the τ which can be related to the leptonic widths via the τ lifetime τ_τ:

$$\Gamma(\tau^- \rightarrow e^- \overline{\nu}_e \nu_\tau) = \frac{B_e}{\tau_\tau} \text{ and } \Gamma(\tau^- \rightarrow \mu^- \overline{\nu}_\mu \nu_\tau) = \frac{B_\mu}{\tau_\tau}. \quad (4.9)$$

Therefore a test of lepton universality for τ decays, as will be discussed in Sect. 4.4, requires the measurement of both the leptonic branching ratio and the τ lifetime and, because of the mass dependence in (4.7), also of the τ mass.

The ARGUS group has contributed precision measurements of both leptonic branching ratios [222]. The analysis was done on two data samples with different event topologies. In one selection a single charged track was required to recoil against a system of three charged tracks (1-3 topology). No additional photon was allowed in the one-prong hemisphere and the number of photons in the three-prong hemisphere was also restricted to suppress background from hadronic annihilation events. With additional cuts to ensure good particle identification on the one-prong side, the single charged track was then classified as electron (e), muon (μ) or hadron (h = pion or kaon, not separated). This allowed the determination of the ratios B_μ/B_e and B_h/B_e which are independent of the three-prong branching ratio.

To resolve the separate branching ratios 1-1 topologies with an identified electron and muon were also selected, i.e. the purely leptonic reaction (4.1). Note that the electron-muon combination has much less of a background problem than the same reaction with two leptons of equal type which has to be separated from the corresponding QED reaction. From this selection the product $B_\mu \cdot B_e$ was determined (updated in [227]). The analyses of both topologies yielded [222, 227]:

$$\begin{aligned} B_\mu \cdot B_e &= 0.0306 \pm 0.0005 \pm 0.0013 \\ B_\mu/B_e &= 0.997 \pm 0.035 \pm 0.040 \\ B_h/B_e &= 0.678 \pm 0.037 \pm 0.044 \end{aligned}$$

From these the branching ratios B_e, B_μ and B_h can be determined independently of any other branching ratio [222, 227]:

$$\begin{aligned} B_e &= (17.5 \pm 0.3 \pm 0.5)\% \\ B_\mu &= (17.4 \pm 0.3 \pm 0.5)\% \end{aligned}$$

The single hadron branching ratio B_h will be discussed in Sect. 4.3.2. The consistency of these results with lepton universality depends also on the mass and lifetime of the τ and will be discussed in Sect. 4.4.

4.2.3 Hadronic Decays

The hadronic current in (4.5) leads to final states with well defined quantum numbers:

- Spin-parity: The space-time transformation properties of the V and A currents fix the allowed spin and parity, J^P, of the hadronic states:

$$\begin{aligned} V_\mu: \quad J^P &= 1^-,\ 0^+ \\ A_\mu: \quad J^P &= 1^+,\ 0^- \end{aligned}$$

- Isospin: Since the hadronic system in τ decays is charged the isospin is $I \geq 1$ for non-strange systems. If the W couples, as expected, initially to $q\overline{q}$ pairs the isospin is further constrained:

$$\begin{aligned} I &= 1 \quad \text{for } u\overline{d} \\ I &= \tfrac{1}{2} \quad \text{for } u\overline{s} \end{aligned}$$

Table 4.1: *The spectral functions and possible $q\overline{q}$ resonances with the same quantum numbers which could be observed in τ decays.*

spectral function	J^{PG}	I	S	resonances
a_0	0^{--}	1	0	π^-
a_1	1^{+-}	1	0	$a_1^-(1260)$
v_0	0^{++}	1	0	–
v_1	1^{-+}	1	0	$\rho^-(770)$
a_0^s	0^-	$\frac{1}{2}$	-1	K^-
a_1^s	1^+	$\frac{1}{2}$	-1	$K_1(1270)$, $K_1(1400)$
v_0^s	0^+	$\frac{1}{2}$	-1	$K_0^*(1430)$
v_1^s	1^-	$\frac{1}{2}$	-1	$K^*(892)$

- G-parity: For non-strange $q\overline{q}$ systems isospin and angular momentum fixes also the G-parity ($G(q\overline{q}) = (-1)^{L+S+I}$) leading to multi-pion final states with either an even or odd number of pions:

$$\begin{aligned} GV_\mu G^{-1} &= +V_\mu \rightarrow 2n\,\pi \\ GA_\mu G^{-1} &= -A_\mu \rightarrow (2n-1)\,\pi \end{aligned}$$

Hadronic final states with the opposite G-parity are called 'second class currents' and are suppressed on the level at which isospin violation is suppressed in strong interactions. The quantum numbers for the different currents are:

	first class current	second class current
V_μ :	$J^{PG} = 1^{-+},\ 0^{++}$	$J^{PG} = 1^{--},\ 0^{+-}$
A_μ :	$J^{PG} = 1^{+-},\ 0^{--}$	$J^{PG} = 1^{++},\ 0^{-+}$

No second class currents have been observed yet, in particular the formation of resonances with the 'wrong' G-parity, e. g.:

$$\begin{aligned} a_0^-(980) &\rightarrow \eta\pi^-\,(S-wave) \quad J^{PG} = 0^{+-} \\ b_1^-(1235) &\rightarrow \omega\pi^-\,(S-wave) \quad J^{PG} = 1^{++} \end{aligned}$$

In the case of the $\eta\pi^-$ a P-wave state with $J^{PG} = 1^{--}$ can also only be produced via a second class current, while the $\omega\pi^-$ P-wave state with $J^{PG} = 1^{-+}$ is allowed. The ARGUS collaboration has analysed both final states in τ decays. No evidence was found for the decay into $\eta\pi^-$ [218] (see sect. 4.3.1) and for the decay into an $\omega\pi^-$ S-wave state [213] (see sect. 4.3.1).

The hadronic τ decay width and spectral functions: The differential decay width of τ leptons into hadrons with a squared invariant mass q^2 $(= m^2(W^*))$ can be decomposed into spectral functions with the allowed quantum numbers for non-strange and strange V and A currents:

$$\begin{aligned} \frac{d\Gamma}{dq^2} &= \frac{G_F^2}{32\pi^2 m_\tau^3}(m_\tau^2-q^2)^2\,\{[(m_\tau^2+2q^2)\,(v_1(q^2)+a_1(q^2))+m_\tau^2\,(v_0(q^2)+a_0(q^2))]\cos^2\theta_c \\ &\quad + [(m_\tau^2+2q^2)\,(v_1^s(q^2)+a_1^s(q^2))+m_\tau^2\,(v_0^s(q^2)+a_0^s(q^2))]\sin^2\theta_c\}\,. \end{aligned} \tag{4.10}$$

In Table 4.1 the currents and their quantum numbers are listed together with the $q\overline{q}$ resonances with the same quantum numbers which could be observed in τ decays.

There are many theoretical predictions for the spectral functions and for single decay channels:

- The τ decay into a single pion (kaon) is related by the universality hypothesis to leptonic pion (kaon) decays.

- The 'conserved vector current' hypothesis (CVC) connects the isovector part of the electromagnetic current in e^+e^- annihilation with the non-strange vector spectral function. It predicts that the scalar vector current (v_0) contribution vanishes.

- Less firm predictions are made for the axial-vector current based on the hypothesis of the 'partially conserved axial-vector current' (PCAC).

- Sum rules connect integrals over spectral functions.

- The ratio of the hadronic to the leptonic decay width has been calculated in the framework of perturbative QCD (very similarly to the corresponding ratio in e^+e^- annihilation).

In the following section the ARGUS results on hadronic τ decays will be discussed in terms of these spectral functions and, where possible, compared to the theoretical predictions.

4.2.4 Non-Standard Decays

Search for Neutrinoless τ Decays

The Standard Model assigns to the leptons of each generation separately a lepton number which is absolutely conserved. Despite intensive experimental efforts there is no convincing indication of lepton number violation, either from muon decays, neutrino oscillations or double-β decays. Nonetheless, there are many extensions of the Standard Model which require lepton number violation. In some of these models lepton number violation in τ decays could be enhanced relative to that in muon decays by some power of the mass ratio. Therefore, due to the large τ mass the τ decay experiments may have similar sensitivity to new physics as the muon decay experiments which profit from several orders of magnitude larger statistics.

Conserving its lepton number a τ lepton can only decay by emitting a τ neutrino. The ARGUS Collaboration published a first search for neutrino-less decays in 1986 based on an integrated luminosity of $177\,pb^{-1}$ [212]. With increased statistics, corresponding to $387\,pb^{-1}$, the analysis was repeated and extended [223]. With a total of 29 investigated channels (Table 4.2) this was at the time of publication the most comprehensive and for many channels the most significant search. Of special interest for GUT theories are the channels which violate both lepton and baryon number like $\tau^- \to \overline{p}\gamma$, $\tau^- \to \overline{p}\pi^0$ and $\tau^- \to \overline{p}\eta$.

Search for a Higgs Decay into τ Pairs

In 1984 the Crystal Ball Collaboration stimulated some excitement by reporting the possible observation of a Higgs particle with a mass of 8.3 GeV/c^2 produced in radiative decays of the Υ resonance. Since the Standard Model Higgs boson would preferentially couple to the heaviest accessible fermions the ARGUS Collaboration searched on the Υ resonance for radiative transitions to τ pairs with a mass around 8.3 GeV/c^2 [209]. The ARGUS group could not confirm the Crystal Ball finding and, also for other reasons, the excitement about the Higgs 'discovery' dissipated.

Table 4.2: *Upper limits* $[10^{-5}]$ *(90% CL) on branching ratios of neutrinoless* τ *decays compared with results from previous experiments [212, 223, 254, 255, 256].*

Decay Channel	MARK II	ARGUS 86	Crystal Ball	CLEO	ARGUS 91
$\tau^- \to e^- e^+ e^-$	40	3.8		3.0	1.3
$\tau^- \to e^- \mu^+ \mu^-$	33	3.3		2.7	1.9
$\tau^- \to e^+ \mu^- \mu^-$				1.6	1.8
$\tau^- \to \mu^- e^+ e^-$	44	3.3		2.7	1.4
$\tau^- \to \mu^+ e^- e^-$				1.6	1.4
$\tau^- \to \mu^- \mu^+ \mu^-$	49	2.9		1.7	1.9
$\tau^- \to e^- \pi^+ \pi^-$		4.2		6.0	2.7
$\tau^- \to e^+ \pi^- \pi^-$				1.7	1.8
$\tau^- \to \mu^- \pi^+ \pi^-$		4.0		3.9	3.6
$\tau^- \to \mu^+ \pi^- \pi^-$					6.3
$\tau^- \to e^- \rho^0$	37	3.9			1.9
$\tau^- \to \mu^- \rho^0$	44	3.8			2.9
$\tau^- \to e^- \pi^+ K^-$		4.2		5.8	2.9
$\tau^- \to e^+ \pi^- K^-$				4.9	2.0
$\tau^- \to \mu^- \pi^+ K^-$		12		7.7	11
$\tau^- \to \mu^+ \pi^- K^-$				4.0	5.8
$\tau^- \to e^- K^{*0}$	130	5.4			3.8
$\tau^- \to \mu^- K^{*0}$	100	5.9			4.5
$\tau^- \to e^- \gamma$	64		20		12
$\tau^- \to e^- \pi^0$	210		14		17
$\tau^- \to \mu^- \gamma$	55				3.4
$\tau^- \to \mu^- \pi^0$	82				4.4
$\tau^- \to e^- \eta$			24		6.3
$\tau^- \to \mu^- \eta$					7.3
$\tau^- \to \bar{p} \gamma$					29
$\tau^- \to \bar{p} \pi^0$					65.5
$\tau^- \to \pi^- \gamma$					28
$\tau^- \to \pi^- \pi^0$					37
$\tau^- \to \bar{p} \eta$					129

4.3 Properties of Hadronic τ Decays

4.3.1 Vector currents

The (first-class) vector currents have even G-parity: $GVG^{-1} = +V$. This restricts the possible hadronic decay channels:

$$\begin{array}{lll} J^{PG} = 1^{-+}: & \tau \rightarrow & 2n\pi\,\nu,\ \eta\pi\pi\nu,\ \omega\pi\nu,\ K\overline{K}\pi\nu,\ \ldots \\ J^{PG} = 0^{++}: & & \text{forbidden by CVC} \end{array}$$

The formation of vector states in τ decays and e^+e^- annihilation is related by the CVC hypothesis. CVC forbids the formation of scalars which is related to the fact that $q\overline{q}$ states with these quantum numbers have even C-parity and hence are not produced in e^+e^- annihilations. The occurrance of states with non-$q\overline{q}$ quantum numbers or second class currents at a level higher than expected by isospin violation effects could point to new physics. None of the following states has been observed (L is the final state angular momentum):

state	L	J^{PG}	class	ARGUS Ref.
$\pi^-\pi^0$	S-wave	0^{++}	exotic	[229]
$\eta\pi^-$	S-wave	0^{+-}	2nd class (e.g. $a^0(980)$)	[218]
$\eta\pi^-$	P-wave	1^{--}	2nd class, exotic	[218]
$\omega\pi^-$	S-wave	1^{++}	2nd class, (e.g. $b_1^-(1235)$)	[213]

The ARGUS limits on these channels are discussed in this section below, except for the limit on the $\pi^-\pi^0$ channel which is discussed in section 4.5.1.

The two-pion final state

The τ decay mode

$$\tau^- \rightarrow \pi^-\pi^0\nu_\tau \tag{4.11}$$

has the largest branching ratio of all τ decays. The two-pion spectrum is dominated by the ρ resonance (Figure 4.3). The ARGUS group has analysed this two-pion channel together with the corresponding strange final state $K^-\pi^0$, which is dominated by the K^* resonance (see Sect. 4.3.3), employing a data sample corresponding to $198\,pb^{-1}$ [217].

With a somewhat larger data sample ($264\,pb^{-1}$) the two-pion analysis was repeated for τ pair events where both τ's decay into the two-pion state [224]. This makes the analysis less dependent on other τ branching ratios. The measured branching ratio is:

$$\mathrm{Br}(\tau^- \rightarrow \pi^-\pi^0\nu_\tau) \;=\; (22.6 \pm 0.4 \pm 0.9)\%.$$

The current world average, dominated by CLEO and LEP results, lies substantially higher: $Br(\tau^- \rightarrow \pi^-\pi^0\nu_\tau) \;=\; (25.2 \pm 0.4)\%$ [17].

CVC comparison: In terms of the spectral function v_1 the $\pi^-\pi^0$ mass spectrum is given by (q^2 is the two-pion invariant mass):

$$\frac{d\Gamma(q^2)}{dq} = \frac{G_F^2}{16\pi^2 m_\tau^3} q(m_\tau^2 - q^2)^2(m_\tau^2 + 2q^2)v_1(q^2)\,. \tag{4.12}$$

The CVC hypothesis relates the isospin $I = 1$ part of $\pi^+\pi^-$ production in e^+e^- annihilations to the spectral function v_1 in τ decays:

$$v_1(q^2) = \frac{q^2 \cdot \sigma^{e^+e^-\rightarrow\pi^+\pi^-}_{I=1}(q^2)}{4\pi^2\alpha^2}\,. \tag{4.13}$$

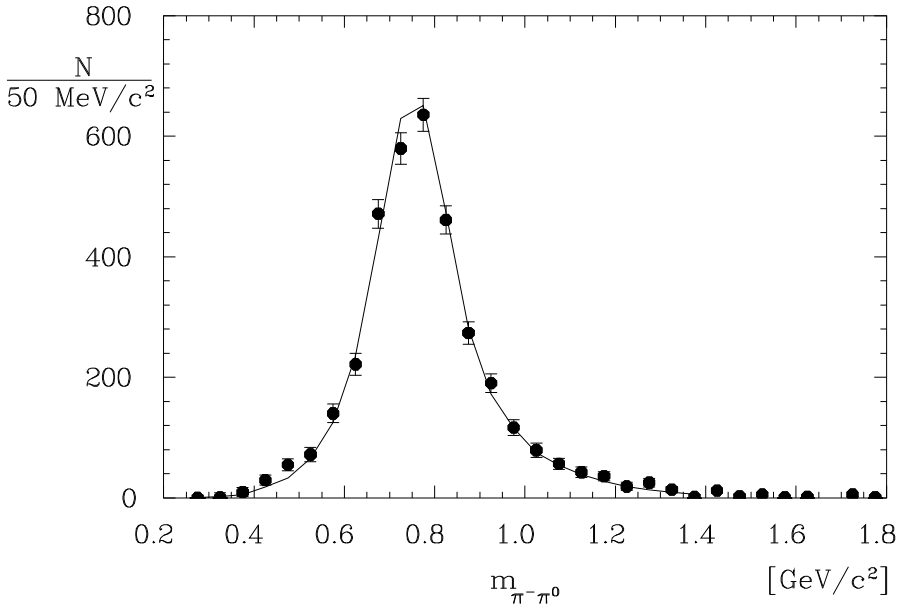

Figure 4.3: *Two-pion mass spectrum of the decay $\tau^- \to \pi^-\pi^0\nu_\tau$ compared to the CVC prediction [224].*

The e^+e^- cross section for $I = 0$ and 1 , on the other hand, can be described by introducing the pion form factor (in the time-like region):

$$\sigma^{e^+e^- \to \pi^+\pi^-}_{I=1,0} = \frac{\pi\alpha^2}{3q^2}\left(1 - \frac{4m_\pi^2}{q^2}\right)^{\frac{3}{2}} |F_\pi(q^2)|^2 \,. \tag{4.14}$$

For the calculation of the spectral function the pion form factor has to be corrected for the $I = 0$ contribution from $\omega \to \pi^+\pi^-$ which leads to the $\rho - \omega$ interference in the e^+e^- cross section. Integrating the spectrum (4.12) with a form factor $|F_\pi^{I=1}|^2$ determined from e^+e^- data yields the prediction $\mathrm{Br}(\tau^- \to \pi^-\pi^0\nu_\tau) = (1.32 \pm 0.05) \cdot \mathrm{Br}(\tau^- \to e^-\bar{\nu}_e\nu_\tau)$ [233]. The experimental value using the ARGUS results for the branching ratios (see Sect. 4.2.2 for the electron branching ratio) is:

$$\frac{\mathrm{Br}(\tau^- \to \pi^-\pi^0\nu_\tau)}{\mathrm{Br}(\tau^- \to e^-\bar{\nu}_e\nu_\tau)} = 1.29 \pm 0.07$$

The comparison shows good agreement between the ARGUS result and the CVC prediction. Using the world averages for the branching ratios the above defined ratio becomes 1.40 ± 0.03 [17].

The two-pion mass spectrum is well fitted by the standard relativistic Breit-Wigner for the ρ resonance except for the high mass tail. The data are fitted much better using the pion form factor parametrisation of [233] which includes besides the dominant ρ resonance additional contributions modifying in particular the high mass region. The deviation from a Breit-Wigner behaviour has been interpreted as a contribution from higher resonances. The $e^+e^- \to \pi^+\pi^-$ data can be fitted by two interfering ρ' resonances (2^3S_1 at $\sim$ 1350 Mev and 1^3D_1 at $\sim$ 1700 MeV) [234]. The τ data are consistent with this description although there is no sensitivity to the higher resonance because of the restricted phase space.

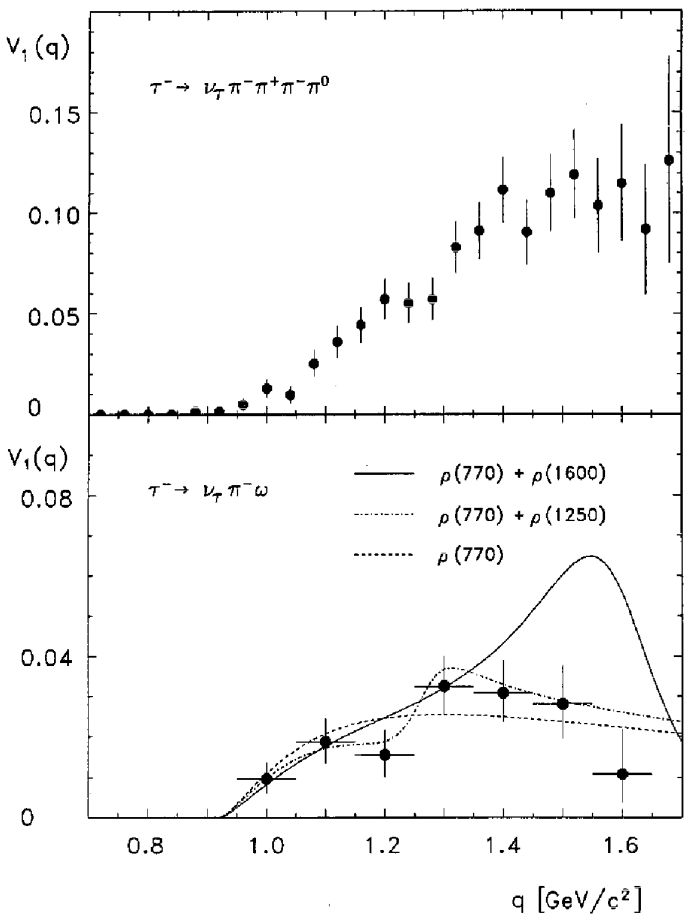

Figure 4.4: *Top: Spectral function for the decay* $\tau^- \to \pi^-\pi^-\pi^+\pi^0\nu_\tau$ *measured by ARGUS [213]. Bottom: Same distribution for the decay* $\tau^- \to \omega\pi^-\nu_\tau$ *with the result of three different fits to* $\sigma_{e^+e^-\to\omega\pi^0}$ *measurements [213].*

The four-pion final states

The four-pion final state in τ decays has been analysed by ARGUS [213, 215, 221] in the three charge mode

$$\tau^- \to \pi^-\pi^-\pi^+\pi^0\nu_\tau. \tag{4.15}$$

The other possible mode, $\tau^- \to \pi^- 3\pi^0\nu_\tau$, makes very high demands on the photon detection efficiency and was not considered by ARGUS.

The decay (4.15) was searched for in τ events with the characteristic 1-3 topology. From an event sample corresponding to an integrated luminosity of $64\,pb^{-1}$ the following branching ratio was obtained [213]:

$$\mathrm{Br}(\tau^- \to \pi^-\pi^-\pi^+\pi^0\nu_\tau) \;=\; (4.2 \pm 0.5 \pm 0.9)\%.$$

The measured spectral function for this decay is shown in Figure 4.4a.

The CVC hypothesis relates this result to the $I = 1$ part of four-pion production in e^+e^- annihilation. The spectral function for the decay (4.15) is given by [235]:

$$v_1^{4\pi} = \frac{q^2}{4\pi^2\alpha^2}\left(\frac{1}{2}\sigma^{I=1}_{e^+e^-\to 2\pi^+2\pi^-}(q^2) + \sigma^{I=1}_{e^+e^-\to\pi^+\pi^-2\pi^0}(q^2)\right). \tag{4.16}$$

Table 4.3: Fraction of resonances produced in the decay $\tau^- \to \pi^-\pi^-\pi^+\pi^0\nu_\tau$ as measured by ARGUS [221].

ρ^0	$0.30 \pm 0.04 \pm 0.02$
$\rho^\pm$	$0.33 \pm 0.06 \pm 0.01$
ρ^-	$0.26 \pm 0.05 \pm 0.01$
ρ^+	$0.10 \pm 0.03 \pm 0.004$
$\rho^0 + \rho^\pm$	$0.64 \pm 0.07 \pm 0.03$
ω	$0.33 \pm 0.04 \pm 0.02$

From the measured e^+e^- cross sections Gilman and Rhie made the prediction [235]:

$$\mathrm{Br}(\tau^- \to \pi^-\pi^-\pi^+\pi^0\nu_\tau) = (0.275^{+0.03}_{-0.09}) \cdot \mathrm{Br}(\tau^- \to \mathrm{e}^-\bar{\nu}_\mathrm{e}\nu_\tau).$$

With the electron branching ratio from ARGUS (Sect. 4.2.2) the prediction becomes

$$\mathrm{Br}(\tau^- \to \pi^-\pi^-\pi^+\pi^0\nu_\tau) = (4.8^{+0.5}_{-1.6})\%$$

which is in agreement with the measurement (although the statistical significance is not overly compelling).

The $\pi^-\pi^-\pi^+\pi^0$ channel was further analysed for resonant substructures [221] and was found to be dominated by the channels $\rho\pi\pi$ and $\omega\pi$. No $\rho\rho$ contribution was observed (Table 4.3).

The $\omega\pi$ final state: The τ decay channel

$$\tau^- \to \omega\pi^-\nu_\tau \tag{4.17}$$

was observed for the first time by ARGUS in 1986 [213]. The branching ratio was determined to be:

$$\mathrm{Br}(\tau^- \to \omega\pi^-\nu_\tau) \;=\; (1.5 \pm 0.3 \pm 0.3)\%.$$

The measured spectral function in Figure 4.4b is compared to different parametrisations of the $e^+e^- \to \omega\pi^0$ cross section [236]. The data are compatible with a $\rho(770) \to \omega\pi$ contribution. The presence of higher ρ resonances could not be proven or disproven.

The $\omega\pi$ system could be produced via a second-class current with $J^{PG} = 1^{++}$, e. g. via the axial-vector resonance $b_1^-(1235)$ (see Sect. 4.2.3). This resonance decays mainly into an $\omega\pi^-$ system in a relative S-wave while the expected first-class vector current with $J^{PG} = 1^{-+}$ leads to a relative P-wave. ARGUS has determined the spin and parity of the $\omega\pi$ system by analysing the distribution of the angle ψ between the normal to the ω decay plane and the direction of the π^- in the ω rest frame. No indication for the presence of a second-class current was found. However, due to the limited statistics only contributions of more than 50% (90% c.l.) could be excluded.

Decay modes involving η mesons

Searches for η's in τ decays were stimulated some years ago by the unconfirmed observation of the decay

$$\tau^- \to \eta\pi^-\nu_\tau \tag{4.18}$$

by the HRS experiment [237]. This hadronic state, independent of its angular momentum, cannot be produced by a first-class current (see discussion in Sect. 4.2.3). It should thus be suppressed in τ decays to a level at which isospin violation occurs (here about $1.5 \cdot 10^{-5}$ [238]).

Figure 4.5: *Distribution of the $\pi^+\pi^-\pi^0$ invariant mass in τ decays of the type $\tau^- \to \pi^-\pi^-\pi^+\pi^0\nu_\tau$ [215].* a*) Simulated events with an η yield corresponding to the HRS measurement; b) data.*

Soon after the HRS announcement the ARGUS group published an upper limit for the $\eta\pi$ channel (less than 1.3% at 95% c.l.) [215] which was in striking contradiction to the HRS result. ARGUS searched for the η decay mode $\eta \to \pi^-\pi^+\pi^0$ in the four-pion final state which exhibits the clean ω signal in the three-pion mass distribution. The disagreement with the HRS result is best seen from the plots in Figure 4.5 where the η signal expected from HRS is compared to the data. In a subsequent publication ARGUS quoted an improved upper limit [218]:

$$\mathrm{Br}(\tau^- \to \eta\pi^-\nu_\tau) \; < \; 0.9\% \text{ at } 95\% \text{ c.l.}$$

In this publication limits were also given for inclusive η production in τ decays and some exclusive channels containing η's. The CLEO group has since substantially improved these limits or, in the case of the $\eta\pi\pi$ final state, has found a positive signal. The most stringent limit for the $\eta\pi$ channel, and in general for second-class currents, comes also from the CLEO Collaboration [239]:

$\mathrm{Br}(\tau^- \to \eta\pi^-\nu_\tau) \; < \; 3.4 \cdot 10^{-4}$ at 95% c.l.

4.3.2 Axial-vector currents

The (first-class) axial-vector currents have odd G-parity: $GAG^{-1} = -A$. It follows that multi-pion final states have an odd number of pions. The non-strange axial-vector currents seem to be nearly saturated by only two states, the π and the $a_1(1260)$:

$$\begin{array}{llrcll} a_0 \text{ current,} & J^{PG} = 0^{--}: & \tau & \to & \pi\nu & \\ a_1 \text{ current,} & J^{PG} = 1^{+-}: & \tau & \to & a_1(1260)\nu & \to \; 3\pi\nu \\ & & \tau & \to & 5\pi\nu & \text{only} \; \approx 0.5\% \end{array}$$

The τ decay into a single pion or kaon

In the Standard Model with universal couplings the τ decay into a pion or kaon,

$$\tau^- \; \to \; \pi^-(K^-)\nu_\tau \,,$$

is related to the corresponding leptonic meson decays via the same decay constants f_π and f_K:

$$\begin{array}{rcl} \Gamma(\tau^- \to \pi^-\nu_\tau) & = & \frac{G_F^2}{16\pi} f_\pi^2 \cos^2\theta_C \, m_\tau^3 \left(1 - \frac{m_\pi^2}{m_\tau^2}\right)^2 (1 + r_\pi) \\ \Gamma(\tau^- \to K^-\nu_\tau) & = & \frac{G_F^2}{16\pi} f_K^2 \sin^2\theta_C \, m_\tau^3 \left(1 - \frac{m_K^2}{m_\tau^2}\right)^2 (1 + r_K) \end{array}$$

Predictions have been obtained with $f_\pi = 0.943\, m_\pi$ and $f_K = 0.313\, m_K$ and the radiative corrections from [232] ($r_\pi = r_K = 0.019 \pm 0.01$).

Together with the determination of the leptonic branching ratios, as described in Sect. 4.2.2, ARGUSalso measured the branching ratio into a single charged pion or kaon where the pions and kaons have not been separated [222] :

$$\mathrm{Br}(\tau^- \to \pi^-/K^-\nu_\tau) \; = \; (11.7 \pm 0.6 \pm 0.8)\%$$

which is in good agreement with the theoretical prediction of $(11.80 \pm 0.12)\%$ obtained from the above expressions for the widths together with world averages for the leptonic branching ratios and the τ lifetime [17].

The τ decay into three pions

Of the two possible three-pion final states in τ decays ARGUS has studied in detail the channel with three charged pions [226]. For this analysis events of the type (1-3 topology)

$$e^+e^- \; \to \; \tau^+\tau^- \; \to \; (1 - prong)^+ \; + \; \pi^+\pi^-\pi^-\nu_\tau$$

were selected from a data sample corresponding to about $264\, pb^{-1}$. The three-pion invariant mass distribution of the selected 10323 events have a relatively large background of 27.6 % from hadronic one-photon annihilation (7.2 %) and from other τ decays, mainly $\tau^- \; \to \; \pi^+\pi^-\pi^-\pi^0\nu_\tau$, (19.3 %). The background was studied in great detail and subtracted from all distributions used for the a_1 analysis (see below).

Since kaons have not been rejected explicitly the data sample contains three-charged-hadron final states with kaons, including $K_S^0\pi^-$ with the K_S^0 decaying into $\pi^+\pi^-$. The kaon modes were estimated to contribute with a branching ratio of 0.75 % and were subtracted as background.

The distribution of unlike- and like-sign two-pion masses in Figure 4.6a demonstrates the dominance of the $\rho\pi$ intermedidate state. The three-pion and two-pion mass distributions are well reproduced by the KORALB Monte Carlo program [240] with adjusted a_1 parameters (m = 1280 MeV,

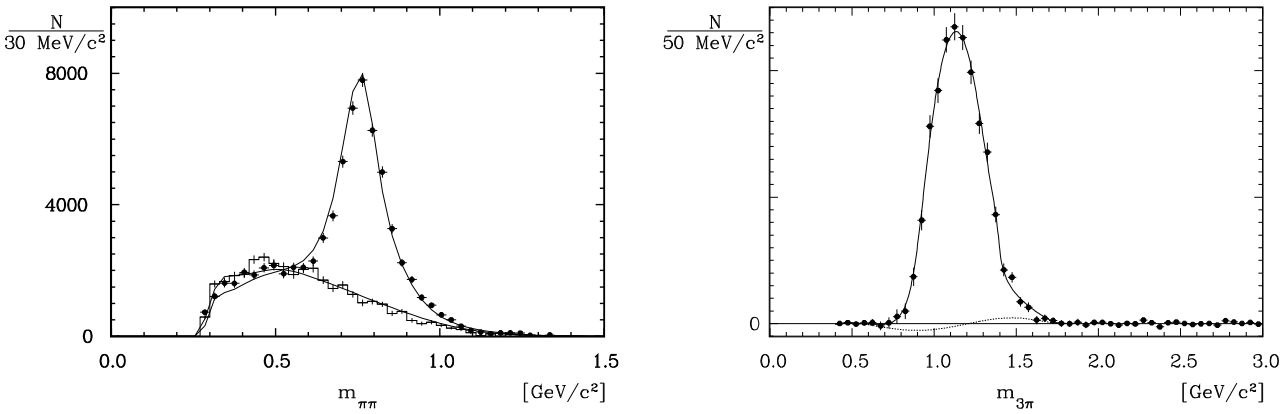

Figure 4.6: *Background corrected two- and three-pion mass spectra of the decay* $\tau^- \to \pi^-\pi^-\pi^+\nu_\tau$ *[226]. The two-pion plot shows the like-sign (one entry per event) and unlike-sign (two entries per event) combinations (curves: KORALB Monte Carlo). The three-pion mass spectrum is fitted by the model of Isgur et al. [241].*

Γ = 599 MeV). Using this Monte Carlo program for efficiency corrections the following branching ratio was obtained:

$$\mathrm{Br}(\tau^- \to \pi^+\pi^-\pi^-\nu_\tau) \;=\; (6.8 \pm 0.1 \pm 0.5)\,\%.$$

This result depends on the one-prong branching ratio (86.13 %) but was found to be quite insensitive to changes in the assumed composition of the one-prong side.

The Particle Data Group quotes a branching ratio for three charged hadrons, i.e. pions and kaons not separated and $K^0_S \to \pi^+\pi^-$ decays included: $\mathrm{Br}(\tau^- \to h^+h^-h^-\nu_\tau) = (8.42 \pm 0.31)\,\%$ [17]. For a comparison the ARGUS branching ratio has to be increased by 0.75 % to account for kaon modes:

$$\mathrm{Br}(\tau^- \to h^+h^-h^-\nu_\tau) \;=\; (7.6 \pm 0.1 \pm 0.5)\,\%.$$

Determination of the $a_1(1260)$ resonance parameters

The τ decay into three pions is dominated by the $a_1(1260)$ resonance ($\mathrm{I^G(J^P)} = 1^-(1^+)$) which decays dominantly via an intermediate $\rho\pi$ into three pions (see Figure 4.6):

$$\tau^- \;\to\; a_1^-\nu_\tau \;\to\; \rho^0\pi^-\nu_\tau \;\to\; \pi^+\pi^-\pi^-\nu_\tau \qquad (4.19)$$

In this decay mode ARGUS observed for the first time parity violation in τ decays [220] (see Sect. 4.5.1). Since the determination of electro-weak parameters from the measured parity violating asymmetry depends sensitively on the structure of the a_1 decay the ARGUS group has carried out a detailed study of the a_1 resonance in τ decays [226].

In this decay the $a_1(1260)$ resonance has a small non-resonant background. Fitting the model of Isgur et al. [241] to the three-pion mass spectrum in Figure 4.6b yields:

$$m_{a1} \;=\; (1.211 \pm 0.007)\ \mathrm{GeV} \text{ and } \Gamma_{a1} \;=\; (0.446 \pm 0.021)\ \mathrm{GeV}.$$

The statistical errors are quite small but the model dependence is large. Using for example the model of Kühn et al. [233], which is implemented in the KORALB and KORALZ Monte Carlo programs and which also describes the data reasonably well, ARGUS obtains:

$$m_{a1} \;=\; (1.274 \pm 0.007)\ \mathrm{GeV} \text{ and } \Gamma_{a1} \;=\; (0.594 \pm 0.023)\ \mathrm{GeV}.$$

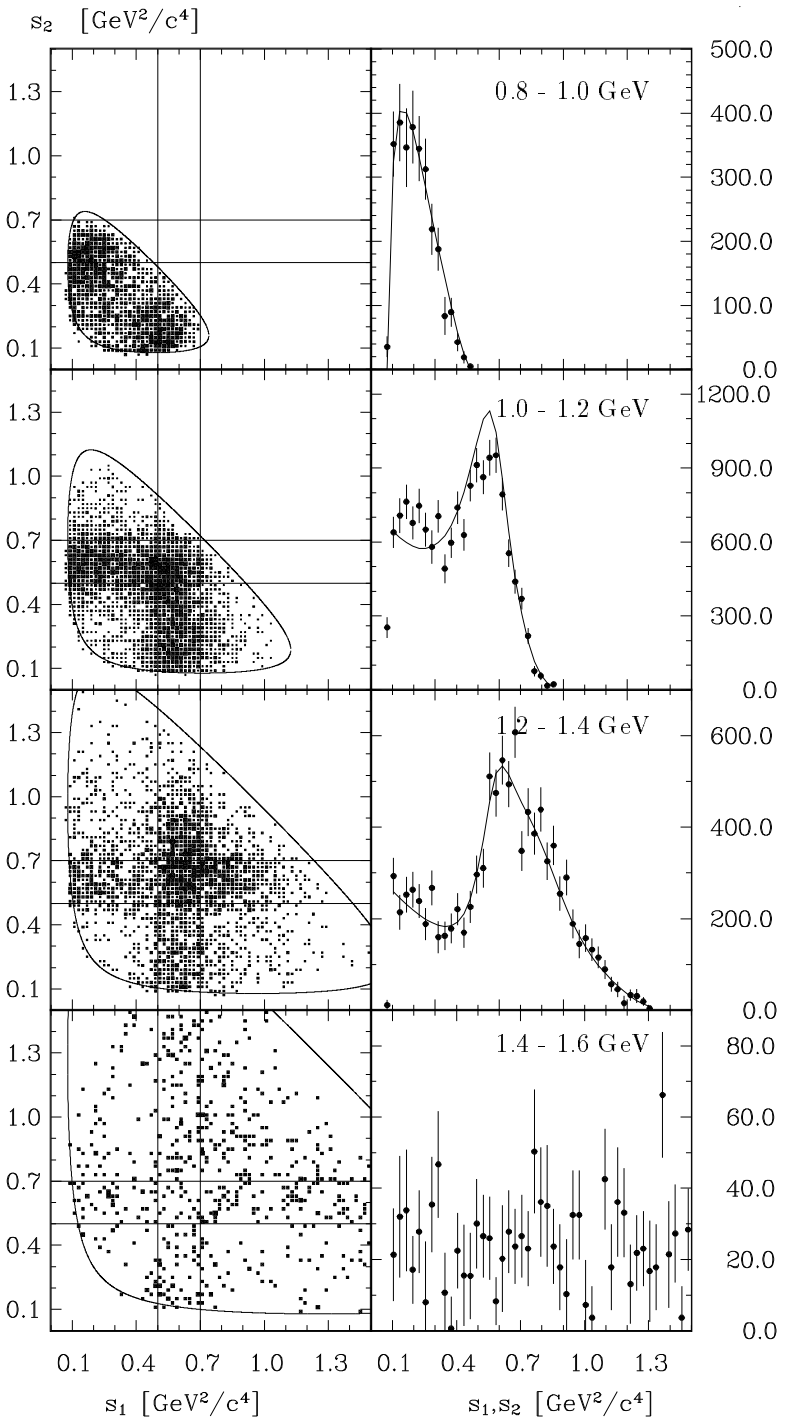

Figure 4.7: *Dalitz-plot projections of the $\pi^-\pi^-\pi^+$ final state in τ decays for four three-pion mass intervals [226]. The curves are fits of the model of Isgur et al. [241] to the data.*

In analyses of the a_1 parameters from diffractive hadronic reactions the width comes out much smaller (see note in [103]). According to Bowler [242] the τ and the hadronic analyses can be made consistent by appropriately treating the Deck amplitude in the hadronic data.

For the interpretation of the observed parity violation in three-pion τ decays [220] it is crucial to know the three-pion angular momentum decomposition (see also Sect. 4.5.1). The ARGUS group has therefore analysed the three-pion final state for intermediate resonances and angular momenta [226]. As is demonstrated in Figure 4.6a the three pions are consistent with being produced completely via $\rho\pi$. ARGUS finds that less than 6% could come from another intermediate state (like $\epsilon\pi$). The $\rho\pi$

system can be in an S or D wave. An analysis of the three-pion Dalitz-plot in different three-pion mass bins using the model of Isgur et al. yields for the ratio of the amplitudes at the nominal a_1 mass:

$$D/S \;=\; -0.11 \pm 0.02$$

The mass dependence of this ratio is build into the model. The fit describes the experimental distributions well (Figure 4.7), except for the bin between 1.0 and 1.2 GeV. In this mass bin the model does not seem to have enough freedom. In [230] it was shown that the fit could be improved by including additional amplitudes. Besides the S- and D-wave amplitudes for $a_1 \to \rho\pi$ the most significant contribution is a $a_1 \to f_2(1270)\pi$ amplitude. Details can be found in [243].

4.3.3 Tau Decays Involving Kaons

Kaons in τ decays can have two sources: associative strangeness production in Cabibbo allowed ($\sim \cos^2\theta_C$) decays and open strangeness production in Cabibbo suppressed ($\sim \sin^2\theta_C$) decays.

Cabibbo allowed decays

Kaon pairs produced in Cabibbo allowed ($\sim \cos^2\theta_C$) decays can have isospin 0 or 1 and thus contribute to both vector and axial-vector currents. As the measurements and QCD predictions of these currents become more precise the knowledge of the kaon contributions to each current becomes increasingly important.

The ARGUS group has analysed the final state $K^-K^+\pi^-$ and finds it consistent with being produced via $K^{*0}K^-$. In this case the branching ratio is:

$$\mathrm{Br}(\tau^- \to K^{*0}K^-\nu_\tau) \;=\; (0.18 \pm 0.05^{+0.03}_{-0.04})\%$$

Cabibbo suppressed decays

As in the non-strange case the strange currents may be dominated by resonances (see Table 4.1). The dominance of the two lowest resonances, K and K^*, in the corresponding currents a_0^s, v_1^s (much like the π and the ρ resonance in the non-strange currents) is well established. The single charged kaons have been measured together with single pions as described in Sect. 4.3.2.

The K^* branching ratio measured by ARGUS is [217]:

$$\mathrm{Br}(\tau^- \to K^{*-}\nu_\tau) \;=\; (1.23 \pm 0.21\,^{+0}_{-0.21})\%$$

It can be related to the non-strange vector current via the Das-Mathur-Okubo sum rule [244]:

$$\int_0^\infty \left[v_1(q^2) - v_1^s(q^2\right] dq^2 \;=\; 0$$

The evaluation of this integral assuming that the vector currents are saturated by the $\pi\pi$ and $K\pi$ channels fulfils the sum rule:

$$\int_0^{m_\tau^2} \left[v_1(q^2) - v_1^s(q^2)\right] dq^2 \;\Big/\; \int_0^{m_\tau^2} v_1^s(q^2) dq^2 \;=\; 0.11 \pm 0.13$$

The search for further decay modes involving K^* mesons and additional pions yielded the following results:

$$\mathrm{Br}(\tau^- \to \overline{K^{*0}}\pi^-\nu_\tau) \;=\; (0.21 \pm 0.09^{+0.05}_{-0.06})\%$$

$$\mathrm{Br}(\tau^- \to K^{*-}(X^0)\nu_\tau) \;=\; (1.19 \pm 0.15^{+0.12}_{-0.18})\%$$

The latter result stands for inclusive K^{*-} production with ≥ 0 additional neutral particles (π^0, K_L). The agreement of this result with the exclusive $\tau^- \to K^{*-}\nu_\tau$ measurement given above shows that most of the K^{*-} mesons are not accompanied by additional neutral particles.

4.4 Test of Lepton Universality

4.4.1 The Leptonic Decay Width

The hypothesis of Lepton Universality implies that the Fermi coupling constant as measured in muon decays also determines the coupling in leptonic τ decays as it was assumed in the partial width formula (4.7). Comparing the partial widths for the two reactions:

$$\tau^- \rightarrow e^- \overline{\nu}_e \nu_\tau \tag{4.20}$$

$$\mu^- \rightarrow e^- \overline{\nu}_e \nu_\mu \tag{4.21}$$

one finds for the ratio of the coupling constants measured in the two decays:

$$\frac{G_F^2(\tau)}{G_F^2(\mu)} = \left(\frac{m_\mu}{m_\tau}\right)^5 \frac{B(\tau \rightarrow e\nu\overline{\nu})}{B(\mu \rightarrow e\nu\overline{\nu})} \frac{\tau_\mu}{\tau_\tau} \frac{f^\mu_{corr}}{f^\tau_{corr}} \tag{4.22}$$

This ratio depends on the leptonic branching ratios, the masses and the lifetimes of the decaying leptons. The correction factors f_{corr} are calculable for the μ and the τ; their ratio is very close to 1.

This ratio deviated for a long time from unity, the Standard Model expectation, by more than two standard deviations. Because of other inconsistencies in the τ decay branching ratios ('missing one-prong problem') the leptonic τ branching ratio has been a prime suspect for the cause of the deviation. However, with an increasing number of measurements and an increasing precision the leptonic branching ratios turned out to be quite stable and reliable. The ARGUS collaboration contributed to this effort with the measurements presented in Sect. 4.2.2 which are in good agreement with the world averages.

In the following we discuss the ARGUS contribution to the measurements of the other two quantities which are important for the universality test, the τ mass and lifetime.

4.4.2 The τ Lifetime

With the Vertex Drift Chamber installed in 1985 into the ARGUS experiment [245] it became possible to reconstruct vertices in τ decays and thus to determine the τ lifetime. For high-momentum tracks the chamber allowed one to reconstruct the impact parameters, i. e. the distance of closest approach to the origin in a plane perpendicular to the beam ($x-y$ plane), with a resolution of $(95 \pm 4)\,\mu m$.

The τ lifetime was measured by analysing the distribution of reconstructed vertices in three-prong τ decays [214]. The three tracks were fitted to a common vertex and the most probable distance, l_{xy}, of the vertex to the center of the beam in the $x-y$ projection was determined. The beam position and width were measured using Bhabha events. The beam width was $\sigma_x = 480\,\mu m$ horizontally and $\sigma_y = 85\,\mu m$ vertically. From the projected decay path l_{xy} the proper decay length was derived for each event:

$$c\tau_\tau = \frac{l_{xy}}{\beta\gamma \sin\theta} \tag{4.23}$$

The polar angle of the τ direction with respect to the beam was approximated by the direction of the three-pion system. The Lorentz factors β, γ yield in the considered energy range $\beta\gamma \approx 2.8$.

Figure 4.8 shows the distribution of the proper decay length for 5696 events. The events were selected from τ events with 1-3 topologies in a data sample corresponding to an integrated luminosity of $166\,pb^{-1}$ collected in 1985 and 1986. From the weighted mean of the distribution, $< c\tau_\tau >= (88.4 \pm 4.3)\,\mu m$, the final result

$$\tau_\tau = (295 \pm 14 \pm 11) \cdot 10^{-15}\,s$$

was obtained. The measured τ lifetime is in full agreement with the current world average of $\tau_\tau = (295.6 \pm 3.1) \cdot 10^{-15}\,s$.

Figure 4.8: *The measured distribution of the proper decay length for the selected three-prong τ decays [214].*

The Vertex Drift Chamber, which was the main tool for the described analysis, was replaced in 1989 by the Micro Vertex Drift Chamber [246] to which later a silicon strip detector [247] was added. With this system the impact parameter resolution could be appreciably improved (about $25\,\mu m$ for particle momenta of 1 GeV/c) due to a better detector resolution and due to a much narrower beam pipe (radius $11\,mm$). The τ lifetime determination is currently beeing repeated with a data sample ($\mathcal{L} = 7\,pb^{-1}$) collected with the new vertex system installed.

4.4.3 The Masses of the τ Lepton and its Neutrino

Determination of the τ Mass with a Pseudo-Mass Technique

Up to 1992 the mass of the τ lepton was based on determinations of the τ pair production threshold at SPEAR and DORIS [103]. Because of the missing neutrino it is not so obvious that the τ mass could also be measured in τ events at energies $\sqrt{s} \approx 10\,GeV$. However, the ARGUS group developed a 'pseudo-mass technique' for the τ mass determination exploiting the kinematical constraints in hadronic τ decays [225].

The pseudo-mass m_τ^* was determined for τ decays into three charged pions, $\tau^- \to \pi^-\pi^-\pi^+\nu_\tau$ using, the measured energy and momentum of the three-pion system ($E_{3\pi}$, $p_{3\pi}$) and the τ energy E_τ equal to the nominal beam energy. The unknown τ direction was approximated by the momentum direction of the three-pion system. In the approximation that the τ and the three-pion momentum are collinear we defined the 'pseudo-momentum' of the τ by $p_\tau^* = p_{3\pi} \pm p_{\nu_\tau}$. For the pseudo-mass calculation only the solution $p_\tau^* = p_{3\pi} + p_{\nu_\tau}$ was used because simulations showed that this is the better approximation for most of the events and leads also to a higher sensitivity to the τ mass. With $E_{\nu_\tau} = E_\tau - E_{3\pi}$, $p_{\nu_\tau} = \sqrt{E_{\nu_\tau}^2 - m_{\nu_\tau}^2}$ and $m_\tau^{*\,2} = E_\tau^2 - p_\tau^{*\,2}$ we finally obtain the formula:

$$m_\tau^{*\,2} = 2E_\tau E_{3\pi} - 2E_{3\pi}^2 + m_{3\pi}^2 + m_{\nu_\tau}^2 - 2p_{3\pi}\sqrt{(E_\tau - E_{3\pi})^2 - m_{\nu_\tau}^2}\,. \tag{4.24}$$

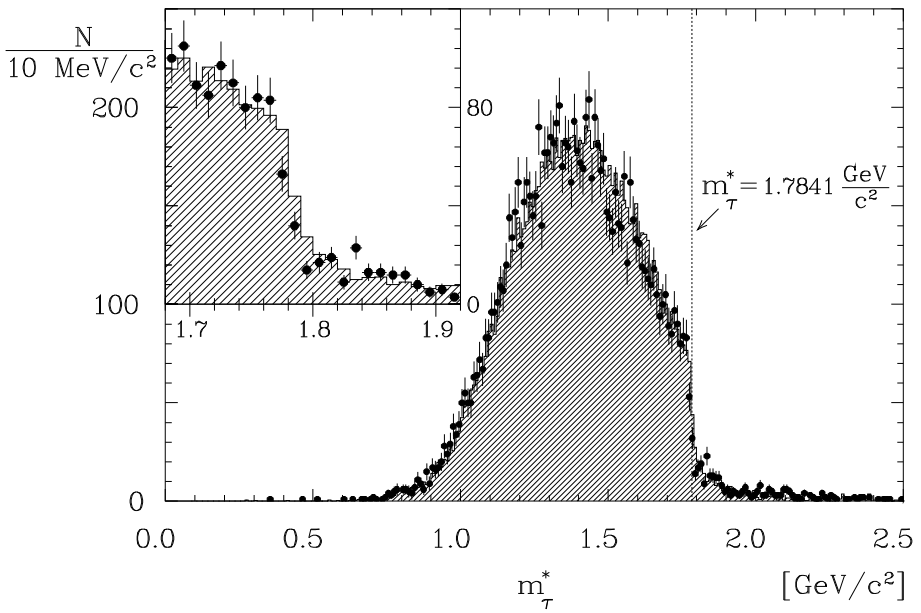

Figure 4.9: *Measured pseudo-mass spectrum of three-pion events compared with the result of a Monte Carlo simulation (hatched histogram) of the same spectrum for the decay* $\tau^- \to \pi^-\pi^-\pi^+\nu_\tau$ *and for background, normalized to the data [225]. The simulation used the old value* $m_\tau = 1.7841$ GeV *[103], indicated by the dotted line. The insert gives an enlarged view of the interesting region around* $m^*_\tau = m_\tau$.

The pseudo-mass spectrum in Figure 4.9 was obtained for an integrated luminosity of $341\,pb^{-1}$ selecting the three-pion decays from events with a 1-3 topology. The distribution has a kinematical limit at the true τ mass. This limit is reached by those events for which the above assumptions hold true, i.e. for which the τ the three-pion system and the neutrino are collinear. The tail at large m^*_τ is due to events with radiative energy loss in the initial state.

The distribution is plotted for $m_{\nu_\tau} = 0$. However, simulations have shown that in the region of the kinematical limit the formula (4.24) is very insensitive to a variation of the ν_τ mass within its limits (see below).

From a comparison of the measured pseudo-mass distribution to simulated mass distributions with variable τ masses as input the following τ mass was determined:

$$m_\tau = (1776.3 \pm 2.4 \pm 1.4)\ \text{MeV}\,.$$

The systematic error accounts for uncertainties in the beam energy, the momentum scale, the mass of the ν_τ, the simulation of the three-pion system and of the background.

The measured mass value was lower by 7.8 MeV than the world average at the time of publication [103]. The shift in the mass is in the right direction to bring the leptonic τ branching ratios in better agreement with Lepton Universality. The ARGUS analysis was soon after confirmed by the BES and CLEO experiments. The current world average is now statistically dominated by a threshold measurement of the BES experiment [17]:

$$m_\tau = (1777.1^{+0.4}_{-0.5})\ \text{MeV}\,.$$

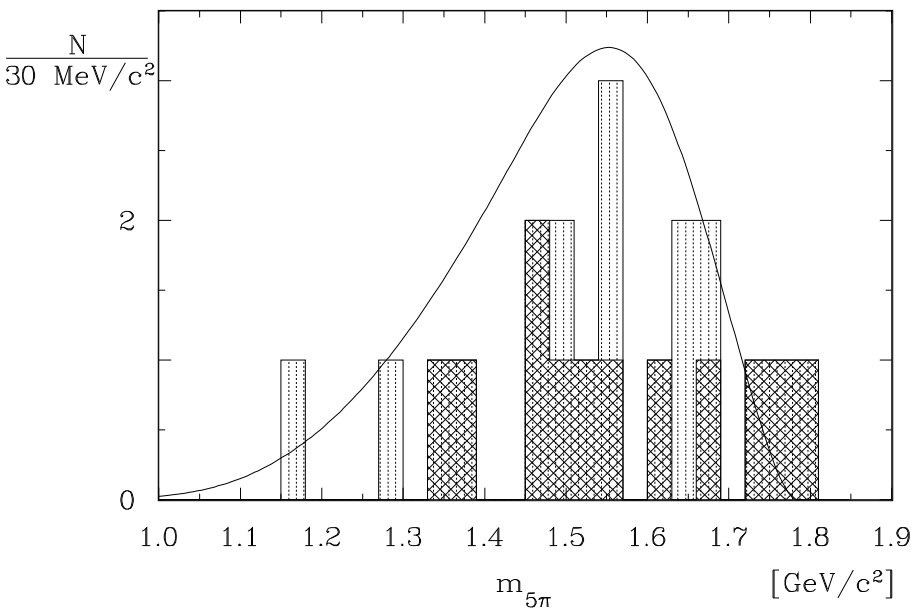

Figure 4.10: *Measured invariant 5π mass spectrum (histogram) [225]. The hatched part indicates the events analysed in the previous analysis [216]. The curve corresponds to the expected shape of a phase-space decay weighted with the weak matrix element (assuming $m_{\nu_\tau} = 0$ MeV). Note that the curve has not been normalized to the data.*

Determination of the ν_τ Mass Limit

The first upper limit on the ν_τ mass was derived by the ARGUS Collaboration from an analysis of the energy spectrum of the three-pion system in the decay $\tau^- \to \pi^-\pi^-\pi^+\nu_\tau$ [210]. The result, $m_{\nu_\tau} < 70$ MeV at 95% c.l., could be improved by analysing the mass spectrum of τ decays into five charged pions.

The peaking of the five-pion mass spectrum near the kinematical limit renders the channel, despite its small branching ratio, well suited to study effects of a finite ν_τ mass. The first analysis of the five-pion mass spectrum [216] was updated with an integrated luminosity of 390 pb^{-1} [225]. From 20 events in the spectrum (Figure 4.10) the ARGUS collaboration found the limit [225]:

$$m_{\nu_\tau} < 31.0 \text{ MeV at } 95\% \text{ c.l.}$$

For a long time the ARGUS limits on m_{ν_τ} were the most stringent. Only recently an improvement (yet unpublished) has been reported by the ALEPH Collaboration [248].

4.4.4 Status of Lepton Universality in τ Decays

Evaluating the Universality test (4.22) with the current world averages [17] for the τ leptonic branching ratios, the τ mass and the τ lifetime one finds good agreement with Standard Model expectation:

$$\frac{G_F^2(\tau)}{G_F^2(\mu)} = 0.9945 \pm 0.0144.$$

Assuming that the τ and the muon decay only via W exchange as in Figure 4.2 one could test the coupling g_l at each $W - l - \nu_l$ vertex. For a τ decaying into a lepton l and neutrinos (reaction

(4.6)), for example, these couplings are related to the Fermi coupling constant as follows:

$$\frac{G_F(\tau)}{\sqrt{2}} = \frac{g_\tau g_l}{8M_W^2}. \tag{4.25}$$

The ratios of coupling constants can be determined again from the measured leptonic branching ratios, masses and lifetimes [17]:

$$\begin{aligned} \frac{g_\mu}{g_e} &= \sqrt{\frac{B_\mu}{0.9726 B_e}} &&= 1.0038 \pm 0.0085 \\ \frac{g_\tau}{g_\mu} &= \sqrt{\left(\frac{m_\mu}{m_\tau}\right)^5 \cdot \frac{\tau_\mu}{\tau_\tau} \cdot B_e} &&= 0.9973 \pm 0.0072 \end{aligned}$$

This means that with a precision of better than 1% all charged current coupling constants in τ decays are equal as expected for a Standard Model sequential lepton.

4.5 Tests of the Lorentz Structure of Tau Decays

The Standard Model Charged Current Lagrangian predicts not only the partial decay widths but also the differential spectra of the final states as induced by the Lorentz structure of the effective four-fermion coupling (4.3). The momentum and angular spectra in leptonic decays can be described by Michel parameters as in muon decays [249]. In τ pair production in e^+e^- annihilation the spins of the τ leptons are correlated. Hence the analysis of angular and momentum correlations increases the sensitivity and even enables the determination of some parameters otherwise unmeasurable. However, with unpolarised beams there remains a sign ambiguity. ARGUS has resolved this ambiguity by the observation of parity violation in a hadronic τ decay which determined the τ neutrino helicity in that decay. In an analysis of the correlations in τ decays where one τ decays into a charged lepton and the other in three pions the signs of the Michel parameters could also be determined. Until recently the sign of the τ polarisation measured on the Z^0 peak at LEP was only fixed by the parity violation measurement of ARGUS. Now the SLD measurements with polarised beams also resolve this ambiguity.

We start with the discussion of polarisation measurements in hadronic τ decays since the results are partly used in the subsequent discussion of the determination of the Michel parameters in leptonic τ decays.

4.5.1 Probing the Electro-Weak Coupling by the Hadronic Final State

The angular momentum of the hadronic final state in τ decays carries information on the Lorentz structure of the leptonic $\tau - \nu_\tau$ vertex. As in the Goldhaber experiment, where the measured polarisation of the emitted photon probes the ν_e helicity, the hadron polarisation in τ decays probes the ν_τ helicity.

ρ polarisation:

The decay angular distribution of the ρ meson in the decay

$$\tau^- \rightarrow \rho^- \nu_\tau \tag{4.26}$$

has the general form

$$\psi(\theta) \sim 1 + b\cos^2\theta \tag{4.27}$$

where the coefficient b depends on the neutrino spin and the interaction structure. The angle θ has to be measured in the ρ rest system relative to the ρ direction of flight. The ARGUS group has

determined b and has compared the value to the prediction of the KORALB Monte Carlo for a $V-A$ interaction of the $\tau - \nu_\tau$ vertex [224]:

$$\begin{aligned} b_{meas} &= 0.57 \pm 0.12 \\ b_{MC} &= 0.57 \pm 0.01 \end{aligned}$$

This result confirms that the interaction is vector-like (V or A or both) and excludes that the ν_τ spin could be 3/2.

Since the sign of the ρ spin cannot be measured the analysis of the ρ channel is not sensitive to the V, A composition of the interaction. The V, A interference and hence parity violation has been observed by the ARGUS Collaboration in τ decays into three pions and in correlations between hadronically decaying τ pairs.

Parity Violation in Hadronic Tau Decays and the Tau Neutrino Helicity

To resolve the sign ambiguity which usually occurs in analyses of the Lorentz structure of τ decays when the τ's are produced by unpolarised beams, one has to determine the sign of particle polarisations in the final state. This is very difficult. However, following an idea of Kühn and Wagner [250] this is in principle possible using those hadronic final states which allow one to construct pseudo-scalar observables from the measured kinematics. Such a pseudo-scalar observable can be employed as an analyser of the ν_τ spin.

Kühn and Wagner suggested as an analyser of the ν_τ spin the three-pion final state in the τ decay channel [250]:

$$\tau^- \rightarrow a_1^- \nu_\tau \rightarrow \rho^0 \pi^- \nu_\tau \rightarrow \pi^+ \pi^- \pi^- \nu_\tau \tag{4.28}$$

It is known that the three charged pion final state is dominated by the axial vector meson resonance $a_1(1270)$ which decays dominantly into an S-wave $\rho\pi$ intermediate state.

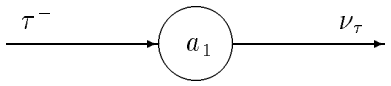

$J_z(\tau^-)$	$J_z(a_1)$	$J_z(\nu_\tau)$
$-\frac{1}{2}$	0	$-\frac{1}{2}$
$+\frac{1}{2}$	$+1$	$-\frac{1}{2}$

Figure 4.11: *Possible spin configurations in the decay (4.28) if the ν_τ is left-handed (a_1^- rest system).*

From Figure 4.11 we see that in the a_1 rest system the spin component of the a_1 in ν_τ direction can only be $J_z(a_1) = 0$ and $+1$ and not -1 if the ν_τ is left-handed and vice versa for a right-handed ν_τ. Note that because of its large mass the τ^- couples with both helicities even for pure V-A. The task is therefore to distinguish $J_z(a_1) = +1$ from $J_z(a_1) = -1$. Preference of either $J_z = +1$ or -1 implies that parity is not conserved.

A parity violating observable is the expectation value of the pseudoscalar

$$\hat{p}_\tau \, \hat{n}_{3\pi} \cdot sign(s_1 - s_2). \tag{4.29}$$

The vector $\hat{p}_\tau$ denotes the direction of the τ and the axial vector $\hat{n}_{3\pi}$ the orientation of the three-pion plane, both taken in the three-pion CM system. The four-vectors of the two like-sign pions are q_1 and q_2, of the third pion q_+, and of the three-pion system Q. The sign term with $s_1 = (q_2 + q_+)^2$ and $s_2 = (q_1 + q_+)^2$ in (4.29) establishes Bose symmetry of the expression (4.29) with respect to the interchange of π_1^- and π_2^- ($\hat{n}_{3\pi} \sim \vec{q_1} \times \vec{q_2}$) and results at the same time in a unique orientation of the three-pion plane defined by $\hat{n}_{3\pi} \cdot sign(s_1 - s_2)$.

The analysis of the parity violation is complicated by the fact that the τ direction is not observable. However $\hat{p}_\tau$ is known to lie on a cone around the measurable three-pion direction (in the three-pion

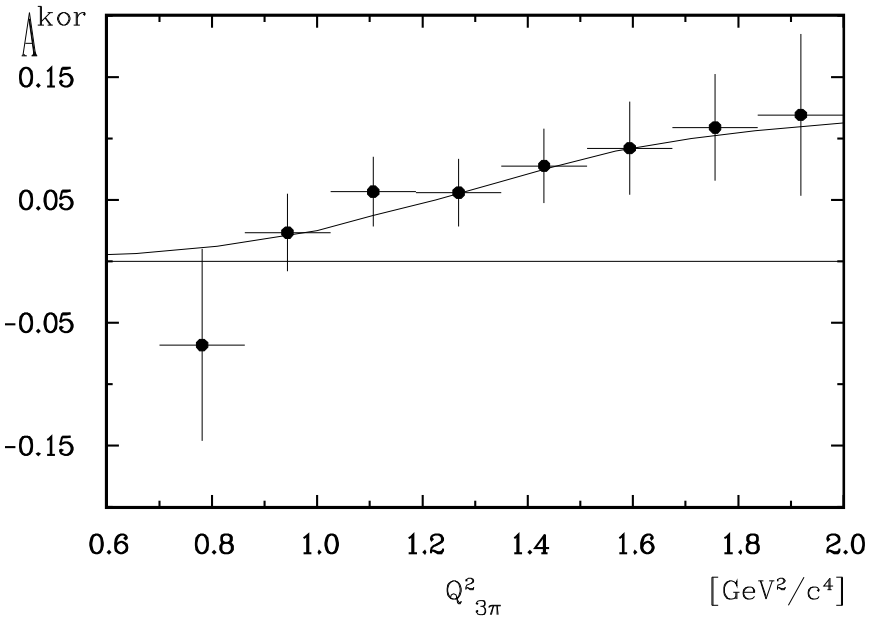

Figure 4.12: *The parity violating asymmetry measured as a function of the square of the three-pion invariant mass combined for τ^- and τ^+ decays [226].*

c.m.system this direction corresponds to the direction of the boost from the laboratory system to the c.m.system) with a half opening angle ψ. This angle is calculable from the three-pion mass Q^2 and the three-pion laboratory energy, $E_{3\pi} = x \cdot E_{beam}$. The parity violating asymmetry corresponding to (4.29) can now be obtained in $Q^2 - x$ bins:

$$A(Q^2, x) = \frac{\langle \hat{Q}\, \hat{n}_{3\pi}\, sign(s_1 - s_2) \rangle}{\langle \cos\psi \rangle} \tag{4.30}$$

where the nominator and the denominator are both average values in a $Q^2 - x$ bin.

The ARGUS group has measured the asymmetry (4.30) as a function of Q^2 and x. The data sample used in this analysis corresponds to about 260 pb^{-1}. Reaction (4.28) was selected from τ pairs decaying into four charged particles with no additional observed photons (1-3 topology). After cuts a sample of 3899 τ pair candidates remained including about 18% background. The by far largest background (about 16%) stems from τ decays of the type $\tau^- \to \pi^+\pi^-\pi^-\pi^0\nu_\tau$.

As expected the parity violating asymmetry was found to have a different sign for particles and anti-particles. In Figure 4.12 the combined asymmetry for τ^+ and τ^- decays is shown as a function of Q^2 averaged over x. Averaging also over Q^2 yields

$$\overline{A}(\tau^- + \tau^+) = 0.063 \pm 0.0155.$$

With a four standard deviation offset from zero this result established for the first time parity violation in τ decays.

The measured asymmetry can be used to determine the electro-weak coupling constants and the helicity of the τ neutrino. To do this one has to evaluate the τ decay matrix element

$$T(\tau^- \to 3\pi\nu_\tau) = L^\mu J_\mu. \tag{4.31}$$

with the leptonic current

$$L^\mu = \frac{G_F}{\sqrt{2}} \overline{u}_{\nu_\tau} (g_V + g_A\gamma_5)\, \gamma^\mu\, u_\tau \tag{4.32}$$

and a model dependent hadronic current J^μ. The squared matrix element contains a parity violating asymmetry

For the first analysis of the ν_τ helicity [220] we have used the Born term ansatz of [250], which represents an almost pure S-wave decay in the considered Q^2 range [251]:

$$J_\mu = G(Q^2)\left[\left(q_{1\mu} - q_{+\mu} - \frac{Q(q_1 - q_+)}{Q^2}Q_\mu\right) B(s_2) \; + \; (1 \leftrightarrow 2)\right] \tag{4.33}$$

with $G(Q^2)$ and $B(s_i)$ being the Breit-Wigner functions for the a_1 and the ρ's, respectively.

The sign of J_z can be determined from the interference between the two possible amplitudes for the $\rho\pi$ final state [250]. Denoting the two π^- mesons in (4.28) by π_1^- and π_2^- we have the two combinations $\pi^+\pi_1^-$ and $\pi^+\pi_2^-$ which can form a ρ^0:

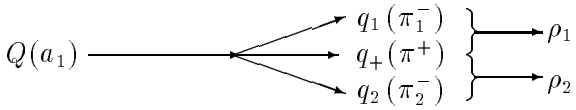

The interference of both amplitudes leads to a parity violating asymmetry in the decay probability:

$$A^{theo} = \mp\frac{2g_A g_V}{g_A^2 + g_V^2} A_{RL}(Q^2) \tag{4.34}$$

with A_{RL} being, for a given hadronic current, a calculable function of Q^2. The signs correspond to τ^- and τ^+ decays, respectively. Fitting this function to the data we obtained for the normalized product of the vector and axial vector coupling constants [226]:

$$\gamma_{AV} = \frac{2g_A g_V}{g_A^2 + g_V^2} = 1.25 \pm 0.23 \; {}^{+0.15}_{-0.18}$$

This is an updated result which was derived with an experimentally determined S- and D-wave composition of the $\rho\pi$ final state (see sect. 4.3.2). The originally published result [220] had a larger systematic error due to the uncertain D-wave amplitude which could contribute even with different sign to the asymmetry [251].

The coupling constants are defined such that the standard model predicts $\gamma_{AV} = +1$. Therefore the observed consistency of the measured γ_{AV} with $+1$ means that the τ neutrino is dominantly left-handed. A right-handed τ neutrino would result in $\gamma_{AV} = -1$.

Tau Neutrino Helicity from Angular Correlations in Hadronic Tau Decays

In the electro-weak production process

$$e^-e^+ \; \rightarrow \; \gamma, Z^0 \; \rightarrow \; \tau^-\tau^+$$

the τ pairs have correlated spins, preferring opposite helicities. This leads in general to correlations between the decay products of both τ's.

The ARGUS group has exploited the angular correlations in the final state of the reaction:

$$e^-e^+ \; \rightarrow \; \tau^-\tau^+ \; \rightarrow \; \nu_\tau\rho^-\,\overline{\nu}_\tau\rho^+ \; \rightarrow \; \nu_\tau\pi^-\pi^0\,\overline{\nu}_\tau\pi^+\pi^0$$

to determine with high precision $|\gamma_{AV}|$ [229]. The matrix element of this reaction depends on 11 variables $\vec{\eta} = (\eta_1, ..., \eta_{11})$. The variables are the two $\pi\pi$ masses, the τ production and decay angles and the ρ decay angles. The matrix element can be expressed as [252]:

$$|\mathcal{M}(\vec{\eta})|^2 \; = \; A(\vec{\eta}) \; + \; \gamma_{AV}^2 \cdot B(\vec{\eta}). \tag{4.35}$$

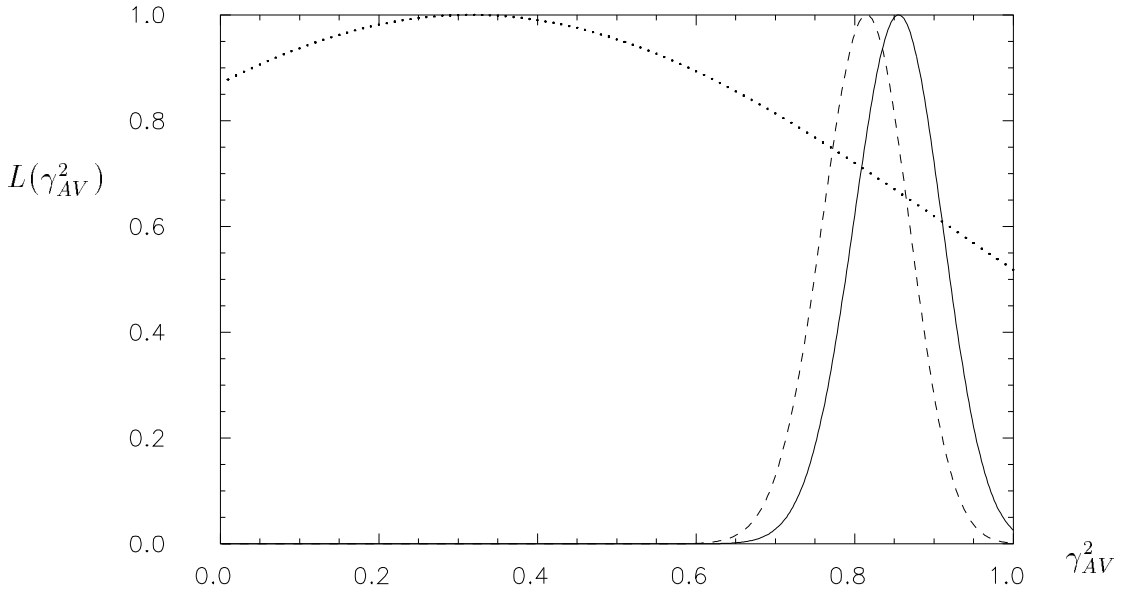

Figure 4.13: *Pseudo-likelihood as a function of γ^2_{AV} (uncorrected) for the selected $\rho^-\rho^+$ events (full line) and for a simulated data sample containing a comparable mixture of signal and background events (dashed line) [229]. The dotted line represents a function using only the energy-energy correlation of the two ρ mesons.*

The explicit expressions A and B can be found in [252]. Since γ^2_{AV} can be interpreted as the product of the neutrino helicities,

$$\gamma^2_{AV} = -h_{\nu_\tau} h_{\overline{\nu}_\tau}, \tag{4.36}$$

the measurement determines the relative sign of the neutrino helicities as well as the absolute value of γ_{AV}.

Experimentally, however, the kinematics can only be reconstructed up to a two-fold ambiguity because of the undetected neutrinos. The ARGUS group defined a likelihood function using the average matrix element for these two solutions. To derive the likelihood function for real data the matrix elements have to be corrected for detector effects and radiative corrections. Lacking an analytic expression for these corrections we used the above defined likelihood function (without corrections) as a 'pseudo-likelihood function' to determine γ^2_{AV} by a maximum likelihood fit. This fitted γ^2_{AV} value was then related to the true γ^2_{AV} by Monte Carlo methods.

Figure 4.13 shows the pseudo-likelihood function of the data compared to the same function for data simulated with $\gamma^2_{AV} = 1$. The data sample comprised ≈ 1700 events from an integrated luminosity of $387\,pb^{-1}$. The simulation also included the expected background, mainly from the $\pi^-\pi^0\pi^0$ final state where one π^0 was lost. The background has a non-negligible asymmetry since about 50% of the $\pi^-\pi^0$ from the a_1 decay form a ρ resonance with the same spin polarisation as in the direct ρ channel (because of the dominant S-wave decay of the a_1).

The sign of the fitted γ^2_{AV} confirms opposite helicities for neutrinos and anti-neutrinos. Together with the sign of γ_{AV} from the three-pion analysis the final result is [229]:

$$\gamma_{AV} = 1.022 \pm 0.028 \pm 0.030.$$

This is at present the most precise determination of the handedness of the τ neutrino ($\gamma_{AV} = -h_{\nu\tau}$). The results sets a lower limit on the mass of a hypothetical right-handed W boson. Assuming that the right-handed couplings have the same strength as the left-handed, i.e. that they are only

suppressed by the W_R propagator, one finds:

$$M_{W_R} \; > \; 227\,GeV/c^2 \qquad (90\%\ \text{c.l.}).$$

A possible scalar and pseudo-scalar coupling to the two-pion final state would result in an asymmetry in the decay angular distribution of the two-pion system. No such asymmetry was observed. Quantitative limits on scalar couplings are however quite model dependent and a detailed discussion can be found in [229, 253].

4.5.2 Leptonic Decays and the Michel Parameters

For a four-fermion pointlike interaction the most general matrix element for the leptonic τ decay is given by [249]:

$$\mathcal{M} \;=\; 4\frac{G_0}{\sqrt{2}} \sum_{\substack{\gamma = S,V,T \\ \epsilon,\mu = R,L}} g^{\gamma}_{\epsilon\mu} \left\langle \overline{l}_{\epsilon} \left| \Gamma^{\gamma} \right| \nu_l \right\rangle \left\langle \overline{\nu}_{\tau} \left| \Gamma_{\gamma} \right| \tau_{\mu} \right\rangle \; . \tag{4.37}$$

This is a sum over products of two currents which behave like scalars (S), vectors (V) and tensors (T) under Lorentz transformations and which connect right- and left-handed (R, L) τ leptons to right- and left-handed electrons and muons (l). There are 10 independent complex coupling constants $g^{\gamma}_{\epsilon\mu}$ yielding 19 independent real parameters. In the Standard Model we have $g^{V}_{LL} = 1$, all other $g^{\gamma}_{\epsilon\mu} = 0$, and G_0 the Fermi coupling constant.

The decay matrix element (4.37) can be written in terms of the coupling constants, the lepton momenta and the polarisation vector of the τ lepton yielding the differential decay width in the τ rest frame:

$$\begin{aligned} \frac{d\Gamma(\tau^{\mp} \to l^{\mp}\nu\overline{\nu})}{d\Omega dx} \;=\; & \frac{G_F^2 m_{\tau}^5}{192\pi^4} x^2 \left[3(1-x) + \frac{2}{3}\rho(4x-3) + 6\eta\frac{m_l}{m_{\tau}}\frac{1-x}{x} \right. \\ & \left. \mp \xi P_{\tau} \cos\theta \left((1-x) + \frac{2}{3}\delta(4x-3) \right) \right] \end{aligned} \tag{4.38}$$

Radiative corrections and terms of order $(m_l/m_{\tau})^2$ have been neglected. In the formula $x = 2E_l/m_{\tau}$ is the normalised lepton energy, P_{τ} the τ polarisation and θ the angle between the τ spin and the lepton momentum. The Michel parameters ρ, η, ξ and δ depend on the coupling constants $g^{\gamma}_{\epsilon\mu}$ (see e.g. [249]). A deviation from the Standard Model prediction,

$$\rho = 3/4,\ \eta = 0,\ \xi = 1,\ \delta = 3/4, \tag{4.39}$$

would indicate new physics.

Determination of the ρ and η parameters

The ARGUS Collaboration started the investigation of the Michel parameters in τ decays with the analysis of single electron and muon spectra in τ events [219]. For this analysis 1 - 3 topologies were selected, i. e. the leptonic decay was required to be accompanied by a three-prong decay of the other τ. With additional cuts 5106 events containing electrons and 3041 containing muons with background contaminations of less than 0.8% and 2.0%, respectively, were found from a data sample corresponding to an integrated luminosity of 455 pb^{-1} (about 450 000 produced τ pairs). The laboratory energy spectra of the electrons and muons are shown in Figure 4.14.

With unpolarised beams these spectra depend only on the parameters ρ and η (the first three terms in (4.38)). The η dependence is proportional to the ratio of the light lepton mass to the τ mass, m_l/m_{τ}, and is only measurable for the decay into a muon and for not too high τ energies. In

Figure 4.14: *Laboratory energy spectra for a) electrons and b) muons in leptonic τ decays [219]. The data are compared to the prediction for a $V-A$ (solid line) and $V+A$ (dashed line) couplings at the $W-\tau-\nu_\tau$ vertex (for the other vertex the standard $V-A$ coupling is assumed in both cases). For the determination of the ρ parameters only the data points above the dotted lines have been used.*

this first Michel parameter analysis the sensitivity to η was too small, so the Standard Model value $\eta = 0$ was assumed and only the ρ parameters for both electrons and muons were determined. The result,

$$\begin{aligned} \rho_e &= 0.746 \pm 0.045 \pm 0.028 \\ \rho_\mu &= 0.734 \pm 0.055 \pm 0.026 \end{aligned}$$

has been the most precise determination of these Michel parameters for leptonic τ decays.

The highest sensitivity to the η parameter is reached at low energies or, equivalently, in the τ rest system. Unfortunately, it is not possible to reconstruct directly the rest system of a leptonic τ decay because of the two undetected neutrinos. However, exploiting also the kinematical information of the recoiling τ the ARGUS group developed a method to approximately reconstruct the τ rest system, called the 'pseudo-rest-frame' [228]. The recoiling τ was again chosen to decay into a three-prong hadronic system (photons were allowed in addition to the three charged tracks). The pseudo-rest-frame was now reconstructed by boosting the lepton into the direction opposite to the reconstructed total momentum of the hadronic system assuming the τ energy to be equal to the beam energy. Since in the τ rest frame the pions in the decay $\tau \to \pi\nu$ are monochromatic, this background for the $\tau \to \mu\nu\overline{\nu}$ decay can be better suppressed in the pseudo-rest-frame. Indeed, for momenta in the pseudo-rest-frame below 0.6 GeV/c it was not necessary to require muon identification which led to a significant increase in the yield in the low momentum region and thus of the sensitivity to the η parameter.

The efficiency corrected spectra of the lepton energies in the pseudo-rest-frame are shown in Figure 4.15. A fit to the electron spectrum yields the improved result for the ρ parameter:

$$\rho_e = 0.735 \pm 0.036 \pm 0.020$$

This value replaces the previous ARGUS result. A combined fit to the electron and the muon spectra is sensitive to both the ρ and η parameters if the equality of the ρ parameter in both leptonic channels

Figure 4.15: *Efficiency corrected electron (left) and muon (right) spectra in the τ pseudo-rest-frame (full points) [228]. The dashed lines show fit results: a) Fit of the electron spectrum with $\eta = 0$; b) result of the combined fit to both spectra shown for the muon spectrum.*

is assumed. The fit yielded:

$$\begin{aligned} \rho_{e\mu} &= 0.732 \pm 0.034 \pm 0.020 \\ \eta_{e\mu} &= 0.03 \pm 0.18 \pm 0.12 \end{aligned}$$

Analysis of Correlations in Purely Leptonic τ Decays

In the differential leptonic decay width (4.38) the Michel parameters ξ and δ appear only in a product with the τ polarisation P_τ. Thus a determination of these parameters from single lepton spectra requires polarised beams. Lacking polarised beams, the ARGUS group has chosen an alternative approach by analysing momentum and angular correlations between the two leptons in events of the type (4.1) [227]:

$$e^+e^- \;\rightarrow\; \tau^+\tau^- \;\rightarrow\; e^+\nu_e\overline{\nu}_\tau\mu^-\overline{\nu}_\mu\nu_\tau$$

Such correlations reflect the fact that τ pairs (or more generally any fermion pair) are produced with correlated spins in e^+e^- annihilation, preferring opposite helicities for the τ^- and the τ^+, i. e. ($P_{\tau^-} = -1$, $P_{\tau^+} = +1$) or ($P_{\tau^-} = +1$, $P_{\tau^+} = -1$). If Z^0 exchange can be neglected, as for the ARGUS measurements, both helicity combinations are produced with equal probability. The squared matrix element of reaction (4.1) contains terms proportional to:

$$P_{\tau^-} \cdot P_{\tau^+} \cdot \xi_e \cdot \xi_\mu \tag{4.40}$$

Since $P_{\tau^-} \cdot P_{\tau^+} \approx -1$ is calculable from the production process from the term (4.40) the product $\xi_{e^+} \cdot \xi_{\mu^-}$ can be determined and thus also the relative sign of the ξ parameters for particles and anti-particles. The absolute sign of the ξ parameter can only be fixed exploiting polarised beams or by measuring final state polarisations. In leptonic decays of both τ's discussed in this paragraph, polarisations in the final state are not measureable with the ARGUS detector (below we will show that the sign ambiguities can be removed by correlating leptonic decays with hadronic decays which exhibit parity violation, see Sect. 4.5.1).

For the correlation analysis 3336 $(e\nu\overline{\nu})(\mu\nu\overline{\nu})$ events were selected ($\mathcal{L} = 333\,pb^{-1}$). In a first step the ρ parameters were determined from the single lepton spectra for fixed $\eta = 0$:

$$\begin{aligned} \rho_e &= 0.79 \pm 0.08 \pm 0.06 \\ \rho_\mu &= 0.76 \pm 0.07 \pm 0.08 \end{aligned}$$

These results are statistically independent from the ρ parameters determined from events with 1-3 topologies. Evaluating the three-dimensional correlations in the lepton momenta p_e, p_μ and the angle α_{acol} between the momenta yields ($\rho = 3/4$ and $\eta = 0$ fixed, δ free):

$$\xi \;=\; \sqrt{\xi_e \cdot \xi_\mu} \;=\; 0.90 \pm 0.15 \pm 0.10$$

The sign comes out to be the same for both ξ_e and ξ_μ. This result excludes $\xi = 0$ with a significance of 3.9 standard deviations. A non-zero ξ parameter means that the electron or muon momenta are correlated with the τ spin leading to a non-vanishing expectation value of a pseudoscalar. Therefore it is clear that the source for $\xi \neq 0$ must be parity violation although the sign of the ξ parameters could not be determined in this analysis.

Determination of the Michel Parameters ξ and δ

In the analysis described in the following the sign of the ξ parameter could also be resolved [230, 243]. This was possible by studying correlations in τ events for one τ decaying leptonically and the other into three charged pions:

$$e^+e^- \;\rightarrow\; \tau^+\tau^- \;\rightarrow\; l^+\nu_l\overline{\nu}_\tau\,\pi^-\pi^-\pi^+\nu_\tau \tag{4.41}$$

As shown in Sect. 4.5.1 the three-pion final state exhibits a parity violating asymmetry which allows one to determine the τ neutrino helicity h_{ν_τ}. The sign of the parity violation fixes then the sign of the $P_\tau\xi$ term in the correlations of the lepton with the hadronic state.

In the Born approximation, the squared matrix element for the reaction (4.41) has, after integration over the unobserved neutrino degrees of freedom and summation over unobserved spins, the following structure [243]:

$$|\mathcal{M}|^2 \;=\; (H_1 + h_{\nu_\tau}H_2)\;P\;(L_1 + \rho L_2 + \eta L_3) \;+\; (h_{\nu_\tau}H'_{1\alpha} + H'_{2\alpha})\;C^{\alpha\beta}\;(\xi L'_{1\beta} + \xi\delta L'_{2\beta}) \tag{4.42}$$

The production of the τ pairs is described by the spin-averaged matrix element P and the spin correlation matrix $C^{\alpha\beta}$, the L- and H-terms being functions of the variables of the leptonic and hadronic decays, respectively. The terms proportional to $H'_{1\alpha}$ allow the determinion of the products $h_{\nu_\tau}\xi$ and $h_{\nu_\tau}\xi\delta$ similar to the purely leptonic case (h_{ν_τ} corresponds here to the ξ parameter of the second leptonic decay). Here, however, the parity violating terms proportional to H_2 and $H'_{2\alpha}$ allow in addition the determination of h_{ν_τ}, ξ and $\xi\delta$ separately.

For this analysis 3622 events of the type (4.41) were selected (2110 with an electron and 1512 with a muon, $\mathcal{L} = 455\,pb^{-1}$), including about 10% background. The four τ decay parameters ρ, h_{ν_τ}, $h_{\nu_\tau}\xi$, and $h_{\nu_\tau}\xi\delta$ were determined in a likelihood fit. The parameter η was used in the fit as determined by ARGUS [228]. The likelihood method took into account radiative corrections and resolution effects.

For the hadronic final state the model of Kühn and Santamaria [233] was tried and found to provide an inadequate description of the data. Only a modified model for the dominant $a_1 \rightarrow \rho\pi$ S- and D-wave amplitudes and the addition of several other amplitudes led to a good likelihood for the data (see also Sect. 4.3.2). The additional amplitudes were separately not very significant, except for an amplitude $a_1 \rightarrow f_2(1270)\pi$ contributing about 4% to the three-charged-pion branching ratio. For the D/S ratio of the $a_1 \rightarrow \rho\pi$ amplitude, which influences sensitively the h_{ν_τ} analysis, the obtained result is consistent with the earlier ARGUS analysis.

The result for the τ decay parameters are:

$$\begin{aligned}
\rho &= 0.721 \pm 0.040 \pm 0.021 \\
h_{\nu_\tau} &= -0.85^{+0.15}_{-0.17} \pm 0.05 \\
h_{\nu_\tau}\xi &= -1.07 \pm 0.17 \pm 0.08 \\
h_{\nu_\tau}\xi\delta &= -0.66 \pm 0.10 \pm 0.03 \\
\xi &= 1.26^{+0.30}_{-0.26} \pm 0.09 \\
\xi\delta &= 0.77^{+0.18}_{-0.16} \pm 0.05
\end{aligned}$$

Table 4.4: *ARGUS results on the Michel parameters and the ν_τ helicity (statistical and systematic errors combined).*

ρ	=	0.738	$\pm$	0.038
η	=	0.03	$\pm$	0.22
h_{ν_τ}	=	-1.017	$\pm$	0.039
ξ	=	0.97	$\pm$	0.14
$\xi\delta$	=	0.65	$\pm$	0.12

Table 4.5: *Decay branching ratios of the τ lepton measured by the ARGUS Collaboration.*

decay channel	branching ratio	reference
$\tau^- \rightarrow e^-\overline{\nu}_e\nu_\tau$	$(17.5 \pm 0.3 \pm 0.5)\%$	[222, 227]
$\tau^- \rightarrow \mu^-\overline{\nu}_\mu\nu_\tau$	$(17.4 \pm 0.3 \pm 0.5)\%$	[222, 227]
$\tau^- \rightarrow \pi^-\pi^0\nu_\tau$	$(22.6 \pm 0.4 \pm 0.9)\%$	[224]
$\tau^- \rightarrow \pi^-\pi^-\pi^+\pi^0\nu_\tau$	$(4.2 \pm 0.5 \pm 0.9)\%$	[213]
$\tau^- \rightarrow \omega\pi^-\nu_\tau$	$(1.5 \pm 0.3 \pm 0.3)\%$	[213]
$\tau^- \rightarrow \eta\pi^-\nu_\tau$	$< 0.9\%$ at 95% c.l.	[218]
$\tau^- \rightarrow \pi^-/K^-\nu_\tau$	$(11.7 \pm 0.6 \pm 0.8)\%$	[222]
$\tau^- \rightarrow \pi^+\pi^-\pi^-\nu_\tau$	$(6.8 \pm 0.1 \pm 0.5)\%$	[226]
$\tau^- \rightarrow K^{*-}\nu_\tau$	$(1.23 \pm 0.21^{+0}_{-0.21})\%$	[217]
$\tau^- \rightarrow K^{*0}K^-\nu_\tau$	$(0.18 \pm 0.05^{+0.03}_{-0.04})\%$	[231]
$\tau^- \rightarrow \overline{K^{*0}}\pi^-\nu_\tau$	$(0.21 \pm 0.09^{+0.05}_{-0.06})\%$	[231]
$\tau^- \rightarrow K^{*-}(X^0)\nu_\tau$	$(1.19 \pm 0.15^{+0.12}_{-0.18})\%$	[231]

These results are in sign and absolute value consistent with the Standard Model $V-A$ structure of the weak couplings in τ decays.

4.5.3 Combing the Results on Michel Parameters and the ν_τ Helicity

The ARGUS Collaboration has measured all four Michel parameters which describe the general form of the lepton spectra in leptonic τ decays. In hadronic τ decays into three charged pions a parity violating asymmetry was observed from which the ν_τ helicity could be determined. The sign of the ν_τ helicity in this channel could then be used to fix all signs of the Michel parameters. This was achieved by exploiting correlations in τ pair events with both leptonic and hadronic decays.

Combining all ARGUS results on the Michel parameters and the ν_τ helicity [219, 220, 226, 227, 228, 229, 230] and assuming that the Michel parameters are the same for electrons and muons we obtain the values given in Table 4.5.3.

All values confirm the Standard Model prediction for the $V-A$ structure of the charged weak currents with universal couplings for all three generations.

4.6 Summary of the ARGUS Tau Results

The results from ARGUS on the decay branching ratios of τ-leptons obtained for various final states are summarized in Table 4.5. Most of the hadronic final states have been analysed in great detail to understand the structure of the weak hadronic currents which can be studied in a unique way

Table 4.6: *Parameters of the τ, ν_τ measured by the ARGUS Collaboration.*

measurement	reference
$\tau_\tau = (295 \pm 14 \pm 11) \cdot 10^{-15}\, s$	[214]
$m_\tau = (1776.3 \pm 2.4 \pm 1.4)$ MeV	[225]
$m_{\nu_\tau} < 31.0$ MeV at 95% c.l.	[225]

in τ physics. The nature of vector and axial vector currents was investigated and compared to theoretical concepts, such as current conservation or the concept of first and second class currents. The comparison of the measured spectral functions of vector currents to e^+e^- data also confirmed the CVC hypothesis for τ decays.

The selection rules for the hadronic weak currents lead to relatively clean final states allowing the study of light quark systems in the resonance region. The most prominent examples are the analyses of the resonance structures in the two- and three-pion systems which are dominated by the ρ and a_1 resonances, respectively. Today, the best knowledge of the a_1 resonance parameters and its angular momentum structure stems from the ARGUS analysis of the three-pion final state in τ decays.

The ARGUS group searched also for τ decay modes which would point to physics beyond the Standard Model. The limits on neutrino-less decays are summarized in Table 4.2.

An important test of the Standard Model is the confirmation of Lepton Universality, i.e. that the τ and its neutrino are sequential leptons with the same coupling strength and structure as for the lighter leptons. The comparison to muon decays involves a precise knowledge of leptonic branching ratios, the τ lifetime and mass. For a long time the measured set of these parameters indicated a deviation from Lepton Universality. ARGUS was the first experiment that presented evidence that the problem was caused by the then-accepted mass value. Though the best mass determinations come now from other experiments the technique developed by ARGUS to derive the mass from a hadronic final state (despite the missing neutrino) is quite interesting and has also been adapted in various modifications for other analyses. For a long time ARGUS had also the best limits on the τ-neutrino mass. The ARGUS results on masses and lifetimes are summarized in Table 4.6.

A special highlight of τ physics with the ARGUS detector is certainly the analysis of the Lorentz-structure of the electro-weak currents in τ decays. Of particular importance is the first observation of parity violation in τ decays and the determination of the τ-neutrino helicity. Starting with the analysis of lepton momentum spectra to determine the Michel parameter ρ ARGUS finally achieved with increasingly sophisticated analysis techniques a complete determination of all four Michel parameters and the τ neutrino helicity (Table 4.5.3). Even the signs of the ξ and δ parameters could be fixed by relating the leptonic decays to hadronic decays which exhibit observable parity violation.

Chapter 5

Bottomonium Spectroscopy

The discovery of the Υ resonances in the $\mu^+\mu^-$ final state [2] in 1977 initiated the era of the third quark family. Until the recent discovery of the top quark [9], the b quark was the only experimentally accessible member of this family, and it will remain the only one to study heavy quarkonium bound systems, since the top quark is itself a very broad state, hiding any possible structure from bound state effects.

The bottomonium spectrum is shown in Figure 5.1. The lowest lying state produced in e^+e^- annihilation is the $\Upsilon(1S)$, which has been closely examined at the DORIS, CESR and VEPP-4 e^+e^- storage rings. The interpretation of the Υ states as $b\bar{b}$ bound systems has been confirmed via many details in these investigations.

Quantum Chromo Dynamics (QCD) is the theory describing the strong interactions between quarks and gluons. While it can be expanded into a converging series of perturbation terms at high momentum transfers, there is no easy way to find definite solutions at low energy scales. Therefore, the theoretical description of bottomonium is governed by classical approximations and phenomenological models.

One approach with a wide application is the notion of a classical potential, where the $b\bar{b}$ system can be described as solution the the Schrödinger equation. The high mass of the b quark allows the use of a non-relativistic description. All potentials considered are modifications to the simple ansatz [257]

$$V(r) = -\frac{4\alpha_s}{3r} + \kappa r$$

with a Coulomb-like part due to one-gluon exchange and a linear term responsible for quark confinement. The wave function at the origin can be obtained from the solutions, and shows only slow variation with the quark mass. Thus, electromagnetic couplings can be used to verify the down-type nature of the b quark, with electric charge $Q = -1/3$. The coupling, proportional to the square of the charge, is four times weaker than that of up-type quarks. The corresponding measurements will be discussed below.

Hadronic decays of all states below the $B\overline{B}$ threshold proceed dominantly via three gluons, which is the lowest order QCD diagram, and leads to an event topology completely different from the continuum process $e^+e^- \rightarrow q\bar{q}$. This has been verified experimentally [258], leading to an upper limit of $< 5.3\%$ of unexpected two-jet events at 95% confidence level from topological distributions (shown in chapter 7 on fragmentation). The decay via fragmenting gluons has further support from the fact that no charm production is observed, leading to upper limits of < 0.019 $D^{*\pm}$ per Υ decay and < 0.034 of any charmed particle [259]. The distinct nature of bottom is also apparent from the absence of transitions to charmonium: less than 0.00068 J/ψ mesons are produced per $\Upsilon(1S)$ decay.

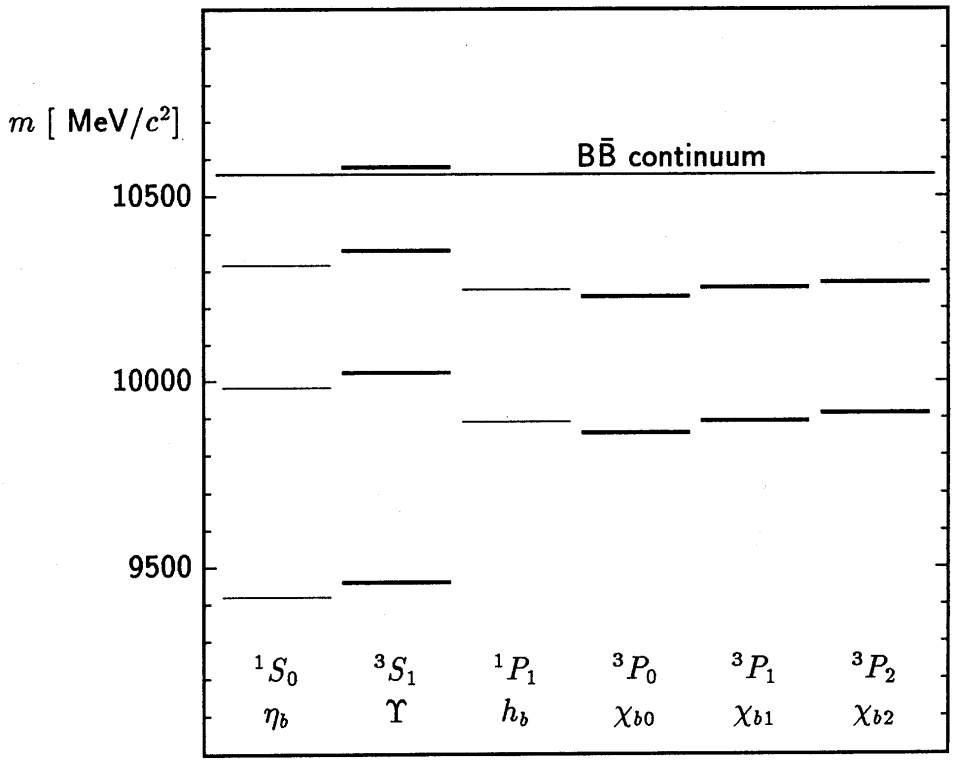

Figure 5.1: Bottomonium spectrum. The thin lines are yet undiscovered states.

5.1 Upsilon Mass Measurement

The masses of the two lowest Υ resonances were measured at a precision of one per mille at the DORIS storage ring soon after their discovery. An order of magnitude improvement was gained only in 1984, when ARGUS and Crystal Ball together with the DORIS machine group [260] used the beam depolarization technique to calibrate the e^+e^- energy.

This technique becomes possible, when the beam particles become vertically polarized by the Sokolov–Ternov effect [261]: If a synchrotron radiation photon is emitted, the spin of the emitting electron may flip. The probability for a spin flip in a homogeneous magnetic field is larger for a transition to the energetically lower parallel orientation than for the energetically higher antiparallel orientation. This leads to a vertical polarization of $\sim 92\%$ after some relaxation time, which may be reduced to lower values and eventually to zero by perturbations.

The spins precesses with a frequency

$$f_P = f_0 \cdot \gamma \cdot a$$

where $a = (g-2)/2 = 0.0011596522[1 \pm 3]$ is the anomalous magnetic moment, $\gamma = 1/\sqrt{1 - v^2/c^2}$ the Lorentz factor, and f_0 the orbital frequency.

If the particle is exposed to a horizontal magnetic field, its spin is tilted. If this field is alternating in phase with the precession, the cone of precession is opened during many revolutions and the beam depolarizes. This will also occur at energies where the precession frequency is in phase with the orbital frequency, since constant horizontal B components are always present in storage rings. At these energies, no polarization will build up.

With a time dependent field, this depolarization can be achieved at other energies, too. The

depolarizing frequency f_D must match

$$\begin{aligned} f_D &= f_P - n \cdot f_0 \\ &= (\gamma a - n) \cdot f_0 \end{aligned}$$

with arbitrary integer n. Choosing a suitable n, one can have

$$f_D = \mathrm{frac}(\gamma a) \cdot f_0$$

with only the fractional part of γa.

Scanning f_D shows a significant dip in beam polarization. The correct n has to be calculated from the approximate energy. Then

$$\gamma a = \frac{f_D}{f_0} + n$$

and

$$E_{\mathrm{beam}} = \gamma m_e.$$

The data points of the scan are shown in Figure 5.2b. The results of the mass measurements for the Υ(2S) were

$(10022.8 \pm 0.5)\mathrm{MeV/c^2}$ Crystal Ball [260]
$(10023.43 \pm 0.45)\mathrm{MeV/c^2}$ ARGUS [260]

leading to a significant step in precision from $\pm 20\mathrm{MeV/c^2}$, which was obtained in energy measurements via the magnetic field in the storage ring dipoles, to $\pm 0.5\mathrm{MeV/c^2}$.

The mass of the Υ(1S) was measured in the same way at the CESR [262] and VEPP-4 [263] storage rings, while at DORIS no polarization builds up at this energy. Another way to obtain this mass is made possible from the Υ(2S) mass measurement and a determination of the mass difference [264]

$$m(\Upsilon(2\mathrm{S})) - m(\Upsilon(1\mathrm{S})) = (562.78 \pm 0.16 \pm 0.57)\mathrm{MeV/c^2}$$

leading to an Υ(1S) mass of

$$(9460.3 \pm 0.7)\mathrm{MeV/c^2}$$

from DORIS measurements alone. This result agrees well with the present world average [17] of $(9460.37 \pm 0.21)\mathrm{MeV/c^2}$.

5.2 Determination of Γ_{ee} and Γ_{tot}

The total width of the Υ resonances below the $b\bar{b}$ threshold is significantly smaller than the beam energy spread of an e^+e^- storage ring due to synchrotron radiation. Therefore, it has to be measured indirectly as

$$\Gamma_{\mathrm{tot}} = \frac{\Gamma(\Upsilon \to e^+e^-)}{\mathrm{BR}(\Upsilon \to e^+e^-)} = \frac{\Gamma_{ee}}{B_{ee}} = \frac{\Gamma_{ee}}{B_{\mu\mu}}$$

where lepton universality is used to relate the decay into an electron positron pair to the equivalent decay into a muon pair.

The e^+e^- partial width of narrow quarkonium resonances is determined from fits to the resonance shape of $e^+e^- \to \Upsilon \to$ hadrons. This shape is significantly modified by QED corrections.

5.2.1 Radiative Corrections

The calculation of the radiative corrections usually divides the bremsstrahlung spectrum into two parts, the soft and the hard photon region. The soft photon correction to the process $e^+e^- \to q\overline{q}$ at beam energy E in the extreme relativistic limit $\frac{m_q^2}{E^2} \ll 1$ cancels partly with the virtual photon corrections, leaving finally

$$\sigma(s) = \sigma_0(s)\left(1 + \delta_{\rm vac} + \delta_{\rm vert} + \beta \ln(\frac{k_1}{E})\right) \tag{5.1}$$

where $\beta = \frac{2\alpha}{\pi}(\ln\frac{s}{m_e^2} - 1)$, the vertex correction is $\delta_{\rm vert} = \frac{2\alpha}{\pi}(\frac{3}{4}\ln\frac{s}{m_e^2} - 1 + \frac{\pi^2}{6})$, and $\delta_{\rm vac}$ is the vacuum polarization of the photon propagator from loops formed by electrons, muons, taus, and hadrons. To include photon energies in the region $k_1 < k \lesssim E$ the following expression has to be evaluated with $\kappa = \frac{k}{E}$, to give the complete first order cross section [265, 266, 267]

$$\sigma(s) = \sigma_0(s)(1 + \delta_{\rm vac} + \delta_{\rm vert} + \beta \ln \kappa_1) + \int_{\kappa_1}^{\kappa_{\rm max}} \frac{{\rm d}\sigma_{hard}}{{\rm d}\kappa}\,{\rm d}\kappa$$

using $\kappa_{\rm max} = 1 - \frac{4m_e^2}{s}$. Up to now no value has been assigned to κ_1: It is limited from below by the fact that for small values of κ_1 the $\beta \ln \kappa_1$ term becomes large and negative and may easily dominate the remaining terms indicating that higher order corrections become necessary. On the other hand, large values of κ_1 are not allowed since they belong to the hard bremsstrahlung spectrum. Therefore, to avoid the division of the cross section into two parts, the leading logs of the higher order soft photon terms are summed up to give

$$\sigma(s) = \int_0^{\kappa_{\rm max}} \sigma_0(s(1-\kappa))\beta\kappa^\beta\,(1 + \delta_{\rm vac} + \delta_{\rm vert})\left(\frac{1}{\kappa} - 1 + \frac{\kappa}{2}\right)\,{\rm d}\kappa \tag{5.2}$$

This result agrees with calculations up to second order of [268] and is also used in [269], while a modified form is used in [270, 271].

5.2.2 Determination of the Resonance Parameters

The process $e^+e^- \to \Upsilon \to$ hadrons is given to lowest order by

$$\sigma_0(s) = 12\pi\frac{\Gamma^0(\Upsilon \to e^+e^-)\Gamma(\Upsilon \to \text{hadrons})}{(s - m_\Upsilon^2)^2 + \Gamma_{\rm tot}^2 m_\Upsilon^2}$$

and the three parameters $\Gamma^0(\Upsilon \to e^+e^-) \equiv \Gamma_{ee}^0$, $\Gamma(\Upsilon \to \text{hadrons}) \equiv \Gamma_{\rm had}$ and $\Gamma_{\rm tot}$ describe the partial widths of the decays $\Upsilon \to e^+e^-$, $\Upsilon \to$ hadrons and the total width, respectively.

A remark has to be made concerning the partial width Γ_{ee}^0. In the derivation of the Breit Wigner cross section use has been made of the fact that the matrix elements are equal for

$$\mathcal{M}(e^+e^- \to \Upsilon) = \mathcal{M}(\Upsilon \to e^+e^-)$$

i.e. the production probability $e^+e^- \to \Upsilon$ equals the decay probability $\Upsilon \to e^+e^-$, if simply phase space factors are replaced by flux factors.

This exchange of final and initial state is no longer possible, if a photon from bremsstrahlung of the e^+e^- is present, since the initial state energy $\sqrt{s}$ and the resonance mass m_Υ uniquely determine the photon energy k in the production process, whereas the decay is always an integral over all k of infinitely many photons,

$$\Gamma_{ee}^{\rm expt} := \sum_{n=0}^{\infty}\Gamma(\Upsilon \to e^+e^- + n\gamma)$$

The connection between Γ_{ee}^0 and $\Gamma_{ee}^{\rm expt}$ to order α^3, i.e. of the process $\Upsilon \to e^+e^-\gamma$, is

$$\Gamma_{ee}^{\rm expt} = \Gamma_{ee}^0 \left(1 + \delta_{\rm vac} + \delta_{\rm virt}^{\rm final} + \int \delta_{\rm brems}^{\rm final}(k)\,{\rm d}k\right)$$

The contributions of the vertex correction and the bremsstrahlung of the final state leptons cancel up to a term $\frac{3}{4}\frac{\alpha}{\pi}$. Together with the remaining vacuum polarization one finds

$$\Gamma_{ee}^{\rm expt} = \Gamma_{ee}^0 \left(1 + \delta_{\rm vac} + \frac{3\alpha}{4\pi}\right)$$

With this, one can formally rewrite the cross section in terms of $\Gamma_{ee}^{\rm expt}$ instead of Γ_{ee}^0. The Breit Wigner cross section with this substitution and first order radiative corrections from equation (5.2) is

$$\sigma(s) = \int_0^{\kappa_{\rm max}} 12\pi \frac{\Gamma_{ee}^{\rm expt}\Gamma_{\rm had}}{(\hat{s} - m_\Upsilon^2)^2 + \Gamma_{\rm tot}^2 m_\Upsilon^2} \cdot \beta\kappa^\beta \left(1 + \delta_{\rm vert}\right)\left(\frac{1}{\kappa} - 1 + \frac{\kappa}{2}\right) {\rm d}\kappa \qquad (5.3)$$

where $\hat{s} = s(1-\kappa)$. In order to apply equation (5.3) to a narrow resonance several approximations are made.

1. Since one is only interested in the region near the resonance peak, the photon spectrum is dominated by its soft photon part and $\sigma(s)$ reduces to

$$\sigma(s) = \int_0^{\kappa_{\rm max}} 12\pi \frac{\Gamma_{ee}^{\rm expt}\Gamma_{\rm had}}{(\hat{s} - m_\Upsilon^2)^2 + \Gamma_{\rm tot}^2 m_\Upsilon^2} \cdot \beta\kappa^{\beta-1} \left(1 + \delta_{\rm vert}\right) {\rm d}\kappa$$

2. In the case of a narrow resonance the Breit Wigner cross section is approximated by a delta function

$$12\pi \frac{\Gamma_{ee}^{\rm expt}\Gamma_{\rm had}}{(s - m_\Upsilon^2)^2 + \Gamma_{\rm tot}^2 m_\Upsilon^2} \to 12\pi^2 \frac{\Gamma_{ee}^{\rm expt}\Gamma_{\rm had}}{\Gamma_{\rm tot}\, m_\Upsilon} \delta(s - m_\Upsilon^2)$$

3. The energy spread of the colliding beam machine has to be taken into account. The energy distribution of the actual e^+e^- energy $\sqrt{\tilde{s}}$ is assumed to have a Gaussian form with a mean energy $\sqrt{s}$

$$G(\sqrt{\tilde{s}}) = \frac{1}{\sqrt{2\pi}\Delta} \exp\left(-\frac{(\sqrt{\tilde{s}} - \sqrt{s})^2}{2\Delta^2}\right)$$

and consequently the experimental cross section at the mean energy $\sqrt{s}$ is a convolution of $\sigma(\tilde{s})$ taken from equation (1) and $G(\sqrt{\tilde{s}})$

$$\sigma_{\rm expt}(s) = \int \sigma(\tilde{s}) G(\sqrt{\tilde{s}})\,{\rm d}\sqrt{\tilde{s}}$$

Performing all integrations, the experimental cross section of the process $e^+e^- \to \Upsilon \to$ hadrons including the first order radiative corrections is of the form

$$\sigma_{\rm expt}(s) = \frac{6\pi^2}{m_\Upsilon^2 \Delta\sqrt{2\pi}} \frac{\Gamma_{ee}^{\rm expt}\Gamma_{\rm had}}{\Gamma_{\rm tot}} e^{-z^2/4} \left(\frac{2\Delta}{\sqrt{s}}\right)^\beta \cdot \Gamma(1+\beta) D_{-\beta}(-z)\left(1 + \delta_{\rm vert}\right) \qquad (5.4)$$

where $z = \frac{\sqrt{s} - m_\Upsilon}{\Delta}$ has been introduced, $\Gamma(x)$ represents the gamma function and $D_{-\beta}(x)$ is the Weber parabolic cylinder function. Equation (5.4) is also obtained from calculations of the radiative corrections in [269, 271] using similar approximations. In the past, different parametrizations have been used, resulting in a significant bias in numbers [272].

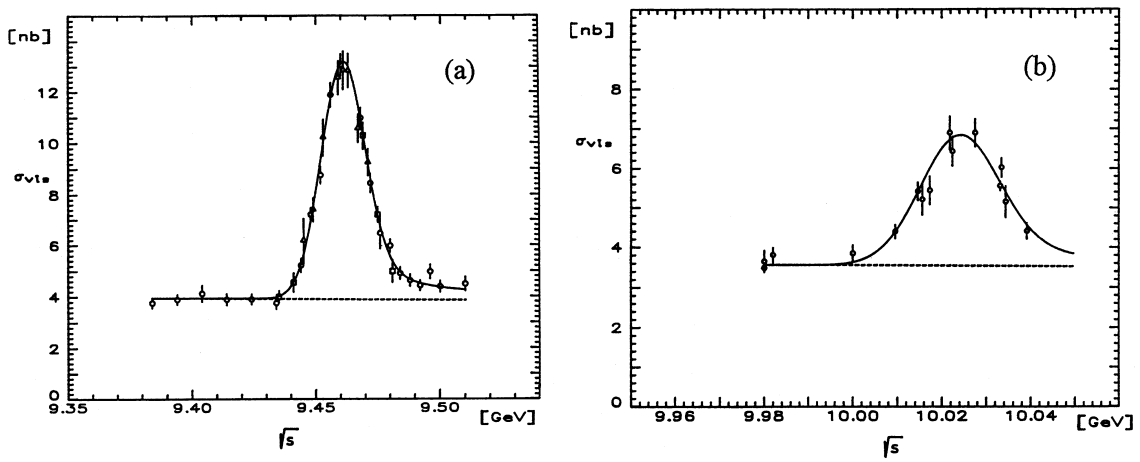

Figure 5.2: *Visible hadronic cross section versus centre of mass energy in the* $\Upsilon(1S)$ *(a) and* $\Upsilon(2S)$ *(b) energy regions [21].*

ARGUS has analysed the resonance curves of the $\Upsilon(1S)$ and $\Upsilon(2S)$ [21]. The scan points are shown in Figure 5.2. The visible cross section is

$$\sigma_{vis}(s) = \eta_\Upsilon \sigma_{\rm expt}(s) + R_{vis}\frac{4\pi\alpha^2}{3s}$$

where the overall acceptance of $\Upsilon(1S)$ decays is $\eta_\Upsilon = 0.912 \pm 0.002 \pm 0.008$, and the corresponding acceptance for the $\Upsilon(2S)$ is slightly higher due to the larger fraction of hadronic modes. The visible continuum cross section is normalized via the free parameter R_{vis}. The best fits are drawn as solid lines in Figure 5.2, and give

$$\begin{aligned}\Gamma_{ee}(\Upsilon(1S)) &= (1.32 \pm 0.04 \pm 0.03)\text{KeV} \\ \Gamma_{ee}(\Upsilon(2S)) &= (0.52 \pm 0.03 \pm 0.01)\text{KeV}\end{aligned}$$

While the difference to an up-type quarkonium is obvious, the precision is well suited to test specific potential models.

5.2.3 Lepton Pair Production

The total width of these resonances can be calculated from the partial widths Γ_{ee}, if in addition, the branching fraction into lepton pairs is known. For a direct measurement, lepton pair events have to be assigned to continuum production $e^+e^- \to \mu^+\mu^-$ and resonance decay. This requires a measurement at continuum energies close to the Υ resonance, and suffers from large background subtraction.

A more precise way to determine both B_{ee} and $B_{\mu\mu}$ of the $\Upsilon(1S)$ meson is via the hadronic transition $\Upsilon(2S) \to \Upsilon(1S)\pi^+\pi^-$, which can be observed both inclusively from the $\pi^+\pi^-$ missing mass spectrum and exclusively as a four-prong final state if the $\Upsilon(1S)$ decays to a charged lepton pair.

This method has been used [264] to determine

$$\begin{aligned}\text{BR}(\Upsilon(1S) \to \mu^+\mu^-) &= (2.30 \pm 0.23 \pm 0.13)\% \\ \text{BR}(\Upsilon(1S) \to e^+e^-) &= (2.42 \pm 0.14 \pm 0.14)\%\end{aligned}$$

The muon pair branching ratio of the $\Upsilon(2S)$ meson has been determined directly [273] from the resonance enhancement of the cross section $\sigma(e^+e^- \to \mu^+\mu^-)$, and found to be

$$\mathrm{BR}(\Upsilon(2S) \to \mu^+\mu^-) = (1.6 \pm 0.6 \pm 0.7)\%$$

The present world averages (including our measurements) are $\mathrm{BR}(\Upsilon(1S) \to \mu^+\mu^-) = (2.48 \pm 0.07)\%$, $\mathrm{BR}(\Upsilon(1S) \to e^+e^-) = (2.52 \pm 0.17)\%$, and $\mathrm{BR}(\Upsilon(2S) \to \mu^+\mu^-) = (1.31 \pm 0.21)\%$ [17].

From these numbers and Γ_{ee}, the total widths can be calculated to be

$$\begin{aligned} \Gamma_{\rm tot}(\Upsilon(1S)) &= (55.5 \pm 4.2)\mathrm{KeV} \\ \Gamma_{\rm tot}(\Upsilon(2S)) &= (33 \pm 19)\mathrm{KeV} \end{aligned}$$

These results are in good agreement with the previous world averages $\Gamma_{\rm tot}(\Upsilon(1S)) = (52.5 \pm 1.8)$KeV and $\Gamma_{\rm tot}(\Upsilon(2S)) = (44 \pm 7)$KeV [17].

5.2.4 The Width of the $\Upsilon(4S)$

The $\Upsilon(4S)$ state has a mass slightly above the open $B\overline{B}$ threshold. It therefore decays dominantly into $B^0\overline{B}^0$ and B^+B^- pairs, is a strong interaction process, and makes it a considerably wider resonance. Therefore, a relativistic Breit–Wigner shape

$$\sigma(s) = 12\pi \frac{\Gamma_{ee}\Gamma(s)}{(s - m^2(s))^2 + M^2\Gamma^2(s)}$$

with energy-dependent $\Gamma(s)$ has to be used in the parametrization of the resonance shape. ARGUS [21] has derived this shape from a quark pair creation model calculation [274]. The matrix element for the decay $\Upsilon(4S) \to B\overline{B}$ is given by the product of a spin dependent amplitude and an overlap integral comprising the meson and quark wave functions involved in the decay. The real part of the propagator is absorbed in a mass shift function $m(s)$, which is related to $\Gamma(s)$ by a dispersion relation.

The fit of the resonance curve yields at the nominal resonance mass the following parameters

$$\begin{aligned} \Gamma_{ee}(\Upsilon(4S)) &= (0.28 \pm 0.05 \pm 0.01)\mathrm{KeV} \\ \Gamma_{\rm tot}(\Upsilon(4S)) &= (10.0 \pm 2.8 \pm 2.7)\mathrm{MeV} \end{aligned}$$

The systematic error on the total width reflects the model uncertainty. This width is substantially smaller than the previous world average, which is obtained from fits using a parametrization similar to (5.4). The approximation $\Delta \gg \Gamma_{\rm tot}$ used for its derivation is, however, not valid for the broad $\Upsilon(4S)$. Actually, a fit of this function to the ARGUS data yields a width which is about a factor two larger than the quoted result, while a convolution of a simple Breit Wigner with the Gaussian machine resolution gives $\Gamma_{\rm tot} = (13.6 \pm 4.4)$MeV, in agreement with the result from the more elaborate model.

The measured parameters correspond to a state $\Upsilon(10580)$, which is, due to its width and overlap with excited D states, most likely not a pure 4S state, but a mixture of $\Upsilon(4S)$ and $\Upsilon_1(2D)$. Widely overlapping S and D states form the structure at even higher energies. They are not accessible with the DORIS storage ring, but have been examined at CESR [275].

5.2.5 Electromagnetic Transitions

One of the first results from ARGUS was on electromagnetic transitions from the $\Upsilon(2S)$ to the χ_b states [276]. For this analysis, the detector was used as a pair spectrometer, looking for photons converted to e^+e^- pairs in the beam pipe or in the inner wall of the drift chamber. This provides a very good resolution $\sigma_E = 1.1$MeV for photon energies from 100 to 180MeV, which could not be

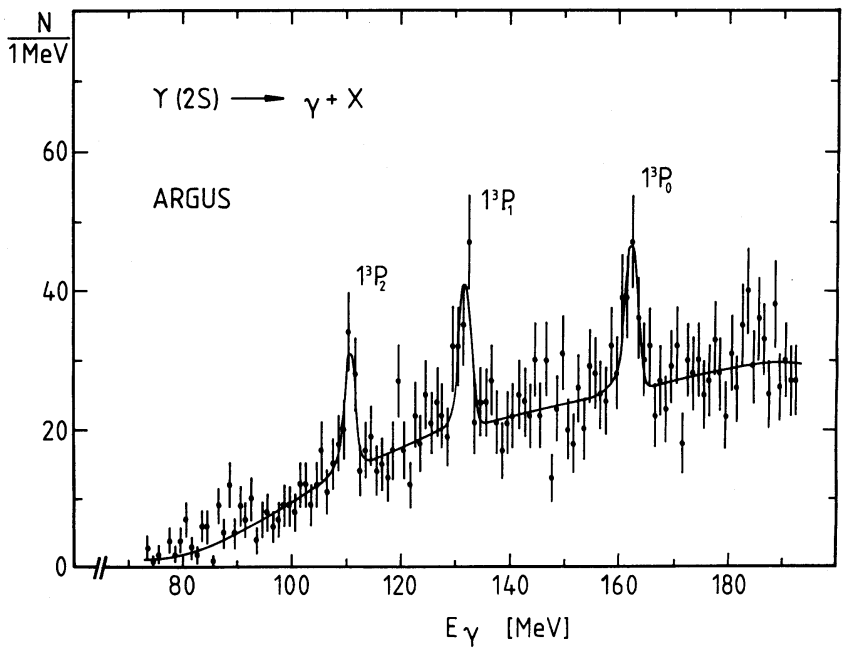

Figure 5.3: *Inclusive spectrum of converted photons from the* $\Upsilon(2S)$ *resonance and the underlying continuum. The width of the peaks is determined by the momentum resolution of the detector. The calibration has been checked with a* π^0 *signal [276].*

Table 5.1: *ARGUS results on the electromagnetic transitions* $\Upsilon(2S) \to \gamma\chi_{bJ}$ *[276].*

J	E_γ	N	$\mathrm{BR}(\Upsilon(2S) \to \gamma\chi_{bJ})$
2	$110.6 \pm 0.3 \pm 0.9$	50 ± 11	$(9.8 \pm 2.1 \pm 2.4)\%$
1	$131.7 \pm 0.3 \pm 1.1$	67 ± 13	$(9.1 \pm 1.8 \pm 2.2)\%$
0	$162.1 \pm 0.5 \pm 1.4$	69 ± 15	$(6.4 \pm 1.4 \pm 1.6)\%$

reached by a calorimeter. The disadvantage, on the other hand, is a low detection efficiency between 0.4% and 0.9%.

The energy distribution is shown in Figure 5.3. Three clear peaks were observed, with energies and numbers of signal events as given in Table 5.1. From the energies and the precision mass measurement of the $\Upsilon(2S)$, the masses of the χ_b states are determined from ARGUS measurements alone [276, 260] to be

$$\begin{aligned} m(\chi_{b0}) &= 9860.0 \pm 0.7 \pm 0.4 \mathrm{MeV/c^2} \\ m(\chi_{b1}) &= 9890.9 \pm 0.5 \pm 1.1 \mathrm{MeV/c^2} \\ m(\chi_{b2}) &= 9912.2 \pm 0.5 \pm 0.9 \mathrm{MeV/c^2} \end{aligned}$$

The mass splitting of the χ_b states is determined by spin-dependent terms, and the transformation properties of the potential. The observed mass splitting favours a confining potential transforming like a Lorentz scalar. This is also in agreement with lattice gauge calculations, which represent a promising method to calculate QCD in the low-energy regime.

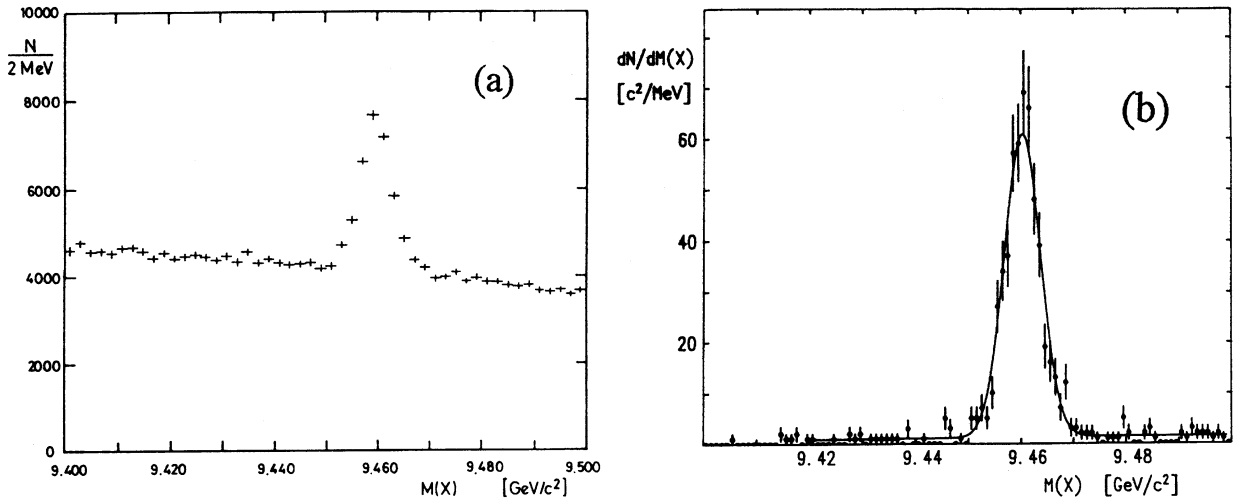

Figure 5.4: *Missing mass for inclusive* $\Upsilon(2S)$ *decays (a) and exclusive events* $\pi^+\pi^- l^+ l^-$ *(b) [264]*

Table 5.2: *Experimental results on* $\mathrm{BR}(\Upsilon(2S) \to \Upsilon(1S)\pi^+\pi^-)$

experiment	BR [%]	15 20 %
LENA[b] 81 [279]	26 ± 13	
LENA[c] 81 [279]	19 ± 8	
CUSB[c] 84 [280]	18.9 ± 2.6	
ARGUS[a] 84 [278]	$17.9 \pm 0.9 \pm 2.1$	
CLEO[a] 84 [281]	$19.1 \pm 1.2 \pm 0.6$	
Crystal Ball[c] 85 [282]	16.9 ± 4.0	
ARGUS[a] 87 [264]	$18.1 \pm 0.5 \pm 1.0$	

[a] inclusive, from $\Upsilon(2S) \to \pi\pi$ + missing mass
[b] inclusive, from $\Upsilon(2S)/\Upsilon(1S)$ charged multiplicities
[c] exclusive, from $\Upsilon(2S) \to \pi\pi(ee/\mu\mu)$

5.3 Hadronic Transitions from $\Upsilon(2S)$ to $\Upsilon(1S)$

In the QCD picture hadronic transitions between the 2S and 1S vector meson states proceed via emission of two gluons, which are dominantly chromoelectric dipole radiation E1E1. The fragmentation of this low-mass gg system is, however, not calculable within the framework of QCD. There exist only phenomenological models describing this part. The possible final states of this hadronization process are $\pi^+\pi^-$, $\pi^0\pi^0$ and η.

The $\pi^+\pi^-$ final state has been investigated with both exclusive decays of the $\Upsilon(1S)$ into e^+e^- and $\mu^+\mu^-$ and with inclusive decays into many final particles. The exclusive events [264, 277] have been selected requiring two positive and two negative tracks, where the low-momentum pair is identified with the $\pi^+\pi^-$ and used to calculate the missing mass m_X for the hypothesis $\Upsilon(2S) \to \pi^+\pi^- X$.

While this distribution is practically background free around the $\Upsilon(1S)$ mass (Fig. 5.4b), the same distribution in inclusive events [264, 278] shows a clear signal above a linear background (Fig. 5.4a). The branching ratio is compared to results from other experiments in Table 5.2.

To obtain the $\pi\pi$ invariant mass distribution, for each bin all data within its boundaries are submitted to a fit of the missing mass distribution. This fit yields the number of events in the Υ

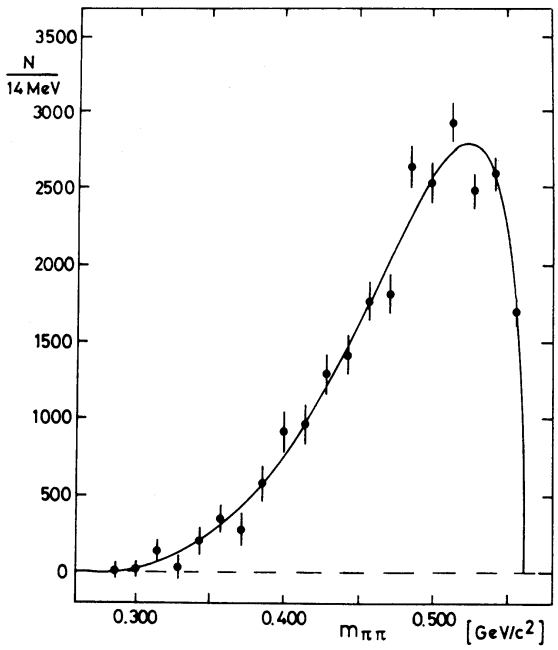

Figure 5.5: *Invariant mass distribution of* $\pi^+\pi^-$ *from* $\Upsilon(2S) \to \pi^+\pi^-\Upsilon(1S)$ *[264].*

mass signal, which make up the $\pi\pi$ invariant mass distribution shown in Fig. 5.5. It shows a shape governed by dynamics, deviating significantly from phase space. Theoretical descriptions start with the emission of two gluons, which subsequently hadronize into two pions. The second step, the conversion to hadrons, determines the $m(\pi\pi)$distribution.

For simple three-body phase space the distribution of $M = m_{\pi\pi}$ would have the form:

$$PS = \sqrt{\frac{(M^2 - 4m_\pi^2)[m_1^4 + m_2^4 + M^4 - 2(m_1^2M^2 + m_2^2M^2 + m_1^2m_2^2)]}{4\,m_2^2}}$$

where we use $m_1 = m(\Upsilon(1S))$ and $m_2 = m(\Upsilon(2S))$.

Brown and Cahn [283] and Voloshin [284] were the first to use chiral symmetry arguments and PCAC to derive a matrix element. Brown and Cahn's ansatz includes three terms with free normalization parameters. Neglecting terms involving non-isotropic angular distributions, they predict

$$\frac{\mathrm{d}\Gamma}{\mathrm{d}M} \propto PS \cdot [M^2 - 2m_\pi^2]^2 \,.$$

Modifications to this ansatz are obtained considering the leading contribution from a colour-field multipole expansion, that is a chromoelectric E1E1 transition, which is the two gluon emission in a non-relativistic limit [285, 286, 287, 288]. These models have one free parameter each, which has been fitted to the data, with results given in the upper part of Table 5.3. The parameter should be independent of the energy scale, i.e. the same for charmonium and bottomonium.

Another idea is scalar meson ($\varepsilon = f_0$) dominance in the $\pi\pi$ channel [289, 290, 291, 292, 293]. Resonance parameters for different models obtained from the data are given in the second part of Table 5.3.

In all theoretical models the pions are expected to be dominantly in an S state. However, on general grounds, $even^{++}$ states are allowed as well, and their contribution has to be found by experiment [294]. An order of magnitude prediction of the d-wave has been made by Novikov and Shifman [288].

Table 5.3: *Fit results for theoretical parametrizations in $m(\pi\pi)$ for $\Upsilon(2S) \to \Upsilon(1S)\,\pi^+\pi^-$ by the ARGUS collaboration [264].*

Yan [285]	B/A	$= -0.154 \pm 0.019$	$\chi^2 = 27.8/19$d.f.
Voloshin/Zakharov [286]	λ	$= 3.30 \pm 0.19$	$\chi^2 = 27.4/19$d.f.
Novikov/Shifman [288]	κ	$= 0.151 \pm 0.009$	$\chi^2 = 27.7/19$d.f.
Schwinger et al. [290]	$m(f_0)$	$= 0.86 \pm 0.11$ GeV/c^2	$\chi^2 = 29.8/18$d.f.
	$\Gamma(f_0)$	$= 2.4 \pm 1.3$ GeV/c^2	
Genz et al. [291]	$m(f_0)$	$= 0.633 \pm 0.018$ GeV/c^2	$\chi^2 = 42.7/18$d.f.
	$\Gamma(f_0)$	$= 0.37 \pm 0.04$ GeV/c^2	
Harrington et al. [293]	$m(f_0)$	$= 0.57 \pm 0.04$ GeV/c^2	$\chi^2 = 28.4/18$d.f.
	$\Gamma(f_0)$	$= 0.39 \pm 0.08$ GeV/c^2	

Since the multipole expansion is expected to be dominated by E1E1 radiation, the angular momentum of the quarkonium is not changed in this process.

Final states with two neutral pions have been reconstructed using exclusive $\Upsilon(1S)$ decays into lepton pairs. This selection yields 17 events with a negligible background, corresponding to

$$\frac{\mathrm{BR}(\Upsilon(2S) \to \Upsilon(1S)\pi^0\pi^0)}{\mathrm{BR}(\Upsilon(2S) \to \Upsilon(1S)\pi^+\pi^-)} = 0.52 \pm 0.10 \pm 0.10$$

which is in good agreement with the expectation of 0.5 from isospin conservation.

5.3.1 $\Upsilon(2S) \to \Upsilon(1S)\,\eta$

The transition $\Upsilon(2S) \to \Upsilon(1S)\,\pi^0$ violates isospin conservation, and is forbidden as a strong interaction process. The last possibility, $\Upsilon(2S) \to \Upsilon(1S)\,\eta$, is allowed but has very little phase space.

A search using exclusive $\Upsilon(1S)$ decays into lepton pairs lead to a zero result, which is quantified as

$$\mathrm{BR}(\Upsilon(2S) \to \Upsilon(1S)\,\eta) < 0.5\%\ (90\%\mathrm{CL})$$

looking for η decays into three pions.

5.3.2 Summary

Our understanding of the mass spectrum and widths of heavy quarkonia has been continuously increasing in the last decade. The measurements of ARGUS at the Υ resonances have contributed significantly to this field, and even stimulated new theoretical efforts. The description of the $\Upsilon(4S)$ resonance shape has added to the qualitative understanding of the parameters describing such a system, and many quantitative results from ARGUS measurements still dominate the world average [17], among them B_{ee} of the $\Upsilon(1S)$, the masses of χ_{b0}, χ_{b1}, and χ_{b2}, and the branching fraction of $\Upsilon(2S) \to \Upsilon(1S)\pi^+\pi^-$.

Chapter 6

Two–Photon Physics

6.1 Introduction

An electron–positron storage ring is a suitable tool for studying reactions induced by two interacting photons (Fig. 6.1):

$$e^+e^- \rightarrow e^+e^-\gamma^*\gamma^* \rightarrow e^+e^-X. \tag{6.1}$$

The two photons exchanged in this reaction are in general virtual. The analysis of ARGUS data was restricted to almost real photons that dominate the photon spectra. Such interactions of quasi-real photons have been selected by requiring the total transverse momentum of the final state X to be small, typically bellow 100 MeV/c. In this case the electrons and positrons preferentially scatter under a very small angle and escape detection (*"no – tag"* measurement).

The ARGUS analysis of two–photon reactions concentrated on the investigation of the spectroscopy of light mesons and charmed quark systems. Since the initial two–photon state has a well defined C-parity and selects certain spin–parity combinations the observation and study of resonances, e.g. by performing partial wave analyses, is in general less complicated than in hadronic reactions. The two–photon partial decay width $\Gamma_{\gamma\gamma}$ of a resonance can be deduced from its formation

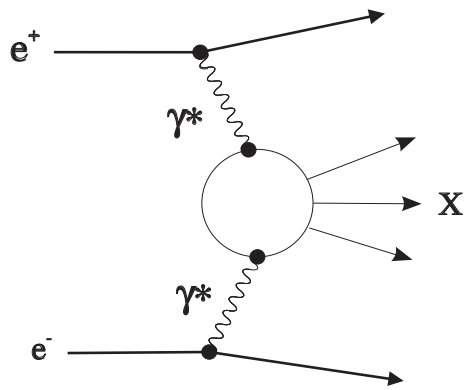

Figure 6.1: *A schematic representation of the two–photon production of final states X.*

cross section. Since $\Gamma_{\gamma\gamma}$ depends on the charges of the hadron constituents, it can be used to determine the flavour content of mesons, as expressed, for example, by the mixing angles of meson nonets. As gluons are electrically neutral, glueballs, i.e. the expected bound gluon states, are expected to have a smaller probability for two–photon formation than quark–antiquark states. A measure of the gluonic content of a resonance X can be obtained by comparing its two–photon width to the branching ratio of the radiative J/ψ decay, $J/\psi \rightarrow X\gamma$. In this decay the formation of glueballs is expected to be favoured since the resonance X is produced via qluon exchange.

A longstanding question has been whether, in addition to standard $q\bar{q}$ mesons and qqq baryons, four– and six–quark bound states are also realized in nature. Two–photon interactions offer a particularly clean possibility to study those four–quark states which are formed by and decay into two vector mesons. In the framework of the vector meson dominance model, such states would be observable in two–photon reactions as an enhancement of the scattering cross section of two vector mesons. The interest in vector meson pair production was in particular stimulated by the observation of a large cross section for $\gamma\gamma \to \rho^0\rho^0$ near the threshold [295]. The cross section was readily explained as the excitation of two interfering four–quark resonances with isospin 0 and 2 [296, 297]. The models predicted a much smaller cross section for $\gamma\gamma \to \rho^+\rho^-$ which was later indeed observed experimentally [298]. These models as well as others, e.g. a t-channel factorization model, attempt to explain the $\rho\rho$ cross section near threshold and make predictions for other vector meson pair production cross sections [296, 297, 299, 300]. In the case of the resonance models, a specific spin–parity, namely $J^P = 2^+$, is predicted. When ARGUS started to analyse vector meson pair production by two photons, including partial wave analyses whenever statistics allowed, only a very few channels had been studied and the spin–parity assignments were even controversial. The ARGUS collaboration has since achieved themost comprehensive study of two–photon production of all possible pairs of the lowest mass nonet of the vector mesons.

In what follows we shall consider the DORIS II storage ring as a source of quasi-real colliding photons. The spectra of photons are continuous and the two–photon invariant mass $W_{\gamma\gamma}$ is defined by the center–of–mass energy of the reaction products. Assuming quasi–real photons the relationship between the two–photon production cross section $\sigma_{\gamma\gamma}$ and the number of events per $W_{\gamma\gamma}$ interval, $\frac{dN}{dW_{\gamma\gamma}}$, that were produced in the reaction, is the following:

$$\frac{dN}{dW_{\gamma\gamma}} = \frac{d\mathcal{L}_{\gamma\gamma}}{dW_{\gamma\gamma}} L_{ee}\sigma_{\gamma\gamma}(W_{\gamma\gamma}) \,, \tag{6.2}$$

where $\frac{d\mathcal{L}_{\gamma\gamma}}{dW_{\gamma\gamma}}$ is the two–photon luminosity function for two transverse photons, and L_{ee} is the time integrated electron–positron luminosity. The two-photon luminosity function involves only electromagnetic interactions and can be calculated using Monte Carlo numerical integration (see ref. [301] for the explicit form of the differential two–photon luminosity function).

Several two–photon final states have been analyzed. In some cases the invariant mass dependence of the cross section shows well separated resonances. In general, however, a partial wave analysis was needed to identify the spins and parities of the intermediate states. Therefore, whenever statistics allowed, an attempt was made to determine the contribution of the leading partial waves.

In this chapter, the ARGUS two–photon results are presented as follows: After describing some general features of data analysis we discuss the two–photon production of vector meson pairs and proceed to two–photon formation of resonances. Almost all ARGUS two–photon results fall into these two categories. An exception is the reaction $\gamma\gamma \to p\bar{p} + (n\pi)$ with $n = 1, 2, 3$ for which the cross section was determined as described in detail in [302].

6.2 Data Analysis Methods

The most powerful selection criterion for reactions induced by two almost real photons is the cut on the total transverse momentum, $|\sum_i \vec{p}_{T,i}| <\approx 100\text{MeV/c}$ of the particles reconstructed in the detector. The scattered electron and positron are assumed to escape along the beam pipe. This cut suppresses background, such as τ decays and incompletely reconstructed two–photon events. The background was subtracted using Monte Carlo simulations of other two–photon reactions, τ–pair production and one–photon annihilation into hadrons based on their measured cross sections.

6.2.1 Partial Wave Analysis

ARGUS is a detector with good solid angle coverage and is thus well suited for partial wave analyses of hadronic final states. Particularly important for a large and well understood acceptance was a trigger scheme with high efficiency for both low energy and low multiplicity events. In general, a two–photon final state particle may evolve via several intermediate states with different spin and parity, which we shall denote by the index k. We determine these contributions by means of a partial wave analysis based on a maximum likelihood method. For this purpose a probability density function is constructed from the squared sum of matrix elements describing the formation and decay of particles for each contribution k. Each matrix element in the sum is multiplied by a free parameter λ_k and appropriately normalized.

The aim of the partial wave analysis is to determine the proportion λ_k^2 of the measured events belonging to different partial waves. The likelihood function is obtained by inserting for each event j the set of measured kinematical variables ξ_j into the probability density function. The likelihood function L is a product of such functions for all events. For practical reasons logarithm of the likelihood function is varied. The following expression is maximized by varying the λ_k's :

$$\ln L = \sum_{j=1}^{N_{acc}} \ln \sum_k P_{kl} \lambda_k \lambda_l \frac{A_k(\xi_j)}{\sqrt{|A_k|^2}} \frac{A_l^*(\xi_j)}{\sqrt{|A_l|^2}} - N_{acc} I \,, \tag{6.3}$$

where

$$I = \sum_k \lambda_k^2 + \sum_{k \neq l} P_{kl} \lambda_k \lambda_l \frac{\overline{A_k A_l^*}}{\sqrt{|A_k|^2 \; |A_l|^2}}. \tag{6.4}$$

Here $A_k(\xi_j)$ is the decay matrix element and N_{acc} the number of accepted events in a given $W_{\gamma\gamma}$ interval. Partial waves with the same parity and helicity J_z interfere with each other and is described by the phases P_{kl}. The diagonal elements of P_{kl} equal to 1; the off–diagonal matrix elements of P_{kl} differ from zero only for the interfering terms in the sum. The acceptances η_k and the matrix elements $\overline{|A_k(W_{\gamma\gamma})|^2}$ for various partial waves averaged over the acceptance were determined using Monte Carlo simulated two–photon events. The maximum likelihood is calculated for each $W_{\gamma\gamma}$ bin independently (see refs.[305, 308, 309] for more details).

The determination of the contribution from the different partial waves is very sensitive to the precise value of the acceptance averaged matrix elements $\overline{|A_k(\xi_j)|^2}$ the evaluation of which requires a good knowledge of the spectrometer. A careful analysis of the performance of detector components during data taking was made, and the results were included in the simulation program.

Having determined λ_k and η_k, the two–photon cross section for the production of a certain partial wave $\sigma_{\gamma\gamma\to k}(W_{\gamma\gamma})$ is calculated as follows:

$$\sigma_{\gamma\gamma\to k}(W_{\gamma\gamma}) = \frac{N_{acc}(W_{\gamma\gamma}) \; \lambda_k^2}{L_{ee} \; \eta_k \int_{W_{\gamma\gamma} - \Delta/2}^{W_{\gamma\gamma} + \Delta/2} \frac{d\mathcal{L}}{dW'_{\gamma\gamma}} \, dW'_{\gamma\gamma}}, \tag{6.5}$$

where Δ stands for the width of the $W_{\gamma\gamma}$ bin.

6.2.2 Treatment of the Final States

In the case of more than two stable particles in the final state it is useful to describe the final state as being composed of two isobars (e.g. $\rho\rho$, $\rho\pi$, $\rho\omega$ etc.) and phase–space distributed multiparticle states, as shown in Fig. 6.2.

The matrix element for the decay into isobars can symbolically be represented as

$$A_k(\kappa \to I_1 I_2;\; I_1 \to X_1,\; I_2 \to X_2) = \mathrm{BW}(I_1)\,\mathrm{BW}(I_2)\,G(\Theta)\,, \tag{6.6}$$

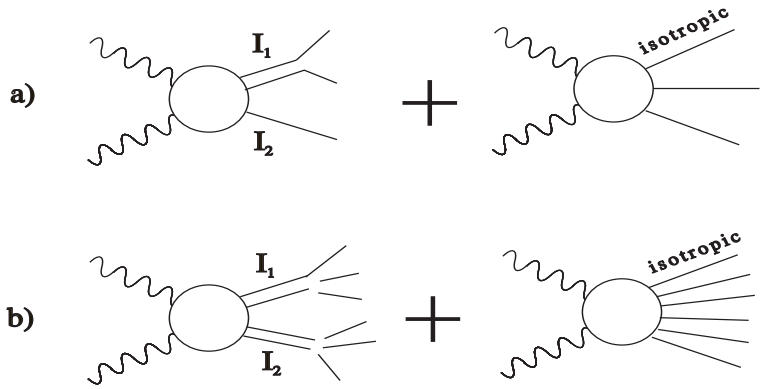

Figure 6.2: *A schematic drawing representing the isobar model for final states with three (a) or more (b) particles. The final state partial waves are treated as being composed of two well defined isobars and phase–space distributed parts.*

where we have denoted by κ the state formed by the two photons, by I_1, I_2 the final state isobars and by $I_1 \to X_1$ and $I_2 \to X_2$ the decay of the isobars to the final state particles. BW(I_1), BW(I_2) represent the Breit–Wigner propagators for the two isobars and $G(\Theta)$ is a geometrical function of the set of measured angles Θ. This expression for A_k has to be symmetrized with respect to identical bosons in the final state. The number of matrix elements k considered in the analysis is limited by the statistics of the experimental data. The presented analyses were restricted to orbital angular momenta (of the isobars) $l = 0$, $l = 1$ and in some cases $l = 2$. The effect of such a restriction has been tested by Monte Carlo simulation.

However, the entire two–photon production of multiparticle final states cannot be described with the isobar model. To approximately account for other processes, additional amplitudes are added in which a phase space distribution is assumed for some or all final state particles.

6.2.3 Systematic Errors

Systematic errors vary from case to case. In general an error between 8% and 15% can be attributed to the total and partial wave cross sections. Some common sources of systematic errors are as follows: detector simulation ($\approx 6\%$), trigger simulation ($\approx 5\%$), luminosity measurement (1.8%) and event generation (1.3%), the value of the first two depending on the particular reaction. The background contamination depends also very much on the particular process under investigation but generally does not exceed 10%.

The results of the partial–wave analyses were systematically checked by comparing measured angular distributions with distributions expected on the basis of fit results. The maximum likelihood method was also tested using the Monte Carlo simulated data sample. Various sets of states were generated and analyzed with different hypotheses in order to test the migration of events from one intermediate state to another. It was found that the invariant mass distributions of final state isobars, such as ω, ρ, ϕ, etc. represent a more severe constraint than angular distributions.

6.3 Two–Photon Production of a Pair of Vector Mesons

ARGUS has started a program of studying two–photon production of vector meson pairs including all members of the lowest vector meson nonet. From the 9 studied combinations 6 have been observed for the first time. ARGUS also performed partial wave analyses of the reactions $\gamma\gamma \to \rho^0\rho^0$, $\gamma\gamma \to \rho^+\rho^-$ and $\gamma\gamma \to \rho^0\omega$.

6.3.1 $\gamma\gamma \to \rho\rho$

The partial wave analysis was done on $\gamma\gamma \to \pi^+\pi^-\pi^+\pi^-$ and $\gamma\gamma \to \pi^+\pi^-\pi^0\pi^0$ events [308, 309]. The following $\rho^0\rho^0$ and $\rho^+\rho^-$ partial waves were included:

$$\begin{aligned}(J^P,\ J_z,\ S) \ &= \ (0^+,\ 0,\ 0),\ (0^-,\ 0,\ 1),\\ &\quad\ (2^+,\ \pm 2,\ 2),\ (2^+,\ 0,\ 2),\ (2^-,\ 0,\ 1),\end{aligned}$$

where J^P are the *spin and parity*, J_z spin component in the beam direction of the initial state and S the total spin of the two ρ's for a particular partial wave.

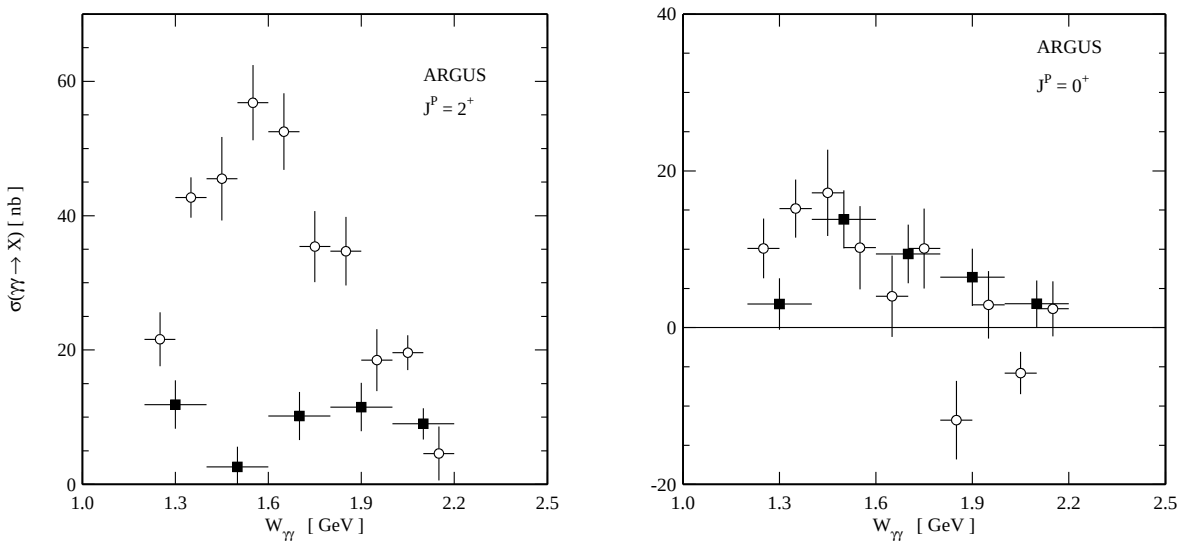

Figure 6.3: *Cross sections for the dominating amplitudes for $\gamma\gamma \to \rho^0\rho^0$ (open circles) and for $\gamma\gamma \to \rho^+\rho^-$ (full squares) [308, 309].*

The results obtained from these analyses are shown in Fig. 6.3. In the case of the reaction $\gamma\gamma \to \rho^0\rho^0$ the amplitude $(2^+, \pm 2, 2)$ dominates with a smaller contribution from the $(0^+, 0, 0)$ amplitude. For the process $\gamma\gamma \to \rho^+\rho^-$ the cross section is dominated by the $(2^+, \pm 2, 2)$ and the $(0^+, 0, 0)$ amplitudes with similar contributions. For an ordinary isospin 0 resonance we expect $\Gamma_{\gamma\gamma\to\rho^+\rho^-}/\Gamma_{\gamma\gamma\to\rho^0\rho^0} = 2$ (1/2 for a pure isospin 2 resonance). Instead, the observed ratio is lower than 1/2. The only possible resonance interpretation for such a result is an interference between an isospin 0 and an isospin 2 resonance. Both four–quark models [296, 297] have predicted such an interference on the basis of the vector meson dominance model using M.I.T.–bag wave functions for the $qq\bar{q}\bar{q}$ states. They also predict the spin–parity to be $J^P = 2^+$. The t–channel factorization model[299] is able to approximately account for the observed $\gamma\gamma \to \rho^0\rho^0$ cross section but has difficulties to describe the large cross section below the nominal reaction threshold [300]. The reaction $\gamma\gamma \to \rho^+\rho^-$ has also been calculated in the framework of perturbative QCD [310]. The $\rho^+\rho^-$ cross section is well reproduced but the same calculation fails to account for the large $K^*\bar{K}^*$ cross sections (see subsection on $\gamma\gamma \to K^*\bar{K}^*$).

6.3.2 $\gamma\gamma \to \rho^0\omega$

The first measurement of the cross section for $\gamma\gamma \to \rho^0\omega$ was published by ARGUS in 1987 [311]. It was followed by several more results from other experiments [312, 313]. By the end of data taking

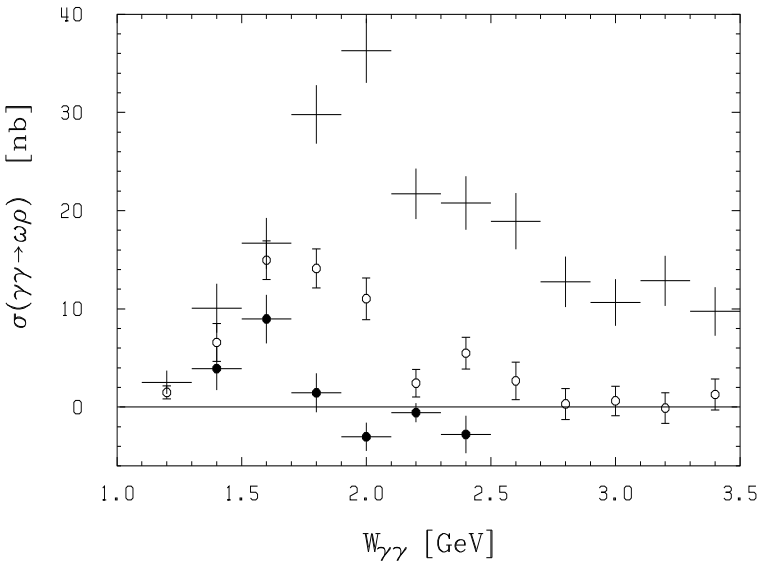

Figure 6.4: *Cross sections for $\gamma\gamma \to \pi^+\pi^+\pi^0\pi^-\pi^-$ (crosses), for $\gamma\gamma \to \rho^0\omega$ (open circles) and for the $(J^P, J_z) = (2^+, 2)$ partial wave of $\gamma\gamma \to \rho^0\omega$ (full circles) [314].*

ARGUS had more than doubled the integrated luminosity. A sample of 2547 $\pi^+\pi^+\pi^0\pi^-\pi^-$ events was selected. This number was sufficient to allow a partial wave analysis [314]. The following partial waves in the $\rho^0\omega$ channel were considered:

$$(J^P,\ J_z,\ S) \quad = \quad (0^+,0,0),\ (0^-,0,1),\ (2^+,\pm2,2),\ (2^+,0,2),\ (2^-,0,1),\ (2^-,0,2).$$

Fig. 6.4 shows the total $\pi^+\pi^-\pi^+\pi^-\pi^0$ cross section, the $\rho^0\omega$ contribution and the $(2^+,2)$ cross section which in the region below 1.7 GeV/c^2 dominates the $\gamma\gamma \to \rho^0\omega$ reaction.

Since no other partial wave analysis exists, only a comparison of the total $\gamma\gamma \to \rho^0\omega$ cross sections can be made. It shows good agreement with the older data within the limits of statistical errors. It appears that the predictions of various models[296, 297, 299] are too dependent on free parameters to make a selection among them possible.

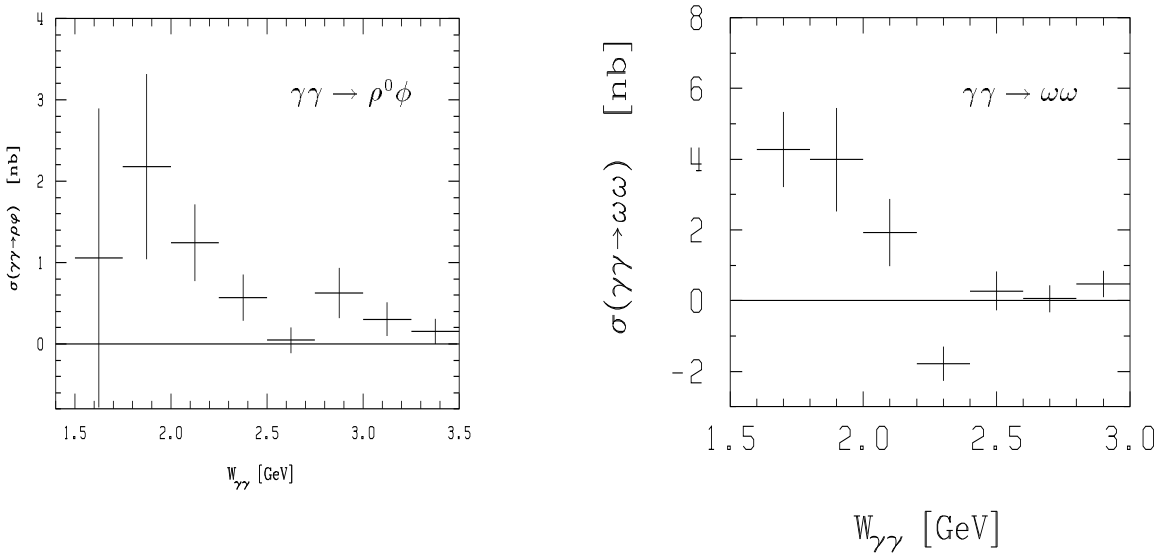

Figure 6.5: *Cross sections for the reactions $\gamma\gamma \to \rho^0\phi$ and $\gamma\gamma \to \omega\omega$ [315].*

6.3.3 $\gamma\gamma \to \rho^0\phi$

The cross section for $\gamma\gamma \to \rho^0\phi$ (Fig. 6.5) was obtained from a sample of $\gamma\gamma \to \pi^+\pi^-K^+K^-$ events. The small number of 33 $\rho^0\phi$ candidates is not sufficient for a partial wave analysis. Therefore, the cross section for $\gamma\gamma \to \rho^0\phi$ was extracted[315] from $\pi^+\pi^-$ invariant mass distributions. The possible spin–parity assignment of the $W_{\gamma\gamma}$ region below 2.5 GeV was tested by studying various projected angular distributions. It was found that the peak can be attributed neither to a pure $J^P = 0^-$ nor to a pure 0^+ or 2^+ wave.

Here, the $qq\bar{q}\bar{q}$ models [296, 297] have the most serious difficulties since one of the strongest predictions of the models is that the $\gamma\gamma \to \rho\phi$ be large (up to about 70 nb in [296]) and in addition the observed signal seems incompatible with the predicted assignment of $J^P = 2^+$. As for the t–channel factorization model of Alexander at al.[299], there is no prediction for the cross section of this reaction.

6.3.4 $\gamma\gamma \to \omega\omega$

ARGUS made its first observation[316] of the reaction $\gamma\gamma \to \omega\omega$ on a part of the total $\gamma\gamma \to \pi^+\pi^+\pi^0\pi^0\pi^-\pi^-$ event sample. The analysis was repeated with the full statistics leading to about 90 $\gamma\gamma \to \omega\omega$ events out of 3200 $\gamma\gamma \to \pi^+\pi^+\pi^0\pi^0\pi^-\pi^-$ events. This number is sufficient for a mass maximum likelihood fit to the three–pion masses but not for a partial wave analysis of $\omega\omega$. In the analysis[317] three contributions to the final state were considered: $\omega\omega$, $\omega 3\pi$ and 6π. Apart from a Breit–Wigner form of the mass distribution for ω mesons (convoluted with the spectrometer response function), the final state particles were approximated by a phase space distribution. This approximation was tested with Monte Carlo simulation and found to represent the main contribution to the systematic error of 25% for the cross section for $\gamma\gamma \to \omega\omega$ shown in Fig. 6.5. Only about 3% of the total integrated $\gamma\gamma \to \pi^+\pi^+\pi^0\pi^0\pi^-\pi^-$ cross section in the mass region between 1.6 and 3 GeV/c^2 is due to the production of omega pairs. Here the t–channel factorisation model has problems since it predicts a cross section of more than 15 *nb* around 2.2 GeV.

6.3.5 $\gamma\gamma \to \omega\phi$

The analysis of the $\pi^+\pi^0\pi^-K^+K^-$ final state[315] showed a weak $\omega\phi$ signal of 4 events (Fig. 6.6) with a background less than 0.6 events (95% c.l.). The signal was obtained from the $\pi^+\pi^0\pi^-$ and K^+K^- invariant–mass spectra. All the observed events fall in the lowest possible $W_{\gamma\gamma}$ interval around 2 GeV/c^2. At higher values of $W_{\gamma\gamma}$ no events were observed, leading to upper limits for the cross section.

6.3.6 $\gamma\gamma \to K^*\bar{K}^*$

A $K^+K^-\pi^+\pi^-$ sample was used to obtain the $\gamma\gamma \to K^{*0}\bar{K}^{*0}$ cross section [318]. The analysis was based on the study of the $K^+\pi^-$ and $K^-\pi^+$ invariant mass spectra.

The two–photon production of $K^{*+}K^{*-}$ was obtained [319] from the reactions $\gamma\gamma \to K^0_S K^0_S \pi^+\pi^-$ and $\gamma\gamma \to K^0_S K^{\mp}\pi^0\pi^{\pm}$. As seen from Fig. 6.6, the cross section for $\gamma\gamma \to K^{*+}K^{*-}$ is about eight times larger than that for $\gamma\gamma \to K^{*0}K^{*0}$.

In the reaction of $\gamma\gamma \to K^{*+}K^{*-}$ and $\gamma\gamma \to K^{*0}\overline{K^{*0}}$, similar to the case of $\gamma\gamma \to \rho^+\rho^-$, vector mesons cannot be produced diffractively. It has been suggested[310] that perturbative QCD might be applicable to the calculation of the processes $\gamma\gamma \to \rho^+\rho^-$, $K^{*+}K^{*-}$, and $K^{*0}\overline{K^{*0}}$ even at relativly low energies. The calculation for the $\gamma\gamma \to \rho^+\rho^-$ cross section is in good agreement with the experimental results but fails completely to account for the large cross section for $\gamma\gamma \to K^{*+}K^{*-}$.

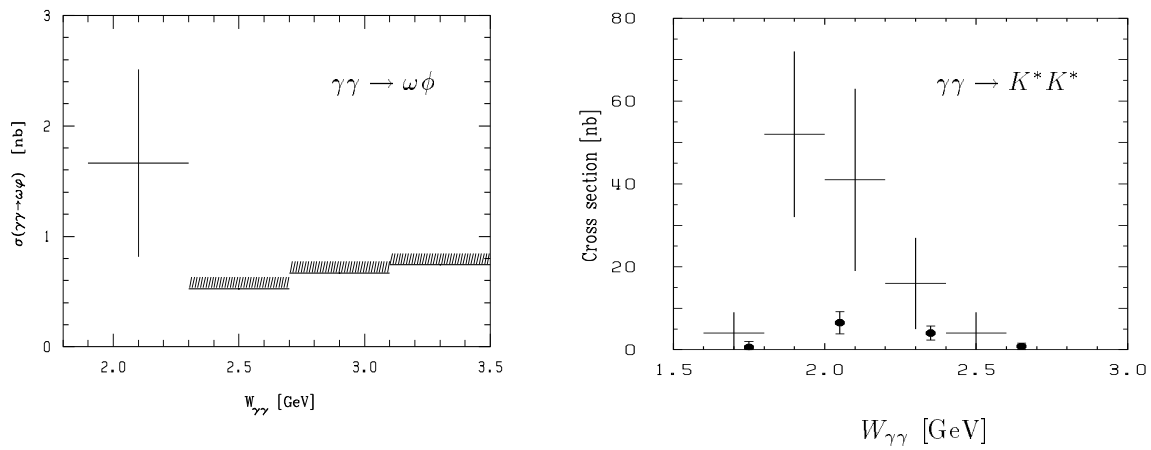

Figure 6.6: Cross sections for the reactions $\gamma\gamma \to \omega\phi$ and $\gamma\gamma \to K^*K^*$ ($K^{*+}K^{*-}$ crosses, $K^{*0}K^{*0}$ full circles) [319].

Due to the heavier s-quark mass only about $\frac{1}{3}$ of the $\rho^+\rho^-$ cross section is expected here. On the other hand, the ratio between the measured $K^{*+}K^{*-}$ and $K^{*0}\bar{K}^{*0}$ cross sections of 8:1 agrees with the prediction of the perturbative QCD calculation. As for the existing four–quark models[296, 297], they are also unable to reproduce the observed large cross sections.

6.3.7 Summary and Discussion of Vector Meson Pair Production

Cross sections for two–photon production of pairs of vector mesons have been measured for the majority of the accessible channels in the $W_{\gamma\gamma}$ range from the production threshold to about 3.5 GeV. In most cases ARGUS data represent either the first observation of the signal or the first partial wave analysis.

At the time when the first ARGUS $\gamma\gamma \to \rho^0\rho^0$ results were published [308] several other measurements [295, 303, 304, 305, 306, 307] existed. They all found a large cross section peaking at about 1.5 GeV. However, the results of the partial wave analyses were not consistent with each other. ARGUS found a dominance of $(J^P, J_z) = (2^+, 2)$.

There are no partial wave analyses of $\gamma\gamma \to \rho^+\rho^-$ to which ARGUS results can be compared. The same is true for $\gamma\gamma \to \rho\omega$ where no partial wave analysis was done by other experiments [313]. The magnitudes of $\rho\omega$ cross sections agree with each other. All other vector pair production reactions have only been measured by ARGUS.

Although we have now a fairly complete set of experimental results on two–photon production of vector mesons in the $W_{\gamma\gamma}$ region below 3 GeV, the theoretical understanding is not yet satisfactory.

6.4 Resonance Production

There are two main motivations for measuring two–photon partial widths: the determination of tensor and pseudoscalar nonet mixing angles, and the understanding of the resonance formation mechanism. One of the aims of hadron spectroscopy is to establish the possible existence of glueball states or a glueball admixture in $q\bar{q}$ resonances.

The resonances that have been studied by the ARGUS collaboration include $f_2(1270)$, $f_2'(1525)$, $a_2(1320)$, $\eta'(958)$ and $\eta_c(2980)$. Their two–photon width can be measured via different hadronic decay channels. Since the ARGUS detector is most suitable for the measurement of charged particles, those decay channels where chosen in which charged particles dominate.

6.4.1 $\gamma\gamma \to K^+K^-$

The K^+K^- invariant mass spectrum (Fig. 6.7) is dominated by the resonances $f_2(1270)$, $a_2(1320)$ and $f_2'(1525)$. The two–photon widths of the first two merged resonances cannot be precisely determined since it is difficult to separate them from each other and from the continuum[1]. Therefore, the study concentrated on $f_2'(1525)$ (Fig. 6.7). The best fit is obtained for a coherent continuum contribution [320]. It results in $\Gamma_{\gamma\gamma} \times \mathrm{Br}(f_2' \to K^+K^-) = (0.0314 \pm 0.0050 \pm 0.0077)$ keV. Less than half of the world average value[2] as quoted by the Particle Data Group [17]. The measurements contributing to this average either assume the absence of continuum in the neutral channel, or an incoherent continuum in the charged channel.

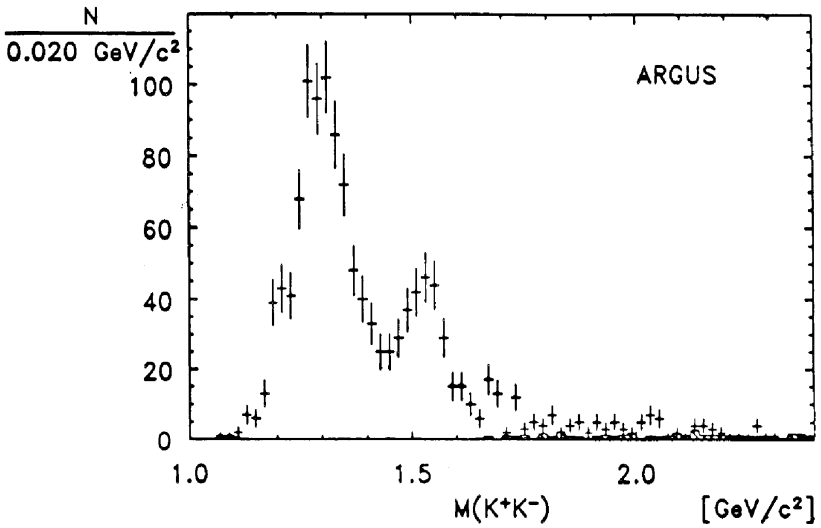

Figure 6.7: *Two–kaon invariant mass spectrum for the reaction* $\gamma\gamma \to K^+K^-$ *[320].*

6.4.2 $\gamma\gamma \to \pi^+\pi^-\pi^0$

The $\gamma\gamma \to \pi^+\pi^-\pi^0$ reaction is dominated by the formation of the $a_2(1320)$ resonance in its helicity 2 state. A maximum likelihood partial wave analysis was performed taking into account the amplitudes [321]

$(2^+, \pm 2)$	$\to$	$\rho^\pm\pi^\mp$		$(0^-, 0)$	$\to$	$\rho^\pm\pi^\mp$
$(2^+, 0)$	$\to$	$\rho^\pm\pi^\mp$		$(0^-, 0)$	$\to$	$f_2\pi^0$
$(2^-, 0)$	$\to$	$\rho^\pm\pi^\mp$		$(0^-, 0)$	$\to$	$f_0(980)\pi^0$
$(2^-, 0)$	$\to$	$f_2\pi^0$		isotropic	$\to$	$\pi^+\pi^-\pi^0$.

The resulting event distributions for the amplitudes $(J^P, J_z) = (2^+, \pm 2)$ and $(2^+, 0)$ in the region of a_2 (below 1.45 GeV) are displayed in Fig. 6.8a. They yield a two–photon partial width of $\Gamma_{\gamma\gamma}(a_2(1320)) = (0.96 \pm 0.03 \pm 0.13)$ keV. The $\gamma\gamma$ helicity 0 fraction of $\Gamma_{\gamma\gamma}$ is $(6.7 \pm 2.2)\%$. The precision of these results equals or exceeds the precision of the world average values.

[1] Two–photon pion pair production is a more convenient method for the study of $f_2(1270)$. The reactions $\gamma\gamma \to 3\pi$ that are suitable for the determination of the $a_2(1320)$ two–photon widths, are discussed in the subsection 4.2.

[2] The Particle Data Group average takes into account the ARGUS value of $(0.067 \pm 0.08 \pm 0.015)$ keV as obtained by assuming an incoherent background contribution.

The ARGUS results confirm the predicted dominance of $J_z = 2$ in the two–photon formation of the a_2 meson. The $J_z = 0$ fraction of about 6% is best accounted for by a relativistic $q\bar{q}$ bound state model [322]

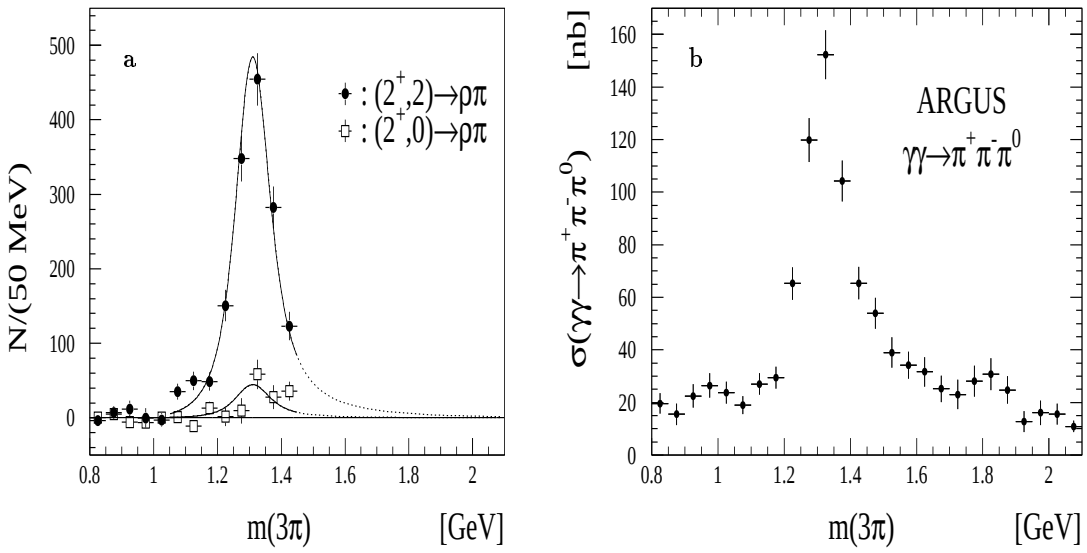

Figure 6.8: a) *Event distributions for the partial waves* $(J^P, J_z) = (2^+, \pm 2)$ *and* $(2^+, 0)$ *of the reaction* $\gamma\gamma \to \pi^+\pi^0\pi^-$ *in the region below 1.45 GeV. b) The total* $\gamma\gamma \to \pi^+\pi^0\pi^-$ *cross section obtained by summing up all the partial wave contributions [321].*

Fig. 6.8b shows the total $\gamma\gamma \to \pi^+\pi^0\pi^-$ cross section obtained by summing up all the partial wave contributions. It is interesting that in the region above 1.45 GeV most of the cross section belongs to the $J^P = 2^+$ waves and that the $J^P = 2^-$ $\rho\pi$ and $f_2\pi$ wave contributions equal zero within the statistical errors. This is in contradiction to an observation of $\pi_2(1670)$ with a two–photon partial width of $(1.41 \pm 0.23 \pm 0.28)$ keV and $(1.3 \pm 0.3 \pm 0.2)$ keV reported by the Crystal Ball [323] and CELLO [324] collaborations, respectively. We note that such a large partial width would be very unusual for an excited state of orbital angular momentum $l = 2$. ARGUS can set only an upper limit of $\Gamma_{\gamma\gamma}(\pi_2) < 0.19$ keV (90% c.l.) in gross disagreement with the other two experiments. Part of the disagreement might be due to different methods used in the data processing; Crystal Ball and CELLO did not perform partial wave analyses. However, even by simply subtracting the a_2 contribution and attributing the remaining cross section to $\pi_2(1600)$ ARGUS is unable to account for such a large two–photon width.

An upper limit of $\Gamma_{\gamma\gamma}(\pi(1300)) \times \mathrm{Br}(\pi(1300)) \leq 0.54$ keV (90% c.l.) was obtained for the pseudoscalar meson $\pi(1300)$.

6.4.3 $\gamma\gamma \to \eta'(958) \to \pi^+\pi^-\gamma$

The spectrum of the reaction $\gamma\gamma \to \eta'(958) \to \rho\gamma \to \pi^+\pi^-\gamma$ of Fig. 6.9 was obtained by tuning the transverse photon momenta to compensate the transverse momenta of the two pions [325]. The background at low $W_{\gamma\gamma}$ comes from the continuum, while at high momenta it is a reflection of the a_2 resonance ($a_2 \to \pi^+\pi^-\pi^0$ where only one photon from the decay $\pi^0 \to \gamma\gamma$ is detected). A two–photon partial width of $\Gamma_{\gamma\gamma}(\eta') = 4.16 \pm 0.09 \pm 0.42$ keV is obtained using $\mathrm{Br}(\eta' \to \pi^+\pi^-\gamma) = 0.301 \pm 0.014$ for the branching ratio.

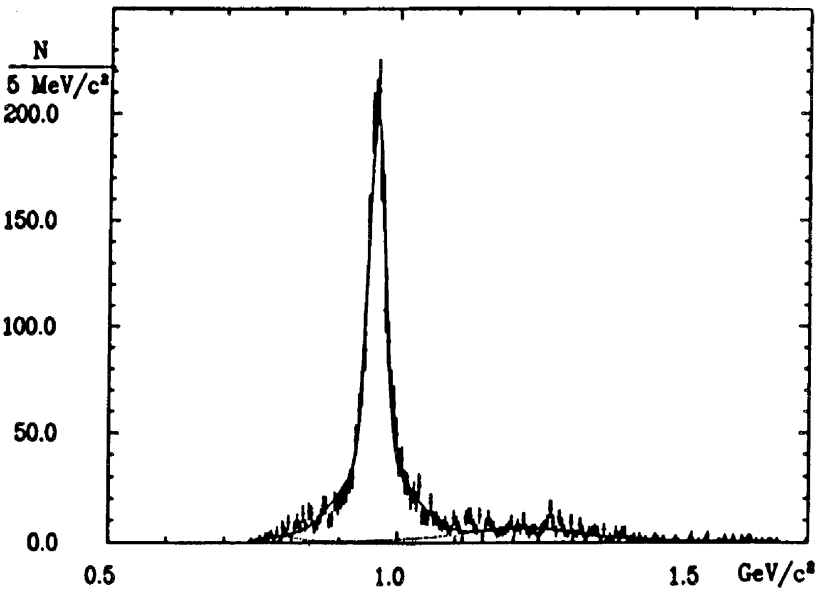

Figure 6.9: $\pi^+\pi^-\gamma$ *invariant mass spectrum after kinematic cuts and* γ *energy tuning [325].*

The ARGUS result for the two–photon decay width based on the whole event sample is the most accurate available and is quite consistent with the old world average of (4.27 ± 0.23) keV.

The $\eta'(958)$ meson is the heaviest member of the pseudoscalar nonet. The pseudoscalar nonet masses span a range of almost an order of magnitude. Therefore, it is interesting to know to what extent the SU(3) flavor symmetry can still be applied. From the two–photon partial widths of the three neutral members of the pseudoscalar nonet one obtains [325] a value of $\theta = -17.5^0 \pm 1.1^0$. The same mixing angle for the η and η' can only be obtained if one allows for breaking of the SU(3) nonet symmetry by introducing an additional parameter. The symmetry breaking could be interpreted as a sign for a glueball component in the η'. This is supported by a strong $J/\psi \to \gamma\eta'$ transition [17].

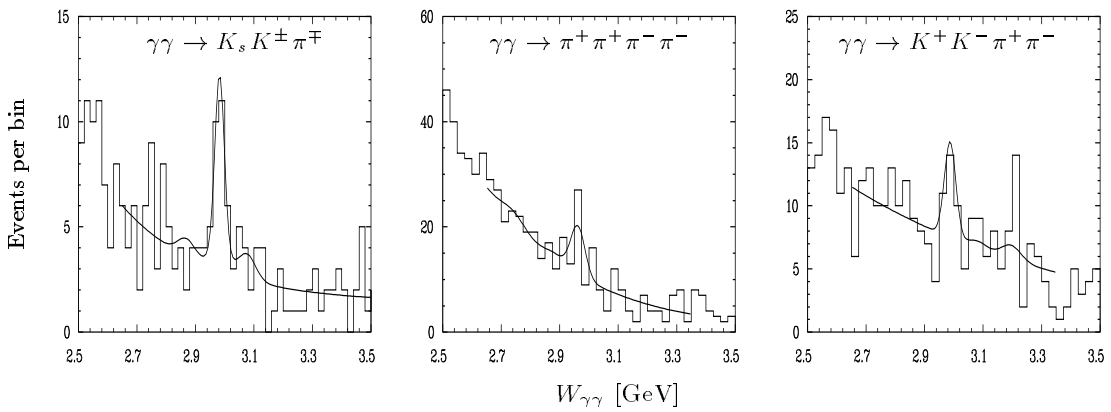

Figure 6.10: *Invariant mass distribution for three* η_c *channels. Solid curves represent fits to the data. The binning is 20 MeV for the the reaction* $\gamma\gamma \to K_s K^\pm \pi^\mp$ *and 25 MeV for other two spectra [326]*

6.4.4 $\gamma\gamma \to \eta_c$

The two–photon production of the pseudoscalar $c\bar{c}$ groundstate η_c was studied via the decay channels displayed in Table 6.4.4 [326]. Invariant mass spectra for the reactions $\gamma\gamma \to K^0_S K^\pm \pi^\mp$, $\gamma\gamma \to \pi^+\pi^+\pi^-\pi^-$ and $\gamma\gamma \to \pi^+\pi^- K^+ K^-$ are shown in Fig. 6.10. The most significant product of the two–photon width times the branching ratio, is $\Gamma_{\gamma\gamma}(\eta_c) \times \mathrm{Br}(\eta_c \to K^0_s K^\pm \pi^\mp) = (0.28 \pm 0.07)$ keV. This value is consistent with the world average of (0.23 ± 0.08) keV. The final result on the two–photon width of the η_c meson,

$$\Gamma_{\gamma\gamma}(\eta_c) = (11.3 \pm 4.2)\ \mathrm{keV}$$

is obtained as the weighted average of the first four decay modes in Table 6.4.4. We note that the main contribution to the error, amounting to 3.2 keV, comes from the uncertainty of the branching ratio $\mathrm{Br}(J/\psi \to \eta_c\gamma)$ which is used to determine the η_c branching ratio.

The ARGUS result on $\Gamma_{\gamma\gamma}(\eta_c)$ can be used to obtain the branching ratio $\mathrm{Br}(\eta_c \to K^+K^-K^+K^-) = 0.021 \pm 0.010 \pm 0.006$. The second error is the uncertainty on the branching ratio for the decay $J/\psi \to \eta_c\gamma$.

Table 6.1: *Results of the analysis of $\gamma\gamma \to \eta_c$. If two errors are given, the first error shown is statistical and the second systematic. In the case of results for the two–photon width, the first error is statistical, the second uncorrelated systematic, and the third correlated systematic error. Upper limits correspond to the 95 % confidence level. $\eta_c \to 2K^+2K^-$ contains all topological modes except $\eta_c \to \phi\phi$ [326].*

Channel	Events	$\Gamma_{\gamma\gamma}(\eta_c) \cdot \mathrm{Br}_i$ in keV	Br_i [327] in %	$\Gamma_{\gamma\gamma}(\eta_c)$ in keV
$K^0_S K^\pm \pi^\mp$	22.0 ± 5.3	$0.281 \pm 0.068 \pm 0.028$	1.78 ± 0.56	$15.8 \pm 3.8 \pm 2.3 \pm 4.5$
$K^+K^-\pi^+\pi^-$	13.9 ± 6.6	$0.17 \pm 0.08 \pm 0.02$	2.13 ± 0.68	$8.2 \pm 3.9 \pm 1.3 \pm 2.3$
$2\pi^+2\pi^-$	21.4 ± 8.6	$0.18 \pm 0.07 \pm 0.02$	1.09 ± 0.37	$16.7 \pm 6.7 \pm 3.5 \pm 4.6$
$\phi\phi \to 2(K^+K^-)$	< 3.0	< 0.0309	0.171 ± 0.062	<24.1
$2K^+2K^{-\,a}$	9.1 ± 3.5	$0.231 \pm 0.090 \pm 0.023$	-	-
ϕK^+K^-	< 6.3	< 0.152	-	-

6.4.5 Summary and discussion of resonance production

The spectroscopy of hadronic bound states is still far from understood, even for the lowest meson multiplets. An important input for a systematic classification of resonances are their electromagnetic couplings which reveal the charge composition of the constituents. The ARGUS experiment has contributed to improving the precision of the measured two–photon widths of resonances.

ARGUS has measured the two–photon width of the pseudoscalar meson $\eta\prime(958)$ and the tensor mesons $a_2(1320)$ and $f_2^{'}(1525)$. Combining the results of all measurements, including the ARGUS data, the mixing angles for the pseudoscalar and tensor nonets are:

$$\Theta_P = -17.5^o \pm 1.1^o \text{ and } \Theta_T = 33.5^{o\,+3.5^o}_{-3.0^o}.$$

The observed properties of the pseudoscalar and tensor states are quite consistent with $SU(3)$ nonet symmetry, except for the two–photon width of the $\eta\prime$ meson which is somewhat low compared to the two–photon width of the η meson. This leaves room for a possible gluon admixture in the $\eta\prime$ meson which is also supported by the relatively abundant $\eta\prime$ production in radiative J/ψ decays.

In the analysis of the $a_2(1320)$ meson ARGUS found the fraction of $(J^P, J_z) = (2^+, 0)$ to be $(6.7 \pm 2.2)\%$. This observation agrees with the expected dominance of $(J^P, J_z) = (2^+, \pm 2)$. The measured fraction favours relativistic bound state calculations.

In the three-pion mass spectrum no sizeable $J^P = 2^-$ contribution was found. In particular, the surprisingly large two–photon width for the orbital excitation $\pi_2(1670)$, observed previously by two other experiments, could not be confirmed by ARGUS.

ARGUS has measured the two-photon width of the pseudoscalar charmonium ground state $\eta_c(2980)$. Including QCD corrections the prediction is $\Gamma_{\gamma\gamma}(\eta_c) = (8.6 \pm 0.6)$ keV [328] which coincides nicely with the combined ARGUS result of (11.3 ± 4.2) keV.

Chapter 7

Fragmentation

7.1 Introduction

Hadron production in high energy e^+e^--annihilation far away from the resonance region is described as a factorizing process [329]. The first step is the production of a quark pair in the reaction $e^+e^- \rightarrow q\bar{q}$, modified by photon and gluon radiation, which are calculated by perturbative methods in the framework of QED and QCD respectively [330]. In the second step the produced quarks and gluons fragment into hadrons [331], which are detected and are the source of all information concerning the underlying parton process. A similar approach is used to interpret hadron production in direct decays of heavy quarkonium states as the $\Upsilon(1S)$-resonances. In this case the Υ-meson in the first step is assumed to decay into gluons via the reactions $\Upsilon \rightarrow 3g$ and $\Upsilon \rightarrow \gamma gg$ respectively, which in the second step hadronize [332].

It is a general feature of all hadronization processes and known since a long time [333] that the produced mesons and baryons align along the direction of the primary partons. The transverse momentum p_t of the hadrons with respect to this direction is, nearly independent of the parton momentum, limited to $p_t \approx 0.3$ GeV/c. The strong correlation between the parton momentum and the direction of these jets allows to extract from measured topological distributions those of the underlying parton reaction.

The understanding of hadron formation in quark- and gluon-jet fragmentation respectively has been a challenge for almost two decades. While the small momentum transfers involved in these reactions will keep this field inaccessible to pure QCD in the foreseeable future, the results on the other side are from a practical point of view of utmost importance, since they are used to bridge the gap between the underlying parton process of interest in QCD studies [330, 334] and the jet of hadrons observed. Lacking a fundamental theory, phenomenological approaches are the basis of our present understanding of the hadronization process. Parton shower models based on QCD leading log approximation [335, 336] and the Lund string model [337] are the most popular phenomenological tools widely used by experimentalists to extract the interesting information from their data.

Common to all these approaches is the production of jets. It is now widely accepted that the probability of a certain hadron to form in the hadronization step is mainly determined by its valence quark content and its spin [338]. Quarks of a given flavor are formed according to probabilities, which are tuned to data. This concept has turned out to be very successful and allows e.g. to describe the relative production rate of strange mesons and baryons with a single parameter s/u, parametrizing the attenuated production of strange quarks during the break up of the color-field [338]. With additional corrections from spin-spin interactions and the shapes of the wave function

one can hope to obtain a basically simple, universal picture of hadron production [337].

In this chapter the contribution of the ARGUS group to our present understanding of fragmentation is summarized. The data collected in this experiment are unique to a certain extent, since a high statistic sample of continuum events can be compared to a data set of direct $\Upsilon(1S)$-decays into gluons. Possible differences of quark and gluon fragmentation should therefore be observable. The paper describes in section 7.2 some general information on the final states. In section 7.3 results of light quark fragmentation into mesons and baryons are presented, while in section 7.4 the production rates of charmed mesons and baryons are discussed. The data are compared with the predictions of presently favored fragmentation models. The results are summarized in section 7.5.

7.2 General Features of the Hadronic Final States

7.2.1 Jet-Structure

As discussed in section 7.1 the hadronic final state produced in the second step of the $e^+e^- \rightarrow q\bar{q}$-reaction is expected to be of jet-like structure. At an energy of $\sqrt{s} = 10$ GeV and a mean total multiplicity of about 12 (section 7.3.1) the mean particle momentum is only a factor of three larger than the transverse momentum with respect to the parton direction. Therefore, pencil-like jets cannot be expected to be observed, rather one has to define proper topological variables to characterize the jet shape [339]. Several shape variables have been proposed, which allow to fix the jet-axis. The sphericity S and the thrust T are most commonly used. The thrust maximizes the parallel component of all particles with respect to the jet-axis of an event

$$T(\hat{\vec{n}}) = \max_{\vec{n}} \frac{\sum \vec{p}_i \cdot \vec{n}}{\sum \mid \vec{p}_i \mid} \ . \tag{7.1}$$

This quantity is linear in the momentum and therefore infrared stable. In Figure 7.1 (a) the thrust distribution derived from charged and neutral hadrons for continuum events and direct $\Upsilon(1S)$-decays is shown [258]. The thrust distribution for continuum events differs from that of direct $\Upsilon(1S)$-decays as expected, since in the continuum two-jet- and in direct $\Upsilon(1S)$-decays three-jet-topologies dominate. Note that the thrust distribution for direct Υ-decays differs only slightly from that of a phase space distribution [332].

QCD predicts the $\Upsilon(1S)$-meson to decay directly into three gluons and into one photon plus two gluons respectively [332]. ARGUS has searched for a two-jet component predicted by Landshoff et al. [340] in direct $\Upsilon(1S)$-decays by an analysis of the second Fox-Wolfram moment [341]

$$H_2 = \frac{\sum_{i=1}^{N} \sum_{j=1}^{N} \{ \mid \vec{p}_i \mid \mid \vec{p}_j \mid \} . (3\cos^2 \alpha_{ij} - 1)}{2 \left(\sum_1^N \mid \vec{p}_i \mid \right)^2} \ , \tag{7.2}$$

where the sum runs over all particles of an event and $\cos \alpha_{ij} = \frac{(\vec{p}_i \, \vec{p}_j)}{(|\vec{p}_i| \ |\vec{p}_j|)}$. At large values of H_2 one expects a contribution of two-jet events in direct $\Upsilon(1S)$-decays (Figure 7.1 (b)). No signal is observed. From this observation an upper limit for two-jet events in direct $\Upsilon(1S)$-decays of 5.3 % at 95 % CL is derived.

As follows from Figures 7.1, the topological variables show a rather broad distribution, hence the jet-axis is not too well fixed. Therefore, an alternative method has been applied to determine the angular distribution of the jet-axis from the data. Fast hadrons should be well aligned with the jet-axis [333] and hence reproduce in good approximation the polar angular distribution of the quarks for continuum events. Far from the threshold this distribution for the reaction $e^+e^- \rightarrow q\bar{q}$ is given by the expression

$$\frac{d\sigma}{d\Omega} \sim (1 + \cos^2 \theta) \ . \tag{7.3}$$

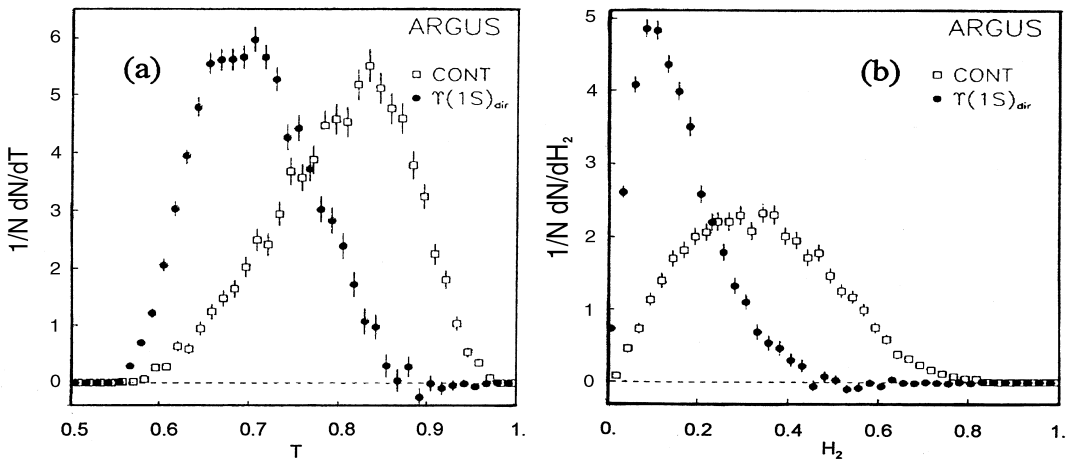

Figure 7.1: *(a) Thrust distributions (from charged and neutral particles) of direct $\Upsilon(1S)$-decays and continuum events at 9.98 GeV cms-energy. (b) Distributions of the second Fox–Wolfram moment (from charged and neutral particles) of direct $\Upsilon(1S)$-decays and continuum events at 9.98 GeV cms-energy [258].*

Fast hadrons should approach this angular distribution. As shown in Figure 7.2 [342] this is indeed the case. In this figure the coefficient A, determined from a fit of

$$\frac{d\sigma}{d\Omega} \sim (1 + A(x_p)\cos^2\theta) \tag{7.4}$$

to the measured angular distribution of hadrons with a fractional momentum $x_p = \frac{p}{p_{max}}$, is plotted. As expected A is compatible with 1.

In the highest momentum bin A seems to decrease. This behavior is expected, since in the limiting case of exclusive π-meson production $e^+e^- \rightarrow \pi^+\pi^-$ the angular distribution of the $\pi^\pm$-mesons at high energies is given by

$$\frac{d\sigma}{d\Omega} \sim (1 - \cos^2\theta) \ . \tag{7.5}$$

The observed deviation from A = 1 in Figure 7.2 might be interpreted as the influence of a higher twist contribution to the inclusive spectrum for $x_p \rightarrow 1$ [343]. It turns out that for $x_p < 0.3$ the parameter $A(x_p)$ decreases [344] as expected, since low momentum hadrons are not strongly aligned with the parton direction [333].

7.2.2 Measurements of α_s

The R value defined as the ratio of nonresonant hadronic cross section to the Born cross section for μ-pair production

$$R = \frac{\sigma_0(e^+e^- \rightarrow hadrons)}{\sigma_0(e^+e^- \rightarrow \mu^+\mu^-)} \tag{7.6}$$

is of special interest. In this expression σ_0 indicates that effects of higher order QED contributions have been corrected. In the quark parton model this ratio equals the sum of the quark charges squared times the number of colors $N_c = 3$. Higher order QCD corrections up to the third order in α_s have been calculated [345]

$$R = 3\sum_{i=1}^{n_f} Q_i^2\,(1 + f(\alpha_s)) \ , \tag{7.7}$$

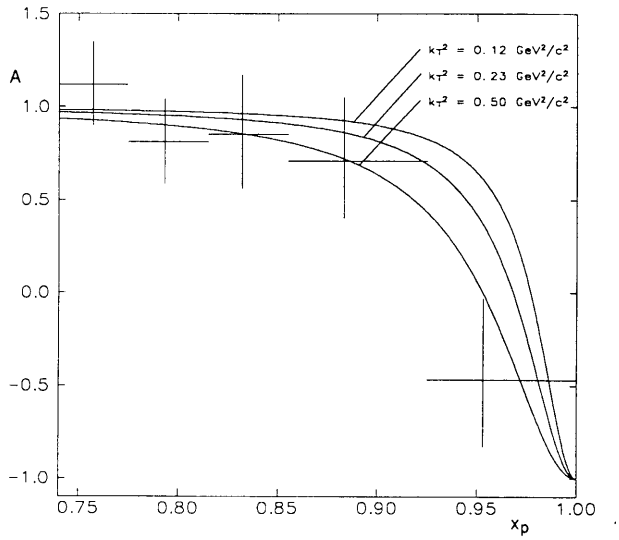

Figure 7.2: *Results of a fit of* $\frac{d\sigma}{d\Omega} \sim 1 + A \cdot cos^2\theta$ *to the acceptance corrected polar angle distribution of charged hadrons compared to predictions from a higher twist calculation [343].*

n_f denotes the number of quark flavors above the production threshold. The expression holds for high enough energies; otherwise known kinematical factors have to be considered. ARGUS [43] has measured $R = 3.46 \pm 0.03 \pm 0.13$ at an energy of $\sqrt{s} = 9.36$ GeV. It is the most precise value at *cms* energies around 9.5 GeV. Averaging the available data in this energy region one gets $\langle R \rangle = 3.515 \pm 0.079$ at $\sqrt{s} = 9.5$ GeV [43]. Using the third order expression for $f(\alpha_s)$ [345] with $n_f = 4$ the number of quark flavors and setting $m_c = m_D$ one gets $\alpha_s \approx 0.14 \pm 0.05$. The error of α_s is dominated by systematic uncertainties. It is still too large to be competitive with the results derived by other methods [334, 346].

An alternative way to derive α_s is the study of the direct decay $\Upsilon(1S) \to \gamma gg$. The ratio

$$R_\gamma = \frac{\Gamma(\Upsilon(1S) \to \gamma gg)}{\Gamma(\Upsilon(1S) \to ggg)} \tag{7.8}$$

depends on the strong coupling constant [347]

$$R_\gamma = \frac{4}{3} \frac{\alpha_{em}}{\alpha_s} \left\{ 1 + (2.2 \pm 0.6) \frac{\alpha_s}{\pi} \right\} . \tag{7.9}$$

Higher order corrections are claimed to cancel almost completely [347]. ARGUS [348] has performed a detailed study of the decay $\Upsilon(1S) \to \gamma gg$. The major problem of this analysis is the careful subtraction of the photon-background from π^0- and η-decays into a γ-pair. This background limits the momentum interval accessible to the study. The acceptance corrected spectrum is shown in Figure 7.3. The data are compared with theoretical predictions [349, 350, 351] folded with the energy resolution of the shower counters. The parton model spectra [349, 350] are clearly ruled out.

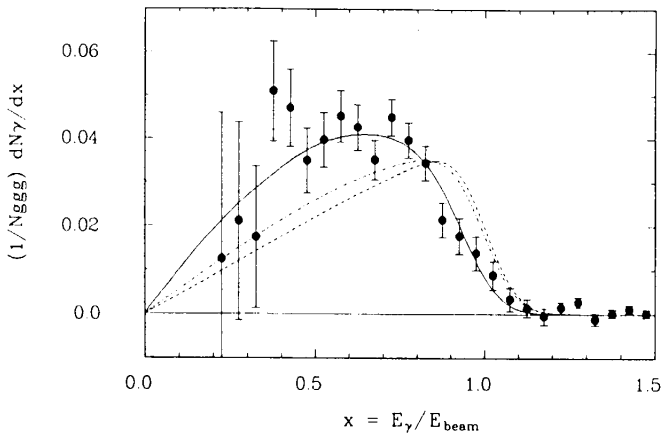

Figure 7.3: *Acceptance-corrected direct photon spectrum compared to the theoretical spectra of ref. [349] (dashed curve), ref.[350] (dotdashed curve) and ref.[351] (solid curve). The error bars represent statistical errors only.*

The prediction of Field [351], which includes the effect of gluon self-coupling in the final state, is in good agreement with the data. This result demonstrates that in the energy interval of interest final state interactions of the partons might distort appreciably the parton distribution. Using the spectra of Field [351] to extrapolate to $x_\gamma = 0$, one gets [348]

$$R_\gamma = (3.00 \pm 0.13 \pm 0.18)\ \% \ , \tag{7.10}$$

which allows to derive $\alpha_s = 0.225 \pm 0.011 \pm 0.019$ at a momentum scale of $0.157 M_\Upsilon$ [347].

7.3 Fragmentation into Mesons and Baryons with Light Valence Quarks

It is now a widely used concept to assume that the probability of a certain hadron to form in fragmentation is determined by its quark content [331, 338]. The observed suppression of strange particles in this framework is due to an attenuation of strange quark production relative to light u- and d-quarks, parametrized by a factor $\frac{s}{u}$ taken from experiment. Similarly the production of vector relative to pseudoscalar mesons is again suppressed by a factor $\frac{V}{V+P}$. Note, however, that decay products have to be considered properly, if one wants to extract these parameters from the data.

Additional corrections are expected from the mixing of different SU(3)-multiplets. It is a priori not clear that the mixing angle of the static quark model can be used. The production of the $\eta'(958)$- and the η-meson in this respect are of special interest. A further crucial ingredient to the total picture of hadronization is the role of hadrons with non-zero angular momentum of the quarks. They finally decay into the observed pseudoscalar- and vector-mesons and can thus distort the observed $\frac{V}{V+P}$ ratio compared to the original one. Due to the scarce information available orbitally excited mesons are usually not considered by fragmentation models.

7.3.1 Production of Stable Mesons

π, η- and K-mesons are besides protons and neutrons the final products of the fragmentation and decay chain. Thus they provide information on the global properties of the fragmentation of quarks and gluons. In Table 7.1 the multiplicities measured by the ARGUS collaboration are collected. In addition the predictions of the Lund string model [337, 352, 353] are entered into the Table 7.1.

Table 7.1: *Measured rates of pseudoscalar mesons in the continuum ($\sqrt{s} = 9.98$ GeV) and for direct $\Upsilon(1S)$-decays [344, 354]. The data are compared to the predictions of the Lund fragmentation model , version JETSET 7.4 [337, 352, 353].*

	ARGUS results		Fragmentation model	
	continuum	$\Upsilon(1S)$	continuum	$\Upsilon(1S)$
$\pi^{\pm}$	6.38 ± 0.14	7.55 ± 0.14	5.98	7.55
π°	3.22 ± 0.32	3.97 ± 0.44	3.57	4.35
$K^{\pm}$	0.89 ± 0.03	0.91 ± 0.03	0.92	0.86
$K^{\circ}/\bar{K}^{\circ}$	0.91 ± 0.06	1.03 ± 0.05	0.81	0.79
η	0.19 ± 0.06	0.40 ± 0.17	0.42	0.64
η'	0.034 ± 0.011	0.115 ± 0.04	0.077	0.112

The data are derived from the measured inclusive energy spectra by extrapolating to $z = \frac{E}{E_{max}} = \frac{m}{E_{max}}$. Note, however, that ARGUS has measured in addition the mean charged multiplicity at $\sqrt{s} = 10.47$ GeV directly by unfolding the recorded multiplicity distribution [43]. From this analysis one gets $\langle n_{ch} \rangle = 8.35 \pm 0.02 \pm 0.20$. Only a small part of the discrepancy between the charged multiplicities derived by the two methods is due to the energy difference between the two data sets analyzed. The remaining discrepancy of ~ 2.7 standard deviations hints to a systematic uncertainty not covered by the errors quoted. The measured $\pi^{\pm}$- and π^0-meson production rates [344, 354] are equal within the errors as expected from isospin invariance.

It is interesting to note that the mean charged particle multiplicity in direct $\Upsilon(1S)$-decays tends to be slightly higher than the continuum data by a factor $r = 1.18 \pm 0.03$. This ratio is by far smaller than the asymptotically expected difference of the multiplicity in quark- and gluon-jets [329, 330, 331]. For charged K-mesons this ratio is $r = 1.02 \pm 0.05$. Note that this trend is not unexpected, since in charm-quark initiated jets K-mesons are enriched. ARGUS has determined the K^0-meson multiplicity in jets induced by light- and charm-quarks separately by tagging the latter with reconstructed D^*-mesons [355]. The statistics are still too low to draw definite conclusions but the result of this study confirms the expected trend: for c-quark initiated jets one gets $\langle n_{K^{\circ}} \rangle = 1.03 \pm 0.07$, while in light quark jets one gets $\langle n_{K^{\circ}} \rangle = 0.84 \pm 0.09 \pm 0.06$.
The shape of the measured $\pi^{\pm}-, \pi^0-, K^{\pm}$- and K^0-meson momenta are reasonably well described by the predictions of the fragmentation models [344, 354]. In this paper they are not discussed in detail, since the decay of the unstable particles distorts the original spectrum. The measured rates compare well with the model predictions, only the η-meson rates are smaller than expected (Table 7.1).

7.3.2 Production of Unstable Mesons

Parameters of the Fragmentation Models

The free parameters of the fragmentation models can advantageously be derived from studies of vector-meson production in direct $\Upsilon(1S)$-decays, since the charm content of these events is negligible (see section 7.4.3) and hence uncertainties due to charm production and subsequent decays do

Table 7.2: *Measured rates of vector mesons in the continuum ($\sqrt{s} = 10.5$) and for direct $\Upsilon(1S)$-decays [46, 358, 359]. The data are compared to the predictions of the Lund fragmentation model, version JETSET 7.4 [337, 352].*

	ARGUS results		Fragmentation model	
	continuum	$\Upsilon(1S)$	continuum	$\Upsilon(1S)$
K^{*+}	0.246 ± 0.034	0.29 ± 0.05	0.33	0.35
$K^{*\circ}$	0.292 ± 0.075	0.328 ± 0.033	0.30	0.35
ρ°	0.326 ± 0.038	0.333 ± 0.042	0.40	0.58
ω	0.295 ± 0.076	0.314 ± 0.116	0.34	0.57
ϕ	0.044 ± 0.0028	0.055 ± 0.0036	0.048	0.045

not influence the interpretation. Note that the number of tagged charm events in the continuum is not large enough to use these events for such a study [355]. However, it should be stressed that the procedure applied in this analysis relies on the assumption that the parameters of fragmentation models are the same for quark and gluon initiated processes.

The production of ω-mesons has been observed for the first time in deep inelastic e^+e^--annihilation by the ARGUS collaboration [46]. Since the ω- and ρ^0-meson have the same valence quark content, the same spin and nearly the same mass, equal production rates for these two mesons are expected. The experiment confirms this prediction, for direct $\Upsilon(1S)$-decays one gets [46]

$$r_\omega = \frac{n(\omega)}{n(\rho^0)} = 0.85 \pm 0.19 \pm 0.14 \tag{7.11}$$

in good agreement with model predictions [353] and with results from soft pp-collisions [356], which find $r_\omega = 1.02 \pm 0.08$. These results confirm the basic assumption of all fragmentation schemes that the valence quark composition determines the production rate. On the other hand in high p_T hadronic reactions the situation is far from being clear [357], depending on the specific reaction under study values $r_\omega = 1$ and $r_\omega = 0.44$ have been measured respectively.
Nearly all particles in the pseudoscalar- and vector-meson nonets have been observed by the ARGUS collaboration [344, 354, 46, 358, 359]. Only the $\rho^{\pm}$-meson rate has not been measured but it can safely be derived by isospin arguments from the measured ρ^0-meson rate. In Table 7.2 the measured rates of unstable light mesons for continuum data and for direct $\Upsilon(1S)$-decays are collected. These rates were derived from the measured inclusive energy spectra by extrapolation, which in most cases is the major source of systematic uncertainties. This comprehensive data set allows to fix the parameters of the fragmentation models with a minimal number of assumptions. Note, however, that the analysis starts from the assumptions that no tensor- and scalar-mesons are produced.

Vector Meson Suppression

It is common practice to characterize the relative abundancy of vector-mesons in fragmentation by the ratio $\frac{V}{V+P}$, where particles from decays of the ground state meson octets are corrected for. Using the ARGUS data [344, 354, 46, 358, 359] and the branching ratios of ref. [17] a ratio $\left(\frac{V}{V+P}\right)_K$ for K-mesons and a corresponding factor $\left(\frac{V}{V+P}\right)_\pi$ for mesons without a s-quark can be calculated:

$$\left(\frac{V}{V+P}\right)_K = \frac{n(K^{*0}) + n(K^{*+})}{n(K^0) + n(K^+) - 2n(\phi) \cdot 0.84} \tag{7.12}$$

Table 7.3: $\frac{V}{V+P}$ *ratio derived from the measured pseudoscalar- and vector-meson rate [46] from direct* $\Upsilon(1S)$*-decay rates.*

$\left(\frac{V}{V+P}\right)_\pi$	0.208 ± 0.041
$\left(\frac{V}{V+P}\right)_K$	0.335 ± 0.034

$$\left(\frac{V}{V+P}\right)_\pi = \frac{n(\rho^0)+n(\omega)-n(Res,\rho^0,\omega)}{n(\rho^0)+n(\omega)+n(\pi^0)+n(\eta)+n(\eta')-n(decay)} \tag{7.13}$$

n symbolizes the measured multiplicities. $n(Res,\rho^0,\omega)$ is the sum of the ρ^0- and ω-meson contribution from ϕ- and η'-decay. $n(decay)$ includes the rate of $\rho^0-,\omega-,\pi^0-$ and η-mesons produced in decays of $\phi-,K^*-,\rho-,\omega-,K^0-,\eta-$ and η'-mesons. All particle rates have been measured or as mentioned have been derived by isospin arguments. The results for $\frac{V}{V+P}$ are collected in Table 7.3. It has been verified that the $\frac{V}{V+P}$-ratio extracted from a Monte Carlo simulation by the same method agrees with the input parameter for $\frac{V}{V+P}$ to better than 10 % [360]. From this observation we conclude that the derived values given in Table 7.3 provide a good estimate of the $\frac{V}{V+P}$-parameter used in fragmentation models. Note that the values derived differ appreciably from the factor $\frac{V}{V+P} = 0.75$ predicted by spin statistics (see section 7.4.1). The small value of $\left(\frac{V}{V+P}\right)_\pi$ is not unexpected, since π-mesons from baryon and tensor meson decays are not considered in Equation (7.12, 7.13).

Strangeness Suppression in Meson Production

The ARGUS data can also be used to determine the attenuated production of s- with respect to u-quarks in the fragmentation step. In the string model [337] quarks are created, when strings break up. s-quark production is suppressed due to their larger mass compared to light u- and d-quarks. The parameter $\frac{s}{u}$ is used to parametrize the relative abundancy of different quark flavors produced, when the string breaks up $n(u) : n(d) : n(s) = 1 : 1 : \frac{s}{u}$. Neglecting vector-mesons produced in secondary decays the ratio $\frac{s}{u}$ can be calculated from the measured rates of vector mesons. Again data from direct $\Upsilon(1S)$-decays have been exploited to avoid complications due to charm decays. In the analysis $n(\omega) = n(\rho^0)$ is assumed. The multiplicities have to be corrected for different values of $\frac{V}{V+P}$ for strange and nonstrange vector mesons respectively. The most precise results are derived from the following uncorrelated ratios:

$$\frac{s}{u} = \frac{2\ n(\phi)}{n(K^{*\pm})} = \frac{1}{2}\ \frac{n(K^{*0})}{n(\rho^0)-n(Res,\rho^0)} \cdot \frac{\left(\frac{V}{V+P}\right)_\pi}{\left(\frac{V}{V+P}\right)_K}\ . \tag{7.14}$$

From these expressions one gets the results collected in Table 7.4.

Table 7.4: *Ratios* $\frac{s}{u}$ *derived from vector-meson rates.*

$\left(\frac{s}{u}\right)_{\rho^0}$	0.355 ± 0.085
$\left(\frac{s}{u}\right)_\phi$	0.375 ± 0.049
$\left\langle\frac{s}{u}\right\rangle$	0.37 ± 0.04

Comparing the input for the ratio $\frac{s}{u}$ with the results of Equation (7.14) in case of Monte Carlo data we have validated the method. The results for mesons given in Table 7.4 are in good agreement with the values derived from hyperon production discussed in section 7.3.3.

SU(3) Multiplet Mixing

The influence of SU(3) multiplet mixing can sensitively be tested by studying the production of $\eta'(958)$-mesons and comparing it to the corresponding η-meson rate. If one attempts to interprete the $\eta'(958)$- and η-meson production rate based on the philosophy that the production of a specific meson type depends on its quark content and its spin, the pseudoscalar mixing angle plays a crucial role, because the observable η- and $\eta'(958)$-meson are constructed by mixing the SU(3)-singlet- and octet-pseudoscalar states with isospin zero. The mixing angle thus influences their strangeness content. Originally the standard fragmentation models [337] assumed the same strangeness content of the η- and $\eta'(958)$-meson, which corresponded to the choice $\theta_p = -10°$. The observed production rate (Table 7.1) was in gross disagreement with the predictions [358, 361]. Using the value of $\theta_p = -20°$ following from the study of η- and $\eta'(958)$-production in $\gamma\gamma$-processes [17] the agreement with the data was improved (Table 7.1). This result strengthens the basic assumption underlying all fragmentation models that the production rate of mesons depends on their valence quark content.

The $\eta'(958)$- and the η-meson have the same quantum numbers but they differ appreciably by their masses and therefore are an ideal place to study explicit hadron mass effects in fragmentation models. The Lund [337] and the UCLA model [362] differ in just this respect. Since no predictions for direct $\Upsilon(1S)$-decays exist in the framework of the UCLA model [363], presently this interesting test cannot be performed.

Production of Angular Excited Mesons

A further crucial ingredient, which has not been studied in detail, is the role of non-zero angular momentum L between the quarks in the fragmentation process. Mesons with $L \neq 0$ decay finally into mesons with $L = 0$ and, therefore, might contribute considerably to the observed pseudoscalar- and vector-meson rates. No model predictions presently exist. ARGUS has observed the f_0-decay into $\pi^+\pi^-$-mesons [358]. In Table 7.5 the results are compared to the ρ^0-meson rate. In addition the results of other experiments are given. The fact that the ratio is independent of $\sqrt{s}$ and the reaction type points to a common production mechanism for the f_0- and the ρ^0-meson, where only the quark angular momentum causes a suppression. A further support for this assumption follows from the similar shape of the inclusive energy spectra [358].

Table 7.5: *Measured ratio* $\frac{n(f_0)}{n(\rho^0)}$ *from different experiments.*

	$\frac{n(f_0)}{n(\rho^0)}\mid_{cont}$	$\frac{n(f_0)}{n(\rho^0)}\mid_{\Upsilon(1S)}$
ARGUS [358]	0.072 ± 0.018	0.117 ± 0.030
HRS [364]	0.063 ± 0.032	–
LEBC [356]	0.059 ± 0.021	–

Inclusive Spectra of Light Mesons

Finally the measured inclusive energy spectra can be compared to the predictions of fragmentation models (Figures 7.4–7.6). The shape of the spectra agrees rather well for the continuum and for direct $\Upsilon(1S)$–decays. Note, however, that slight discrepancies exist in the total rate (Tables 7.1,7.2). Compared to previous versions of the Lund model the situation has improved [46]. As expected the meson spectra from direct $\Upsilon(1S)$–decay are softer than the continuum data. This behavior reflects the different parton structure underlying the events.

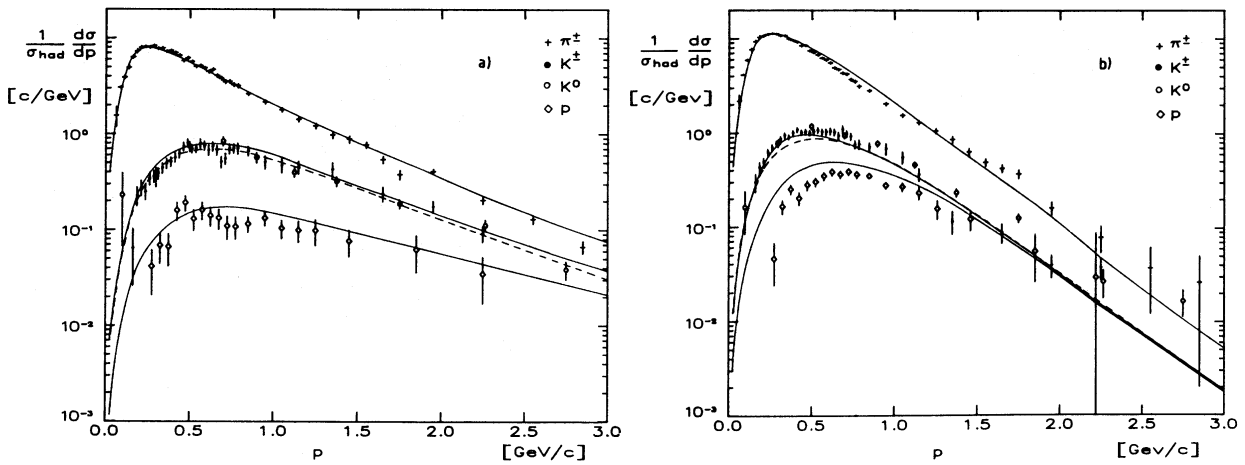

Figure 7.4: *Measured π^+, K^+, K^0 and p spectra for continuum events (a) and direct $\Upsilon(1S)$ decays (b) [344] compared to model predictions [337].*

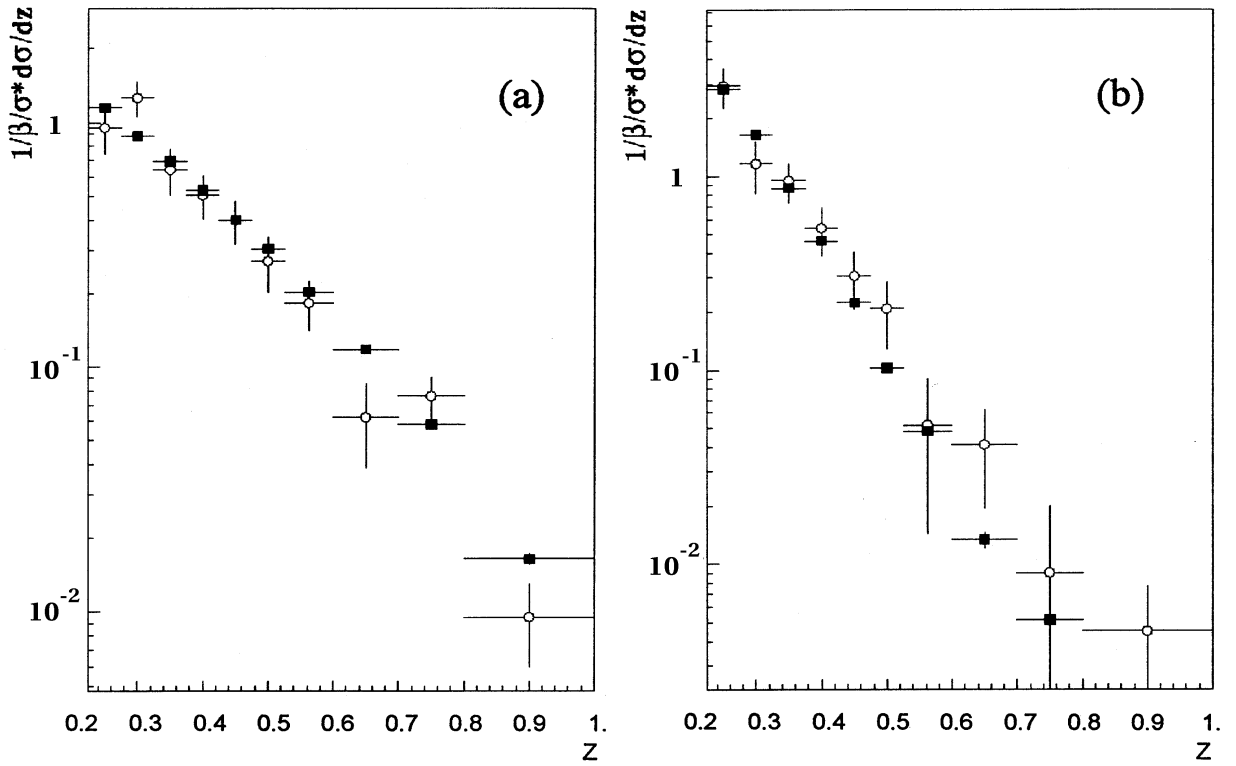

Figure 7.5: *(a) Measured $K^{*+}(896)$–meson spectrum (○) for continuum events. (b) Measured inclusive $K^{*+}(896)$–meson spectrum (○) in direct $\Upsilon(1S)$–decays [46] compared to model predictions [337, 353] .*

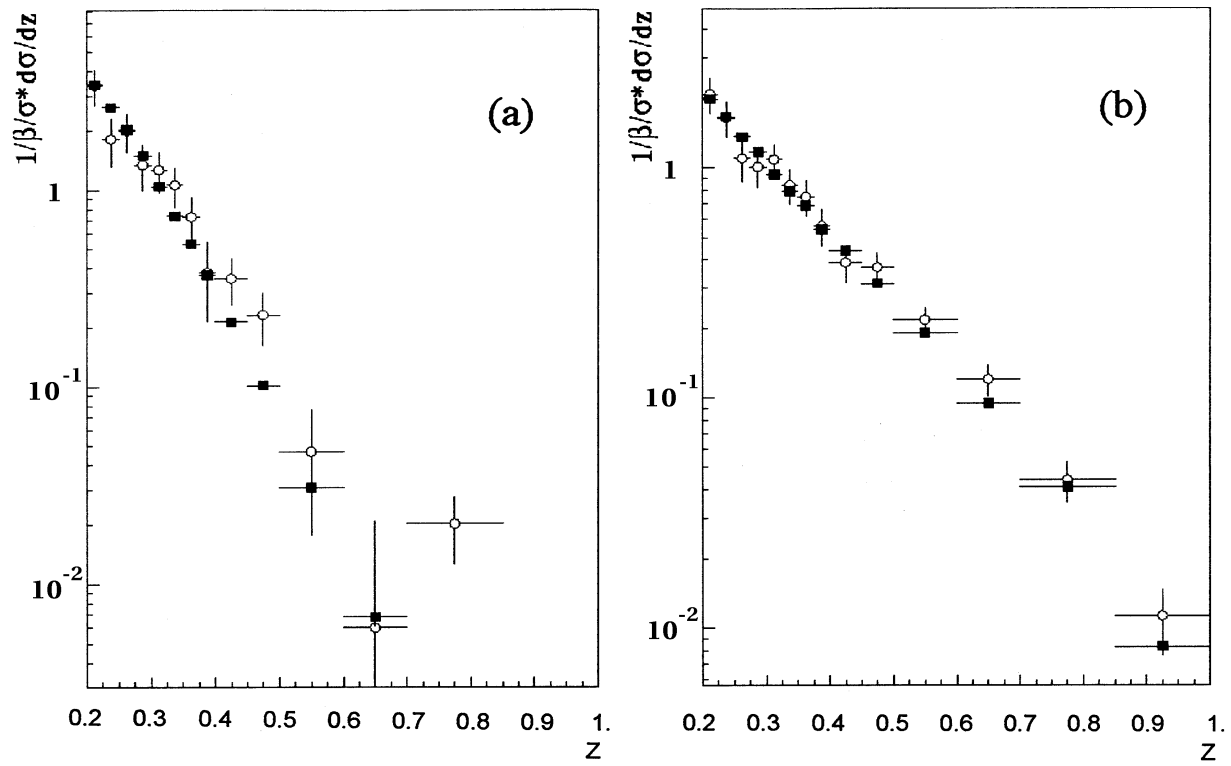

Figure 7.6: *(a) Measured $\rho^0(770)$–meson spectrum (○) in continuum events. (b) Measured $\rho^0(770)$–meson spectrum (○) in direct $\Upsilon(1S)$–decays [46] compared to model predictions [337, 353] .*

7.3.3 Baryon Production

Inclusive Spectra

The basic processes underlying fragmentation are more clearly revealed by the study of heavy particles which can be considered as direct products of the fragmentation chain [365]. Baryon production in this respect is of special interest, since the heavier hyperons are not expected to be to a large extent decay particles. Moreover, mesons are produced in a natural way in the fragmentation process, while for baryons – because of their more complicated valence quark structure – special mechanisms have to be introduced. A series of questions can be attacked by a detailed study of baryon production:

- are baryons formed by a coalesance of three independent quarks [366] or are diquarks popped out of the vacuum?
- can the observed baryon enhancement [367] in direct $\Upsilon(1S)$–decays in comparison to continuum data be explained as an effect of the parton topology or do gluons indeed fragment differently from quarks?
- does the observed enhancement depend on the particle mass as predicted by some models [365, 362] or is it connected with specific baryon production?
- do symmetry breaking effects as strangeness and higher spin suppression observed for mesons also exist for baryons?

The ARGUS collaboration has performed an extensive analysis of baryon production in the continuum and in direct $\Upsilon(1S)$–decays [344, 368, 369, 370, 371, 372]. Typical $\Lambda\pi^-$ mass spectra are shown in Figure 7.7a,b. In Figure 7.7a the Λ and π^- do not point to the interaction vertex, therefore, a

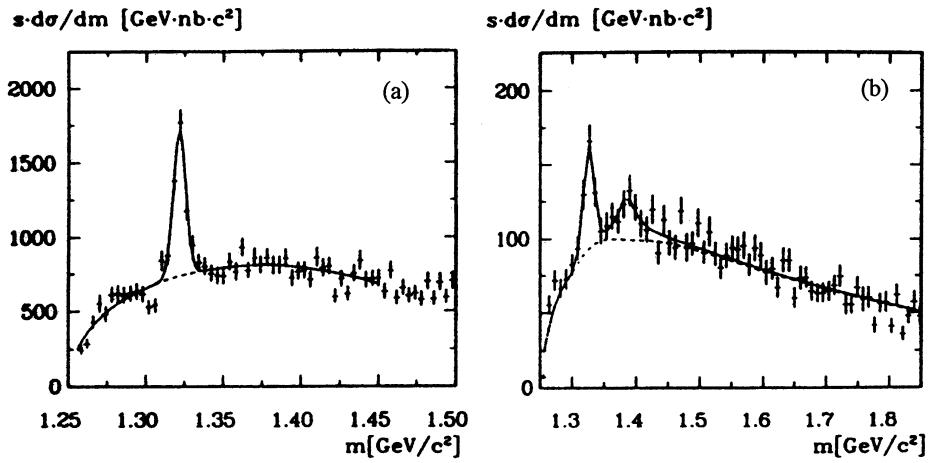

Figure 7.7: *(a) Mass distributions of* $\Lambda\ \pi^-$ *combinations with* $x_p > 0.15$ *for*$\Upsilon(1S)$ *data; (b) mass distributions of combinations with* $x_p > 0.15$ *of* Λ *candidates with a prompt* π^-*–track for* $\Upsilon(1S)$ *and* $\Upsilon(2S)$ *data [369].*

clear Ξ^-–signal is observed. On the other hand both the $\Sigma^-(1385)$– and the Ξ^-–hyperon show up [369], if the π^-–meson is forced to point to the interaction vertex (Figure 7.7a).

The observation of the $\Sigma^{\pm}(1385)$–hyperon proves the production of decuplet baryons in the fragmentation of quarks and gluons. Typical inclusive momentum spectra of baryons as measured in the continuum and in direct $\Upsilon(1S)$–decays are shown in Figures 7.8–7.9. They are compared with the predictions of the Lund string model [337, 353]. The data are in reasonable agreement with the predictions though at a closer look systematic differences show up for the high statistics Λ–spectra: the data from direct $\Upsilon(1S)$–decay have a harder momentum spectrum than the model predicts, on the other hand the measured continuum spectrum is softer than the model predictions. The continuum results indicate that baryons are only in rare cases leading particles in a jet. A further observation is worthwhile to note. The baryon spectrum observed for direct $\Upsilon(1S)$–decays is softer than the spectrum of baryons from continuum data.

The measured total rates are collected in Table 7.6, they are compared with the predictions of the Lund string model [337, 353]. At least one isospin partner of each state in the baryon octet and decuplet has been observed. Again data and predictions agree reasonably well, though for certain cases significant differences show up.

Baryon Enhancement in Direct $\Upsilon(1S)$–Decays

Comparing the data from direct $\Upsilon(1S)$–decays with those from continuum, one observes the well–known baryon enhancement in direct $\Upsilon(1S)$–decays. This is demonstrated in Figure 7.10, where the ratio

$$r = \frac{\#\ \text{hadrons/direct}\Upsilon(1S)-\text{decay}}{\#\ \text{hadrons/continuum event}} \tag{7.15}$$

is plotted as a function of the particle mass. Several points are worth mentioning.

The strong enhancement is only observed for baryons in contrast to predictions from cluster models [365], which explain the enhancement of baryons as a mass effect. In this context the high precision ϕ–data [359], which are included into Figure 7.10, are of special interest. Also the Lund model [337, 352] fails to reproduce the strength of the enhancement. It predicts values $r \leq 2$, while on the average one gets for ground state baryons a value of $r = 2.64 \pm 0.17$. The origin of

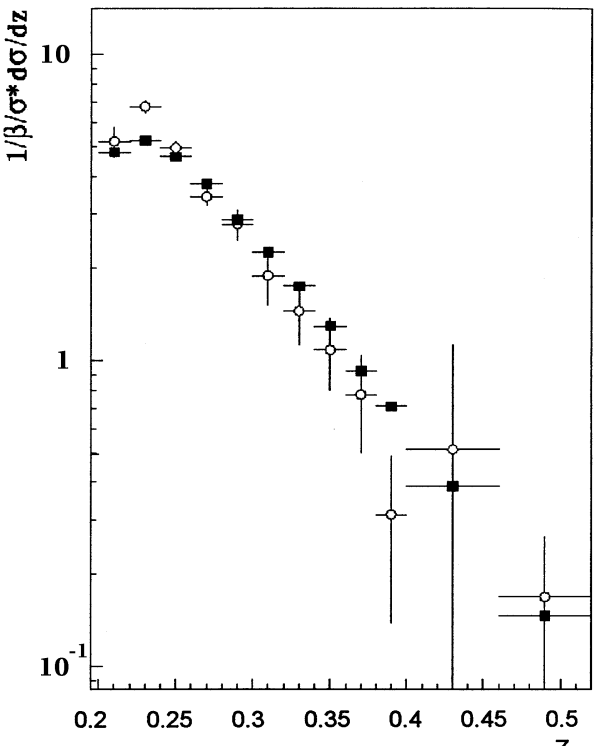

Figure 7.8: *Measured proton spectrum in direct $\Upsilon(1S)$–decays [344] (○) compared to model predictions [337, 353] .*

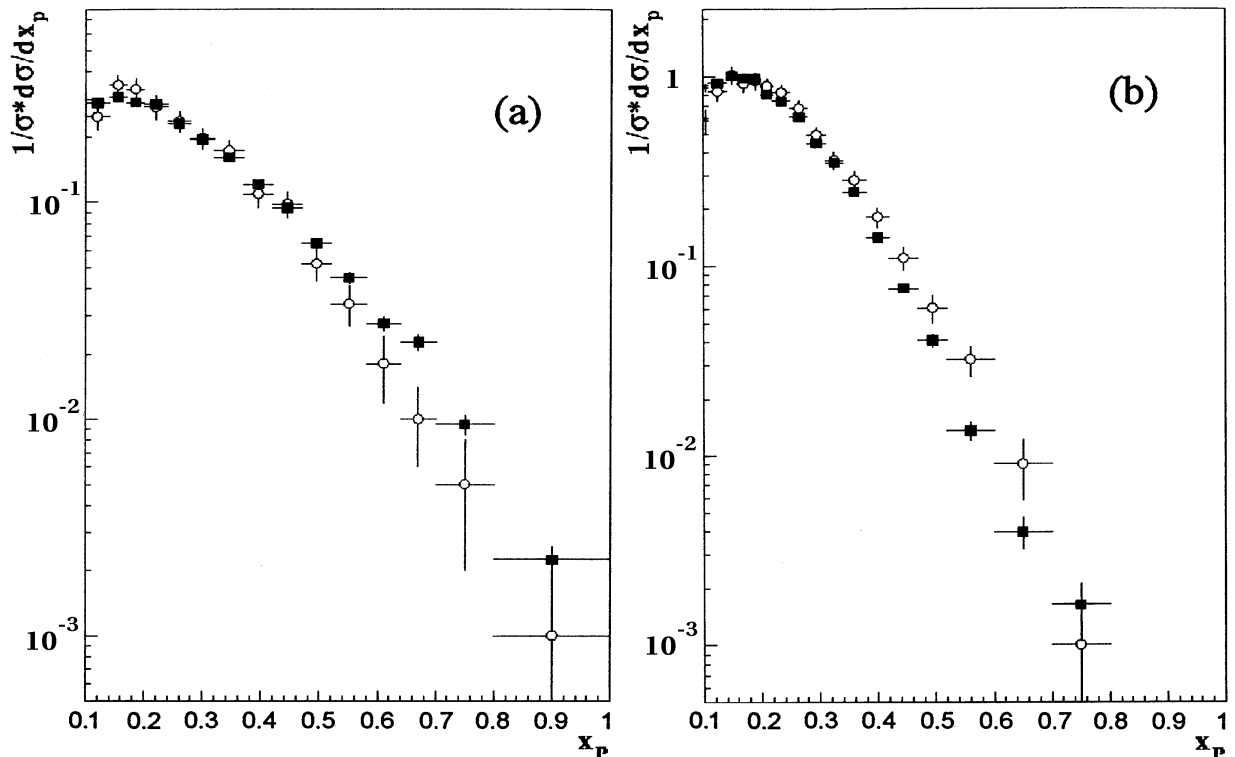

Figure 7.9: *(a) Measured Λ–spectrum (○) in continuum events. (b) Measured Λ–spectrum (○) in direct $\Upsilon(1S)$–decays [369] compared to model predictions [337, 353] .*

Table 7.6: *Rate of baryons produced in direct $\Upsilon(1S)$–decays and in continuum fragmentation [344, 369, 371, 370]. The data are compared with the predictions of the Lund model [337, 352] (JETSET7.4).*

	Data		**Monte Carlo**	
	$\Upsilon(1S)$	continuum	$\Upsilon(1S)$	continuum
$2\bar{p}$	$(5.08 \pm 0.03)10^{-1}$	$(2.72 \pm 0.16)10^{-1}$	$5.54 \cdot 10^{-1}$	$3.26 \cdot 10^{-1}$
2Λ	$(2.28 \pm 0.03 \pm 0.21)10^{-1}$	$(0.92 \pm 0.03 \pm 0.08)10^{-1}$	$1.66 \cdot 10^{-1}$	$1.04 \cdot 10^{-1}$
$2\Sigma^0$	$(5.64 \pm 1.69 \pm 1.13)10^{-2}$	$(2.29 \pm 0.69 \pm 0.49)10^{-2}$	$3.34 \cdot 10^{-2}$	$2.04 \cdot 10^{-2}$
$2\Xi^-$	$(2.06 \pm 0.17 \pm 0.23)10^{-2}$	$(0.67 \pm 0.06 \pm 0.07)10^{-2}$	$1.18 \cdot 10^{-2}$	$0.77 \cdot 10^{-2}$
$2\Delta^{++}$	$(1.24 \pm 0.16 \pm 0.15)10^{-1}$	$(0.40 \pm 0.08 \pm 0.06)10^{-1}$	$0.83 \cdot 10^{-1}$	$0.48 \cdot 10^{-1}$
$2\Sigma^+(1385)$	$(1.68 \pm 0.29 \pm 0.23)10^{-2}$	$(0.51 \pm 0.10 \pm 0.09)10^{-2}$	$1.62 \cdot 10^{-2}$	$0.89 \cdot 10^{-2}$
$2\Sigma^-(1385)$	$(1.42 \pm 0.17 \pm 0.20)10^{-2}$	$(0.55 \pm 0.11 \pm 0.10)10^{-2}$	$1.61 \cdot 10^{-2}$	$0.67 \cdot 10^{-2}$
$2\Xi^0(1530)$	$(4.78 \pm 1.14 \pm 0.62)10^{-3}$	$(1.46 \pm 0.51 \pm 0.23)10^{-3}$	$2.30 \cdot 10^{-3}$	$1.26 \cdot 10^{-3}$
$2\Omega^-$	$(1.83 \pm 0.62 \pm 0.32)10^{-3}$	$(0.72 \pm 0.36 \pm 0.13)10^{-3}$	$2.34 \cdot 10^{-4}$	$1.66 \cdot 10^{-4}$
$2\Lambda(1520)$	$(1.15 \pm 0.21 \pm 0.16)10^{-2}$	$(0.80 \pm 0.17 \pm {}^{0.10}_{0.13})10^{-2}$	-	-

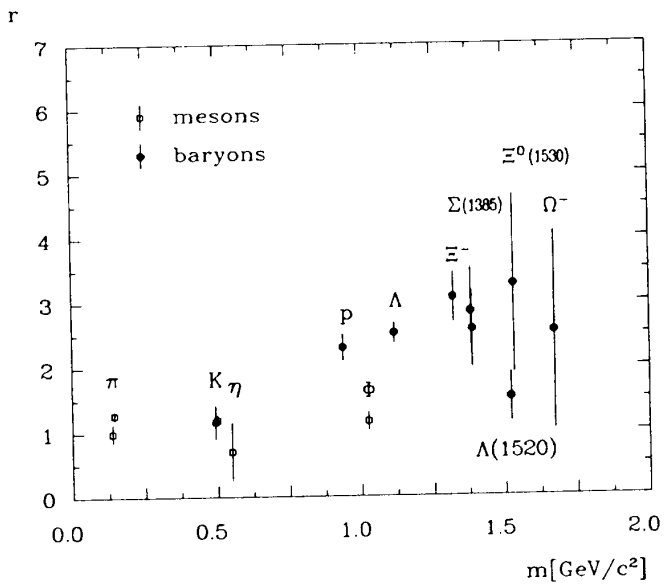

Figure 7.10: *Ratio r for hadrons*

baryon enhancement in the Lund string model is twofold [337]. Generally the particle multiplicity is higher, in addition the possibility to produce diquarks in the break–up of the closed 3–gluon string is enhanced with respect to continuum events. Since about 40 % of the continuum events are $c\bar{c}$–jets, baryon production in the continuum is in addition reduced by phase space [372]. Since no further way exists in this model to explain the discrepancy, the present data might indicate that quarks and gluons fragment differently. Another source of the observed differences, not considered up to now in the Lund string model [337], are contributions of octet strings to 3–gluon fragmentation, which might produce a different topology of the string configuration [337].

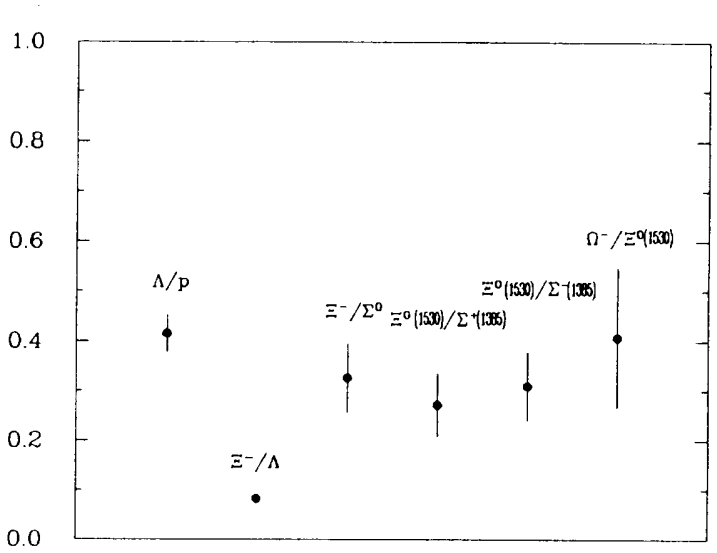

Figure 7.11: *Strangeness suppression in hyperon production*

Symmetry Breaking Effects in Baryon Production

The strangeness suppression in hyperon production is derived from the production ratio of hyperons differing by one unit in strangeness (Figure 7.11). The results from 3–gluon decay and continuum fragmentation have been averaged, since they are equal within errors. The strangeness suppression is about 0.3 independent of the baryon spin. The strength of strangeness suppression is comparable to the value derived from meson production in section 7.3.2. This is not expected generally in diquark models [373], which usually assume a suppression of diquarks carrying spin 1. The most natural explanation for this observation is that the three quarks forming a baryon are produced independently in the fragmentation process. This conclusion is corroborated by the study of baryon correlation discussed in section 7.3.3. The low Ξ^-/Λ ratio can be explained by the high feed–down rate of Λ particles from hyperon–decays. Taking the Σ^0 rate as an approximate measure of the direct Λ–rate, the strangeness suppression amounts to $\frac{n(\Xi^-)}{n(\Lambda)} = 0.33 \pm 0.07 \pm 0.06$. It is not fully reproduced by the Lund model [337, 352] predictions.

Another symmetry breaking effect in the fragmentation process follows from the comparison of octet and decuplet baryon production rates with the same flavor. The spin suppression for the ratios $\Sigma^{\pm}(1385)/\Sigma^0$ and $\Xi^-(1530)/\Xi^-$ is shown in Figure 7.12. Corrections for feed–down are applied. A strong spin–suppression of 0.2...0.3 in agreement with the prediction of the Lund string model is observed. It is by far larger than predicted by cluster models, which assume hadron production to be proportional to spin statistics [365]. Note that the suppression cannot be explained as for meson production by phase space effects, since the mass differences between octet and decuplet baryons are small. Hence, this observation reveals a dynamical feature of fragmentation.

The suppression of orbital angular momentum is expressed quantitatively by the ratio of $\Lambda(1520)$ and Σ^0 production, provided both hyperons are not produced by the decay of heavier resonance. This ratio is found to be $r_L = 0.35 \pm 0.13 \pm 0.09$. It can be compared to the ratio of tensor and vector meson production, which has been determined to be of the order of 0.1 (Table 7.5). Hence, the suppression of states with non–zero orbital momentum is similar for baryons and mesons. In this context it is of interest to note that the enhancement of $\Lambda(1520)$–baryons in direct $\Upsilon(1S)$–decays in comparison to continuum data seems to be substantially smaller than for the ground–state baryons (Figure 7.10).

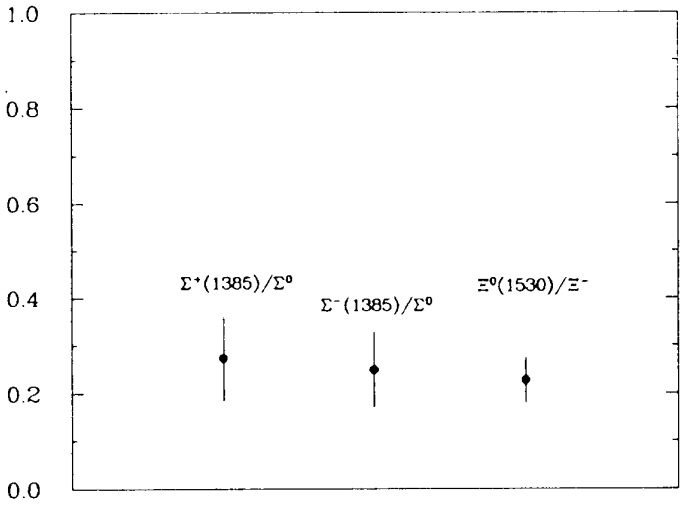

Figure 7.12: *Spin suppression in hyperon production*

Baryon Correlations

The measured baryon production rates and inclusive spectra discussed in section 7.3.3 do not discriminate between the different production models in a unique way, since the number of free parameters to be tuned is large. Correlation studies turn out to be very effective in this respect. ARGUS has measured baryon–antibaryon and baryon–baryon correlations [374, 375] and as a special case of the latter correlations the production of antideuterons in direct $\Upsilon(1S)$–decays [376, 377].

Three different correlations have been studied for the baryon–antibaryon data set [374]. Identifying the jet–axis of the event with the thrust axis one can study the azimuthal angular correlation of $p\bar{p}$–pairs in the plane transverse to the jet–axis. A weak anticorrelation is observed which is reproduced by the Lund model, if a popcorn parameter [337, 378] $\rho > 0.85(0.71)$ at 90% CL is chosen for continuum and $\Upsilon(1S)$–data respectively. Note, however, that the effect can also be reproduced by a pure diquark model [379], if one allows for global instead of local p_t compensation [380] in a jet.

Also flavor correlations allow to discriminate between different production schemes for baryons. The ratio

$$\lambda = 2\frac{n(\Lambda\bar{\Lambda})}{n(\Lambda) + n(\bar{\Lambda})} \tag{7.16}$$

reflects the probability in a multihadron event that a Λ–hyperon is accompanied by a $\bar{\Lambda}$, provided the number of events with two Λ–hyperons is small. ARGUS measured

$$\lambda = 0.306 \pm 0.044 \pm 0.021 \quad (0.328 \pm 0.025 \pm 0.023) \tag{7.17}$$

in continuum events and $\Upsilon(1S)_{dir}$ decays respectively. One expects $\lambda = 1$, if $\Lambda\bar{\Lambda}$ are produced as pairs and $\lambda = 0.2$, if they are produced uncorrelated. The Lund model predictions are compatible with the experimental results, if a popcorn parameter $\rho > 0.73$ (90% CL) is chosen.
The study of dibaryon pp– and $\Lambda\Lambda$–correlations [375] is sensitively dependent on the popcorn parameter ρ. In Tables 7.7,7.8 the measured rates are compared to the predictions of the Lund model with a popcorn parameter $\rho = 0$ (diquark model) and $\rho = 0.9$ (popcorn model). Clearly the continuum data are in good agreement with the popcorn model prediction, while the pure diquark model predicts a too high rate. Evidently, the baryon pair rate serves as a very sensitive tool to probe the

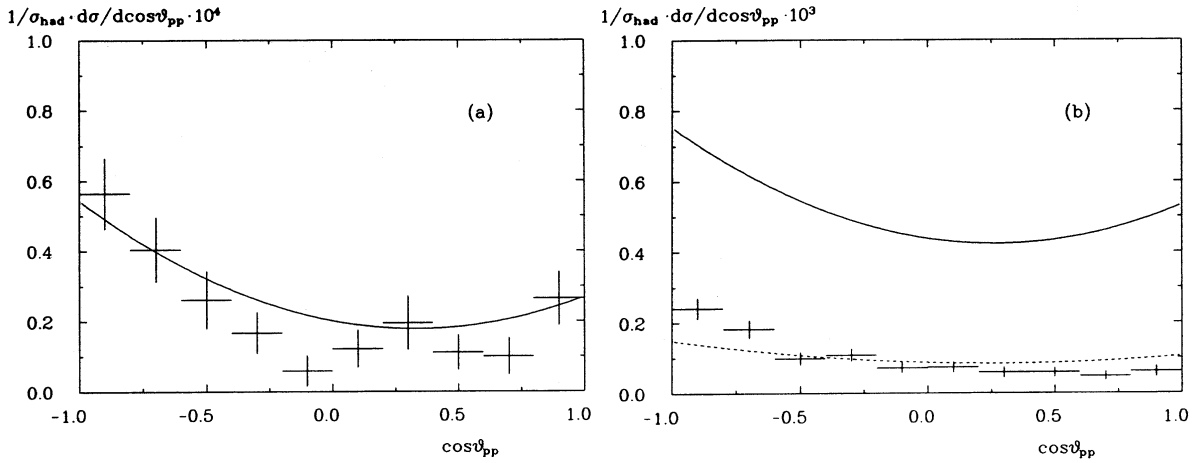

Figure 7.13: *Distribution of the opening angle between two protons (antiprotons) for (a) continuum data and direct (b) Υ–decays. The errors shown include both statistical and systematic uncertainties. The solid line represents the prediction of the Lund model with a popcorn fraction of 0.9. In (b) the dashed line corresponds to the Lund prediction, where the integral of the curve has been normalized to the experimental data.*

popcorn parameter. The baryon single and pair production rates for direct $\Upsilon(1S)$–decays are not reproduced by either of the models.

Table 7.7: Production rate of pp– and $\Lambda\Lambda$–pairs for continuum events. The proton rate is restricted to protons with 0.4 GeV $\leq p \leq$ 1.2 GeV.

	ARGUS	Popcorn	Diquark
$n(p)+n(\bar{p})$	$(9.65 \pm 0.08 \pm 0.24)\ 10^{-2}$	$10.6 \cdot 10^{-2}$	$13.1 \cdot 10^{-2}$
$n(pp)+n(\bar{p}\bar{p})$	$(4.5\ \pm 0.4\ \pm 0.2)\ 10^{-4}$	$5.6 \cdot 10^{-4}$	$18.6 \cdot 10^{-4}$
$n(\Lambda\Lambda)+n(\bar{\Lambda}\bar{\Lambda})$	$(5.1\ \pm 3.6\ \pm 0.8)\ 10^{-4}$	$1.8 \cdot 10^{-4}$	$12.2 \cdot 10^{-4}$

Table 7.8: *Production rate of pp– and $\Lambda\Lambda$–pairs for direct $\Upsilon(1S)$–decays. The proton rate is restricted to protons with 0.4 GeV $\leq p \leq$ 1.2 GeV.*

	ARGUS	Popcorn	Diquark
$n(p)+n(\bar{p})$	$(22.4 \pm 0.2 \pm 0.6)\ 10^{-2}$	$33.1 \cdot 10^{-2}$	$33.3 \cdot 10^{-2}$
$n(pp)+n(\bar{p}\bar{p})$	$(2.00 \pm 0.07 \pm 0.10)\ 10^{-3}$	$10.3 \cdot 10^{-3}$	$16.6 \cdot 10^{-3}$
$n(\Lambda\Lambda)+n(\bar{\Lambda}\bar{\Lambda})$	$(1.81 \pm 0.41 \pm 0.27)\ 10^{-3}$	$1.7 \cdot 10^{-3}$	$5.3 \cdot 10^{-3}$

A further test is provided by the measurement of the opening angle distribution

$$cos\ \theta_{pp} = \frac{\vec{p}_1 \cdot \vec{p}_2}{|\vec{p}_1 \cdot \vec{p}_2|} \tag{7.18}$$

shown in Figure 7.13. For the continuum the popcorn model and the data are in good agreement.

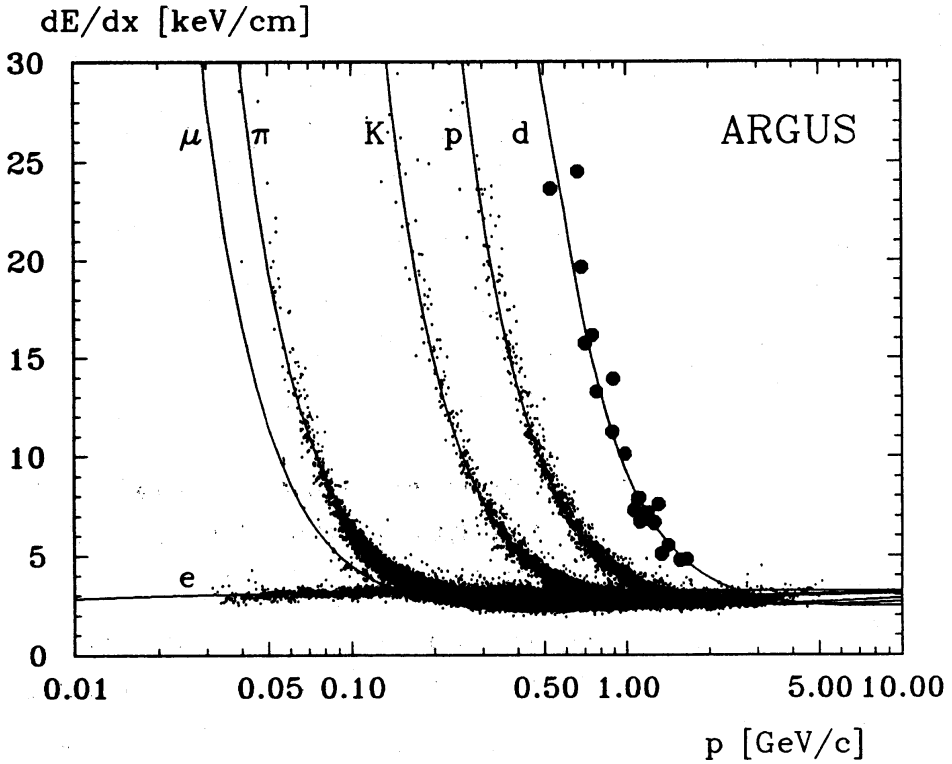

Figure 7.14: *Distribution of the energy loss dE/dx versus momentum p for the 21 antideuteron candidates (big dots), together with the expected curves for e, μ, π, K, p and d (solid lines). The mean dE/dx values of other particles, as measured in a multihadronic event sample, are also included [377]*

The angular distribution of pp–pairs produced in direct $\Upsilon(1S)$–decays is neither reproduced in its absolute rate nor in its shape. It appears that the string dynamics in the three gluon system is not accurately simulated by the models.

The excellent particle identification abilities of the ARGUS detector allowed to observe antideuteron production in e^+e^- annihilation [376, 377]. Figure 7.14 shows the distribution of the energy loss in the drift chamber versus the particle momentum [377]. The bands corresponding to e, μ, π, K, p and $\overline{d}$ are clearly visible. The measurements of time-of-flight and the energy distribution in the shower counters confirm the antideuteron assignment.

The study of antideuteron production allows to test the production of baryon pairs with small relative momentum [376, 377]. $n_{\bar{d}} = (6.0 \pm 2.0 \pm 0.6) \cdot 10^{-5}$ antideuterons/event are observed in direct $\Upsilon(1S)$–decays, while $n_{\bar{d}} < 1.7 \cdot 10^{-5}$/event at 90% CL are detected in the continuum. With respect to the baryon pair production this corresponds to a suppression by a factor of 30. A similar suppression factor is observed with respect to the rate of $\bar{\Lambda}$–production. This result indicates that the direct production of antideuteron is rather unlikely.

However, the antideuteron production can be related to the antiproton production in direct $\Upsilon(1S)$–decays. A coalesance model with one free parameter characterizing the deuteron wave function in momentum space reproduces the measured rate and the shape of the observed momentum spectrum [377].

In summary the baryon correlations favor the popcorn model and exclude the production of point-like diquark–systems in the fragmentation chain. Moreover, the present description of the string dynamics in the three gluon decay seems to be not realistic enough to reproduce data.

7.3.4 Color Coherence Effects

Parton cascades are the basis of jets produced in quark and gluon fragmentation [335, 336]. The development of these cascades is strongly influenced by color coherence effects [385]. Note that the latter are basic for any gauge theory, hence their observation is of great interest. The coherence effects enforce an angular ordering $\theta_1 > \theta_2 > \theta_3$ ... of sequential parton decays, since large angle gluons are unable to resolve separate color sources in a cascade and hence their production is suppressed, when the shower develops. On the other hand, the parton model can only be applied, if the transverse momentum is greater than the inverse hadronization scale $R : k_T > R^{-1}$. Decreasing emission angles due to color coherence, therefore, enforce the increase of the momenta of the produced partons. Combining this prediction with the conjecture of "local–parton–hadron–duality" (LPHD), which postulates the proportionality between the cross–section on the parton and hadron level [381, 382], one expects a relative suppression of low momentum particles.
The observable $\xi = ln\ 1/x_p$, derived from the scaled particle momentum $x_p = \frac{2\ p}{\sqrt{s}}$, is sensitive to this prediction. If coherence effects exist, they lead to a suppression of particle production at small (large) values of $x_p (\xi = ln\ \frac{1}{x_p})$. Since in addition $\frac{d\sigma}{d\xi}$ decreases at small values of ξ due to energy–momentum conservation, $\frac{d\sigma}{d\xi}$ is expected to peak at a value $\xi_{max} > 0$. An analytical expression for the parton spectrum in "modified leading–log approximation" (MLLA) [383] has been derived [384]

$$\frac{1}{\sigma}\ \frac{d\sigma}{d\xi} = C_{LPHD} \cdot f_{MLLA}\left(\xi, \frac{\sqrt{s}}{Q_0}\right) \tag{7.19}$$

which describes also hadron spectra if LPHD is assumed to hold [385]. f_{MLLA} depends only on the momentum variable ξ and the ratio $\sqrt{s}/Q_0$, it is calculable on parton level. Q_0 is an effective QCD scale and is conjectured to grow with the hadron mass m [381, 382]. C_{LPHD} is a phenomenological parameter and has to be derived from the data. According to [385, 386] f_{MLLA} can be approximated by a Gaussian. The peak position of (19) is independent of C_{LHPD} and is predicted [385, 386] by perturbative QCD:

$$\xi_{max} = \frac{1}{2}\ ln\frac{\sqrt{s}}{Q_0} + \frac{k}{2}\ \sqrt{ln\frac{\sqrt{s}}{Q_0}} + O(1) \tag{7.20}$$

$$k = \frac{1}{18}\ \frac{297 + 2\ n_f}{\sqrt{297 - 18 n_f}} = \frac{101}{162}\ \sqrt{3}\ . \tag{7.21}$$

Following the observation that only light flavors are produced in quark and gluon jet fragmentation (see section 7.4), $n_f = 3$ has been chosen in (21).

Two experimentally verifiable predictions follow from Equation (7.20).The position of the peak ξ_{max} increases logarithmically with the center–of–mass–energy $\sqrt{s}$. In addition, due to the conjectured increase of Q_0 with the hadronic mass m, the peak position ξ_{max} should decrease logarithmically with m.
These predictions of color coherence effects can be confronted with ARGUS data discussed in section 7.3.2 and 7.3.3. A typical spectrum $\frac{d\sigma}{d\xi}$ is shown in Figure 7.15 (a) for charged π–mesons produced in the continuum. A Gaussian is a good approximation of the data. The peak position has been determined by fitting a Gaussian to the data, the results are collected in Table 7.9. As demonstrated by Figure 7.15 (b) the expected logarithmically dependence of ξ_{max} on the center–of–mass–energy is reproduced for charged particles. The mass dependence for continuum data shown in Figure 7.16 (a) is as conjectured logarithmic. Baryons and mesons are lying on different curves. Similar observations have been made previously at LEP energies [334].

Comparing data from continuum and direct $\Upsilon(1S)$–decay reveals further interesting aspects. According to Figure 7.17 the relation $\mid \frac{d\xi_{max}}{dm}(\Upsilon) \mid < \mid \frac{d\xi_{max}}{dm}(cont) \mid$ holds. This observation is in agreement with a prediction of a next to leading order MLLA-calculation [386]. Moreover, the meson

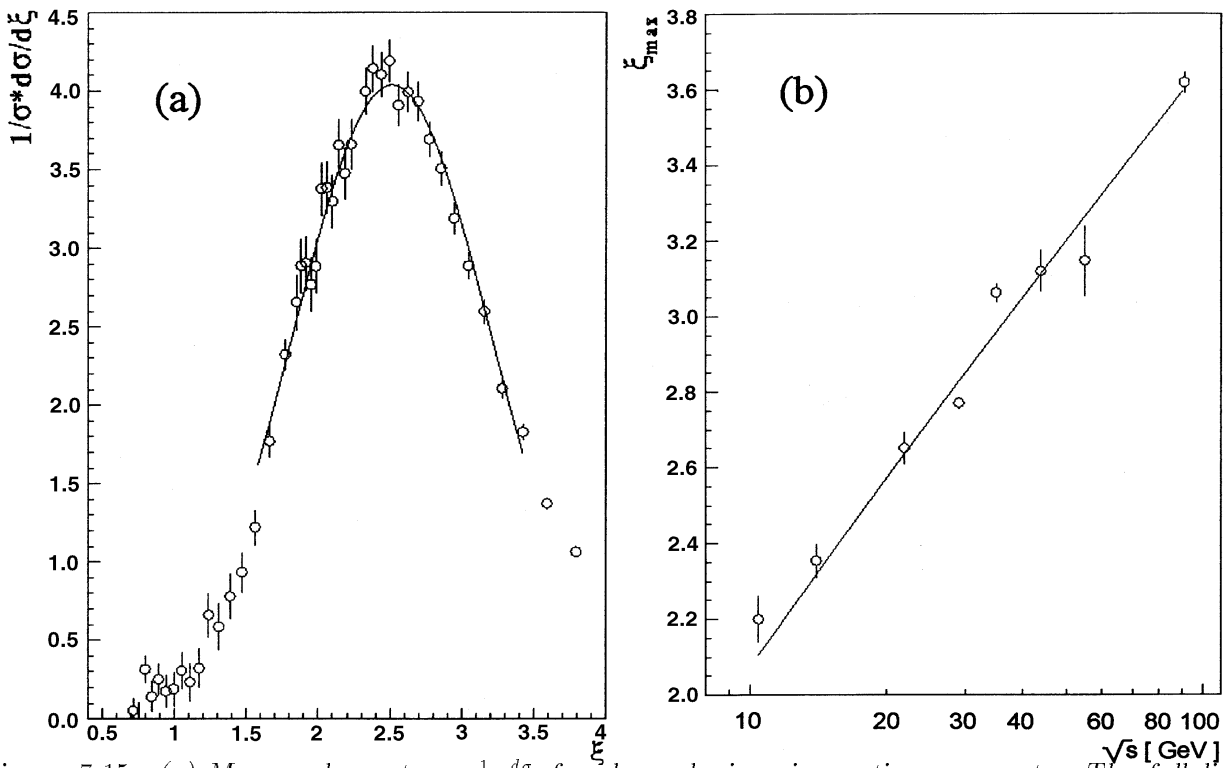

Figure 7.15: *(a) Measured spectrum* $\frac{1}{\sigma}\frac{d\sigma}{d\xi}$ *for charged pions in continuum events. The full line represents a Gaussian fit to the data. (b)* ξ_{max} *as a function of* $\sqrt{s}$*. The data points for* $\sqrt{s} > 10$ *GeV are taken from ref. [334].*

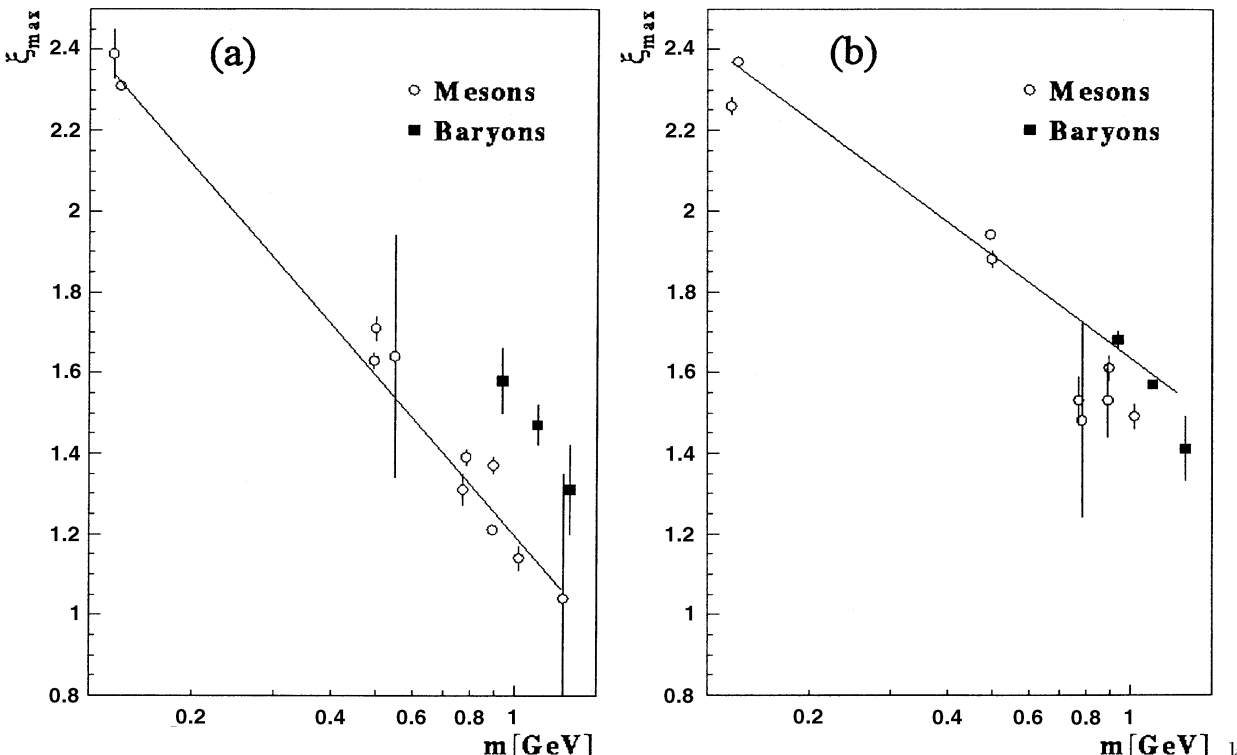

Figure 7.16: *(a)* ξ_{max} *for continuum events at* $\sqrt{s} = 10.45$ *GeV as a function of the particle mass. (b)* ξ_{max} *for direct* $\Upsilon(1S)$*–decays as a function of the particle mass. The full lines represents a fit of an exponential to the meson data*

Table 7.9: *Values of ξ_{max} derived by a fit of a Gaussian to the $\frac{d\sigma}{d\xi}$ spectra measured by the ARGUS collaboration for continuum data and direct $\Upsilon(1S)$–decays.*

Particle	$\xi_{max}(cont)$	$\xi_{max}(\Upsilon(1S))$
π^0	2.39 ± 0.06	2.26 ± 0.02
$\pi^\pm$	2.31 ± 0.02	2.37 ± 0.02
K^0	1.71 ± 0.03	1.88 ± 0.02
$K^\pm$	1.63 ± 0.02	1.94 ± 0.01
η	1.64 ± 0.30	–
ρ^0	1.31 ± 0.04	1.53 ± 0.06
ω	1.39 ± 0.02	1.48 ± 0.24
K^{*0}	1.37 ± 0.02	1.61 ± 0.03
K^{*+}	1.21 ± 0.02	1.53 ± 0.09
ϕ	1.14 ± 0.03	$1,49 \pm 0.03$
$\bar{p}$	1.58 ± 0.08	1.68 ± 0.02
Λ	1.47 ± 0.05	1.57 ± 0.02
Ξ	1.31 ± 0.11	1.41 ± 0.08

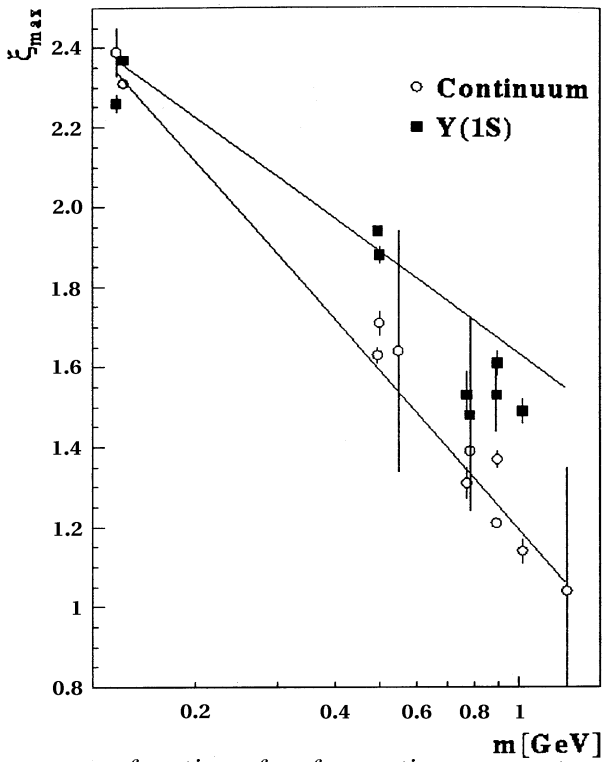

Figure 7.17: *ξ_{max} for mesons as a function of m for continuum events and direct $\Upsilon(1S)$–decays.*

and baryon data for direct $\Upsilon(1S) \to ggg$ decays (Figure 7.16 (b)) differ less than for the continuum results plotted in Figure 7.16 (a).

7.4 Charmed Quark Fragmentation

Charm quark production in the fragmentation process is expected to be suppressed due to their large mass. Thus the observed charmed mesons and baryons as leading particles in a $c\bar{c}$–jet contain the primary charm quark produced in $e^+ e^-$ annihilation itself and hence are an important source of information on fragmentation functions.
The shape of the expected fragmentation function has been predicted by Peterson et al. [99] using kinematical ideas of Suzuki [387] and Bjorken [388]. The amplitude for the transition $Q \rightarrow H + q$ of the heavy quark Q is assumed to be proportional to ΔE^{-1}, the inverse of the energy transfer in the hadronization of Q. Hence the spectrum of hadrons H containing the heavy quark is given by

$$D_Q^H(x_p) \sim \frac{1}{x_p}\left(1 - \frac{1}{x_p} - \frac{\varepsilon}{1-x_p}\right)^{-2} \quad . \tag{7.22}$$

The parameter ε is interpreted in the framework of this model, for mesons as the square of the spectator quark mass to the heavy quark mass

$$\varepsilon = \left(\frac{m_q}{m_Q}\right)^2 \tag{7.23}$$

Note, however, that charmed mesons produced in the decay of heavier states have a softer spectrum.

Since for electromagnetic interactions at high energies helicity is conserved, the spins of the produced charmed quarks are strongly correlated. Hence a measurement of the charmed hadron polarization allows to determine to which extent the fragmentation process dilutes the spin alignment of the primary heavy quarks. Such investigations provide unique information on the hadronization process.

7.4.1 Charmed Meson Production

The ARGUS collaboration has performed an extensive study of charmed meson production [47]. The states observed in these studies are collected in Table 7.10 to the extent that they are of interest for fragmentation studies. Note that a few of these states were observed for the first time by this experiment.

Table 7.10: *Charmed meson states studied by the ARGUS collaboration to determine the Peterson parameter ε by a fit of Equation (7.22) to the momentum spectrum.*

State	ε	Reference
D^0	0.25 ± 0.03	[47]
D^+	0.19 ± 0.04	[47]
$D^{*+}(2010)$	0.19 ± 0.03	[390, 47]
D_s^+	$0.50 \pm {}^{0.22}_{0.14}$	[390]
D_s^{*+}	0.07 ± 0.04	[111]
$D_1^0(2420)$	0.07 ± 0.04	[119]
$D_2^{*0,+}(2460)$	0.06 ± 0.03	[115, 119]
$D_{s\,1}^+(2536)$	$0.06 \pm {}^{0.02}_{0.01} \pm 0.02$	[119, 130]

An example of a measured particle spectrum is shown in Figure 7.18 (a). They are compared to the predictions of the most recent version of the Lund model (JETSET 7.4). Model predictions and data are in reasonable agreement.

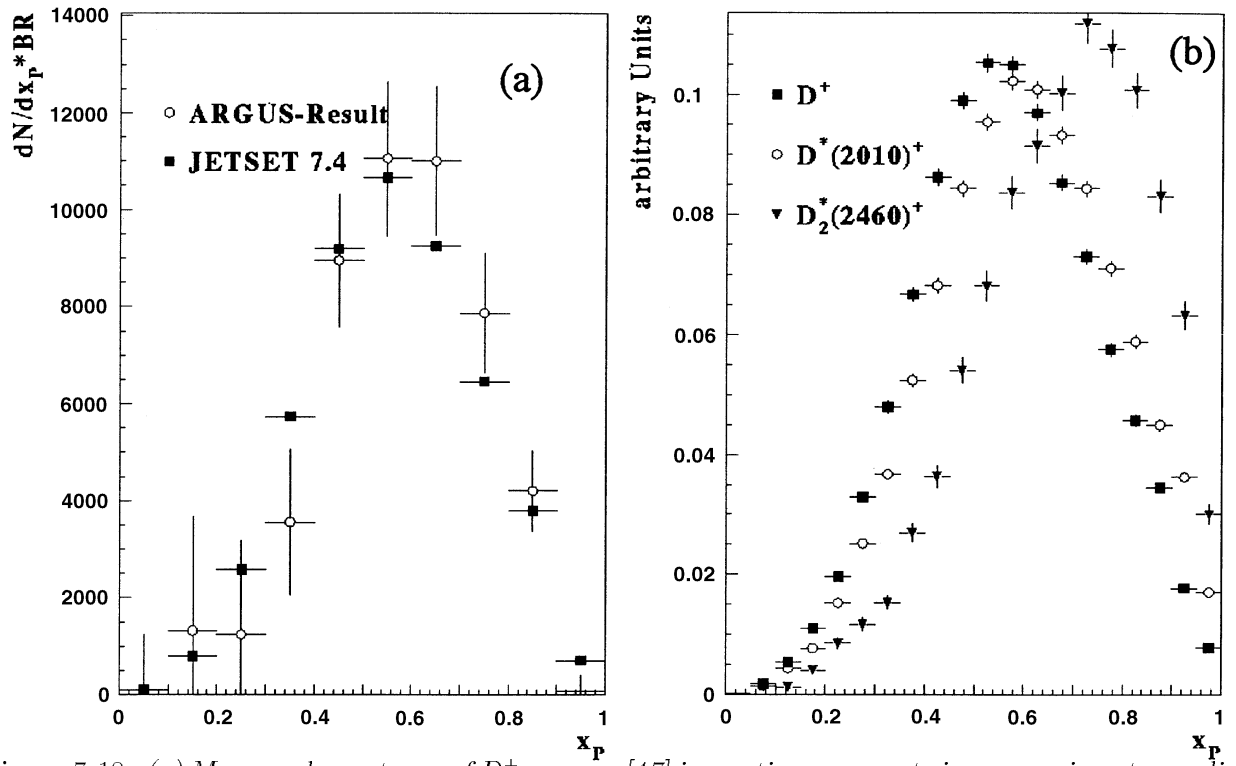

Figure 7.18: *(a) Measured spectrum of D^+–meson [47] in continuum events in comparison to predictions of the Lund model [337, 353]. (b) Comparison of the predicted inclusive spectrum for different charmed mesons [353].*

Note, however, that the spectra have not been corrected for initial state photon radiation, gluon radiation in the beginning of the fragmentation process and most importantly not for decays of excited states. All these processes tend to soften the particle spectra and hence dilute the primary fragmentation function. While the first processes have been extensively studied [392], the latter effect is demonstrated in Figure 7.18 (b). It shows that even the $D^{*+}(2010)$–distribution is not a particularly good measure of the fundamental fragmentation function. The fitted values of the Peterson parameter ε of Equation (7.22) collected in Table 7.10 support this conclusion. They clearly demonstrate the softening of the fragmentation function for low mass charmed mesons.

In two cases the ARGUS collaboration was able to estimate the contribution of excited states to the production rate of the ground state mesons. $(24 \pm {}^{8}_{6} \pm 8)\%$ of the observed $D^{*+}(2010)$–mesons are decay products of the $D_1^0(2420)$–meson [116], while $(11 \pm 4 \pm 5)\%$ of the observed D^+–mesons result from the decay of the $D_2^{*0}(2460)$–meson [115].

Another important information of the fragmentation process follows from the comparison of the production rate of the $D_2^{*0}(2460)$– and the $D_1^0(2420)$–meson. Both decay into the same final state $D^{*+}(2010)\ \pi^-$ [117]. Supposing isospin invariance to hold and assuming that decays to $D\pi$ and $D^*(2010)\pi$ saturate the total width one derives

$$r = \frac{\sigma(D_2^{*0}(2460))}{\sigma(D_1^0(2420))} = 2.3 \pm 0.6 \pm 1.0 \tag{7.24}$$

in agreement with the naive expectation 5/3 of spin statistics.

Spin Alignment and Spin Correlations

No precise knowledge is presently available for the influence of spin on the fragmentation distributions. Hence an independent measurement which is sensitive to the spin distribution is extremely helpful. This is especially the case, if the spin distribution of one of the quarks forming the observed hadron is known. D^*–production fulfills these requirements, since the spin of the primary c–quark is known from helicity conservation and the D^*–meson has been shown to be the leading particle in a c–quark jet (section 7.4.1). Two sets of measurement are possible. For the single D^*–meson the alignment can be determined. Additional information follows from the study of helicity correlations between two D^*–mesons detected in one event.

The expected spin alignment can easily be derived by statistical arguments. If we assume that the spin of the heavy quark is not flipped by the hadronization process, the different $D^*(D)$ helicity states should be populated according to the numbers given in Table 7.11. $\sigma = 2$ corresponds to spin statistics.

Table 7.11: *Probabilities to observe different helicity states of $D^*(D)$–mesons according to a statistical model. $\sigma = 2$ corresponds to the undiluted statistical distribution.*

λ_c	λ_q	$\lambda(D^*) = 1$	$\lambda(D^+) = -1$	$\lambda(D^*) = 0$	$\lambda(D) = 0$
1	1	1	-	-	
1	-1	-	-	$1/\sigma$	$1 - 1/\sigma$
-1	1	-	-	$1/\sigma$	$1 - 1/\sigma$
-1	-1	-	1	-	

The population of different helicity states implies for the ratio of directly produced $D^*(D)$–mesons

$$\frac{N(D^*)}{N(D)} = \frac{V}{P} = \frac{\sigma + 1}{\sigma - 1} \ . \tag{7.25}$$

For the alignment of D^*–mesons one gets

$$\frac{N(\lambda = +1) + N(\lambda = -1)}{N(\lambda = 0)} = \sigma \ . \tag{7.26}$$

A dynamical model for this process has been proposed by Suzuki [393], who treats the heavy meson production perturbatively. The ratio $\frac{V}{V+P}$ is predicted to depend on $z = \frac{P+E}{\sqrt{s}}$. Averaged over the momentum spectrum Suzuki gets $\langle \frac{V}{V+P} \rangle = 0.74$.
If θ, φ are the polar and azimuthal angle of the π^+–meson from the decay $D^{*+} \to D^0 \ \pi^+$ measured in the D^{*+}–rest–frame with respect to the D^{*+}–direction, the angular distribution can be expressed with the help of the D^* spin density matrix elements R_{ij}:

$$\frac{dN}{d\ cos\theta} \sim R_{++}|Y_{11}(\theta,\varphi)|^2 + R_{00}|Y_{10}(\theta,\varphi)|^2 + R_{--}|Y_{1-1}(\theta,\varphi)|^2 \tag{7.27}$$

$$\sim 1 + \left(\frac{2R_{00}}{R_{++} + R_{--}} - 1 \right) cos^2\theta = 1 + \alpha \ cos^2\theta \ . \tag{7.28}$$

The following conclusions follow from this formula

- the alignment can be zero though the D^{*+} is polarized ($R_{++} \neq R_{--}$),
- the statistical model predicts $\alpha = \frac{2-\sigma}{\sigma}$, i.e. for spin statistics ($\sigma = 2$)$\alpha = 0$,

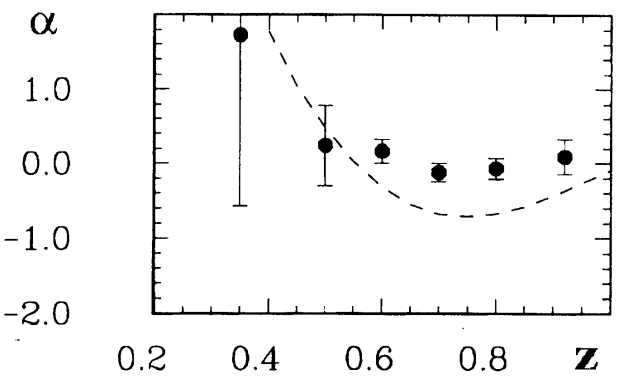

Figure 7.19: *Measured values of α (z) compared to the prediction of the Suzuki model given as a broken line*

- according to Suzuki [393] $\alpha = \alpha(z)$ (Figure 7.19).

The analysis is based on 10^4 $D^{*+} \rightarrow D^0\ \pi^+$ decays ($D^0 \rightarrow K^-\ \pi^+$, $K^-\ \pi^+\ \pi^+\ \pi^-$, $K_s^0\ \pi^+\ \pi^-$). The mass spectra were fitted for different $cos\theta$ intervals and corrected for acceptance effects. A fit of the angular distribution (Equation (7.27)) provided $\alpha = \alpha(z)$, which is plotted in Figure 7.19 and compared with the model of Suzuki [393]. Using the measured $\sigma \cdot B$ of ARGUS [115, 116, 117, 130] and CLEO [394], the influence of $D^*\ -p$ wave decays was studied. At the present level of precision the helicity angular distributions are not disturbed [395].
The results of the ARGUS experiment together with those of previous experiments are collected in Table 7.12. Good agreement between the different experiments is observed. The experimental results exclude the dynamical model of Suzuki [393] (Figure 7.19). The measurement is compatible with predictions of the statistical model. The ratio of vector to pseudoscalar meson production can be derived:

$$\frac{V}{V\ +\ P} = \frac{3+\alpha}{4}\ . \tag{7.29}$$

The results are included in Table 7.12.

Table 7.12: *Measured angular coefficient α.*

	α	$\frac{V}{V\ +\ P}$
ARGUS	$0.01 \pm 0.06 \pm 0.03$	$0.753 \pm 0.015 \pm 0.01$
CLEO [396]	$0.13 \pm 0.07 \pm 0.03$	$0.77 \pm 0.02 \pm 0.01$
HRS [397]	0.14 ± 0.23	0.79 ± 0.06
TPC [398]	$-0.14 \pm 0.17 \pm 0.03$	$0.72 \pm 0.04 \pm 0.01$

It is well known that the spins of the c– and $\bar{c}$–quark produced in $e^+\ e^-$–annihilation are strongly correlated, if the QED amplitude dominates and the cms–energy is high enough. Of course also in this case the correlation strength observed depends on details of the hadronization process. Since at $\sqrt{s} = 10.4$ GeV B–meson contributions can be excluded by a straight forward momentum cut, it is the ideal place for the study of $D^{*+}\ D^{*-}$–helicity correlations. The decay serves as polarization analyzer. Dalitz et al. [399] have studied for the first time this correlation, Mankel [400] has extended their analysis taking into account the finite charm mass, which a priori may be important,

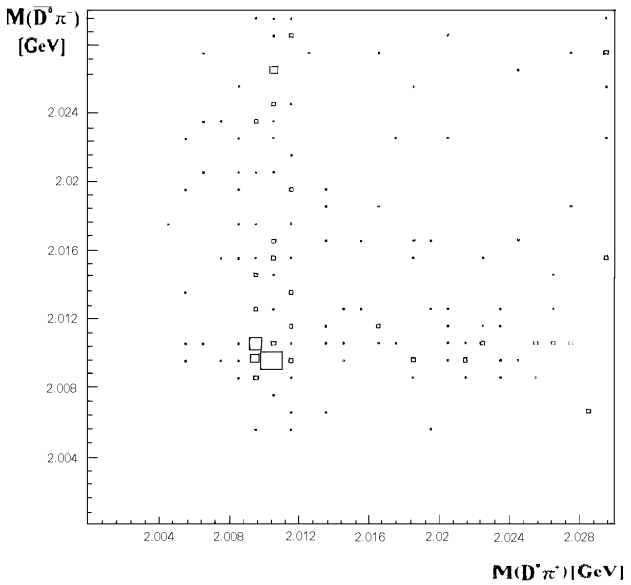

Figure 7.20: *Scatter–plot of $D^{o}\pi^{+}$ $D^{o}\pi^{-}$ invariant masses*

since m_c/E_c at the energies available in this analysis is large. The angular distribution is given by [399, 400],

$$\frac{d\ N}{d\Omega_{+}d\Omega_{-}} \sim \left\{\frac{\sigma}{2} + (1-\frac{\sigma}{2})cos^2\theta\right\}\left\{\frac{\sigma}{2} + (1-\frac{\sigma}{2})cos^2\bar{\theta}\right\} + \frac{\sigma}{2}\ \frac{sin^2\theta_p}{1+cos^2\theta_p}\ sin\ 2\bar{\theta}\ cos(\varphi\ +\bar{\varphi})\ . \quad (7.30)$$

θ_p is the jet angle with respect to the beam axis. Mankel has shown that finite mass effects introduce corrections of the order $0(\frac{m_c^2}{E_c^2})$ and hence can be neglected. The hadronization process is described by the statistical model of Table 7.11.

The observed scatter plot of D^{*}–candidate masses is shown in Figure 7.20, a clear peak is observed in the D^{*}–mass region. Subtracting the background of 12 events ARGUS gets a signal of 19 events. A maximum likelihood fit in the 5 angles of Equation (7.30) is applied with $\alpha_p = \frac{\sigma\ -1}{2\ \sigma}$ as fit parameter. The quantisation axis is approximated by

$$\vec{p}_c = \vec{p}_{D^{*}-}\ -\ \vec{p}_{D^{*}+}\ . \quad (7.31)$$

One finds $\alpha_p = 0.25 \pm 0.12$ corresponding to $\sigma = 2\ ^{+\ 1.8}_{-\ 0.65}$ in good agreement with the conclusion drawn from the alignment study $\alpha_p = 0.252 \pm 0.018 \pm 0.01$. In accordance with the expectations from spin statistics one gets

$$\frac{V}{V\ +\ P} = 0.753 \pm 0.015 \pm 0.01\ . \quad (7.32)$$

Comparing these values with the results of section 7.3.2 (Table 7.3) for light quarks not unexpectedly the latter show an attenuation of vector meson production due to heavy particle decay. The observed polarization correlation is of great interest for further LEP studies of quark polarization, since they demonstrate that hadronization does not dilute the primordial polarization of heavy quarks.

7.4.2 Charmed Baryon Production

$e^{+}\ e^{-}$–annihilation is a clean source of charmed baryons. The large data sample collected by the ARGUS collaboration was searched for new baryon states with charm and for studies of weak decays.

In addition, information on the hadronization process was extracted from the data. The observed states, their decay channels, mass and fragmentation parameters are collected in Table 7.13.

Table 7.13: *Charmed baryon states observed by the ARGUS collaboration. ε is the parameter of the Peterson fragmentation function (Equation (7.22)).*

	Decay channels	ϵ	Quark	Multiplet	Reference
Λ_c^+	$p\ K^-\pi^+$, $\Lambda\pi^+\pi^-\pi^+, \bar{K}^0_P$	$0.24^{+\ 0.07}_{-\ 0.05}$	$c\ d\ u$	$\bar{3}$	[127]
Σ_c^{++} Σ_c^0	$\Lambda_c^+\ \pi^+$ $\Lambda_c^+\ \pi^-$	0.29 ± 0.06	$c\ u\ u$ $c\ d\ d$	6	[129]
Ξ_c^+ Ξ_c^0	$\Xi^-\pi^+\pi^+$ $\Xi^-\pi^+, \Xi^-\pi^-\pi^+\pi^+$	0.24 ± 0.08	$c\ s\ u$ $c\ s\ d$	$\bar{3}$	[128]
Ω_c^0	$\Xi^-\ K^-\ \pi^+\ \pi^+$	-	$c\ s\ s$	6	[130]
Λ_c^{*+} or Σ_c^{*+}	$\Lambda_c^+\ \pi^+\ \pi^-$	0.044 ± 0.018	$c\ d\ u$	-	[14]

As expected the charmed baryons have a hard momentum spectrum proving that also charmed baryons are leading particles in a c–quark jet. The comparison of Tables 7.10,7.13 demonstrates that the Peterson parameter ε for the ground state $\overline{3}(6)$ baryons is appreciably larger than for observed excited charmed meson states. Since the QED and QCD radiative corrections should be similar for charmed meson and baryon production this observation indicates that to a large extent the observed ground state charmed baryons are decay products.

The relative fraction of c–quarks hadronizing into charmed baryons is estimated from the measured [129] fractional Λ_c^+ production $R_{c\bar{c}}\ Br(\Lambda_c^+ \to K^-p\ \pi^+) = (10.8 \pm 1.4 \pm 1.2) \cdot 10^{-3}$. $R_{c\bar{c}}$ is defined according to Equation (7.6) for charmed hadrons. Combining the published branching ratio for the $\Lambda_c^+ \to K^-p\ \pi^+$ decay [17] with the parton model prediction for $\Lambda_c^+ \to K^-p\ \pi^+$ one estimates the fraction of charmed quarks hadronizing into a charmed baryon to be $\sim 20\%$.

7.4.3 Charm Production in Gluon Jets

As shown in the previous section charmed quark production is strongly suppressed in the fragmentation process. This is not unexpected, since the large charm quark mass and the limited energy density of the strong force field inhibit the production of $c\ \bar{c}$–pairs in the "soft" fragmentation step. Since the $\Upsilon(1S)$ decays preferentially through the intermediate state of 3 gluons, it provides an ideal laboratory to search for an uncommon mechanism of charm production. Clearly the $q\bar{q}$–jet contribution due to the continuum beneath the resonance and to the vacuum polarization effects has to be correctly subtracted. Theoretical ideas for charm production in 3–gluon decays of the $\Upsilon(1S)$–resonance were developed more than a decade ago. Bigi and Nussinov [401] proposed gluon fusion as a possible charm source (Figure 7.21). Note that this ansatz follows the same line of reasoning as is applied for charm production in hadronic interactions. No quantitative predictions were made. Fritzsch and Streng [402] estimated the branching ratio to be of the order of a few percent for the process shown in Figure 7.21, where a gluon splits into a $c\bar{c}$–pair.

ARGUS has performed an extensive search for $D^{*+}(2010)$– and ψ–meson production in direct $\Upsilon(1S)$–decays [259]. No signal was observed. Note that due to limited acceptance only $D^{*+}(2010)$–mesons with a fractional momentum $x_p > 0.2$ were studied. The 90 % confidence limits derived are $Br(\Upsilon(1S)_{dir} \to D^{*+}(2010)\ +\ x) < 0.019$ and $Br(\Upsilon(1S)_{dir} \to \psi\ +\ x) < 0.68 \cdot 10^{-3}$. The data thus exclude a large contribution of the gluon reactions sketched in Figure 7.21 to charm production.

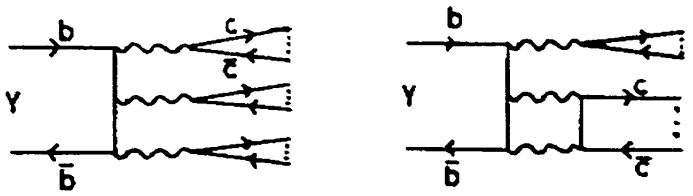

Figure 7.21: *Sources of charmed particles in direct* $\Upsilon(1S)$*–decays*

Recently OPAL has observed charm production in gluon jets. $(2.74 \pm 0.05)\%$ of all gluon jets contain a $c\bar{c}$-pair [403]. This result does not contradict the ARGUS limit, since the mean energy in case of gluon jets tagged in Z^0–decays is appreciably higher than those typical for the ARGUS measurement.

7.5 Summary

The ARGUS collaboration has performed an extensive study of hadron production in $e^+e^- \to q\bar{q}$ and $\Upsilon(1S) \to ggg$ reactions. Three aspects of the data are of special interest:

- The topology of the hadron final state observed in $e^+e^- \to q\bar{q}$ and $\Upsilon(1S) \to ggg$ reactions is compatible with a two–jet and three–jet structure of the original parton system respectively. A two–jet component in direct $\Upsilon(1S)$–decays can be excluded. The angular distribution of the leading hadrons in $e^+e^- \to q\bar{q}$ events agrees with the expectations.
  The influence of angular ordering in the parton cascade, which directly follows from the underlying gauge structure of the theory, has been observed by analyzing the low momentum part of the inclusive hadron spectra. It peaks at finite values of $\xi = ln1/x_p$. For the first time this effect has been observed for a great variety of mesons and baryons. ξ_{max} increases logarithmically with the particle mass. As predicted by higher order calculations ξ_{max} of a given hadron species in gluon jets is larger than in quark jets.

- The study of light meson and baryon spectra allows to determine in a nearly model–independent way free parameters of fragmentation models. The production of vector mesons is suppressed with respect to that of pseudoscalar mesons by a factor 2 to 3 compared to expectations based on spin statistics. Similarly the rate of decuplet baryons is reduced in comparison to octet baryons. The production of strange mesons and baryons is suppressed by a factor $\frac{s}{u} = 0.37 \pm 0.04$ (0.33 ± 0.09) for mesons (baryons). This observation indicates the same origin of strangeness suppression in meson– and baryon–production.
  All fragmentation models are based on the assumption, that the production of a hadron species depends only on its quark content. This idea is supported by the observed equality of ρ^0– and ω–meson production as well as by the measured η– to η'–rate, which depends sensitively on the pseudoscalar nonet mixing angle. Baryon pair and baryon–antibaryon pair production turn out to depend sensitively on the mechanism assumed for baryon production. Hence these measurements provide a powerful tool to discriminate between fragmentation models. The results of the ARGUS experiment exclude pure diquark production and favor the popcorn model [378] as the source of baryons.

- Baryon production turns out to be strongly enhanced in direct $\Upsilon(1S)$–decays in comparison to continuum events. None of the presently available fragmentation models allows to reproduce this observation. It might indicate an inherent difference between quark– and gluon–fragmentation.

- A variety of charmed mesons and baryons has been observed and their spectra have been measured with high precision. From the shape of the spectra follows that the ground state baryons to a large extent are secondary decay products of excited states produced in the first fragmentation step. One further observation is of general interest, especially for the polarization studies of heavy quarks performed at LEP: ARGUS has shown that the polarization of the primary quark is transferred to the leading heavy fragment, no dilution is observable.

In summary the ARGUS data provide a sensitive benchmark for all fragmentation models due to the large variety of hadron states studied and the high statistics achieved. A few of the results a decade after their first observation still provide a challenge to theorists trying to formulate a consistent scheme of the fragmentation process.

Chapter 8

Summary

In summary, ARGUS has made substantial contributions to high energy physics for more than one decade. Many discoveries and measurements have widened our understanding of the Standard Model, particularly in the heavy flavour sector. The most important observations and measurements, first made by ARGUS, are

- the observation of $B^0\overline{B}^0$mixing,
- the observation of semileptonic charmless B decays,
- the first measurements of exclusive semileptonic B decays to D^* and D mesons,
- the model independent determination of the inclusive semileptonic branching ratio of B mesons,
- the reconstruction of B mesons,
- the observation of J/ψ, $\psi^{'}$, and χ_c mesons in B decays,
- the observation of the decay $D^0 \rightarrow \phi\overline{K}^0$,
- the observation of excited charmed mesons,
- the observation of excited charmed baryons,
- an upper limit on the ν_τ mass and the measurement of the mass of the τ lepton,
- the observation of parity violation in τ decays and determination of the ν_τ helicity,
- the determination of several Michel Parameters in τ decays,
- the measurement of direct photon spectrum in $\Upsilon(1S)$ decays,
- the observation and systematic investigation of vector meson pair production in $\gamma\gamma$ interactions,
- a systematic study of meson and baryon production in the continuum and Υ decays including the observation of antideutron production in e^+e^- annihilation.

Chapter 9

Acknowledgement

It is a pleasure to thank the DESY directors, Profs. H.Schopper, V.Sörgel, B.Wiik, G.Weber, E.Lohrmann, P.Söding, A.Wagner and G.Voss, who provided us an excellent opportunity to do exciting physics. We thank the DORIS machine group, especially Prof. K.Wille, Dr. H.Nesemann and B.Sarau, for their efficient running of the storage ring and their cooperation.

Chapter 10

ARGUS Publications

10.1 B Physics

Observation of B Meson Decay into J/ψ, H.Albrecht *et al.* [1] , *Phys. Lett.* **162B** (1985) 395.

Determination of the Branching Ratio for the Decay $B^0 \to D^{*-}\pi^+$, *Phys. Lett.* **182B** (1986) 95.

Reconstruction of B Mesons, *Phys. Lett.* **185B** (1987) 218.

Observation of Inclusive D_s Production in B Meson Decays, *Phys. Lett.* **187B** (1987) 425.

Observation of $B^0\overline{B}^0$Mixing, *Phys. Lett.* **192B** (1987) 245.

Measurement of the Decay $B^0 \to D^{*-}\ell^+\nu$, *Phys. Lett.* **197B** (1987) 452.

B Meson Decays into Charmonium States. *Phys. Lett.* **199B** (1987) 451.

Observation of Charmless B Meson Decays. *Phys. Lett.* **209B** (1988) 119.

Search for the Decay $B \to K^*\gamma$. *Phys. Lett.* **210B** (1988) 258.

Observation of Inclusive B Meson Decays into Λ_c Baryons. *Phys. Lett.* **210B** (1988) 263.

B Meson Decays to $D\pi$ and $D\rho$. *Phys. Lett.* **215B** (1988) 424.

Measurement of Inclusive B Meson Decays into Baryons. *Z. Phys.* **C42** (1989) 519.

Measurement of D^{*+} Polarization in the Decay $\overline{B}^0 \to D^{*+}\ell^-\overline{\nu}$. *Phys. Lett.* **219B** (1989) 121.

Measurement of the Decay $B^0 \to D^-\ell^+\nu$. *Phys. Lett.* **229B** (1989) 175.

Search for $b \to s\gamma$ in Exclusive Decays of B Mesons. *Phys. Lett.* **229B** (1989) 304.

Measurement of the Lifetime Ratio $\tau(B^+)/\tau(B^0)$. *Phys. Lett.* **232B** (1989) 554.

[1] All ARGUS papers on physics results have H.Albrecht as the first author

Observation of Semileptonic Charmless B Meson Decays. *Phys. Lett.* **234B** (1990) 409.

Search for Hadronic $b \to u$ Decays. *Phys. Lett.* **241B** (1990) 278.

Search for Rare Semileptonic B Meson Decays. DESY 89-163, December 1989.

Search for $b \to sX^+X^-$ in Exclusive Decays of B Mesons. DESY 89-166, August 1989.

Study of inclusive semileptonic B meson decays. *Phys. Lett.* **249B** (1990) 359.

Exclusive Hadronic Decays of B Mesons. *Z. Phys.* **C48** (1990) 543.

Search for $b \to s\ gluon$ in B Meson Decays. *Phys. Lett.* **254B** (1991) 288.

Reconstruction of Semileptonic $b \to u$ Decays. *Phys. Lett.* **255B** (1991) 297.

Determination of the Branching Ratios of $\overline{B}^0 \to D^{*+}D_s^{*-}$ and $D_s \to \phi\pi$. DESY 90-157, December 1990.

Inclusive Production of D^0, D^+ and $D^*(2010)^+$ Mesons in B Decays and Nonresonant e^+e^- Annihilation at 10.6 GeV. *Z. Phys.* **C52** (1991) 353.

A Measurement of $\tau(B^-)/\tau(B^0)$ from the Lepton and Dilepton Rates in $\Upsilon(4S)$ decays. DESY 91-056, June 1991.

Production of D_s^+ Mesons in B Decay and Determination of f_{D_s} . *Z. Phys.* **C54** (1992) 1.

Measurement of the Decay $B^- \to D^{*0}\ell^-\overline{\nu}$. *Phys. Lett.* **275B** (1992) 195.

First Evidence of χ_c Production in B Meson Decays. *Phys. Lett.* **277B** (1992) 209.

Exclusive Semileptonic Decays of B Mesons to D Mesons. DESY 92-029, February 1992.

A New Determination of the $B^0\overline{B}^0$ Oscillation Strength. *Z. Phys.* **C55** (1992) 357.

Measurement of Inclusive Baryon Production in B Mesons Decays. *Z. Phys.* **C56** (1992) 1.

Investigation of the decays $B^0\overline{B}^0 \to D^{*+}\ell^-\overline{\nu}$ and $\overline{B} \to D^{**}\ell^-\overline{\nu}$. *Z. Phys.* **C57** (1993) 533.

Inclusive production of charged pions, kaons and protons in $\Upsilon(4S)$ decays. *Z. Phys.* **C58** (1993) 191.

Search for rare B meson decays into D_s^+ mesons. *Z. Phys.* **C60** (1993) 11.

Kaons in Flavour Tagged B Decays. *Z. Phys.* **C62** (1994) 371.

A Model-Independent Determination of the Inclusive Semileptonic Decay Fraction of B Mesons. *Phys. Lett.* **318B** (1993) 397.

A Study of $\overline{B}^0 \to D^{*+}\ell^-\overline{\nu}$ and $B^0\overline{B}^0$ Mixing Using Partial D^{*+} Reconstruction. *Phys. Lett.* **324B** (1994) 249.

Reconstruction of the Decay $B^- \to D_1^0(2414)\pi^-$. *Phys. Lett.* **335B** (1994) 526.

A Measurement of the Polarization in the Decay $B \to J/\psi K^*$. *Phys. Lett.* **340B** (1994) 217.

Search for Rare B Decays. *Phys. Lett.* **353B** (1995) 554.

10.2 Charm Physics

Evidence for F^* Production in e^+e^- Annihilation at 10 GeV Centre-of-Mass Energy. *Phys. Lett.* **146B** (1984) 111.

Production and Decay of the Charged D^* Meson in e^+e^- Annihilation at 10 GeV Centre-of-Mass Energy. *Phys. Lett.* **150B** (1985) 235.

Production and Decay of the F Meson in e^+e^- Annihilation at 10 GeV Centre-of-Mass Energy. *Phys. Lett.* **153B** (1985) 343.

Direct Evidence for W Exchange in Charmed Meson Decay. *Phys. Lett.* **158B** (1985) 525.

Observation of a New Charmed Meson. *Phys. Rev. Lett.* **56** (1986) 549.

Observation of F Decays into $\overline{K}^* K$ *Phys. Lett.* **179B** (1986) 398.

The Decay $D^0 \to \overline{K}^0 \phi$ *Z. Phys.* **C33** (1987) 359.

Search for the Decay $D_s \to \rho^0\pi$ as Evidence for Quark annihilation *Phys. Lett.* **195B** (1987) 102.

An Upper Limit on $D^0 - \overline{D}^0$ Mixing *Phys. Lett.* **199B** (1987) 447.

Observation of the Charmed Baryon Λ_c in e^+e^- annihilation at 10 GeV. *Phys. Lett.* **207B** (1988) 109.

Measurement of D_s^* - D_s Mass Difference. *Phys. Lett.* **207B** (1988) 349.

Search for D^0 Decays into Lepton Pairs. *Phys. Lett.* **209B** (1988) 380.

Lifetimes of Charmed Mesons. *Phys. Lett.* **210B** (1988) 267.

Observation of the Charmed Baryon Σ_c in e^+e^- Annihilations. *Phys. Lett.* **211B** (1988) 489.

Observation of the $D^{*0}(2459)$ in e^+e^- Annihilation. *Phys. Lett.* **221B** (1989) 422.

Measurement of D^0 Decays into $\overline{K}^0\omega, \overline{K}^0\eta$ and $\overline{K}^{0*}\eta$. *Z. Phys.* **C43** (1989) 181.

A Study of Cabibbo-Suppresses D^0 Decays. *Z. Phys.* **C46** (1990) 9.

Observation of a New Charmed-Strange Meson. *Phys. Lett.* **230B** (1989) 162.

Observation of the Charged Isospin Partner of the $D^*(2459)^0$. *Phys. Lett.* **231B** (1989) 208.

Resonance Decomposition of the $D^*(2420)^0$ Through a Decay Angular Analysis. *Phys. Lett.* **232B** (1989) 398.

Observation of the Decay $D_s^+ \to \eta' \pi^+$. *Phys. Lett.* **245B** (1990) 315.

Measurement of Ξ_c production in e^+e^- annihilation at 10.5 GeV center-of-mass energy. *Phys. Lett.* **247B** (1990) 121.

Observations of the Decays $D_s^- \to \phi e^- \overline{\nu}$ and $D^- \to K^{*0} e^- \overline{\nu}$. *Phys. Lett.* **255B** (1991) 634.

Observations of Λ_c^+ Semileptonic Decay. *Phys. Lett.* **269B** (1991) 234.

The Measurement of D_s^+ and D^+ Meson Decays into $K^{*+}K^{*0}$. *Z. Phys.* **C53** (1992) 361.

A Measurement of Asymmetry in the Decay $\Lambda_c^+ \to \Lambda \pi^+$
Phys. Lett. **274B** (1992) 239.

A Measurement of the Inclusive Semileptonic Decay Fraction of Charmed Hadrons. *Phys. Lett.* **278B** (1992) 202.

Evidence for the Production of the Charmed, Doubly Strange Baryon Ω_c in e^+e^- Annihilation. *Phys. Lett.* **288B** (1992) 367.

A Search for $D^0 \to K^+\pi^-$. DESY 92-056, April 1992.

New Results on D^0 Decays. *Z. Phys.* **C56** (1992) 7.

Observation of the Decays $D_{s1}(2536) \to D^{*0}K^+$. *Phys. Lett.* **297B** (1992) 425.

Observation of the Ξ_c^0 semileptonic decay. *Phys. Lett.* **303B** (1993) 368.

A partial wave analysis of the decay $D^0 \to K_s^0\pi^+\pi^-$. *Phys. Lett.* **308B** (1993) 435.

Observation of a new charmed baryon. *Phys. Lett.* **317B** (1993) 227.

Observation of polarization effects in Λ_c semileptonic decay. *Phys. Lett.* **326B** (1994) 320.

A Study of D^0 and D^+ decays into final states with two or three kaons. *Z. Phys.* **C64** (1994) 375.

Measurement of the Absolute Branching Fractions for D^0 Decays into $K^-\pi^+, K^-\pi^+\pi^+\pi^-, \overline{K}^0\pi^+\pi^-$.
Phys. Lett. **340B** (1994) 125.

Measurement of the Decay Fractions of D^* Mesons. *Z. Phys.* **C66** (1995) 63.

Evidence for W Exchange in Charmed Baryon Decays. *Phys. Lett.* **342B** (1995) 397.

A Measurement of the Decay $D_{s2}^{*+} \to D^0 K^+$. DESY 95-129, July 1995.

Measurement of the Semileptonic Branching Fractions of the D^0 Meson. DESY 95-187, October 1995.

10.3 τ Physics

An Upper Limit on the Mass of the Tau Neutrino. *Phys. Lett.* **163B** (1985) 404.

Measurement of Tau Decays into Three Charged Pions. *Z. Phys.* **C33** (1986) 7.

Evidence for the Decay $\tau^- \to \nu_\tau \omega \pi^-$. *Phys. Lett.* **185B** (1987) 223.

Search for Lepton-Number and Lepton-Flavor Violation in Tau Decays. *Phys. Lett.* **185B** (1987) 228.

Search for the Decay $\tau^- \to \nu_\tau \eta \pi^-$. *Phys. Lett.* **195B** (1987) 307.

A Measurement of the Tau Lifetime. *Phys. Lett.* **199B** (1987) 580.

An Improved Upper Limit on the ν_τ-Mass from the Decay $\tau \to \pi^-\pi^-\pi^-\pi^+\pi^+\nu_\tau$. *Phys. Lett.* **202B** (1988) 149.

Measurement of the Decays $\tau^- \to K^{*-}\nu_\tau$ and $\tau^- \to \rho^-\nu_\tau$. *Z. Phys.* **C41** (1988) 1.

Upper Limits for the Decay of τ-Leptons into η-Mesons. *Z. Phys.* **C41** (1988) 405.

Determination of the Michel parameter in tau decay. *Phys. Lett.* **246B** (1990) 278.

Determination of the tau-neutrino helicity. *Phys. Lett.* **250B** (1990) 164.

Observations of the Decay $\tau \to \rho\pi\pi\nu_\tau$. *Phys. Lett.* **260B** (1991) 259.

Measurement of Exclusive One-Prong and Inclusive Three-Prong Branching Ratios of the τ Lepton. *Z. Phys.* **C53** (1992) 367.

Search for Neutrinoless τ Decays. *Z. Phys.* **C55** (1992) 179.

A Measurement of the Tau Mass. *Phys. Lett.* **292B** (1992) 221.
Measurement of the Decay $\tau^- \to \rho^-\nu_\tau$. *Z. Phys.* **C56** (1992) 339.

Analysis of the decay $\tau \to \pi^-\pi^-\pi^+\nu_\tau$ and the determination of the $a_1(1260)$ resonance parameters. *Z. Phys.* **C58** (1993) 61.

A Determination of Two Michel Parameters in Purely Leptonic τ Decays. *Phys. Lett.* **316B** (1993) 608.

Determination of the stucture of τ decays in the reaction $e^+e^- \to \tau^+\tau^- \to \rho^+\overline{\nu}_\tau\rho^-\nu_\tau$ and a precision measurement of the τ-neutrino helicity. *Phys. Lett.* **337B** (1994) 383.

The First Measurement of the Michel Parameter η in τ Decays. *Phys. Lett.* **341B** (1995) 441.

Determination of the Michel parameters ξ und δ in Leptonic τ Decays. *Phys. Lett.* **349B** (1995) 576.

A search for the lepton-flavour violating decays $\tau \to e\alpha, \tau \to \mu\alpha$. *Z. Phys.* **C68** (1995) 25.

Tau decays into K* mesons. *Z. Phys.* **C68** (1995) 215.

10.4 Υ Spectroscopy

Branching Ratio and Mass Spectrum of the Decay $\Upsilon' \to \Upsilon\pi^+\pi^-$. *Phys. Lett.* **134B** (1984) 137.

A Precision Mesurement of the Υ' Meson Mass. D.Barber *et al. Phys. Lett.* **135B** (1984) 498.

A Determination of the μ Pair Branching Ratio of the Υ' Meson. *Z. Phys.* **C28** (1985) 45.

Radiative Decays of the $\Upsilon(2S)$ into the Three χ_b States. *Phys. Lett.* **160B** (1985) 331.

The Hadronic Transitions from Υ(2S) to Υ(1S) . *Z. Phys.* **C35** (1987) 283.

Search for Exclusive Radiative Decays of Υ(1S) and Υ(2S) Mesons. *Z. Phys.* **C42** (1989) 349.

A Measurement of the Electronic Width Γ_{ee} of the $\Upsilon(1S), \Upsilon(2S)$, and $\Upsilon(4S)$ Resonances , and of the Total Decay Width Γ of the $\Upsilon(4S)$. *Z. Phys.* **C65** (1995) 619.

10.5 Two Photon Physics

First Observation of $\gamma\gamma \to \omega\rho^0$. *Phys. Lett.* **196B** (1987) 101.

First Observation of $\gamma\gamma \to K^{*0}\overline{K}^{*0}$. *Phys. Lett.* **198B** (1987) 255.

First Observation of $\gamma\gamma \to \omega\omega$. *Phys. Lett.* **198B** (1987) 577.

Measurement of $\eta \to \pi^+\pi^-\gamma$ in $\gamma\gamma$ Collisions. *Phys. Lett.* **199B** (1987) 457.

A Search for $\omega\phi$ and $\phi\phi$ Production in the Reactions $\gamma\gamma \to K^+K^-\pi^+\pi^-\pi^0$ and $\gamma\gamma \to 2K^+2K^-$. *Phys. Lett.* **210B** (1988) 273.

First Observation of $\gamma\gamma \to K^{*+}K^{*-}$. *Phys. Lett.* **212B** (1988) 528.

A Measurement of $\gamma\gamma \to \rho^+\rho^-$. *Phys. Lett.* **217B** (1989) 205.

Two-Photon Production of Final States with a $p\overline{p}$ Pair. *Z. Phys.* **C42** (1989) 543.

Measurement of K^+K^- Production in $\gamma\gamma$ Collisions. *Z. Phys.* **C48** (1990) 183.

Observation of Spin-Parity 2^+ Dominance in the Reaction $\gamma\gamma \to \rho^0\rho^0$ near Threshold. *Z. Phys.* **C50** (1991) 1.

A Spin-Parity Analysis of $\gamma\gamma \to \rho^+\rho^-$. *Phys. Lett.* **267B** (1991) 535.

Observation of $\gamma\gamma \to \phi\rho^0$ and $\gamma\gamma \to \phi\omega$. *Phys. Lett.* **332B** (1994) 451.

Determination of the radiative width of the η_c meson. *Phys. Lett.* **338B** (1994) 390.

10.6 Fragmentation

Observation of Antideuteron Production in e^+e^- Annihilations at 10 GeV Center of Mass Energy. *Phys. Lett.* **157B** (1985) 326.

Observation of Octet and Decuplet Hyperons in e^+e^- annihilation at 10 GeV Centre-of-Mass Energy. *Phys. Lett.* **182B** (1987) 95.

Determination of α_s from a Measurement of the Direct Photon Spectrum in Υ(1S) Decays. *Phys. Lett.* **199B** (1987) 291.

Hyperon Production in e^+e^- Annihilation at 10 GeV Center of Mass Energy. *Z. Phys.* **C39** (1988) 177.

Observation of the Orbitally Excited Λ (1520) Baryon in e^+e^- Annihilation. *Phys. Lett.* **215B** (1988) 429.

Inclusive ϕ-Meson Production in Electron-Positron Interactions in the Energy Region of the Υ-Resonances. *Z. Phys.* **C41** (1989) 557.

Results on Baryon Antibaryon Correlations in e^+e^- Annihilation. *Z. Phys.* **C43** (1989) 45.

Inclusive Production of Charged Pions, Charged and Neutral Kaons and Antiprotons in e^+e^- Annihilation at 10 GeV and in Direct Υ Decays. *Z. Phys.* **C44** (1989) 547.

Observation of $\Delta(1232)^{++}$ Production in e^+e^- Annihilation around 10 GeV. *Phys. Lett.* **230B** (1989) 169.

Inclusive π^0 and η Production in e^+e^- Annihilation at $\sqrt{s}$ = 10 GeV. *Z. Phys.* **C46** (1990) 15.

Study of Antideuteron Production in e^+e^- Annihilation at 10 GeV Centre - of - Mass Energy. *Phys. Lett.* **236B** (1990) 102.

Evidence for a Higher Twist Effect in Electron Positron Annihilation into Hadrons at 10 GeV Centre - of - Mass Energy. DESY 89-164, December 1989.

Study of pp and $\Lambda\Lambda$ production in e^+e^- Annihilation at 10 GeV Center of Mass Energy. *Z. Phys.* **C49** (1991) 349.

Measurement of R and Determination of the Charged-Particle Multiplicity in e^+e^- Annihilation at $\sqrt{s}$ around 10 GeV. *Z. Phys.* **C54** (1992) 13.

Search for Charm Production in Direct Decays of the $\Upsilon(1S)$ Resonance. *Z. Phys.* **C55** (1992) 25.

Inclusive production of $\eta'(958)$ and $f_0(975)$ mesons in the Υ energy region. *Z. Phys.* **C58** (1993) 199.

Inclusive Production of $K^*(892)$, $\rho^0(770)$, and $\omega(783)$ Mesons in the Υ Energy region. *Z. Phys.* **C61** (1994) 1.

10.7 Searches

Search for Narrow States Coupling to τ pairs in radiative Υ Decay. *Phys. Lett.* **154B** (1985) 452.

Search for Fractionally Charged Particle in e^+e^- Annihilation. *Phys. Lett.* **156B** (1985) 134.

Upper Limit for the Emission of Monoenergetic Photons in Υ(1S) and
Υ(2S) Meson Decays. *Z. Phys.* **C29** (1985) 167.

Search For Gluinos in the Decays of the $\chi_b(1^3P_1)$ Meson. *Phys. Lett.* **167B** (1986) 360.

An Upper Limit for Two-Jet Production in Direct Υ(1S) Decays. *Z. Phys.* **C31** (1986) 181.

Search for Exotic Decay Modes of the Υ(1S) . *Phys. Lett.* **179B** (1986) 403.

10.8 Detector Instrumentation

Electron energy and position measurement using lead scintillator calorimeters with a new light collection system. W. Hofmann *et al.* , *Nucl. Instr. Meth.* **163** (1979) 77.

Characteristics of lead scintillator sampling shower counters for the detection of electrons and photons in the energy range from 70 Mev to 6 GeV. W. Hofmann *et al.* , *Nucl. Instr. Meth.* **195** (1982) 475.

The ARGUS electron - photon calorimeter. 1. Detection of low-energy electromagnetic showers. A. Drescher *et al.* , *Nucl. Instr. Meth.* **205** (1983) 125.

The ARGUS electron / photon calorimeter. 2. Properties of the light collection system of the lead scintillator shower counters. A. Drescher *et al.* , *Nucl. Instr. Meth.* **216** (1983) 35.

The ARGUS drift chamber. M. Danilov *et al.* , *Nucl. Instr. Meth.* **217** (1983) 153.

The ARGUS time-of-flight system. R. Heller *et al.* , *Nucl. Instr. Meth.* **A235** (1985) 26.

The ARGUS electron - photon calorimeter. 3. Electron - hadron separation. A. Drescher *et al.* , *Nucl. Instr. Meth.* **A237** (1985) 464.

Calibration and monitoring of the ARGUS shower counters. A. Drescher *et al.* , *Nucl. Instr. Meth.* **A249** (1986) 277.

The ARGUS vertex drift chamber. K.W. Edwards *et al.* , *Nucl. Instr. Meth.* **A252** (1986) 384.

Muons chambers of the ARGUS detector (in Russian). A. V. Arefiev *et al.* , *Prib. Tekh. Eksp.* **2** (1986) 66.

Study of drift chamber aging with propane. M. Danilov *et al.* , *Nucl. Instr. Meth.* **A274** (1989) 189.

ARGUS: A universal detector at DORIS-II. H. Albrecht *et al.* , *Nucl. Instr. Meth.* **A275** (1989) 1.

The ARGUS microvertex drift chamber. E. Michel *et al.* , *Nucl. Instr. Meth.* **A283** (1989) 554.

The ARGUS silicon vertex detector. E. Michel *et al.* , *Nucl. Instr. Meth.* **A348** (1994) 465.

The ARGUS Vertex Trigger. N.Koch *et al.* , DESY 95-176, September 1995. Submitted to *Nucl. Instr. Meth.*

Bibliography

[1] H. Albrecht *et al.* (ARGUS), *Phys. Lett.* **B192** (1987), 245.

[2] S.W. Herb *et al.*, *Phys. Rev. Lett.* **39** (1977), 252.

[3] H. Hasemann *et al.*, DESY-Proposal Nr. **148**, Oct. 1978.

[4] H. Nesemann *et al.*, DESY preprint DESY M-80/89, 1980, publ. in Geneva Accel. Conf. (1980) 315.

[5] H. Albrecht *et al.* (ARGUS), *Nucl. Instr. Meth.* **A275** (1989), 1.

[6] H. Albrecht *et al.* (ARGUS), *Phys. Lett.* **B185** (1987), 218.

[7] H. Albrecht *et al.* (ARGUS), *Phys. Lett.* **B197** (1987), 452.

[8] H. Albrecht *et al.* (ARGUS), *Phys. Lett.* **B234** (1990), 409.

[9] F. Abe *et al.* (CDF), *Phys. Rev. Lett.* **74** (1995), 2626;
S. Abachi *et al.* (D0), *Phys. Rev. Lett.* **74** (1995), 2632.

[10] T. Lohse *et al.* (HERA-B), DESY-PRC 93/04 (1993).

[11] D. Boutigny *et al.* (BABAR), SLAC-0443 (1994).

[12] M.T. Cheng *et al.* (BELLE), KEK Report 94-02 (1994).

[13] H. Albrecht *et al.* (ARGUS), *Phys. Rev. Lett.* **56** (1985), 549.

[14] H. Albrecht *et al.* (ARGUS), *Phys. Lett.* **B317** (1993), 227.

[15] H. Albrecht *et al.* (ARGUS), *Phys. Lett.* **B158** (1985), 525.

[16] M.Kobayashi and T.Maskawa, *Progr. Theor. Phys.* **49** (1973) 652.

[17] Particle Data Group, *Phys. Rev.* **D 50** (1994), 1.

[18] M. Bauer, B. Stech, and M. Wirbel, *Z. Phys.* **C 34** (1987), 103.

[19] N. Isgur, *Phys. Rev.* **D 43** (1991), 810.

[20] M.Voloshin and M.Shifman, *Yad. Fiz.* **41** (1985) 187; J.Chay *et al. Phys. Lett.* **B247** (1990), 399; I.Bigi *et al. Phys. Lett.* **B293** (1992), 430; I.Bigi *et al. Phys. Rev. Lett.* **71** (1993), 496.

[21] H. Albrecht *et al.* (ARGUS), *Z. Phys.* **C 65** (1995), 619.

[22] H. Albrecht *et al.* (ARGUS), *Phys. Lett.* **B249** (1990), 359.

[23] S. Behrends *et al.* (CLEO), *Phys. Rev. Lett.* **50** (1983), 881.

[24] C. Bebek *et al.* (CLEO), *Phys. Rev.* **D 36** (1987), 1289.

[25] H. Albrecht *et al.* (ARGUS), *Z. Phys.* **C 48** (1990), 543.

[26] D. Bortoletto *et al.* (CLEO), *Phys. Rev.* **D 45** (1992), 45.

[27] M.S. Alam *et al.* (CLEO), *Phys. Rev.* **D 50** (1994), 43.

[28] T.E. Browder and K. Hohnscheid, "B Mesons", to appear in *Progress in Nuclear and Particle Physics*, Vol. 35. and M. Lindner, World Scientific Publishers (1992).

[29] M. Neubert *et al.*, *Heavy Flavours*, edited by A.Buras and M.Lindner, World Scientific Publishers (1992).

[30] H. Albrecht *et al.* (ARGUS), *Z. Phys.* **C 54** (1992), 1.

[31] J.G. Körner, in Proceedings of the International Symposion on Production and Decay of Heavy Hadrons, Heidelberg, Germany, edited by K.R. Schubert and R. Waldi (1986).

[32] F. Hussain, M.D. Scadron, *Phys. Rev.* **D 30** (1984), 1492.

[33] T. Mannel, W. Roberts, Z. Ryzak, *Phys. Lett.* **B259** (1991), 485.

[34] I. Dunietz *et al.*, *Phys. Rev.* **D 43** (1991), 2193;
B. Kayser *et al.*, *Phys. Lett.* **B237** (1990), 508.

[35] H. Albrecht *et al.* (ARGUS), *Phys. Lett.* **B340** (1994), 217.

[36] H. Albrecht *et al.* (ARGUS), *Phys. Lett.* **B277** (1992), 209.

[37] H. Albrecht *et al.* (ARGUS), *Phys. Lett.* **B241** (1990), 278.

[38] H. Albrecht *et al.* (ARGUS), *Z. Phys.* **C 60** (1993), 11.

[39] J.R. Patterson, Proceedings of the XXVII International Conference on High Energy Physics, Glasgow 1994, p. 149.

[40] A. Ali and C. Greub, *Z. Phys.* **C 60** (1993), 433.

[41] W.S. Hou, A. Soni and H. Steger, *Phys. Rev. Lett.* **59** (1987), 1521; // R. Grigjannis *et al.*, *Phys. Lett.* **B224** (1989), 209.

[42] H. Albrecht *et al.* (ARGUS), *Phys. Lett.* **B353** (1995), 554.

[43] H. Albrecht *et al.* (ARGUS), *Z. Phys.* **C 54** (1992), 13.

[44] H. Albrecht *et al.* (ARGUS), *Phys. Lett.* **B254** (1991), 288.

[45] H. Albrecht *et al.* (ARGUS), *Z. Phys.* **C 58** (1993), 191.

[46] H. Albrecht *et al.* (ARGUS), *Z. Phys.* **C 61** (1994), 1.

[47] H. Albrecht *et al.* (ARGUS), *Z. Phys.* **C 52** (1991), 353.

[48] W. Wirbel, Y.L. Wu, *Phys. Lett.* **B228** (1989), 430.

[49] H. Albrecht *et al.* (ARGUS), *Phys. Lett.* **B162** (1985), 395.

[50] P. Haas *et al.* (CLEO), *Phys. Rev. Lett.* **55** (1985), 1248.

[51] H. Albrecht *et al.* (ARGUS), *Phys. Lett.* **B199** (1987), 451.

[52] M.S. Alam *et al.* (CLEO), *Phys. Rev.* **D 50** (1994), 43.

[53] H. Albrecht *et al.* (ARGUS), *Phys. Lett.* **B210** (1988), 263.

[54] H. Albrecht *et al.* (ARGUS), *Z. Phys.* **C 42** (1989), 519.

[55] H. Albrecht *et al.* (ARGUS), *Z. Phys.* **C 56** (1992), 1.

[56] H. Albrecht *et al.* (ARGUS), *Z. Phys.* **C 62** (1994), 371.

[57] M.S. Alam *et al.* (CLEO), *Phys. Rev. Lett.* **58** (1987), 1814;
P.L.Lipton (CLEO), Ph.D. Thesis, University of Rochester, UR 984 (1987).

[58] G. Altarelli *et al.*, *Nucl. Phys.* **B208** (1982), 365.

[59] B. Grinstein, N. Isgur, D. Scora, M.B. Wise, *Phys. Rev.* **D 39** (1989), 799;
N. Isgur, D. Scora, *Phys. Rev.* **D 40** (1989), 1.

[60] M.A. Shifman *et al.*, *Phys. Rev.* **D 51** (1995), 2217

[61] R. Rückl, Habilitationsschrift, CERN (1983).

[62] H. Schröder, Proceedings of the XXIV International Conference on High Energy Physics, Munich 1988, p. 73.

[63] R. Rückl, Preprint MPI-Ph/36/89;
G.Altarelli and S. Petrarca, *Phys. Lett.* **B261** (1991), 303;
I.I. Bigi *et al.*, *Phys. Lett.* **B323** (1994), 408.

[64] H. Albrecht *et al.* (ARGUS) *Phys. Lett.* **B318** (1993), 397.

[65] B. Barish *et al.* (CLEO), Cornell preprint CLNS-95-1362, October 1995.

[66] R. Fulton *et al.* (CLEO), *Phys. Rev. Lett.* **64** (1990), 16.

[67] H. Albrecht *et al.* (ARGUS), *Phys. Lett.* **B255** (1991), 297.

[68] M. Wirbel *et al.*, *Z. Phys.* **C 29** (1985), 637.

[69] J.G. Körner, G.A. Schuler, *Z. Phys.* **C 38** (1988), 511 and Erratum in *Z. Phys.* **C 41** (1989), 690.

[70] B. Grinstein, M.B. Wise and N. Isgur, *Phys. Rev. Lett.* **56** (1986), 298.

[71] H. Pietschmann and F. Schöberl, *Europhys. Lett.* 2 (1986) 583.

[72] S. Balk, F. Hussain, J.G. Körner, G. Thompson, MZ-TH-92-22 (1992).

[73] P. Ball, HD-THEP-92-25, 27th Rencontres de Moriond, Proceedings (1992).

[74] M.A. Shifman, M.B. Voloshin, *Sov. J. Nucl. Phys.* **45** (1987), 292 and **47** (1988), 511.

[75] H. Albrecht *et al.* (ARGUS), *Z. Phys.* **C 57** (1993), 533.

[76] M. Neubert, *Phys. Lett.* **B264** (1991), 455; *Phys. Lett.* **B338** (1994), 84.

[77] M. Neubert, CERN-TH 7395/94.

[78] H. Albrecht *et al.* (ARGUS), *Phys. Lett.* **B324** (1994), 249.

[79] H. Albrecht *et al.* (ARGUS), *Phys. Lett.* **B275** (1992), 195.

[80] H. Albrecht *et al.* (ARGUS), *Phys. Lett.* **B229** (1989), 175.

[81] H. Albrecht *et al.* (ARGUS), DESY preprint DESY 92-029 (1992).

[82] H. Albrecht *et al.* (ARGUS), DESY preprint DESY 89-163 (1989).

[83] T. Skwarnicki, Proceedings of the XXVIII International Conference on High Energy Physics, Beijing 1995.

[84] H. Albrecht *et al.* (ARGUS), DESY preprint DESY 89-163 (1989).

[85] H. Albrecht *et al.* (ARGUS), *Phys. Lett.* **B232** (1989), 554.

[86] R.K. Böck *et al.* (UA1), Proceedings of the XXII International Conference on High Energy Physics, Leipzig 194, p. 2.

[87] J.S. Hagelin, *Phys. Rev.* **D 20** (1979), 2893; *Nucl. Phys.* **B193** (1981), 123.

[88] M.J. Vysotzki, *Sov. J. Nucl.Phys.* **31** (1980), 797.

[89] A.J. Buras, M. Jamin and P.H. Weisz, *Nucl. Phys.* **B347** (1990), 491.

[90] H. Albrecht *et al.* (ARGUS), *Z. Phys.* **C 55** (1992), 357.

[91] S.Narison, *Phys. Lett.* **B322** (1994), 247, S.Narison and A.Pivovarov, *Phys. Lett.* **B327** (1994), 341.

[92] M.Artuso *et al.* (CLEO), *Phys. Rev. Lett.* **62** (1989), 2233.

[93] S.L. Glashow, J. Iliopoulos, and L. Maiani *Phys. Rev.* **D 2** (1970), 1285.

[94] J.J. Aubert *et al.*, *Phys. Rev. Lett.* **33** (1974), 1404.

[95] J.E. Augustin *et al.*, *Phys. Rev. Lett.* **33** (1974), 1406.

[96] G. Goldhaber *et al.*, *Phys. Rev. Lett.* **37** (1974), 255;
J.E.Wiss *et al.*, *Phys. Rev. Lett.* **37** (1974), 1531.

[97] C.E.K. Charlesworth, *A Study of the Decay Properties of the Charmed Baryon* Λ_c, Ph.D. thesis, University of Toronto, 1992.

[98] H. Albrecht *et al.* (ARGUS), *Phys. Lett.* **B150** (1985), 235.

[99] C. Peterson *et al.*, *Phys. Rev.* **D 27** (1983), 105.

[100] V.G. Kartvelishvili *et al.*, *Yad.Fiz.* **38** (1983), 1563.

[101] Particle Data Group, *Rev. Mod. Phys.* **56** (1984), 1.

[102] S. Ono, *Phys. Rev. Lett.* **37** (1976), 655.

[103] Particle Data Group, *Phys. Rev.* **D 45** (1992), 1.

[104] L. Angelos, G.P. Lepage, *Phys. Rev.* **D 45** (1992), 3021.

[105] F. Batler *et al.* (CLEO), *Phys. Rev. Lett.* **69** (1992), 2041.

[106] H. Albrecht *et al.* (ARGUS), *Z. Phys.* **C 66** (1995), 63.

[107] D. Bortoletto *et al.* (CLEO), *Phys. Rev. Lett.* **69** (1992), 2046.

[108] A. Chen *et al.* (CLEO), *Phys. Rev. Lett.* **51** (1983), 634.

[109] M. Althoff *et al.* (TASSO), *Phys. Lett.* **B136** (1984), 130.

[110] H. Albrecht *et al.* (ARGUS), *Phys. Lett.* **B153** (1985), 343.

[111] H. Albrecht *et al.* (ARGUS), *Phys. Lett.* **B146** (1984), 111.

[112] H. Albrecht *et al.* (ARGUS), *Phys. Lett.* **B207** (1988), 349.

[113] J.L. Rosner, *Comm. Nucl. Part. Phys.* **16** (1987) 321.

[114] J.C. Anjos *et al.* (E691), *Phys. Rev. Lett.* **62** (1989), 1717.

[115] H. Albrecht *et al.* (ARGUS), *Phys. Lett.* **B221** (1989), 422.

[116] H. Albrecht *et al.* (ARGUS), *Phys. Lett.* **B232** (1989), 398.

[117] H. Albrecht *et al.* (ARGUS), *Phys. Lett.* **B231** (1989), 208.

[118] J. Parsons, *A Study of Orbitally Excited Charm Mesons*, Ph.D. Thesis, University of Toronto (1990). Unpublished.

[119] H. Albrecht *et al.* (ARGUS), *Phys. Lett.* **B230** (1989), 162.

[120] H. Albrecht *et al.* (ARGUS), *Phys. Lett.* **B297** (1992), 425.

[121] K.W. Edwards *et al.* (CLEO), *Phys. Rev. Lett.* **74** (1995), 3331.

[122] H. Albrecht *et al.* (ARGUS), *Preprint* DESY 95-129 (1995).

[123] E.J.Eichten, C.T.Hill, and C.Quigg, *Phys. Rev. Lett.* **71** (1993) 4116.

[124] A.B.Kaidalov and A.V.Nogteva, *Yad. Fiz.* **47** (1988) 505.

[125] S.Godfrey and N.Isgur, *Phys. Rev.* **D32** (1985) 189; J.Morishita *et al.*, *Phys. Rev.* **D37** (1988) 159; V.Gupta and R.Koegeler, *Z. Phys.* **C41** (1988) 277; S.Godfrey and R.Kokoski, *Phys. Rev.* **D43** (1991) 1679; S.N.Gupta and J.M.Johnson, *HEP-PH-9409432*, Wayne State University, Detroit, 1994; J.Zeng *et al.*, *CEBAF-TH-94-08*, Old Dominion University, Norfolk, 1994.

[126] R. Werding (WA89), *Proc. of the XXVIIIth International Conference on High Energy Physics*, Glasgow, Scotland,1994.

[127] H. Albrecht *et al.* (ARGUS), *Phys. Lett.* **B207** (1988), 109.

[128] H. Albrecht *et al.* (ARGUS), *Phys. Lett.* **B247** (1990), 121.

[129] H. Albrecht *et al.* (ARGUS), *Phys. Lett.* **B211** (1988), 489.

[130] H. Albrecht *et al.* (ARGUS), *Phys. Lett.* **B288** (1992), 367.

[131] J.G. Koerner and H.W. Siebert, "Charm Baryon: Theory and Experiment", *Ann. Rev. Nucl. Part. Sci.* **41** (1991), 511.

[132] S. Biagi *et al.* (WA62), *Z. Phys.* **C 28** (1985), 175.

[133] J. Stiewe (ARGUS), *Proc. of the XXVIth International Conference on High Energy Physics*, Dallas, USA, 1992.

[134] P.L. Frabetti *et al.* (E687), *Phys. Lett.* **B300** (1993), 190.

[135] P.L. Frabetti *et al.* (E687), *Phys. Lett.* **B338** (1994), 106.

[136] N. Isgur, and G. Karl, *Phys. Lett.* **B 74** (1978), 353;
L.A. Copley,N. Isgur and G. Karl, *Phys. Rev.* **D 20** (1979), 768;
S. Capstick and N. Isgur, *Phys. Rev.* **D 34** (1986), 2809;
C.S. Kalman and B. Tran, *Nuovo Cim.* **A102** (1989) 835.

[137] N. Ushida *et al.* (E531), *Phys. Rev. Lett.* **45** (1980), 1049,1053.

[138] M.A. Shifman, *Proc. of the 1987 International Symposium on Lepton and Photon Interactions at High Energies*, Hamburg, 1987.

[139] H. Albrecht *et al.* (ARGUS), *Phys. Lett.* **B210** (1988), 267.

[140] M.K. Gaillard, B.W.Lee, and J.L.Rosner, *Rev. Mod. Phys.* **47** (1975) 277;
J.Ellis, M.K. Gaillard, and D.V.Nanopoulos, *Nucl. Phys.* **B100** (1975), 313;
D. Fakirov and B. Stech, *Nucl. Phys.* **B133** (1978), 315;
N. Cabibbo and L. Maiani, *Phys. Lett.* **B 73** (1978), 418.

[141] I. Bigi and M. Fukugita, *Phys. Lett.* **B 91** (1980), 121.

[142] H. Albrecht *et al.* (ARGUS), *Z. Phys.* **C 33** (1987), 359.

[143] M. Lusignoli and A. Pugliese, *preprint* 515, Roma (1986).

[144] A.N. Kamal, *Phys. Rev.* **D 33** (1986), 377.

[145] M. Bauer, B. Stech and M. Wirbel, *Z. Phys.* **C 34** (1987), 103.

[146] B.Yu. Blok, M.A. Shifman, *Yad.Fiz.* **45** (1987) 211;478;841.

[147] H.J. Lipkin, *Phys. Lett.* **B 90** (1980), 710;
M. Bauer and B. Stech, *Phys. Lett.* **B152** (1985), 380;
J.F. Donoghue, *Phys. Rev.* **D 33** (1986), 1516.

[148] U. Baur *et al.*, *Phys. Lett.* **B175** (1986), 377.

[149] H. Albrecht *et al.* (ARGUS), *Phys. Lett.* **B195** (1987), 102.

[150] H. Albrecht *et al.* (ARGUS), *Phys. Lett.* **B179** (1986), 398.

[151] B. Guberina, R. Rückl, and J. Trampetic, *Z. Phys.* **C 33** (1986), 297.

[152] P. Avery *et al.* (CLEO), *Phys. Rev. Lett.* **71** (1993), 2391.

[153] H. Albrecht *et al.* (ARGUS), *Phys. Lett.* **B342** (1995), 397.

[154] J.G. Koerner and M. Kramer, *Z. Phys.* **C 55** (1992), 659.

[155] R. Rameika *et al.*, *Phys. Rev.* **D 33** (1986), 3172;
P. Dauber *et al.*, *Phys Rev.* **179** (1969), 1262;
D. Aston *et al.*, *Phys. Rev.* **D 32** (1985), 2270.

[156] see, *e.g.*, G. Källen, Elementary particle physics, Addison-Wesley, Reading MA 1964)

[157] H. Albrecht *et al.* (ARGUS), *Phys. Lett.* **B274** (1992), 239.

[158] S. Pakvasa, S.P. Rosen, and S.F. Tuan, LA-UR 90-700 (1990).

[159] J.D. Bjorken, *Phys. Rev.* **D 40** (1989), 1513.

[160] T. Mannel, W. Roberts, and Z. Ryzak, *Phys. Lett.* **B255** (1991), 593.

[161] P. Avery *et al.* (CLEO), *Phys. Rev. Lett.* **65** (1990), 2842.

[162] T.D.L ee and C.N. Yang, *Phys. Rev.* **D 108** (1957), 1645.

[163] J.C. Anjos *et al.* (E691), *Phys. Rev. Lett.* **62** (1989), 722.

[164] G. Crawford *et al.* (CLEO), *Phys. Rev.* **D 44** (1991), 3394.

[165] Z. Bai *et al.* (MARK III), *Phys. Rev. Lett.* **66** (1991), 1011.

[166] H. Albrecht *et al.* (ARGUS), *Phys. Lett.* **B255** (1991), 634.

[167] S. Semenov (ARGUS), *Proc. of the XXVIIth International Conference on High Energy Physics*, Marseille, France, 1993.

[168] P. Ball, V.M. Braun, and H.G. Dosch, *Phys. Rev.* **D 44** (1991), 3567.

[169] C.W. Bernard, A.X. El-Khadra, and A. Soni, *Phys. Rev.* **D 47** (1993), 998.

[170] H.Albrecht *et al.*(ARGUS Collaboration), *DESY* **95-187** October 1995.

[171] J. Alexander *et al.* (CLEO), *Phys. Rev. Lett.* **65** (1990), 1531;
P.L. Frabetti *et al.* (E687), *Phys. Lett.* **B313** (1993), 253.

[172] R. Perez-Marcial *et al.*, *Phys. Rev.* **D 40** (1989), 2955;
R. Singleton Jr. Preprint SLAC-PUB-5335 (1990).

[173] H. Albrecht *et al.* (ARGUS), *Phys. Lett.* **B269** (1991), 234.

[174] H. Albrecht *et al.* (ARGUS), *Phys. Lett.* **B303** (1993), 368.

[175] E. Vella *et al.* (MARK II), *Phys. Rev. Lett.* **48** (1982), 1515.

[176] H.C. Ballagh *et al.*, *Phys. Rev.* **D 24** (1981), 7.

[177] S.R. Klein *et al.* (MARK II), *Phys. Rev. Lett.* **62** (1989), 2444.

[178] P. Utzat, *Suche nach semileptonischen Zerfällen des Baryons mit Charm und doppelter Strangeness* Ω_c., Diplomarbeit, Univ. Heidelberg/D (1993);
J.Spengler (ARGUS) in Proceedings of HADRON 93, Como 1993.

[179] H. Albrecht *et al.* (ARGUS), *Phys. Lett.* **B340** (1994), 125.

[180] S. Abachi *et al.* (HRS), *Phys. Lett.* **B205** (1988), 411.

[181] D. Decamp *et al.* (ALEPH), *Phys. Lett.* **B266** (1991), 218.

[182] H. Albrecht *et al.* (ARGUS), *Z. Phys.* **C 56** (1992), 7.

[183] H. Albrecht *et al.* (ARGUS), *Z. Phys.* **C 43** (1989), 181.

[184] H. Albrecht *et al.* (ARGUS), *Z. Phys.* **C 46** (1990), 9.

[185] P. Avery *et al.* (CLEO), *Phys. Rev.* **D 43** (1991), 3599.

[186] M. Procario *et al.* (CLEO), *Phys. Rev.* **D 48** (1993), 4007.

[187] D.S. Akerib *et al.* (CLEO), *Phys. Rev. Lett.* **71** (1994), 3070.

[188] H. Albrecht *et al.* (ARGUS), *Phys. Lett.* **B308** (1993), 405.

[189] H. Albrecht *et al.* (ARGUS), *Z. Phys.* **C 53** (1992), 361.

[190] H. Albrecht *et al.* (ARGUS), *Z. Phys.* **C 64** (1994), 375.

[191] R. Ammar *et al.* (CLEO), *Phys. Rev.* **D 44** (1991), 3383.

[192] see, for example, M. Wirbel, *Nucl. Phys.* **B268** (1988), 33.

[193] R. Shindler *et al.* (MARK II), *Bul. Am. Phys.* **24** (1979) 600.

[194] R.M. Baltrusaitis *et al.* (MARK III), *Phys. Rev. Lett.* **55** (1985), 150.

[195] A.N. Kamal and R. Sihna, *Phys. Rev.* **D 36** (1987), 3510;
A.N. Kamal and R.C. Verma, *Phys. Rev.* **D 35** (1987), 3515;
A. Czarnecki,A.N. Kamal and Q.Xu, *Z. Phys.* **C 54** (1992), 410.

[196] M. Gluck, *Phys. Lett.* **B 88** (1979), 145;
G. Eilam and J.P. Leveille, *Phys. Rev. Lett.* **44** (1980), 1648;
J. Finjord, *Nucl. Phys.* **B171** (1980), 413.

[197] J.C. Anjos *et al.* (E691), *Phys. Rev.* **D 43** (1991), R635.

[198] S. Barlag *et al.* (ACCMOR), *Z. Phys.* **C 48** (1990), 29.

[199] M.K. Gaillard and B. W.Lee, *Phys. Rev.* **D 10** (1974), 897.

[200] H.-Y. Cheng, *Phys. Rev.* **D 26** (1982), 143;
A. Datta and DK̇umbhakar, *Z. Phys.* **C 27** (1985), 515.

[201] L. Wolfenstein, *Phys. Lett.* **B164** (1985), 170.

[202] I. Bigi and A.I. Sanda, *Phys. Lett.* **B171** (1986), 320;
I. Bigi, *Proceedings of the Charm Physics Workshop,* Peking, 1987.

[203] L.L. Chau and H.Y. Cheng, *Phys. Lett.* **B280** (1992), 281.

[204] H. Albrecht *et al.* (ARGUS), *Phys. Lett.* **B199** (1987), 447.

[205] H. Albrecht *et al.* (ARGUS), *Preprint* DESY 92-56 (1992).

[206] R. Ammar *et al.* (CLEO), *Phys. Rev. Lett.* **72** (1994), 1406.

[207] M.L.Perl *et al.*, *Phys. Rev. Lett.* **35** (1975), 1489.

[208] H. Albrecht *et al.* (ARGUS), *Z. Phys.* **C 54** (1992), 13.

[209] H. Albrecht *et al.* (ARGUS), *Phys. Lett.* **B154** (1985), 452.

[210] H. Albrecht *et al.* (ARGUS), *Phys. Lett.* **B163** (1985), 404.

[211] H. Albrecht *et al.* (ARGUS), *Z. Phys.* **C 33** (1986), 7.

[212] H. Albrecht *et al.* (ARGUS), *Phys. Lett.* **B185** (1987), 228.

[213] H. Albrecht *et al.* (ARGUS), *Phys. Lett.* **B185** (1987), 223.

[214] H. Albrecht *et al.* (ARGUS), *Phys. Lett.* **B199** (1987), 580.

[215] H. Albrecht *et al.* (ARGUS), *Phys. Lett.* **B195** (1987), 307.

[216] H. Albrecht *et al.* (ARGUS), *Phys. Lett.* **B202** (1988), 149.

[217] H. Albrecht *et al.* (ARGUS), *Z. Phys.* **C 41** (1988), 1.

[218] H. Albrecht *et al.* (ARGUS), *Z. Phys.* **C 41** (1988), 405.

[219] H. Albrecht *et al.* (ARGUS), *Phys. Lett.* **B246** (1990), 278.

[220] H. Albrecht *et al.* (ARGUS), *Phys. Lett.* **B250** (1990), 164.

[221] H. Albrecht *et al.* (ARGUS), *Phys. Lett.* **B260** (1991), 259.

[222] H. Albrecht *et al.* (ARGUS), *Z. Phys.* **C 53** (1992), 367.

[223] H. Albrecht *et al.* (ARGUS), *Z. Phys.* **C 55** (1992), 179.

[224] H. Albrecht *et al.* (ARGUS), *Z. Phys.* **C 56** (1992), 339.

[225] H. Albrecht *et al.* (ARGUS), *Phys. Lett.* **B292** (1992), 221.

[226] H. Albrecht *et al.* (ARGUS), *Z. Phys.* **C 58** (1993), 61.

[227] H. Albrecht *et al.* (ARGUS), *Phys. Lett.* **B316** (1993), 608.

[228] H. Albrecht *et al.* (ARGUS), *Phys. Lett.* **B341** (1995), 441.

[229] H. Albrecht *et al.* (ARGUS), *Phys. Lett.* **B337** (1994), 383.

[230] H. Albrecht *et al.* (ARGUS), *Phys. Lett.* **B349** (1995), 576.

[231] H. Albrecht *et al.* (ARGUS), DESY-95-087 (1995).

[232] W.J. Marciano an A. Sirlin, *Phys. Rev. Lett.* **61** (1988), 1815.

[233] J.H. Kühn and A. Santamaria, *Z. Phys.* **C 48** (1990), 445.

[234] A. Donnachie, Proc. of the HADRON '91 Conference, College Park, MD (USA), eds. S. Oneda and D.C. Peaslee, World Scientific 1992.

[235] F.J. Gilman and S.H. Rhie, *Phys. Rev.* **D 31** (1985), 1066.

[236] S.I. Dolinsky *et al.*, *Phys. Lett.* **B174** (1986), 453.

[237] M. Derrick *et al.* (HRS), *Phys. Lett.* **B189** (1987), 260.

[238] A. Pich, *Phys. Lett.* **B196** (1987), 561.

[239] M. Artuso *et al.* (CLEO), *Phys. Rev. Lett.* **69** (1992), 3278.

[240] S. Jadach and Z. Was, Comp. Phys. Comm. **36** (1985) 191;
S. Jadach and Z. Was, CERN-TH-5855/90;
S. Jadach, J.H. Kühn, and Z. Was, CERN-TH-5856/90.

[241] N. Isgur, C. Morningstar, and C. Reader, *Phys. Rev.* **D 39** (1989), 1357.

[242] M. Bowler, *Phys. Lett.* **B209** (1988), 99.

[243] M. Schmidtler, Doctoral Thesis, Universität Karlsruhe (1995).

[244] T. Das, V.S. Mathur, and S. Okubo, *Phys. Rev. Lett.* **18** (1967), 761.

[245] K.W. Edwards *et al.*, *Nucl. Instr. Meth.* **A252** (1986), 384.

[246] E. Michel *et al.*, *Nucl. Instr. Meth.* **A283** (1989), 544.

[247] E. Michel *et al.*, *Nucl. Instr. Meth.* **A348** (1994), 465.

[248] D. Buskulic *et al.* (ALEPH) *Phys. Lett.* **B349** (1995), 585.

[249] W. Fetscher, H.J. Gerber and K.F. Johnson, *Phys. Lett.* **B137** (1986), 102;
W. Fetscher, *Phys. Rev.* **D 42** (1990), 1544.

[250] H. Kühn und F. Wagner, *Nucl. Phys.* **B236** (1984), 16.

[251] M. Feindt, *Z. Phys.* **C 48** (1990), 681.

[252] H. Thurn and H. Kolanoski, *Z. Phys.* **C 60** (1993), 277.

[253] H. Thurn, Doctoral Thesis, University of Dortmund, 1994.

[254] K.G. Hayes *et al.* (MARK II), *Phys. Rev.* **D 25** (1982), 2869.

[255] S. Keh *et al.* (Crystal Ball), *Phys. Lett.* **B212** (1988), 123.

[256] T. Bowcock *et al.* (CLEO), *Phys. Rev.* **D 41** (1990), 805.

[257] E. Eichten *et al.*, *Phys. Rev.* **D 17** (1978), 3090; *Phys. Rev.* **D 21** (1980), 203.

[258] H. Albrecht *et al.* (ARGUS), *Z. Phys.* **C 31** (1986), 181.

[259] H. Albrecht *et al.* (ARGUS), *Z. Phys.* **C 55** (1992), 25.

[260] D.P. Barber *et al.* (DORIS Machine Group, ARGUS, CRYSTAL BALL), *Phys. Lett.* **B135** (1984), 498.

[261] A.A. Sokolov, I.M. Ternov, *Sov. Phys. Dokl.* **8** (1964), 1203.

[262] W.W. MacKay *et al.* (CUSB), *Phys. Rev.* **D 29** (1984), 2483.

[263] A.S. Artamov *et al.*, *Phys. Lett.* **B137** (1984), 272;
S.E. Baru *et al.* (MD1), *Z. Phys.* **C 56** (1992), 547.

[264] H. Albrecht *et al.* (ARGUS), *Z. Phys.* **C 35** (1987), 283.

[265] G. Bonneau and F. Martin, *Nucl. Phys.* **B 27** (1971), 381.

[266] F.A. Berends and R. Kleiss, *Nucl. Phys.* **B177** (1981), 237.

[267] F.A. Berends and R. Kleiss, *Nucl. Phys.* **B178** (1981), 141.

[268] F.A. Berends, G.J.H. Burgers, and W.L. van Neerven, *Phys. Lett.* **B185** (1987), 395.

[269] Y.S. Tsai, SLAC-PUB-3129 (1983).

[270] J.P. Alexander, G. Bonvicini, P.S. Drell and R. Frey, *Phys. Rev.* **D 37** (1988), 56.

[271] E.A. Kuraev, V.S. Fadin, Sov. J. Nucl. Phys. 41 (1985), 466.

[272] *detailed discussions on this topic are found in* W. Buchmüller, S. Cooper, in High Energy Electron-Positron Physics, ed. by A. Ali, P. Söding, World Scientific 1988, p. 412, *and* J.P. Alexander *et al.*, *Nucl. Phys.* **B320** (1989), 45.

[273] H. Albrecht *et al.* (ARGUS), *Z. Phys.* **C 28** (1985), 45.

[274] A. Le Yaouanc *et al.*, *Phys. Rev.* **D 8** (1973), 2223. and *Phys. Lett.* **B 71** (1977), 397;
S. Ono, *Phys. Rev.* **D 23** (1981), 1118;
A. Le Yaouanc *et al.*, Hadron Transitions in the Quark Model, Gordon and Breach Science Publ. (1988).

[275] D.M.J. Lovelock *et al.* (CUSB), *Phys. Rev. Lett.* **54** (1985), 377;
J. Besson *et al.* (CLEO), *Phys. Rev. Lett.* **54** (1985), 381.

[276] H. Albrecht *et al.* (ARGUS), *Phys. Lett.* **B160** (1985), 331.

[277] R. Heller, Dissertation, IHEP-HD/84-08, Heidelberg 1984.

[278] H. Albrecht *et al.* (ARGUS), *Phys. Lett.* **B134** (1984), 137.

[279] B. Niczyporuk *et al.* (LENA), *Phys. Lett.* **B100** (1981), 95.

[280] V. Fonseca *et al.* (CUSB), *Nucl. Phys.* **B242** (1984), 31.

[281] J. Besson *et al.* (CLEO), *Phys. Rev.* **D 30** (1984), 1433.

[282] D. Gelphman *et al.* (Crystal Ball), *Phys. Rev.* **D 32** (1985), 2893.

[283] L.S. Brown, R.N. Cahn, *Phys. Rev. Lett.* **35** (1975), 1.

[284] M.B. Voloshin, JETP Lett. 21,347(1975).

[285] T.-M. Yan, *Phys. Rev.* **D 22** (1980), 1652.

[286] M. Voloshin, V. Zakharov, *Phys. Rev. Lett.* **45** (1980), 688.

[287] D. Morgan, M.R. Pennington, *Phys. Rev.* **D 12** (1975), 1283.

[288] V.A. Novikov, M.A. Shifman, *Z. Phys.* **C 8** (1981), 43.

[289] R. Decker, M. Moreno, Lett. al Nuovo Cim. 13, 407 (1975).

[290] J. Schwinger *et al.*, *Phys. Rev.* **D 12** (1975), 2617.

[291] H. Genz, C.B. Lang, Il Nuovo Cim. 32A, 513 (1976).

[292] T.N. Pham, B. Pire, T.N. Truong, *Phys. Rev.* **D 13** (1976), 620.

[293] B.J. Harrington, S.Y. Park, A. Yildiz, *Phys. Rev.* **D 12** (1975), 2765.

[294] R.N. Cahn, *Phys. Rev.* **D 12** (1975), 3559.

[295] R. Brandelik *et al.* (TASSO), *Phys. Lett.* **B 97** (1980), 448.

[296] N.N. Achasov *et al.*, *Phys. Lett.* **B108** (1982), 134; *Z. Phys.* **C 27** (1985), 99; *Phys. Lett.* **B203** (1988), 309.

[297] B.A. Li and K.F. Liu, *Phys. Rev. Lett.* **51** (1983), 1510; *Phys. Rev.* **D 30** (1984), 613; *Phys. Rev. Lett.* **58** (1987), 2288.

[298] H. Albrecht *et al.* (ARGUS),

[299] G. Alexander, A. Levy, U. Maor, *Z. Phys.* **C 30** (1986), 65;
G. Alexander and U. Maor, *Phys. Rev.* **D 46** (1991), 2882.

[300] H. Kolanoski, *Z. Phys.* **C 39** (1988), 543.

[301] V.M. Budnev, I. F. Ginzburg, G.V. Meledin, V. G. Serbo, *Phys. Rep.* **15C** (1975) 181.

[302] H. Albrecht *et al.* (ARGUS) *Z. Phys.* **C 42** (1989), 543.

[303] D.L. Burke *et al.* (MarkII), *Phys. Lett.* **B103** (1981), 153.

[304] H. Aihara *et al.* (TPC/2γ), *Phys. Rev.* **D 37** (1988), 28.

[305] M. Althoff *et al.* (TASSO), *Z. Phys.* **C 16** (1982), 13.

[306] H.-J. Behrend *et al.* (CELLO), *Z. Phys.* **C 21** (1984), 205.

[307] Ch. Berger *et al.* (PLUTO), *Z. Phys.* **C 38** (1988), 521.

[308] H. Albrecht *et al.* (ARGUS), *Z. Phys.* **C 50** (1991), 1.

[309] H. Albrecht *et al.* (ARGUS), *Phys. Lett.* **B267** (1991), 535.

[310] S.J. Brodsky, G. Köpp and P.M. Zerwas, *Phys. Rev. Lett.* **58** (1987), 443.

[311] H. Albrecht *et al.* (ARGUS), *Phys. Lett.* **B196** (1987), 101.

[312] A. Wegner *et al.* (JADE), *Z. Phys.* **C 48** (1990), 393.

[313] H.-J. Behrend *et al.* (CELLO), *Phys. Lett.* **B257** (1991), 493.

[314] E. Križnič, *Production of $\omega\rho^0$, $\rho^0\phi$ and $\omega\phi$ in Two–Photon Interactions at the ARGUS Spectrometer*, Doctor thesis, University of Ljubljana, Slovenia (1993).

[315] H. Albrecht *et al.* (ARGUS), *Phys. Lett.* **B332** (1994), 451.

[316] H. Albrecht *et al.* (ARGUS), *Phys. Lett.* **B198** (1987), 577.

[317] H. Albrecht *et al.* (ARGUS), DESY 95-227.

[318] H. Albrecht *et al.* (ARGUS), *Phys. Lett.* **B198** (1987), 255.

[319] H. Albrecht *et al.* (ARGUS), *Phys. Lett.* **B212** (1988), 528.

[320] H. Albrecht *et al.* (ARGUS), *Z. Phys.* **C 48** (1990), 183.

[321] T. Podobnik, *Resonances Observed in the Reaction* $\gamma\gamma \to \pi^+\pi^-\pi^0$, Doctor thesis, University of Ljubljana, Slovenia (1995).

[322] Z.P. Li, F.E. Close, T. Barnes, *Phys. Rev.* **D 43** (1991), 2161.

[323] D. Antreasyan *et al.* (Crystal Ball), *Z. Phys.* **C 48** (1990), 561.

[324] H.-J. Behrend *et al.* (CELLO), *Z. Phys.* **C 46** (1990), 583.

[325] H. Albrecht *et al.* (ARGUS), *Phys. Lett.* **B199** (1987), 457.

[326] H. Albrecht *et al.* (ARGUS), *Phys. Lett.* **B338** (1994), 390.

[327] D. Bisello *et al.*, *Nucl. Phys.* **B350** (1991), 1.

[328] R. Barbieri *et al.*, *Phys. Lett.* **B106** (1981), 497.

[329] P. Mättig, Phys. Rep. 177 (1989) 141.

[330] S. Bethke and J.E. Pilcher, Ann. Rev. Nucl. Sc. 42 (1992) 251.

[331] W. Hofmann, Ann. Rev. Nucl. Sc. 38 (1988) 279.

[332] D. Wegener in A. Ali and P. Söding, High Energy e^+e^- Reactions, World Publishing, Singapore 1988, p. 489.

[333] S. Brandt *et al.*, *Phys. Lett.* **B 12** (1964), 57.

[334] M. Schmelling, CERN/PPE 94-184

[335] B.R. Webber, *Nucl. Phys.* **B238** (1984), 492.

[336] R.D. Field and S. Wolfram, *Nucl. Phys.* **B213** (1983), 65.

[337] B. Andersson *et al.*, Phys. Rep. 97 (1983) 31.

[338] R.P. Feynman and R. D.Field, *Nucl. Phys.* **B136** (1978), 1.

[339] S. Brandt and H.D. Dahmen, *Z. Phys.* **C 1** (1979), 61.

[340] A. Donnachie and P.V. Landshoff, *Z. Phys.* **C 4** (1980), 231.

[341] G.C. Fox and S. Wolfram, *Nucl. Phys.* **B149** (1979), 413.

[342] H. Albrecht *et al.* (ARGUS) DESY 89-164.

[343] E.L. Berger, *Z. Phys.* **C 4** (1980), 289.

[344] H. Albrecht *et al.*, (ARGUS) *Z. Phys.* **C 44** (1989), 547.

[345] S.G. Goroshny *et al.*, *Phys. Lett.* **B259** (1991), 144.

[346] S. Bethke, Summary of α_s measurements, PITHA-94-30.

[347] S.J. Brodsky *et al.*, *Phys. Rev.* **D 28** (1983), 228.

[348] H. Albrecht *et al.* (ARGUS) *Phys. Lett.* **B199** (1987), 291.

[349] A. Ore and J.L. Powell, *Phys. Rep.* 75 (1949), 1696

[350] D.M. Photiadis, *Phys. Lett.* **B164** (1985), 160.

[351] R.D. Field, *Phys. Lett.* **B133** (1983), 248.

[352] T. Sjostrand, Comp. Phys. Comm. 43 (1987) 367.

[353] T. Sjostrand CERN-TH-7112-93 (Rev.1994).

[354] H. Albrecht *et al.* (ARGUS), *Z. Phys.* **C 46** (1990), 15.

[355] R. Waldi (ARGUS) Joint Intern. Lepton–Photon Symposium & Europhysics Conference on High Energy Physics, Geneva 1991, Vol.I, p. 424.

[356] M. Aguilar-Bonitez *et al.*, (LEBC-EHS) *Z. Phys.* **C 50** (1991), 405.

[357] W. Geist *et al.*, Phys.Rep. 197 (1990) 263.

[358] H. Albrecht *et al.* (ARGUS), *Z. Phys.* **C 58** (1993), 199.

[359] H. Albrecht *et al.* (ARGUS), *Z. Phys.* **C 41** (1989), 557.

[360] A. Lindner, PhD thesis, Dortmund 1992

[361] A. Zimmermann, Diplomarbeit, Dortmund 1992

[362] C.D. Buchanan and S.B. Chun, *Phys. Rev. Lett.* **59** (1987), 1997.

[363] C.D. Buchanan, private communication

[364] S. Abachi *et al.* (HRS), *Phys. Rev. Lett.* **57** (1986), 1990.

[365] R.D. Field, *Phys. Lett.* **B135** (1984), 203.

[366] W. Hofmann, *Z. Phys.* **C 10** (1981), 351.

[367] H. Albrecht *et al.* (DASP2), *Phys. Lett.* **B102** (1981), 291.

[368] H. Albrecht *et al.* (ARGUS), *Phys. Lett.* **B183** (1987), 419.

[369] H. Albrecht *et al.* (ARGUS), *Z. Phys.* **C 39** (1988), 177.

[370] H. Albrecht *et al.* (ARGUS), *Phys. Lett.* **B215** (1988), 429.

[371] H. Albrecht *et al.* (ARGUS), *Phys. Lett.* **B230** (1989), 169.

[372] H. Scheck, *Nucl. Phys.* B Conf. Suppl. 1B (1988), 291.

[373] S. Ekelin *et al.*, *Phys. Rev.* **D 30** (1984), 2310.

[374] H. Albrecht *et al.* (ARGUS), *Z. Phys.* **C 43** (1989), 45.

[375] H. Albrecht *et al.* (ARGUS), *Z. Phys.* **C 49** (1991), 349.

[376] H. Albrecht *et al.* (ARGUS), *Phys. Lett.* **B157** (1985), 326.

[377] H. Albrecht *et al.* (ARGUS), *Phys. Lett.* **B236** (1990), 102.

[378] A. Casher *et al.*, *Phys. Rev.* **D 20** (1979), 179.

[379] H. Scheck, PhD thesis, Dortmund 1988

[380] D. Drijard *et al.* (ABCDHW), *Nucl. Phys.* **B155** (1979), 269.

[381] Y.L. Azimov *et al.*, *Z. Phys.* **C 27** (1985), 65.

[382] Y.L. Azimov *et al.*, *Z. Phys.* **C 31** (1986), 213.

[383] Yu.L. Dokshitzer *et al.*, Rev. Mod. Phys. 60 (1988) 373.

[384] C.P. Fong and R.R. Webber, *Nucl. Phys.* **B355** (1991), 54.

[385] Y.L. Dokshitzer *et al.*, Basics of Perturbative QCD, Edition Frontier 1991.

[386] V.A. Khoze, CERN-TH 5849.

[387] M. Suzuki, *Phys. Lett.* **B 71** (1977), 139.

[388] J.D. Bjorken, *Phys. Rev.* **D 17** (1978), 171.

[389] G. Harder, PhD thesis, Hamburg 1989, DESY F15 – 89/01.

[390] H. Albrecht *et al.* (ARGUS), *Phys. Lett.* **B150** (1985), 135.

[391] H. Albrecht *et al.* (ARGUS), *Phys. Lett.* **B297** (1992), 426.

[392] S. Bethke, *Z. Phys.* **C 29** (1985), 175.

[393] M. Suzuki, *Phys. Rev.* **D 33** (1986), 676.

[394] P. Avery *et al.* (CLEO), *Phys. Rev.* **D 41** (1990), 774.

[395] D. Wegener, Proc. XXIII Intern. Symp. on Multiparticle Dynamics Aspen 1993, p. 520.

[396] Y. Kubota *et al.* (CLEO), *Phys. Rev.* **D 44** (1991), 593.

[397] S. Abachi *et al.* (HRS), *Phys. Lett.* **B199** (1987), 585.

[398] S. Aihara *et al.* (TPC), *Phys. Rev.* **D 43** (1991), 21.

[399] R.H. Dalitz *et al.*, *Phys. Lett.* **B215** (1988), 783.

[400] R. Mankel, to be published.

[401] I.Y. Bigi and S. Nussinov, *Phys. Lett.* **B 82** (1979), 281.

[402] H. Fritzsch and K.H. Streng, *Phys. Lett.* **B 77** (1978), 299.

[403] R.D. Heuer (OPAL), talk LEP FRC meeting April 1995.

List of Figures

1.1 The ARGUS Detector 2
1.2 *ARGUS luminosity* 4

2.1 *Measurements of CKM matrix elements* 7
2.2 *Description of the unitarity triangle (see text).* 8
2.3 $\Upsilon(4S)$ *resonance cross section [21, 22]* 10
2.4 *View of a fully reconstructed* $\Upsilon(4S) \to B^- B^+$ *decay along the beam axis (see text)* . 11
2.5 *Mass distributions for B candidates in the decay channels* $D^{*+} n\pi (n \leq 3)$ *[25]. The hatched area shows the same spectrum for wrong-charge combinations.* 12
2.6 *Mass distributions for B candidates in clean two-body channels [25]:* **(a)** B^- *candidates from the channels* $B^- \to D^0\pi^-$, $D^{*0}\pi^-$, $D_J^{(*)0}\pi^-$, $J/\psi(K^-, K^{*-})$, *and* $\psi' K^-$; **(b)** $\overline{B}^0$ *candidates from the channels* $D^+\pi^-$, $D^{*+}\pi^-$, *and* $J/\psi(K_s^0, K^{*0})$ 13
2.7 $|\cos\theta|$ *distribution for B mesons [25]. The curve is a fit using a* $\sin^2\theta$ *distribution.* . 13
2.8 *Comparison between the experimentally measured branching ratios (points with combined statistical and systematic errors; [25]) and the prediction of Bauer, Stech, and Wirbel [18] with* $a_1 = 1.03$ *and* $a_2 = -0.20$ *(squares)* 15
2.9 *Invariant mass distribution for all eight decay modes* $B \to D_s^{(*)} D^{(*)}$ *(points with error bars; [30]). The solid line is the result of a fit using a Gaussian for the signal plus a constant to parametrize the background. The corresponding distribution for the continuum contribution is shown as a hatched histogram.* 17
2.10 *Comparison of the ratio of branching ratios* $BR(B^+ \to D_s^{*+}\overline{D}^0)/BR(B^+ \to D_s^+\overline{D}^0)$, $BR(B^+ \to D_s^{*+}\overline{D}^{*0})/BR(B^+ \to D_s^+\overline{D}^{*0})$, $BR(B^0 \to D_s^{*+}D^-)/BR(B^+ \to D_s^+ D^-)$, *and* $BR(B^0 \to D_s^{*+}D^{*-})/BR(B^+ \to D_s^+ D^{*-})$ *[30] with theoretical predictions of Bauer-Stech-Wirbel [18] (triangles), Körner [31] (circles), Hussain-Scadron [32] (squares), and Mannel-Roberts-Ryzak [33] (diamonds)* 18
2.11 *Angular distributions for the decay* $B \to J/\psi K^*$ *[35]. The solid lines show the fit results to the (a)* $\cos\theta_{J/\psi}$ *and (b)* $\cos\theta_{K^*}$ *angular distributions* 19
2.12 *Penguin diagrams for B decays* 20
2.13 *Completely reconstructed event with a* $B^0 \to K^+\pi^-$ *candidate [42]* 21
2.14 *Momentum spectra for (a)* D^0, *(b)* D^+, *and (c)* D^{*+} *mesons from inclusive B decays in the* $\Upsilon(4S)$ *rest frame [47]. The curves are the results of a calculation of Wirbel and Wu [48], normalized to the data.* 23
2.15 *Momentum spectrum of* D_s *mesons from B decays [30]. The curves are the result of a fit of expected spectra for two-body decays* $B \to D_s^{(*)} D^{(*)}$ *and three-body decays* $B \to D_s^{(*)} D^{(*)}\pi/\rho/\omega$ 24
2.16 *Lepton spectra on the* Υ(4S) *[22]* 27
2.17 *Lepton spectra from* Υ(4S) *decays; continuum subtracted [64]* 27
2.18 *Electron spectrum of* $B \to e\nu X$ *decays [64] The solid line is the fit with the ACM model [58] to the data, the dashed line that of the GISW model [59]* 29

2.19 *Combined lepton momentum spectrum for direct Υ(4S) decays [8]. The histogram is the $b \to c$ contribution normalized in the region $2.0 - 2.3\, GeV/c$* 30

2.20 *Completely reconstructed event containing the decay $\Upsilon(4S) \to B^0\overline{B}^0$, $B^0 \to \overline{B}^0$ where one $\overline{B}^0$ decays into $\pi^+\mu^-\overline{\nu}$ and the other into $D^{*+}\rho^-$ [67]* 31

2.21 *Measured M^2_{rec} distributions (points with error bars) for the two D^0 decay channels [75] The blank and shaded areas correspond to the rates for the signal process and the feeddown process, respectively. The continuum process is shown as a dashed line* 33

2.22 *Measured distribution $\Delta BR(\overline{B}^0 \to D^{*+}\ell^-\overline{\nu})/\Delta y$ transformed to correspond to $|V_{cb}| \cdot \xi(y)$ [75]. The dotted line corresponds to $\xi(y) = 1 - \rho^2(y-1)$ for the Isgur-Wise Function where ρ is the charge radius* 35

2.23 *Continuum and fake lepton subtracted M^2_{rec} spectrum for $l^+\pi^-$ (points with errors) and $l^+\pi^+$ (histogram) combinations [78]* 35

2.24 *Background subtracted M^2_{rec} spectrum for right-sign ($\ell^+\pi^-$) combinations [78]. The curves show the result of the fit described in the text* 37

2.25 *$D^0\gamma$ invariant mass distribution for $|M^2_{rec}| < 1\ GeV^2/c^4$ after subtraction of the background under the D^0 signal and of the contribution from faked leptons [79]. The solid line represents the fit result for the D^{*0} signal, the calculated background is shown as the dashed line* 37

2.26 *$|V_{cb}| \cdot \xi(y)$ distribution for $\tau_{B^0} = 1.27$ ps [79]. The solid line shows the fit result for a linear parametrization of the Isgur-Wise Function. The dotted line shows the fit result with a single pole parametrization* 38

2.27 *M^2_{rec} distribution for the $D^-\ell^+$ system [80]. The dashed curve shows the contribution from the cascade decay $B^0 \to D^{*-}\ell^+\nu, D^-(\pi^0,\gamma)\ell^+\nu$* 39

2.28 *Invariant ($D^{*+}\pi^-$) mass (points with error bars) obtained for $M^2_{rec} > 0$ [75]. The dotted curve describes the background obtained from the ($D^{*+}\pi^-$) mass distribution for $M^2_{rec} < 0$* 40

2.29 *Box diagrams for $B^0\overline{B}^0$ transitions* 42

2.30 *Completely reconstructed event consisting of the decay $\Upsilon(4S) \to B^0B^0$ (see text; [1])* 43

2.31 *M^2_{rec} spectra [90] for $l^+\pi^-$ (points with errors) for events with an additional lepton with momentum $1.4 < p_l < 2.5$: background (dotted histogram) and the result of the fit (full histogram) a) for like-sign leptons; b) for unlike-sign leptons* 45

3.1 *$d\sigma/dx_p$ for the D^{*+} mesons produced in charm fragmentation [98]. The dotted and solid curves result from fits to theoretical models [99] [100].* 48

3.2 *Mass difference plots from D^{*+} analysis for $K^-\pi^+$ and $K^-\pi^+\pi^+\pi^-$ D^0 final states. Combinations in (c) are required to have $x_E > 0.6$ [98].* 49

3.3 *$\phi\pi^+$ and $\phi\pi^+\pi^-\pi^+$ invariant mass distributions from D_s^+ analysis [110].* 50

3.4 *Plots from analysis of $D_s^{+*} - D_s^+$ mass difference from the updated ARGUS analysis of 1988 [112]. the left and right plots respectively, show the $D_s^+\gamma$ invariant mass distributions obtained using shower photons (γ_s) and converted photons (γ_c). In each case both signal and sideband distributions are provided ((a) and (b)).* 50

3.5 *Observed charmed mesons (schematic)* 51

3.6 *$D^{*+}\pi^-$ invariant mass distributions for all final states [13].* 52

3.7 *Plots from analysis of the $D^+\pi^-$ final state. (a) shows the invariant mass distribution obtained using selection criteria described in the text. (b) shows the $\cos\theta_\pi$ angular distribution for signal (data points) and background (histogram). In both plots the overlaid lines are the results of the fits described in the text [115].* 53

3.8 *Mass difference plots from analysis of $D^0\pi^+$ final states for each of the two D^0 final states. (a) and (b) were fitted using a polynomial background function and a single Breit-Wigner to describe signal contributions. Signal contributions in (c) and (d) were fitted with three Breit-Wigners in order to account for the feeddown contributions described in the text [117].* 54
3.9 *Plots from the $D^{*+}K_s^0$ analysis using the (a) $K^-\pi^+$,$K^-\pi^+\pi^+\pi^-$ (b) $K^-\pi^+\pi^0$ for the D^0 reconstruction [119].* 55
3.10 *Plots from analysis of $D^{*0}K^+$ final state. (a) and (b) are from the full reconstruction of using the $D^0\pi^0$ and $D^0\gamma$ D^{*0} final states respectively. (c) is from the partial reconstruction where the neutral from the D^{*0} decay is unobserved [120].* 57
3.11 *Invariant mass spectrum for all accepted D^0K^+ combinations. The histogram represents the total contribution of feed-down structures described in the text. The arrows (1) and (2) point to the region populated by the reflections from decays $D_1^+(2420) \to D^{*0}\pi^+$ and $D_2^{*+}(2460) \to D^{*0}\pi^+$, and the feed-down from the decay $D_2^{*+}(2460) \to D^0\pi^+$ respectively [122].* 58
3.12 *ARGUS signals for the Σ_c^0 and Σ_c^{++} states. Mass difference spectra for (a) $\Lambda_c^+\pi^-$ and (b) $\Lambda_c^+\pi^+$ combinations, using $\Lambda_c{}^+$ candidates from the decay modes $pK^+\pi^-$, $\Lambda\pi^+\pi^-\pi^+$, and $\overline{K^0}p$. The overlaid lines are from fits using a Gaussian and a polynomial background [129].* 60
3.13 *ARGUS signals for the a) $\Xi_c{}^0$ and b) $\Xi_c{}^+$ states reconstructed in the $\Xi\pi^+\pi^+\pi^-$ and $\Xi\pi^+\pi^+$ final states respectively. Overlaid are fit results using a Gaussian for the Ξ_c signal and a polynomial to describe the background [128].* 60
3.14 *ARGUS signal for Ω_c in the $\Xi^-K^-\pi^+\pi^+$ final state [130].* 61
3.15 *Invariant mass distribution for all accepted $\Lambda\pi^+\pi^-$ combinations. The solid histogram results from using the Λ_c^+ sidebands. Overlaid is the result of the fit described in the text [14].* 61
3.16 *The x_p spectrum of the Λ_c^{*+}. The solid curve is the result of the fit with the Peterson fragmentation function [14].* 62
3.17 *W-exchange diagram for the decay $D^0 \to \phi\overline{K}^0$* 63
3.18 *$K_s^0K^+K^-$ invariant mass distribution [142].* 64
3.19 *K^+K^- invariant mass distribution from $K_s^0K^+K^-$ combinations in the D^0 mass region [142].* 64
3.20 *(a) The invariant mass of all accepted $\Xi^-K^+\pi^+$ combinations. (b) The wrong sign distribution [153].* 66
3.21 *The $\Xi^-K^+\pi^+$ invariant mass spectrum after a cut around the Ξ^{*0} signal (unshaded histogram). Shaded: The scaled mass spectrum obtained from the Ξ^{*0} sidebands; it displays no enhancement in the Λ_c^+ signal region [153].* 66
3.22 *Number of events as a function of cosθ for signal (circles) and background (squares). The shape of the signal distribution is well parametrized by the fit described in the text [157].* 68
3.23 *The $K_s^0\pi^-$ invariant mass distribution for events containing a positron candidate [167]* 69
3.24 *The $K^+\pi^-$ invariant mass distribution for events containing a positron candidate [166]* 69
3.25 *K^+K^- invariant mass distribution for events containing electron candidate [166]* . . 70
3.26 *The (a)Λe^+ (b) $\Lambda\mu^+$ invariant mass distributions for $x_p > 0.5$, after wrong-sign subtraction(solid squares). Overlaid are the results of Gaussian fits to the corresponding Monte Carlo distributions. Bins with zero contents are not displayed [173].* 71
3.27 *Invariant mass Ξ^-l^+ combinations with $x_p > 0.45$ for events with: (a)the right-sign lepton(histogram) and wrong-sign+sideband (solid squares); (b)the right-sign lepton after background subtraction [174].* 72
3.28 *Distribution of* cosΘ *for two intervals of pion momenta [179]* 73

3.29 *$K^0_S K^0_S K^+$ invariant mass [190]* 74
3.30 *Mass spectrum of accepted $K^{*+}\overline{K}^{*0}$ combinations [189]* 76

4.1 *A typical τ event with 1-3 topology produced in e^+e^- annihilation.* 79
4.2 *The decay of a τ lepton via W exchange into a fermion pair.* 80
4.3 *Two-pion mass spectrum of the decay $\tau^- \to \pi^-\pi^0\nu_\tau$ compared to the CVC prediction [224].* 86
4.4 *Top: Spectral function for the decay $\tau^- \to \pi^-\pi^-\pi^+\pi^0\nu_\tau$ measured by ARGUS [213]. Bottom: Same distribution for the decay $\tau^- \to \omega\pi^-\nu_\tau$ with the result of three different fits to $\sigma_{e^+e^-\to\omega\pi^0}$ measurements [213].* 87
4.5 *Distribution of the $\pi^+\pi^-\pi^0$ invariant mass in τ decays of the type $\tau^- \to \pi^-\pi^-\pi^+\pi^0\nu_\tau$ [215]. a) Simulated events with an η yield corresponding to the HRS measurement; b) data.* 89
4.6 *Background corrected two- and three-pion mass spectra of the decay $\tau^- \to \pi^-\pi^-\pi^+\nu_\tau$ [226]. The two-pion plot shows the like-sign (one entry per event) and unlike-sign (two entries per event) combinations (curves: KORALB Monte Carlo). The three-pion mass spectrum is fitted by the model of Isgur et al. [241].* 91
4.7 *Dalitz-plot projections of the $\pi^-\pi^-\pi^+$ final state in τ decays for four three-pion mass intervals [226]. The curves are fits of the model of Isgur et al. [241] to the data.* 92
4.8 *The measured distribution of the proper decay length for the selected three-prong τ decays [214].* 95
4.9 *Measured pseudo-mass spectrum of three-pion events compared with the result of a Monte Carlo simulation (hatched histogram) of the same spectrum for the decay $\tau^- \to \pi^-\pi^-\pi^+\nu_\tau$ and for background, normalized to the data [225]. The simulation used the old value $m_\tau = 1.7841$ GeV[103], indicated by the dotted line. The insert gives an enlarged view of the interesting region around $m^*_\tau = m_\tau$.* 96
4.10 *Measured invariant 5π mass spectrum (histogram) [225]. The hatched part indicates the events analysed in the previous analysis [216]. The curve corresponds to the expected shape of a phase-space decay weighted with the weak matrix element (assuming $m_{\nu_\tau} = 0$ MeV). Note that the curve has not been normalized to the data.* 97
4.11 *Possible spin configurations in the decay (4.28) if the ν_τ is left-handed (a_1^- rest system).* 99
4.12 *The parity violating asymmetry measured as a function of the square of the three-pion invariant mass combined for τ^- and τ^+ decays [226].* 100
4.13 *Pseudo-likelihood as a function of γ^2_{AV} (uncorrected) for the selected $\rho^-\rho^+$ events (full line) and for a simulated data sample containing a comparable mixture of signal and background events (dashed line) [229]. The dotted line represents a function using only the energy-energy correlation of the two ρ mesons.* 102
4.14 *Laboratory energy spectra for a) electrons and b) muons in leptonic τ decays [219]. The data are compared to the prediction for a $V-A$ (solid line) and $V+A$ (dashed line) couplings at the $W-\tau-\nu_\tau$ vertex (for the other vertex the standard $V-A$ coupling is assumed in both cases). For the determination of the ρ parameters only the data points above the dotted lines have been used.* 104
4.15 *Efficiency corrected electron (left) and muon (right) spectra in the τ pseudo-rest-frame (full points) [228]. The dashed lines show fit results: a) Fit of the electron spectrum with $\eta = 0$; b) result of the combined fit to both spectra shown for the muon spectrum.* 105

5.1 Bottomonium spectrum. The thin lines are yet undiscovered states. 110
5.2 *Visible hadronic cross section versus centre of mass energy in the Υ(1S) (a) and Υ(2S) (b) energy regions [21].* 114

5.3 *Inclusive spectrum of converted photons from the Υ(2S) resonance and the underlying continuum. The width of the peaks is determined by the momentum resolution of the detector. The calibration has been checked with a π^0 signal [276].* 116
5.4 *Missing mass for inclusive Υ(2S) decays (a) and exclusive events $\pi^+\pi^- l^+ l^-$ (b) [264]* 117
5.5 *Invariant mass distribution of $\pi^+\pi^-$ from $\Upsilon(2S) \to \pi^+\pi^-\Upsilon(1S)$ [264].* 118

6.1 *A schematic representation of the two–photon production of final states X.* 120
6.2 *A schematic drawing representing the isobar model for final states with three (a) or more (b) particles. The final state partial waves are treated as being composed of two well defined isobars and phase–space distributed parts.* 123
6.3 *Cross sections for the dominating amplitudes for $\gamma\gamma \to \rho^0\rho^0$ (open circles) and for $\gamma\gamma \to \rho^+\rho^-$ (full squares) [308, 309].* 124
6.4 *Cross sections for $\gamma\gamma \to \pi^+\pi^+\pi^0\pi^-\pi^-$ (crosses), for $\gamma\gamma \to \rho^0\omega$ (open circles) and for the $(J^P, J_z) = (2^+, 2)$ partial wave of $\gamma\gamma \to \rho^0\omega$ (full circles) [314].* 125
6.5 *Cross sections for the reactions $\gamma\gamma \to \rho^0\phi$ and $\gamma\gamma \to \omega\omega$ [315].* 125
6.6 Cross sections for the reactions $\gamma\gamma \to \omega\phi$ and $\gamma\gamma \to K^*K^*$ ($K^{*+}K^{*-}$ crosses, $K^{*0}K^{*0}$ full circles) [319]. 127
6.7 *Two–kaon invariant mass spectrum for the reaction $\gamma\gamma \to K^+K^-$ [320].* 128
6.8 *a) Event distributions for the partial waves $(J^P, J_z) = (2^+, \pm 2)$ and $(2^+, 0)$ of the reaction $\gamma\gamma \to \pi^+\pi^0\pi^-$ in the region below 1.45 GeV. b) The total $\gamma\gamma \to \pi^+\pi^0\pi^-$ cross section obtained by summing up all the partial wave contributions [321].* 129
6.9 *$\pi^+\pi^-\gamma$ invariant mass spectrum after kinematic cuts and γ energy tuning [325].* . . . 130
6.10 *Invariant mass distribution for three η_c channels. Solid curves represent fits to the data. The binning is 20 MeV for the the reaction $\gamma\gamma \to K_s K^\pm\pi^\mp$ and 25 MeV for other two spectra [326]* 130

7.1 *(a) Thrust distributions (from charged and neutral particles) of direct $\Upsilon(1S)$-decays and continuum events at 9.98 GeV cms-energy. (b) Distributions of the second Fox–Wolfram moment (from charged and neutral particles) of direct $\Upsilon(1S)$-decays and continuum events at 9.98 GeV cms-energy [258].* 135
7.2 *Results of a fit of $\frac{d\sigma}{d\Omega} \sim 1 + A \cdot cos^2\theta$ to the acceptance corrected polar angle distribution of charged hadrons compared to predictions from a higher twist calculation [343].* . . 136
7.3 *Acceptance-corrected direct photon spectrum compared to the theoretical spectra of ref. [349] (dashed curve), ref.[350] (dotdashed curve) and ref.[351] (solid curve). The error bars represent statistical errors only.* 137
7.4 *Measured π^+, K^+, K^0 and p spectra for continuum events (a) and direct $\Upsilon(1S)$ decays (b) [344] compared to model predictions [337].* 142
7.5 *(a) Measured $K^{*+}(896)$–meson spectrum ($\circ$) for continuum events. (b) Measured inclusive $K^{*+}(896)$–meson spectrum ($\circ$) in direct $\Upsilon(1S)$–decays [46] compared to model predictions [337, 353]* 142
7.6 *(a) Measured $\rho^0(770)$–meson spectrum ($\circ$) in continuum events. (b) Measured $\rho^0(770)$–meson spectrum ($\circ$) in direct $\Upsilon(1S)$–decays [46] compared to model predictions [337, 353]* 143
7.7 *(a) Mass distributions of $\Lambda\,\pi^-$ combinations with $x_p > 0.15$ for$\Upsilon(1S)$ data; (b) mass distributions of combinations with $x_p > 0.15$ of Λ candidates with a prompt π^-–track for $\Upsilon(1S)$ and $\Upsilon(2S)$ data [369].* 144
7.8 *Measured proton spectrum in direct $\Upsilon(1S)$–decays [344] ($\circ$) compared to model predictions [337, 353]* 145
7.9 *(a) Measured Λ–spectrum ($\circ$) in continuum events. (b) Measured Λ–spectrum ($\circ$) in direct $\Upsilon(1S)$–decays [369] compared to model predictions [337, 353]* 145

7.10 *Ratio r for hadrons* 146
7.11 *Strangeness suppression in hyperon production* 147
7.12 *Spin suppression in hyperon production* 148
7.13 *Distribution of the opening angle between two protons (antiprotons) for (a) continuum data and direct (b) Υ–decays. The errors shown include both statistical and systematic uncertainties. The solid line represents the prediction of the Lund model with a popcorn fraction of 0.9. In (b) the dashed line corresponds to the Lund prediction, where the integral of the curve has been normalized to the experimental data.* 149
7.14 *Distribution of the energy loss dE/dx versus momentum p for the 21 antideuteron candidates (big dots), together with the expected curves for e, μ, π, K, p and d (solid lines). The mean dE/dx values of other particles, as measured in a multihadronic event sample, are also included [377]* 150
7.15 *(a) Measured spectrum $\frac{1}{\sigma}\frac{d\sigma}{d\xi}$ for charged pions in continuum events. The full line represents a Gaussian fit to the data. (b) ξ_{max} as a function of $\sqrt{s}$. The data points for $\sqrt{s} > 10$ GeV are taken from ref. [334].* 152
7.16 *(a) ξ_{max} for continuum events at $\sqrt{s} = 10.45$ GeV as a function of the particle mass. (b) ξ_{max} for direct $\Upsilon(1S)$–decays as a function of the particle mass. The full lines represents a fit of an exponential to the meson data* 152
7.17 *ξ_{max} for mesons as a function of m for continuum events and direct $\Upsilon(1S)$–decays.* . 153
7.18 *(a) Measured spectrum of D^+–meson [47] in continuum events in comparison to predictions of the Lund model [337, 353]. (b) Comparison of the predicted inclusive spectrum for different charmed mesons [353].* 155
7.19 *Measured values of α (z) compared to the prediction of the Suzuki model given as a broken line* 157
7.20 *Scatter–plot of $D^o\pi^+$ $D^o\pi^-$ invariant masses* 158
7.21 *Sources of charmed particles in direct $\Upsilon(1S)$–decays* 160

List of Tables

1.1 *ARGUS data* 4

2.1 *Masses of B mesons (MeV)* 13
2.2 *Branching ratios for decays* $B \to D^{(*)} n \cdot \pi$ *(%)* 14
2.3 *Branching ratios for decays* $B \to J/\psi/\chi_c K^*$ *(%)* 14
2.4 *Parameters* a_1 *and* a_2 *of the model of Bauer, Stech, and Wirbel* 16
2.5 *Branching ratios for decays* $B \to D_s^{(*)} D^{(*)}$ *(%)* 16
2.6 *Limits on charmless B decays from ARGUS [37]* 20
2.7 *Mean kaon multiplicities in B meson decays. Mixing of* B^0 *mesons is taken into account* 26
2.8 *Semileptonic branching ratios of B mesons [22]* 28
2.9 *Observed single-lepton and dilepton events in the momentum interval* $2.3 < p_\ell < 2.6$ *GeV/c and estimated backgrounds (ARGUS [8])* 31
2.10 A_{FB} *and* α_{pol} *in the decay* $\overline{B} \to D^* \ell^- \overline{\nu}$ *[75]* 34
2.11 *Summary on exclusive semileptonic B decays* 39
2.12 *Observed* $\overline{B}^0 \ell^\pm$ *rates [90]* 43
2.13 *Dilepton rates from ARGUS [90]* 44

3.1 *Experimental (ARGUS) measurements and theoretical predictions for masses of P-wave charmed excited mesons.* 58
3.2 *Summary of ARGUS ground state baryons measurements.* 59
3.3 D^0 *decay branching ratios in % . Absolute normalization was obtained using PDG [17] branching ratios for* $D^0 \to \overline{K}^0 \pi^+ \pi^-$ *(for channels with* K_s^0 *) and* $D^0 \to K^- \pi^+$ *(for all other channels)* 74
3.4 *Cabibbo-suppressed D Decays* 75

4.1 *The spectral functions and possible* $q\overline{q}$ *resonances with the same quantum numbers which could be observed in* τ *decays.* 82
4.2 *Upper limits* $[10^{-5}]$ *(90% CL) on branching ratios of neutrinoless* τ *decays compared with results from previous experiments [212, 223, 254, 255, 256].* 84
4.3 88
4.4 *ARGUS results on the Michel parameters and the* ν_τ *helicity (statistical and systematic errors combined).* 107
4.5 *Decay branching ratios of the* τ *lepton measured by the ARGUS Collaboration.* . . . 107
4.6 *Parameters of the* τ, ν_τ *measured by the ARGUS Collaboration.* 108

5.1 *ARGUS results on the electromagnetic transitions* $\Upsilon(2S) \to \gamma \chi_{bJ}$ *[276].* 116
5.2 *Experimental results on* $\mathrm{BR}(\Upsilon(2S) \to \Upsilon(1S)\pi^+\pi^-)$ 117
5.3 *Fit results for theoretical parametrizations in* $m(\pi\pi)$ *for* $\Upsilon(2S) \to \Upsilon(1S)\,\pi^+\pi^-$ *by the ARGUS collaboration [264].* 119

6.1 *Results of the analysis of $\gamma\gamma \to \eta_c$. If two errors are given, the first error shown is statistical and the second systematic. In the case of results for the two–photon width, the first error is statistical, the second uncorrelated systematic, and the third correlated systematic error. Upper limits correspond to the 95 % confidence level. $\eta_c \to 2K^+2K^-$ contains all topological modes except $\eta_c \to \phi\phi$ [326].* 131

7.1 *Measured rates of pseudoscalar mesons in the continuum ($\sqrt{s} = 9.98$ GeV) and for direct $\Upsilon(1S)$-decays [344, 354]. The data are compared to the predictions of the Lund fragmentation model , version JETSET 7.4 [337, 352, 353].* 138
7.2 *Measured rates of vector mesons in the continuum ($\sqrt{s} = 10.5$) and for direct $\Upsilon(1S)$-decays [46, 358, 359]. The data are compared to the predictions of the Lund fragmentation model, version JETSET 7.4 [337, 352].* 139
7.3 *$\frac{V}{V+P}$ ratio derived from the measured pseudoscalar- and vector-meson rate [46] from direct $\Upsilon(1S)$-decay rates.* 140
7.4 *Ratios $\frac{s}{u}$ derived from vector-meson rates.* 140
7.5 *Measured ratio $\frac{n(f_0)}{n(\rho^0)}$ from different experiments.* 141
7.6 *Rate of baryons produced in direct $\Upsilon(1S)$–decays and in continuum fragmentation [344, 369, 371, 370]. The data are compared with the predictions of the Lund model [337, 352] (JETSET7.4).* 146
7.7 149
7.8 *Production rate of pp– and $\Lambda\Lambda$–pairs for direct $\Upsilon(1S)$–decays. The proton rate is restricted to protons with 0.4 GeV $\leq p \leq$ 1.2 GeV.* 149
7.9 *Values of ξ_{max} derived by a fit of a Gaussian to the $\frac{d\sigma}{d\xi}$ spectra measured by the ARGUS collaboration for continuum data and direct $\Upsilon(1S)$–decays.* 153
7.10 *Charmed meson states studied by the ARGUS collaboration to determine the Peterson parameter ε by a fit of Equation (7.22) to the momentum spectrum.* 154
7.11 *Probabilities to observe different helicity states of $D^*(D)$–mesons according to a statistical model. $\sigma = 2$ corresponds to the undiluted statistical distribution.* 156
7.12 *Measured angular coefficient α.* 157
7.13 *Charmed baryon states observed by the ARGUS collaboration. ε is the parameter of the Peterson fragmentation function (Equation (7.22)).* 159